## ABSTRACT

Title of Document: QUANTITATIVE ANALYSIS OF MICROCRACKS IN CONCRETE FROM DELAYED ETTRINGITE FORMATION BY AUTOMATED PROCESSING OF LASER SHEAROGRAPHY IMAGES

Shivam Sharma, Master of Science 2021

Directed By: Professor Amde M. Amde

Department of Civil and Environmental Engineering

The objective of this research was to determine which image processing algorithms were most effective in quantifying the microcrack distribution in concrete in laser shearography images.

The motivation is the need for a nondestructive method to measure the development of damage in concrete due to expansive stresses generated by delayed ettringite formation (D.E.F.). This produces networks of fine microcracks. These may not be visible to the human eye or detectable by conventional imaging techniques. However, laser shearography provides a means to visualize them at very early stages of growth. This nondestructive method generates a first derivative image of the surface topography. This can make cracks less than 1 μm visible. These can in turn be quantified by automated image processing algorithms. These crack pattern images can then be analyzed to obtain sets of statistics that can be tracked over time for investigating the D.E.F. process which can provide insights into the crack propagation mechanisms.

This research thus concerned the application of automated image processing to a set of laser shearography images of concrete prisms where D.E.F. damage had been induced by an accelerated test method. Four prisms were involved. Two were treated to accelerate the D.E.F. rate of development. The other two were controls. They were imaged periodically at roughly month intervals by laser shearography for up to 200 days. A commercial automated image processing software, ImagePro was used. Two approaches were tried to identify the cracks in each image: manually or by an automated macro. Once a crack was identified, its track was traced by an auto tracing algorithm. It was found that the macro generated too many artifacts, so the manual method was used.

The results showed significant differences between the control prisms and the treated ones in terms of crack numbers and their length. Over time the cracks in the treated specimens tended to grow longer but fewer in number as the individual cracks joined up. In the controls, the cracks tended to disappear with time. This may be because they were only superficial in the first place and then were covered by a thin surface layer of calcium hydroxide that precipitated from the lime water bath.

The conclusion is that it is feasible to apply automated imaging techniques to quantify damage due to D.E.F. However, a disadvantage of using the existing commercial software was that it produced crack tracks that were only one pixel wide. Thus, it was not possible to measure actual crack width and their changes with expansion. Another issue is that it is designed for images of surfaces in real space whereas the laser shearography image is the first derivative of the surface topography. This contains information that could be used to estimate crack widths. It could also be

used to automate the detection of cracks, possibly by the application of artificial intelligence techniques.

# QUANTITATIVE ANALYSIS OF MICROCRACKS IN CONCRETE FROM DELAYED ETTRINGITE FORMATION BY IMAGE PROCESSING OF LASER SHEAROGRAPHY IMAGES

by

Shivam Sharma

Thesis submitted to the Faculty of the Graduate School of the

University of Maryland, College Park, in partial fulfillment

of the requirements for the degree of

Master of Science

2021

Advisory Committee:

Professor Amde M. Amde, Chair

Professor M. Sherif Aggour

Research Professor, Chung C. Fu

© Copyright by

Shivam Sharma

2021

Acknowledgements

I would like to thank Professor Amde and Professor Richard for their time, knowledge, and guidance in helping me write this thesis. Their support was valuable throughout this process specially in these trying times.

Also, thanks for Media Cybernetics for making me a Beta tester for Image Pro and letting me use it for the image processing.

I would also like to thank my father Vikram Sharma, my mother Seema Sharma and my sister Vasundhara Sharma who supported me continuously throughout my work.

Finally, a thanks to all my friends who helped me with my work.

Table of Contents

**List of Tables**

**List of Figures**

## Table of Symbols and abbreviations

**Symbols**

| | |
|---|---|
| Tx1 | Concrete Sample 1 |
| Tx2 | Concrete Sample 2 |
| Tx3 | Concrete Sample 3 |
| Tx4 | Concrete Sample 4 |
| $K_2CO_3$ | Potassium carbonate |
| $C_3A$ | Tricalcium Aluminate |
| $C_4AF$ | Calcium Aluminoferrite |

**Abbreviations**

| | |
|---|---|
| D.E.F. | Delayed Ettringite Formation |
| S.E.M. | Scanning Electron Microscope |
| R.G.B. | Red Green Blue |
| A.S.T.M. | American Society of testing and materials |
| F.F.T. | Fast Fourier Transform |
| D.F.T. | Discrete Fourier Transform |
| D.I.C. | Differential Interference Contrast |
| A.S.R. | Alkali-Silicate Reaction |

# Chapter 1 Introduction

## 1.1 Background

Concrete is the foundation of modern society, with its use in most structures it has become imperative for us to identify every possible form of damage and develop ways to mitigate and deal with them for long lasting structures. In this study the aim is to use images taken using the laser shearography method and detect microcracks caused by Delayed Ettringite Formation (D.E.F.) then quantifying them using ImagePro software, this would help with understanding more about the cracks formed on the surface of the concrete.

The Prestressed industry needs to track the formation of D.E.F. in their structural members as they use specialized heating methods after casting which generally involves steam curing at 70$^{o}$ C to induce early strength in concrete, it was concluded after extensive research review that prestressed members are prone to D.E.F. formation by Day (Day 1992). Which makes understanding more about the deleterious effects of D.E.F. all the more important.

Since its official discovery in 1965 by R. A. Kennerley (1965) in dams that were built using fly ash D.E.F. has been identified in various other structures which including both precast and cast in place concrete structures. The exact formation process of D.E.F. is still debatable but it is most likely seen in concrete or mortar samples that have undergone heating and curing cycles of temperatures above 70 degree Celsius

and where an excess amount of potassium, $CO_3$, $SO_3$ was reported in the concrete mixture. D.E.F. is formed within the concrete mixture it causes expansion in the hardened concrete which in turn leads to a phenomenon of map cracking on the concretes surface, which are a series of microcracks that have developed larger over time and caused premature degradation to the strength of concrete, leading to a decrease in the serviceable life or increased project life costs because of unaccounted repairs.

The exact method of the formation of D.E.F. is still not known. The two main leading theories are that the D.E.F. is in the form of crystals, which are formed when the C-S-H gel at high curing temperatures absorbs the sulphates and slowly releases them mostly from admixtures generally clinker to form the Ettringite crystal, Fu et al. (1996).The second theory is that the D.E.F. exists in a gel like state and hardens over a long period of time which is mainly driven by the presence of monosulphates in the mixture which is replaced by D.E.F. overtime causing the unwanted expansion. Taylor et al. (2001).

To further study the development of D.E.F. in concrete samples this paper uses the following approaches to track the effects of D.E.F. :-

### 1.2 Problem Statement

As pointed out above the formation of D.E.F. overtime in Concrete can cause various problems in concrete. In order to better understand the behavior of D.E.F. and

mitigate it's growth Laser Shearography Technology (L.S.T.) is used which will make use of non-destructive testing and allows one to look at and quantify microcracks on the concrete surface, the concrete was mixed in two batches with the first batch being the test specimen which would undergo the modified Duggan Heat cycle and further divided into batches with the first (TX1) being normal concrete and the second (Tx2) with the elevated levels of Potassium Carbonate to promote the formation of D.E.F. The second batch being the control, was divided further into two sections with first (Tx3) with nothing added to it and the second with (Tx4) with the elevated levels of Potassium Carbonate added to the concrete. The first batch was cast at an earlier date and the second batch was cast at a later date, the other difference between the two batches is that the second batch did not undergo the Modified Duggan Heat Cycle. Before imaging the samples, to induce strain in the samples hot air was blown over the samples to create the stress within the concrete in order to get it to expand and give better readings with the imaging.

The imaging of the samples was done at various different dates and a total of 195 images were collected from the samples. The images were then stored on CDs for future processing.

The images will allow us to quantify the number of cracks being developed on the surface and then lead us to make better descriptions about the underlying principles involved with the formation and effects of D.E.F.

The objective of this thesis is to make use of the available data along with the use of readily available image analysis software which use well established and cutting-edge image processing algorithms in order to quantify and measure the required values and support a working theory about the formation and effects of D.E.F.

The following are the main objectives of the Thesis:-

1) Organize the available data images according to their dates and sides

2) Filter the images using Fast Fourier transform images to reduce noise and increase visibility of cracks

3) Manually trace the cracks using ImagePro software

4) Use spatial calibration to get the unit per pixel ratio for all the images

4) Quantify the traced cracks using measurement features of ImagePro

5) Use the collected data to observe trends in the cracking

## Chapter 2 Delayed Ettringite formation (D.E.F.)

### 2.1 Factors causing D.E.F.

Over the last three decades the formation of D.E.F. has been identified as deleterious to concrete's durability and longevity. Since its initial discovery in the last century the formation of D.E.F. has been noted in various concrete structures (Divet 2013). The initial formation of Ettringite is referred to as the primary Ettringite formation, which is not the D.E.F. itself, but a normal reaction product created from the reaction of $C_3A$ and $C_4AF$ with gypsum during the plastic stage of the hydration process of cement. The secondary formation of Ettringite is after the concrete has hardened and had been exposed to higher temperatures (70$^{o}$C+). During hardening to get high early strength, this process is slow and the Ettringite formed after the setting of concrete is known as D.E.F. For the Ettringite formed after setting to be classified as D.E.F. there should not be an external source of sulphates to the concrete. The formation of D.E.F. therefore takes a lot of time which could take months or even years to form and the damage to be noticeable. The presence of D.E.F. has been identified in concrete mixes that used admixtures usually clinker containing high amounts of sulfur trioxide which in the presence of $C_3A$ forms the Ettringite over a period of time (Diamond, 1996). Making the presence of sulfur in the concrete a critical part of the delayed Ettringite formation.

Due to the requirement of high heat for the D.E.F. to form it has been seen in various structures which were exposed to high temperatures while setting, which could include cases such as massive cast-in-place concrete causing high heat of hydration or the concrete simply being cast in high temperature areas during the summer. Although these could be the reason for D.E.F. formation most of the time D.E.F. has been found in precast concrete structures, which underwent some kind of heat treatment and the addition of admixtures into the mix of concrete.

**2.2 Damage caused by D.E.F.**

The mechanism of damage done by D.E.F. is very unique. It forms over a period of time and causes microcracks on the surface of the concrete. These cracks are initially not visible by visual inspections and over a period of time these cracks allow for moisture to seep deep into the concrete which causes more Ettringite to form causing the cracks to get wider over time and let more moisture into the cracks, forming a positive feedback loop, and accelerating the degradation of concrete over time.

Although it is believed that D.E.F. is found in precast structures like Precast/Prestress concrete walls, railway ties (Mielenz, 1995, Vitousova,1991), but a study done at University of Maryland(U.M.D.) and the Maryland State Highway Administration (M.D.S.H.A.) found that D.E.F. formed throughout the bridges in Maryland and they always presented in the form of map cracking on the surface of the bridges. These bridges were cast-in-place thus showing that D.E.F. is present in the cast in place

concrete as well. (Ceary 2007)  Thus making the formation of D.E.F. a more widespread problem.

### 2.3 Detecting D.E.F.

D.E.F. has been detected using various methods throughout the years, with the most common being the use of a Scanning Electron Microscope (S.E.M.) which gives the best result. There are other methods which include, differential scanning calorimetry, Quantitative X-Ray Diffraction and X-Ray Tomography. Since the S.E.M. requires core samples from the concrete under question to be able to be scanned in a lab it is not the most desirable, therefore there is a gap in the lack of techniques available for the detecting D.E.F. using Non-Destructive testing.

## Chapter 3 Laser Shearography

### 3.1 Introduction

Laser shearography is a form of laser-based imaging interferometry to detect, analyse and measure defects on the surface and the subsurface of materials by detecting almost microscopic deformities of the surface being tested when the required amount of stress is applied to form the said deformities. Shearography is a no contact, no contamination and non-destructive testing method which offers near real time information. Laser light itself is a non-penetrating radiation, shearography is capable of inspecting aerospace structures for damage ranging from impact damage, desponds, delamination's, near surface porosity, wrinkled fibres, and foreign objects in the material. As laser shearography has been used throughout various industries and a great track record in detecting damages, there is a need to use new technologies in the Civil Engineering field on cement samples. Concrete is pretty much watertight after its setting and hardening but the introduction of cracks allows water or aggressive chemical ions into the concrete which brings about faster deterioration of the concrete.

### 3.2 Principles of Laser Shearography

The setup of Laser Shearography has a laser sight source, a shearing image interferometer, a computer, and a setup to provide the appropriates stress to the material surface in a controlled environment. Shearography offers two significant

advantages, first the shearography image shows the first derivative of the out of plane deformation of the test part of the surface, which makes it insensitive to the test part bending or deforming due to the applied stress, but it makes it highly sensitive to the local deformities on the surface being scanned. In the case of concrete rigid materials contrast highly with the opening of cracks and the closing due to surface temperatures. Second the shearography cameras are sensitive to the changes in the distances in the x and y directions making any formation of cracks highly visible on the surface of the concrete. The field of View (F.O.W.) for a shearography camera hinges upon the decided maximum defect size, camera resolution, laser illumination power, the ability to apply uniform stress and background noise. The trade-off for crack detection is between field of view and the minimum detectable crack size.

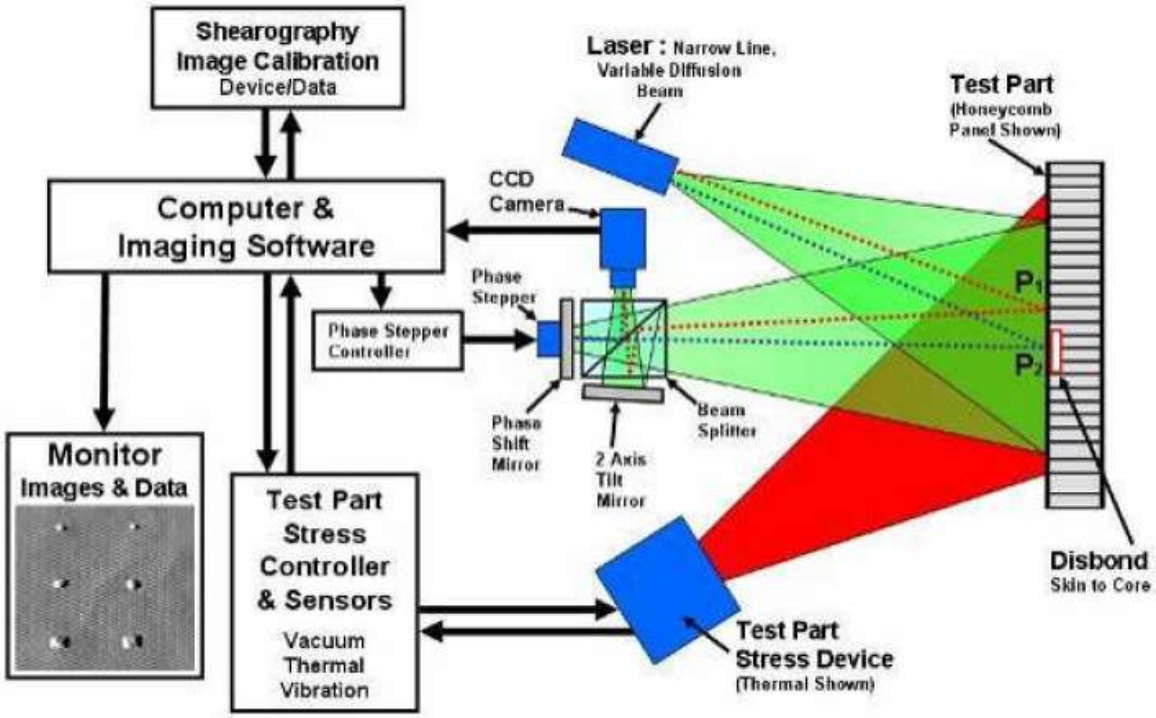


**Figure 1 Laser Shearography setup (Adapted from Newman J, Made, A. M. 2011)**

## Chapter 4 Sample preparation and earlier work

### 4.1 Sample Preparation and mix design components

The samples were casted long before the writing of this thesis, around 13 years ago in a joint study conducted by AMA and associates and Laser Technology Incorporated, which aimed at developing a portable Laser Shearography system. The data obtained in that report is being used for this research. The samples were casted by graduate students of the Civil Engineering department at University of Maryland of that time.

The samples were made in accordance with the American Society for Testing and Materials, the Concrete prisms were in accordance with ASTM C157/157M, and the Concrete cylinders were in accordance with ASTM C190. The prisms were used for the laser shearography imaging along with expansion measurement and the Concrete cylinders were used for compressive strength testing.

In earlier studies done at UMD (Ceesay 2007) it was found that addition of Potassium above the normal levels of concrete will promote the formation of ettringite. The different samples prepared were developed after using the experience gained overtime with working on different types of DEF samples.

To mimic the steam curing and the Modified Duggan heat cycle the following procedure was used on the first batch of samples: -

For steam curing the samples were put in oven while still in the steel moulds with the temperature being around 85$^{o}$ C in a water bath, the exposed parts were covered with foil to prevent over drying and shrinkage. The Samples were in the oven for 4 hours with constant temperature.

For the Modified Duggan Heat Cycle the procedure is as follows: -

1St Day: The samples are heated in an oven at 82$^{o}$C.

2nd Day: 1.5-hour cooling and then stored in water at room temperature.

3rd Day: The samples are heated in an oven at 82$^{o}$C.

4th Day: 1.5-hour cooling and then stored in water at room temperature.

5th, 6th & 7th Day: Heated continuously in an oven at 82$^{o}$C.

At the end of the cycle the specimens are allowed to cool for two days, and then stored in lime water.

Only the First batch of samples casted underwent heat cycles which Included Tx1-6 and Tx2-6.

The mix design of the Concrete was as follows: -

The first batch was casted on 1/25/2008 it was split into two groups Tx1-6 and Tx2-6 this batch went under the Modified Duggan Heat cycle.

**Table 1 Mix design of Concrete used (Adapted from Newman J, Made, A. M. 2011)**

| Mix | Tx1 | Tx2 |
|---|---|---|
| Cement | Type III | Type III |
| Coarse Aggregate | Limestone #57 | Limestone #57 |
| Fine Aggregate | Texas Sand - Alkali Reactivity - 0.05 | Texas Sand - Alkali Reactivity - 0.05 |
| $K_2CO_3$ | - | Total 1.2% |
| No. of Prisms | 9 | 9 |
| No. of Cylinders | 12 | 12 |

| Mix | Tx3 | Tx4 |
|---|---|---|
| Cement | Type III | Type III |
| Coarse Aggregate | Limestone #57 | Limestone #57 |
| Fine Aggregate | Texas Sand - Alkali Reactivity - 0.05 | Texas Sand - Alkali Reactivity - 0.05 |
| $K_2CO_3$ | - | Total 1.2% |
| No. of Prisms | 9 | 9 |
| No. of Cylinders | 12 | 12 |

The second batch was casted on 5/2/2008 it was split into two groups Tx3-6 and Tx4-6 this batch did not undergo the Modified Duggan Heat cycle.

### 4.2 Compression testing Results from earlier work

Compression testing was done on the Cylinder samples of Tx1, Tx2, Tx3 and Tx4. The results of the testing were as expected of the mix designs, Tx3 and Tx4 which were about 98 days younger than the first batch, another round of test was conducted about 231 days after the first round of testing and it was found that the Tx3 sample gained 19% more strength with Tx4 gaining 25% more strength than their previous tests, with the added potassium being in the Tx4 sample it showed lowered strength as expected when compared to Tx3. Tx1 and Tx2 were much older at the time of testing and have undergone the Modified Duggan heat cycle, therefore they showed lower strength as expected, between Tx1 and Tx2 potassium was added to the Tx2 sample, which showed much less strength when compared with Tx1 with an average drop in compressive strength of about 27%. (Newman et al 2011)

Therefore, the addition of Potassium Carbonate and the use of modified heat cycles is showing reduced compressive strength. It was expected for this to happen due to the formation of D.E.F. which was confirmed in an earlier study done at U.M.D. (Ceesay 2007).

To check whether there is D.E.F. in fact present in the Concrete samples Laser shearography was done of the Concrete prisms at Different dates throughout a period of 2 Years.

### 4.3 Expansion data

Expansion tests were also conducted on the samples used for the shearography data; results provided below.

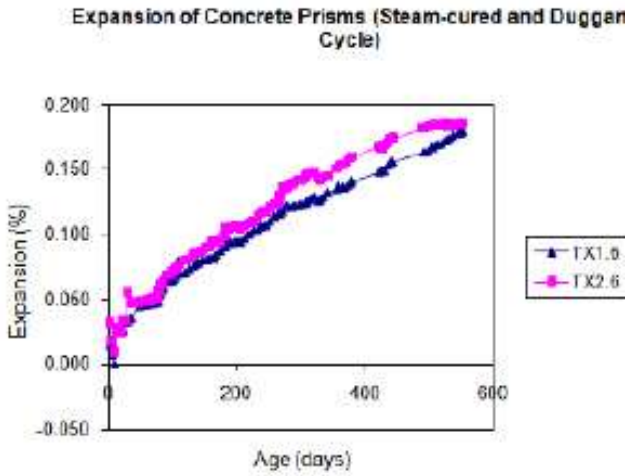


**Figure 2 Expansion results of Tx1 and Tx2 sample data (Adapted from Newman J, Made, A. M. 2011)**

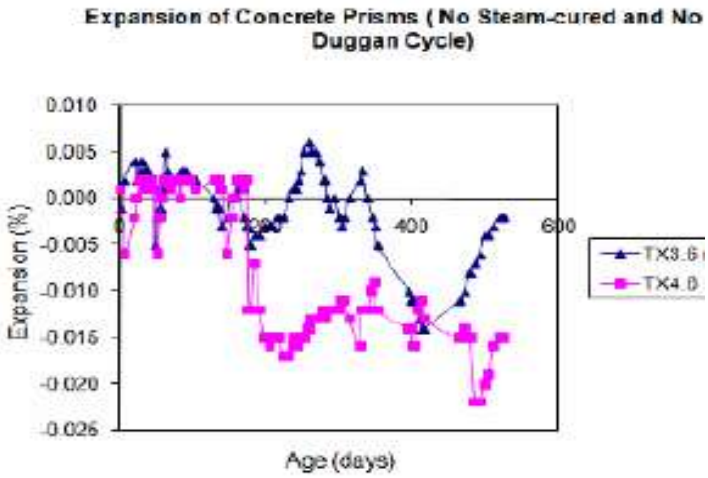


**Figure 3 Expansion Results of Tx3 and Tx4 (Adapted from Newman J, Made, A. M. 2011)**

The presence of the Potassium Carbonate and the application of the Modified Duggan Heat Cycle was causing some expansion in the specimens.

### 4.4 Laser Shearography imaging

Laser shearography is a type of interferometry non-destructive testing which utilizes laser-based image interferometry to detect small defects on the surface or the subsurface. It has been used extensively in the aerospace industry. Using Laser Shearography the damage done on the concrete surface due to D.E.F. the length and the number of Microcracks forming on the surface can be detected and Quantified through subsequent data processing, the scanning of the samples was done at Laser Technology Incorporated, in Pennsylvania. The four samples were scanned at 45, 97, 128, 367, 548 days after casting. Some sides were missing in the final dataset at dates, so they have been left out from the final data.

## Chapter 5 Image Analysis and Data collection

### 5.1 About the software use for this study

Image –Pro® Version 10 was used for the purpose of Image Processing in this study, it was decided to use and industry software other than an in house developed algorithm in the interest of time. Image Pro is very powerful, versatile, and easy to use software which utilizes the concepts for image processing in an easy format to be used in the industry. It works for almost any kind of image format which can be from a variety of sensors including the laser shearography setup used in this study. With the track records of it being used in an earlier study done at U.M.D. and its extensive use in various industries such as Life Sciences, Manufacturing, Pathology and Material Sciences cemented our decision in using Image Pro for this study. It is very advance and easy to use thus making it a valuable tool for this study.

Image Pro has a lot of features and of this study our interest was in the following capabilities: -

1) Basic Image Processing
2) Image Processing and Manipulation
3) One clicks advanced filtering of the Images
4) Ability to develop macros
5) Trace the required cracks using object trackers
6) Data collection tools

### 5.2 Methodology followed in this study

To use Image Pro effectively a methodology was developed on the form of the following steps: -

1) Upload the required Image into the software
2) Apply the required filters to the image
3) Crop the image to the required size
4) Use Polyline trace to manually trace the cracks
5) Use Calibration Button to apply Calibration to the Image
6) Use Measurement Button to get the required Measurements
7) Create mask of the Image to get just the traced Image
8) Export the collected data for further processing

Brief Overview of the Methodology involved through images: -

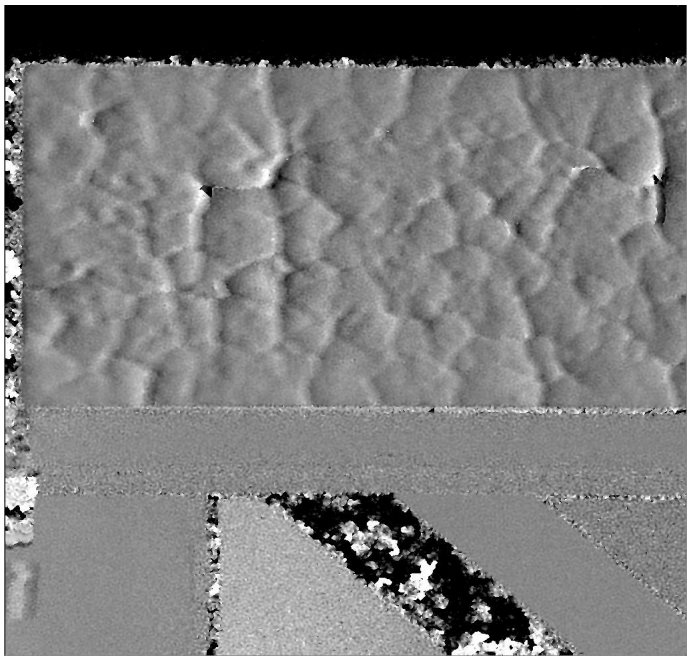

**Figure 4 Original Uncropped Image (Adapted from Newman J, Made, A. M. 2011)**

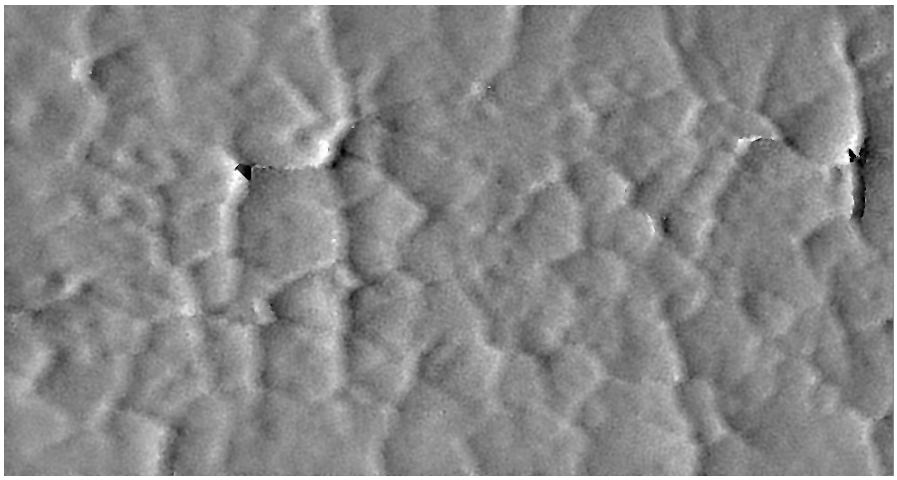

**Figure 5 After Cropping the Region of interest**

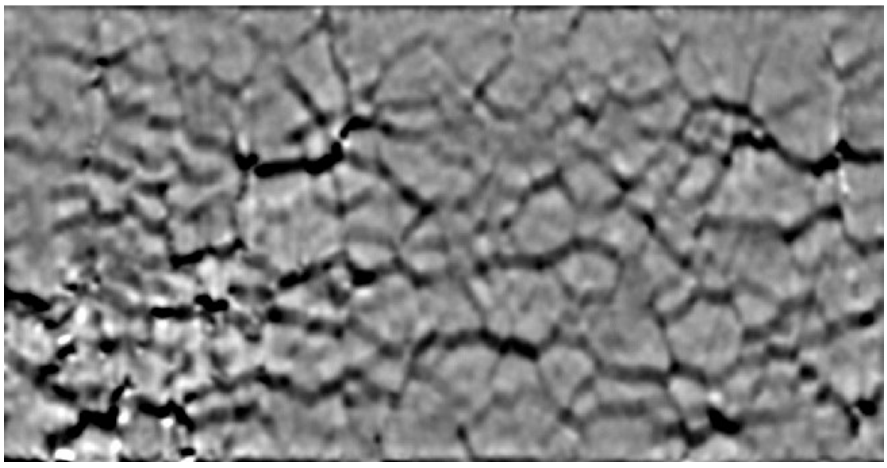

**Figure 6 Image after Running the filter macro**

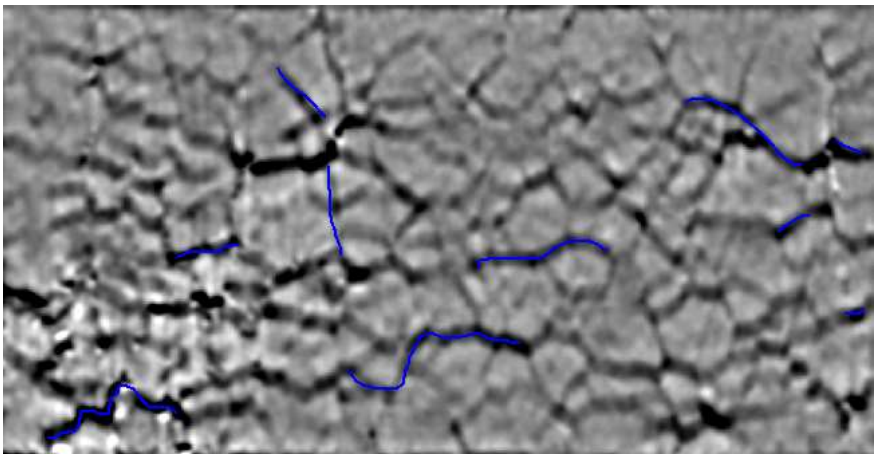

**Figure 7 After Using Polyline tool and tracing manually on the image**

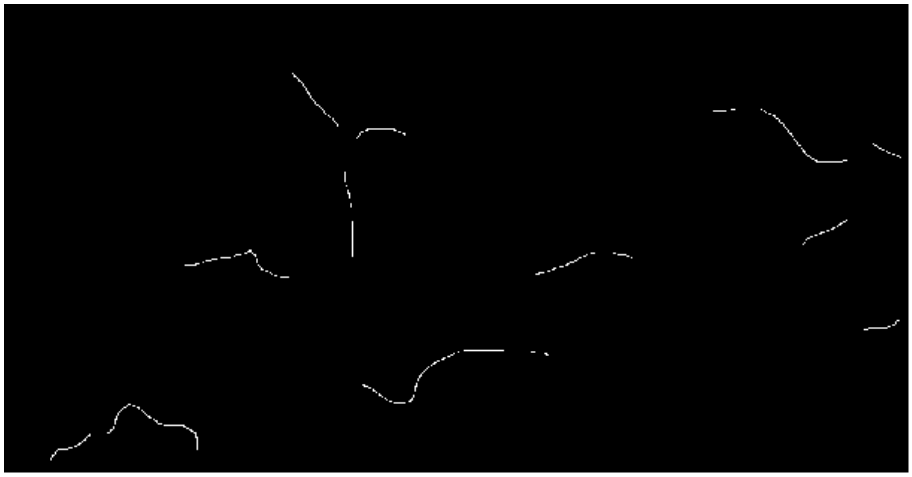

**Figure 8 Taking a mask of the traced objects**

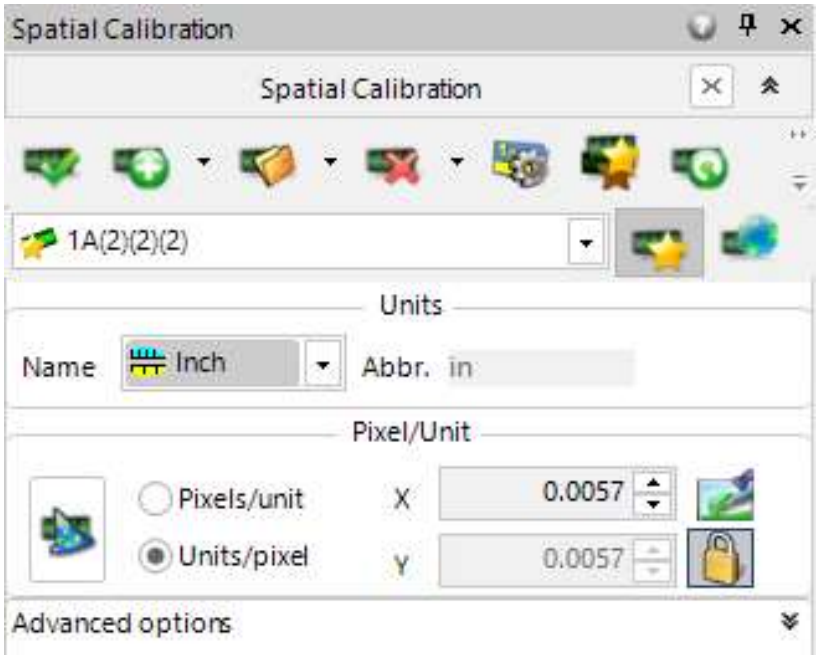


**Figure 9 Setting Spatial calibration for Measurement**

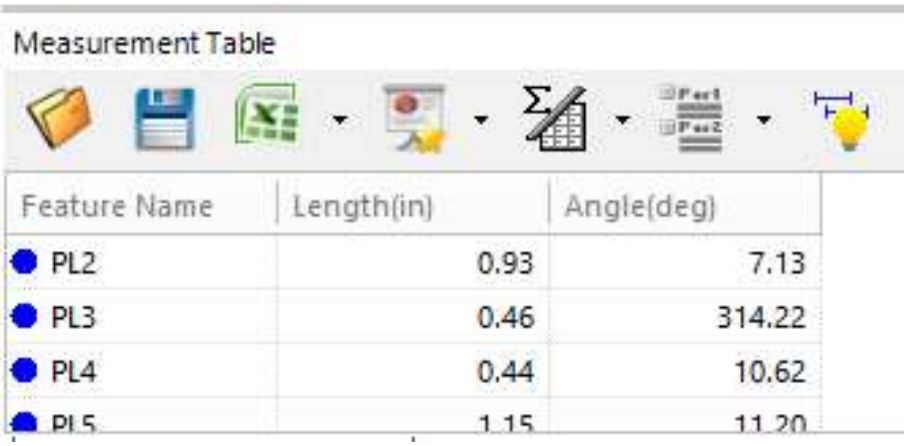


**Figure 10 Collect and export the required data**

These steps have been explained more in the following parts of this chapter.

### 5.3 Calibration of the Image

An image is just a collection of pixels being displayed on the screen, there are a lot of types of images from R.G.B. to Greyscale. The images taken by the Laser shearography system in their original format are 8-bit Greyscale images which are very basic in terms of images. After the tracing of cracks on the filtered surface there was a need to have a calibration system as the recorded measurements will be in terms of number of pixels being traced therefore a need of having a conversion ration arises to get accurate measurements from the images. ImagePro has a Calibration tool that allows us to make the pixel to unit conversion factor.

To create that factor the sides of the Sample Image were used which is the following image: -

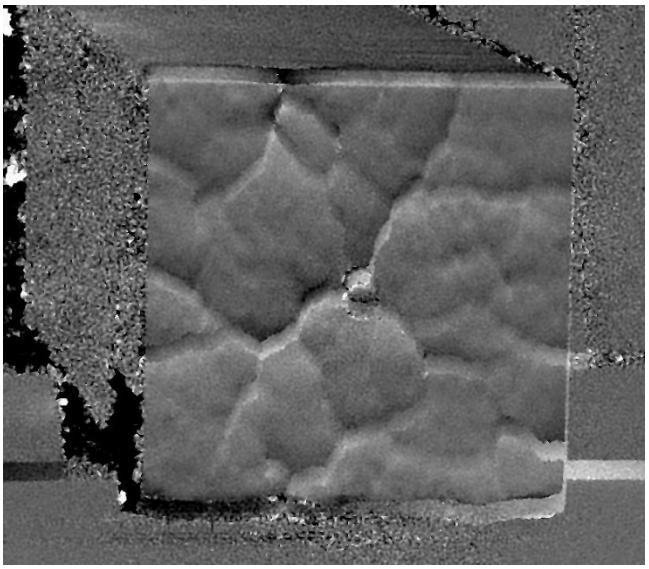

**Figure 11 Smaller side of the Concrete Prism Sample (Adapted from Newman J, Made, A. M. 2011)**

In this study the samples are standardized 3” x 3” x 11.25” concrete prisms as per ASTM C157/157M, therefore we know that the side displayed in the above image is 3” we use this information to set the calibration of the image.

Image Pro allows us to create a calibration which can be applied to any image that we need to, it works by allowing the user to create a line over the object as seen in the image below and then we can put in the known size of the feature and the required units, it will take the pixels under the drawn object and create a unit per pixel ratio which will be saved as a module which you can apply to any image.

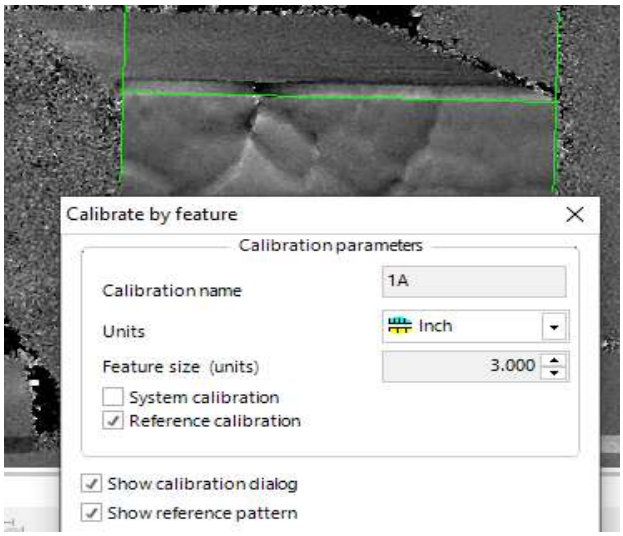


**Figure 12 Creating Calibration**

### 5.4 Image Filtering used in this study

The original Image has a lot of noise in it which made it harder to trace the cracks on the image using the Polyline tool, therefore a need for filtering the image arises to reduce the amount of noise, there are many filters that can be used, for example the Gaussian blur filter, which uses a Gaussian distribution function and removes noise and details from the image being processed, the following images have been processed using the Gaussian filter. This was used earlier in a study done at UMD (Hung 2007).

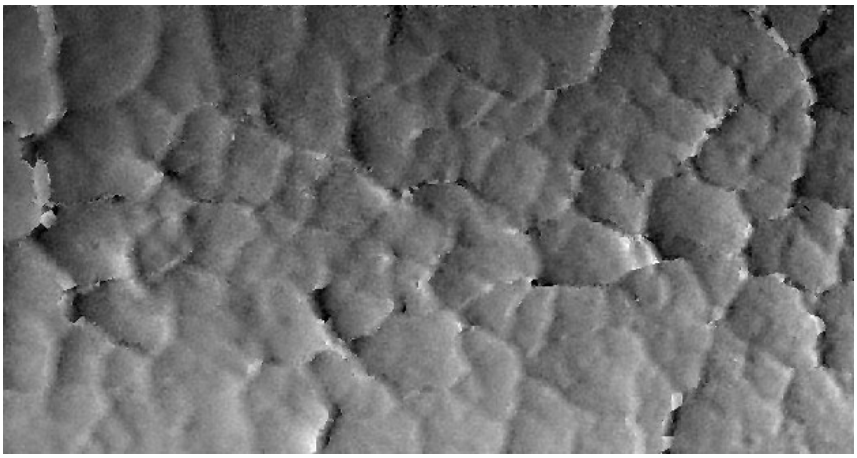

**Figure 13 Tx2 Sample Image (Adapted from Newman J, Made, A. M. 2011)**

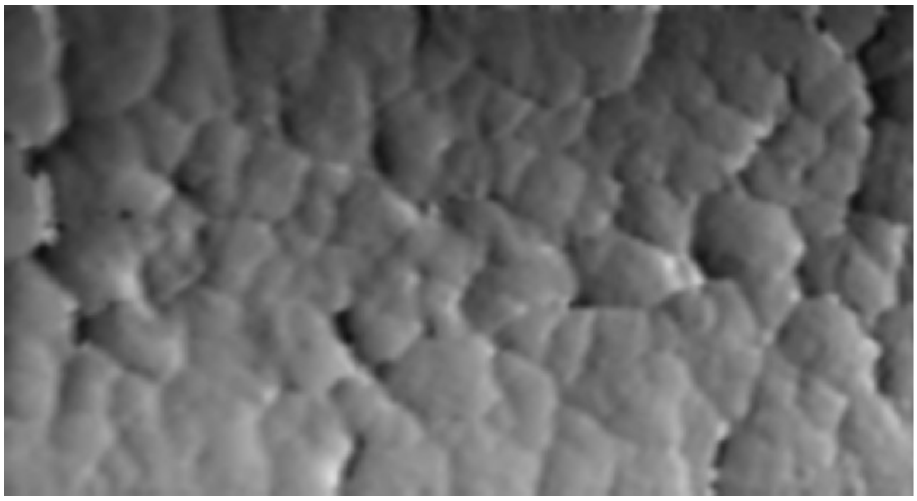

**Figure 14 Tx2 Sample after using Gaussian filter**

Since the Gaussian filter is removing features using it will not be the best option in doing so, therefore a more advanced solution would be required to process the images.

Advanced filtering techniques will be used to filter the images as they have a lot of features and noise in the image, Image pro provides a host of filters that can be used for reducing noise and enhancing the features we want to enhance, therefore I used filters that deal with the images in the Frequency spectrum, i.e., the images will be converted down to their frequency signal and then the appropriate changes made to it. Selecting the filters used was a bit hit and try with the help of people from Media Cybernetics the makers of Image pro.

Filters used in this study include the following: -

1) Low Pass filter
2) DIC Restore filter
3) Band pass large

These filters were combined and used on the images; each filter works in the following described manner: -

### 5.4.1 Fast Fourier transform

The fast Fourier transform is a function that is a basis for the filters used in this study, the F.F.T. calculates the discrete Fourier transform of a sequence, the sequence in this study being the pixel values from the images taken using the laser shearography method. The F.F.T. was created as an alternative to directly calculating the D.F.T. the F.F.T. utilizes matrix factorization to be faster.

The F.F.T. computes the D.F.T. and then plots them in the frequency domain the output image looks like this: -

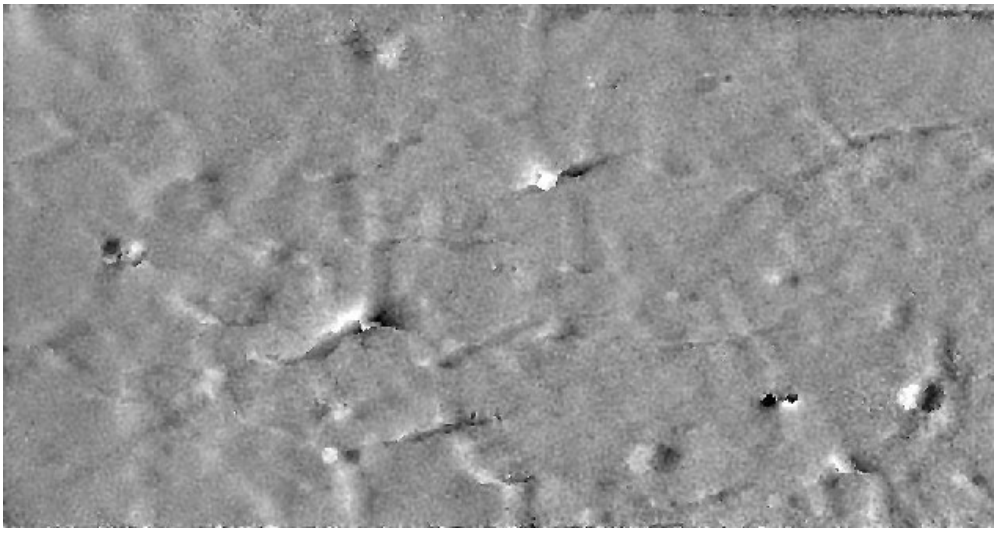

**Figure 15 Tx2 Sample Image**

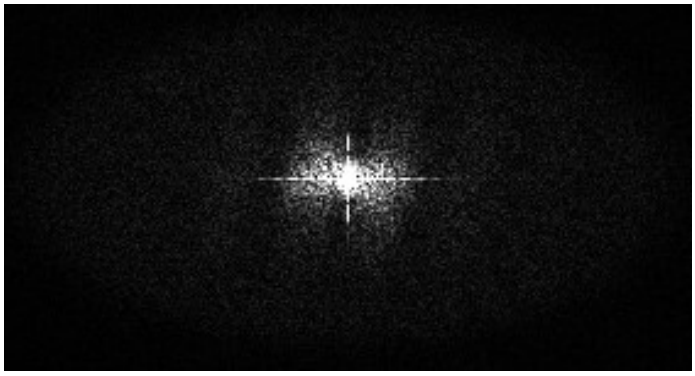

**Figure 16 Tx2 sample image after Fast Fourier transformation**

The white part of the above image shows the highest frequency, and the darker parts represent the lower frequencies, there are no recognizable shape in the image due to it being in the frequency spectrum.

The filter is then applied on the image in the frequency spectrum then the image is converted back into the image format with the filter applied, it will give us better image for further processing.

### 5.4.2 Low Pass Filter

The Low pass filter is applied when the image is in its frequency spectrum in the background of the application, the low pass filter only allows the low frequencies to pass through, the lower frequency in the image is the pixel values that are changing slowly. With the low pass filter the higher frequencies have been blocked, the output image will have lower number of noisy pixels giving us an image with lower amount of noise.

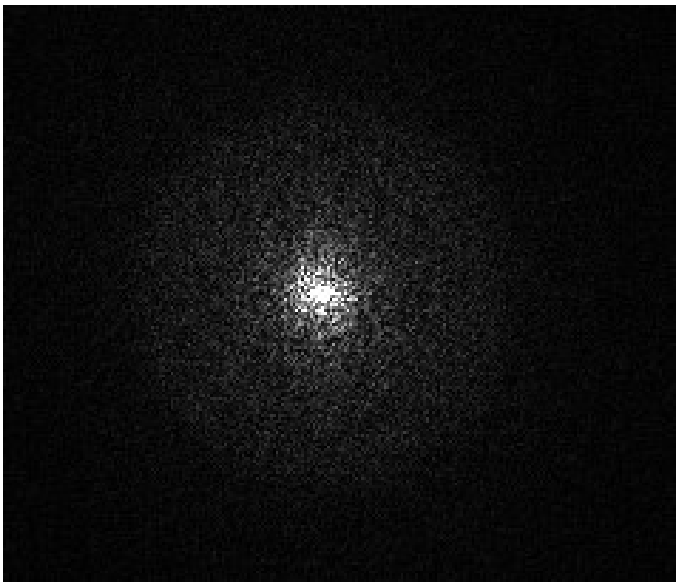

**Figure 17 Image before low pass filter in frequency spectrum**

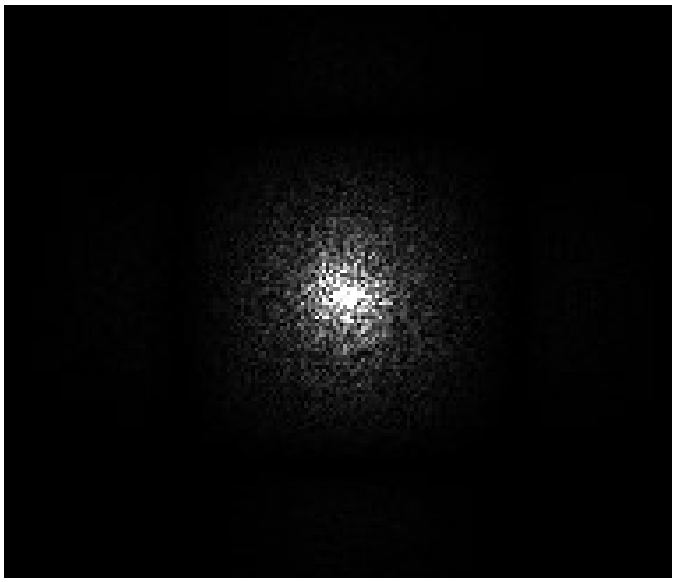

**Figure 18 Image before low pass filter in frequency spectrum**

The filter settings for the Low pass filter were as follows: -

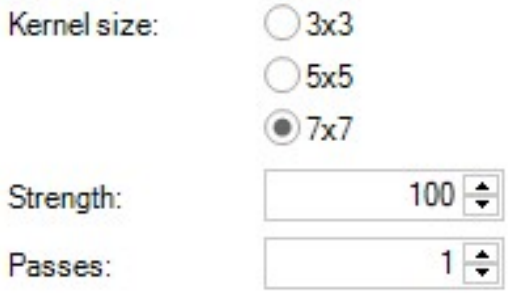


**Figure 19 Filter Setting for Low pass filter**

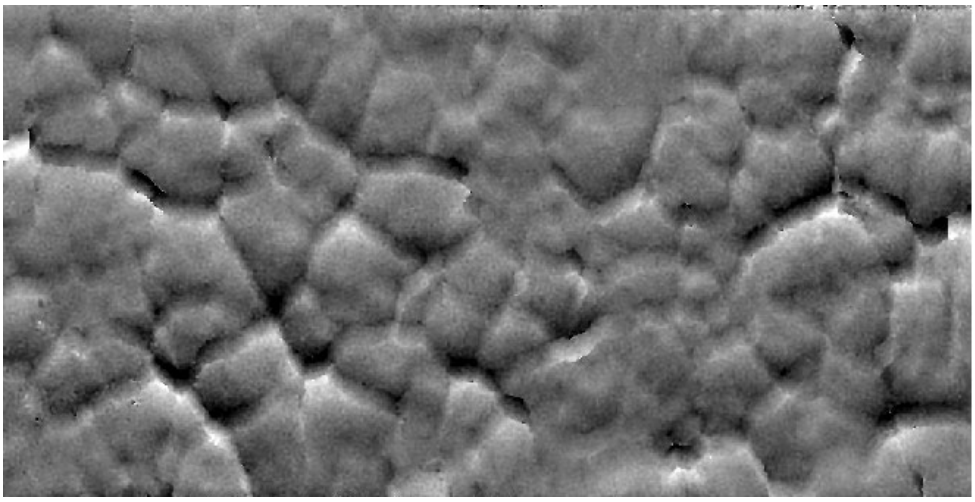

**Figure 20 Tx2 Sample Image before Low pass filter**

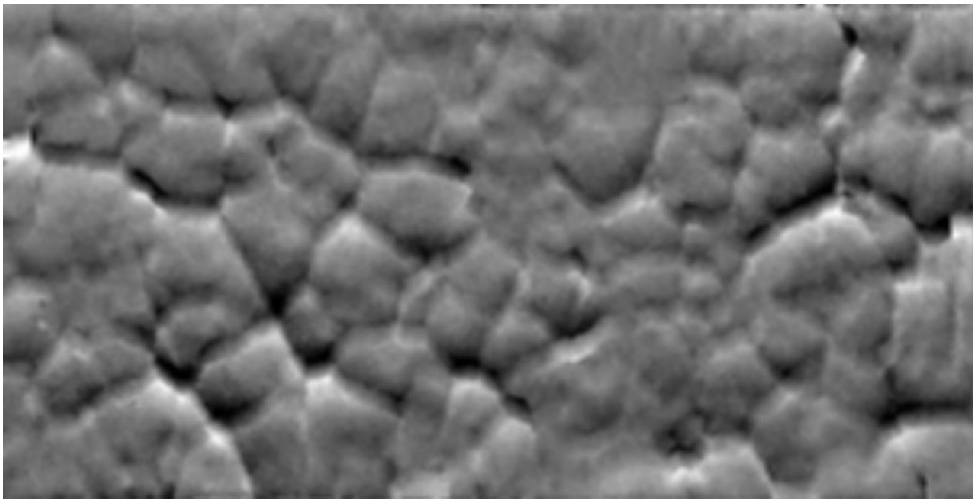

**Figure 21 Tx2 sample image after applying Low Pass Filter**

The output images have a lot lower amount of noise in them, and they have gotten a bit blurry after applying the Low Pass filter due to removal of the high frequency range pixels from the image, but this lets us have a clear view of the cracks on the

image. As there are still certain features on the image that require removal and sharpening on the image more filters need to be applied.

### 5.4.3 Differential Interference contrast (D.I.C.) restore filter

The Differential Interference contrast (D.I.C.) restore filter is used in cases when there are objects that are very small, and the cracks that we are trying to detect are smaller than 10 Micrometres, the cracks need to be separate from the background so that they can be traced manually later, as distinction needs to be apparent for the cracks to be visible.

The D.I.C. method was originally created for use in the biological microscopy industry (Zhaozheng 2014) the reversing of the D.I.C. is done to obtain better images. D.I.C. restore is used in this study due to its ability to restore images for having greater separation between the surrounding and the objects in question it will be applied to the shearography images.

Since there are 2 sets of images for each direction in X and Y the angle setting for the D.I.C. restore feature which allows us to select the features that need to be enhanced in an image as most features will have a common direction, the angle of feature is measured from the horizontal direction clockwise in degrees perpendicular to the feature edges, therefore for the X direction images $90^{o}$ angle was used and for the Y direction images $-90^{o}$ angle was used, these angles were selected after going through multiple images and angles and selecting the direction which highlighted the

maximum amount of features. This filter is applied in conjunction with the Low Pass filter.

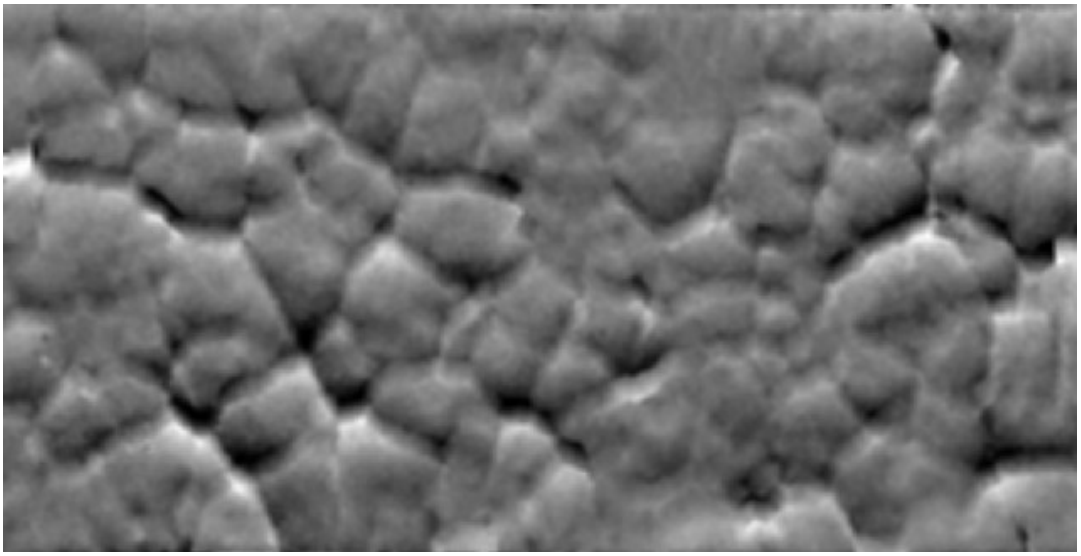

**Figure 22 Tx 2 Sample image after Low Pass filter**

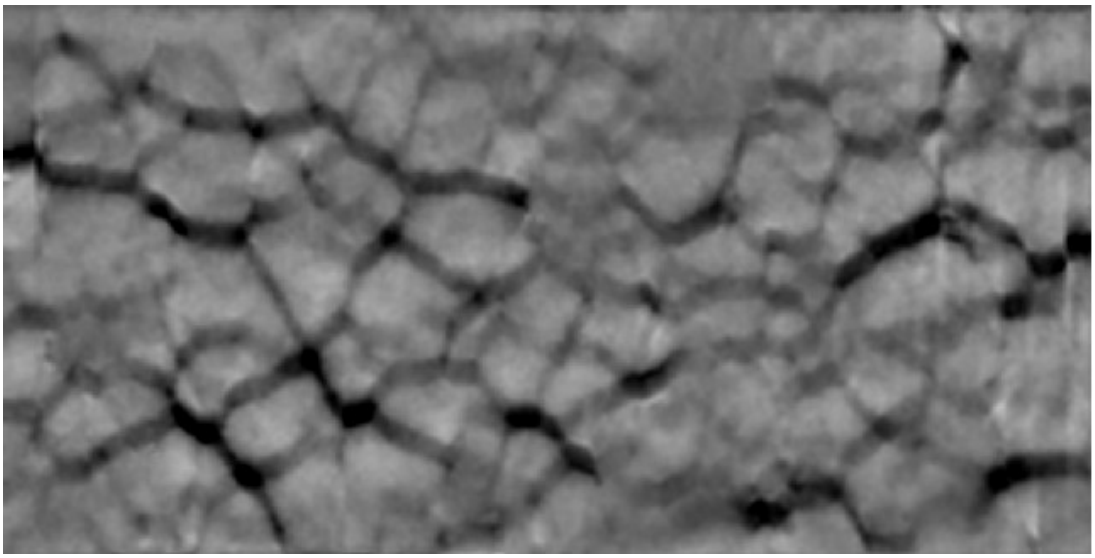

**Figure 23 Tx2 Sample Image after D.I.C. restore**

As it is apparent many cracks on the image have been highlighted as the black parts in the image. To make the visible cracks more highlighted in the surface there is a need for applying a further filter.

### 5.4.4 Band Pass Filter

The Band Pass Filter works on the principles described for the Low pass filter, it is a combination of the high pass and the low pass filter combined, i.e., it will remove pixels of higher frequency and low frequency. This filter can simultaneously reduce noise in an image and remove noise from an image which allows us to get better images.

The threshold will be set by us as setting for the filter, the software allows us to select the size of the low and high frequency to be removed, it also allows us to put it the strength required for the contrast and for the number of passe taken by the filter over and image also can be adjusted. These values were decided after going over multiple images and trying out various values for each parameter.

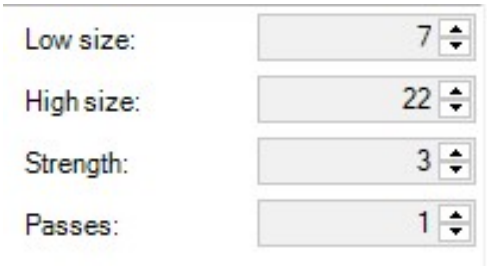


**Figure 24 Settings for the Band pass filter**

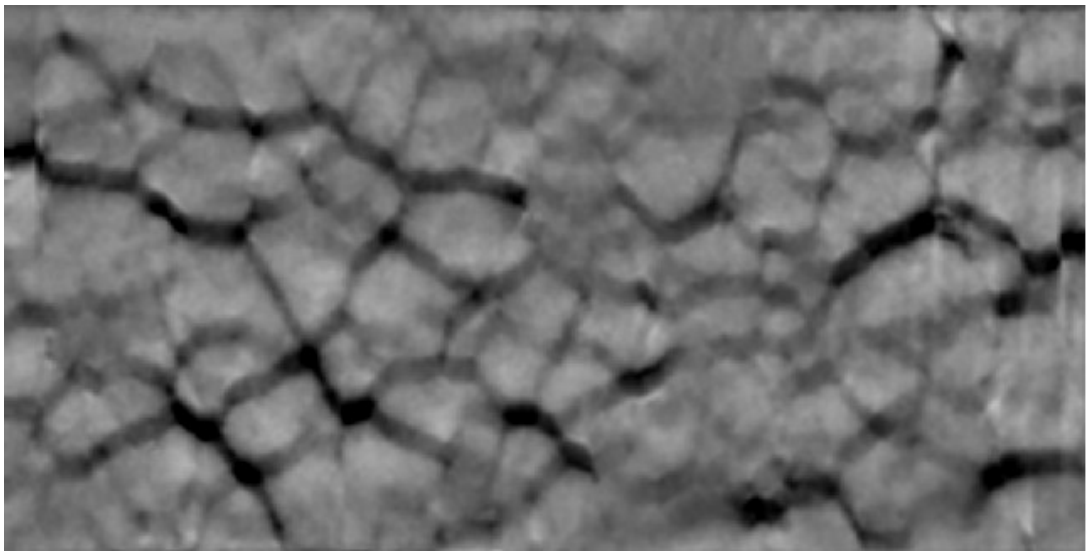

**Figure 25 Tx2 Sample image after applying D.I.C. filter**

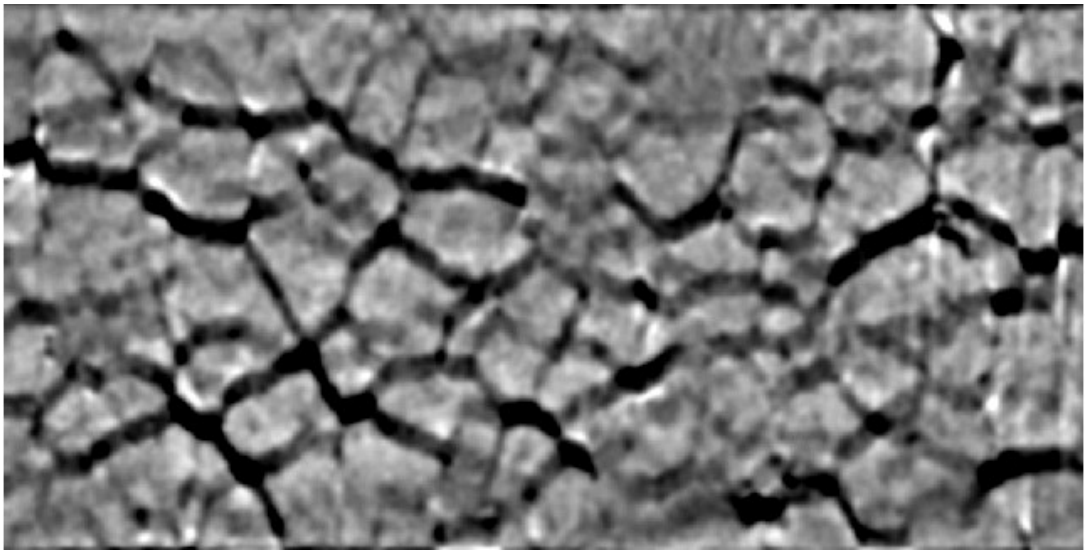

**Figure 26 Tx2 Sample Image after applying band Pass filter**

As it is evident the depth of the cracks has deeply improved, and we can see clear boundaries between what part of the image is a crack and what part of the image is

not a crack. The above obtained image is the final image that will be used for the manual tracing of the cracks.

### 5.5 Macro Creation

For the application of the filtering macros were create in the Image pro platform, 2 sets of macros were created for the 2 direction of the laser shearography images with the only difference between them being the angle of the D.I.C. restore filter used the other filters had the same settings. This would allow us to save time in applying filters on the 196 images that we have.


**Figure 27 Macro for y direction Images**

### 5.6 Crack Tracing

To trace the cracks automatically macros were developed using the features described above to create a macro that could automatically detect the cracks in the image. It utilized the histogram of the image and used it to detect the pixels within a certain range. And the pixels detected are in the form of lines making them one pixel wide. Using the auto tracing was not feasible as the software was picking up a lot of

artefacts on the image. Since the image was a derivative of the topography of the test surface, which made the image much more non-linear in nature than anticipated. Adjusting the threshold of the detection did not yield good results either as there were still too many objects being detected on the image.

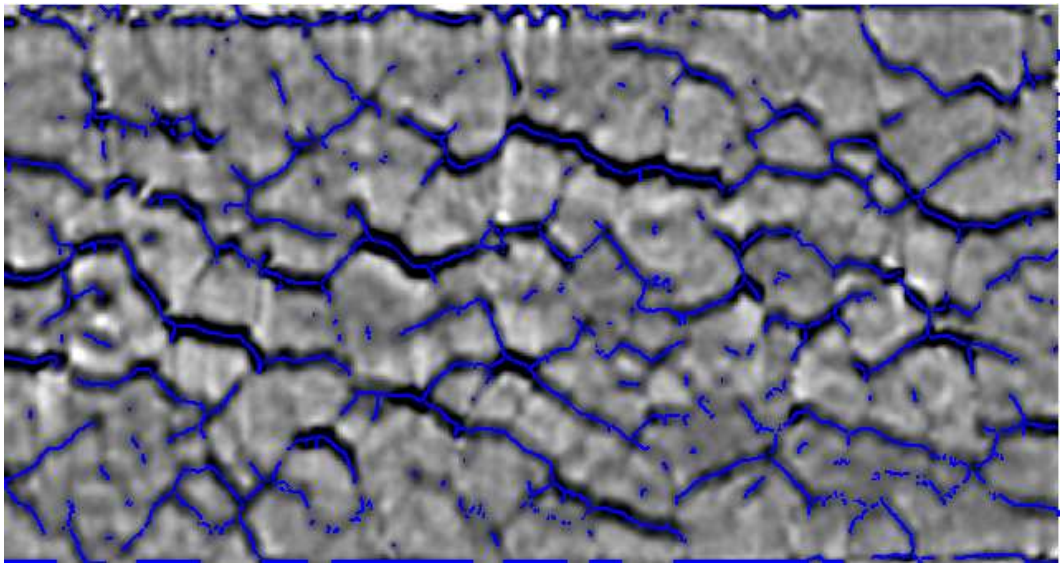

**Figure 28 Image after filtering and auto tracing**

As shown in Figure 26 the cracks in the image have been traced but there are lots of other parts of the image that have been picked up. The traced cracks also were not continuous which made the line length measurement inaccurate. The software also picked up 573 different objects on the image which was way above the number of cracks present on the concrete surface. Because of these problems the auto trace option was dropped for now.

Therefore, the tracing of the cracks was carried out manually using Image pro's polyline tool, each image had to be manually traced, there was an attempt in making this process automated also for the entire dataset but the non-linearities and the differences between each image made it very hard for any one algorithm to accurately pickup on the cracks. Therefore, we decided in the interest of time it would be best to use the polyline tool for tracing manually.

The polyline tool takes the cracks as lines which would allow us to get the lengths of the cracks from the images. Only the darkest parts of the cracks after filtering were used as cracks and an upper limit of 10 cracks to be taken per image was set in the interest of time and having a consistent data set.

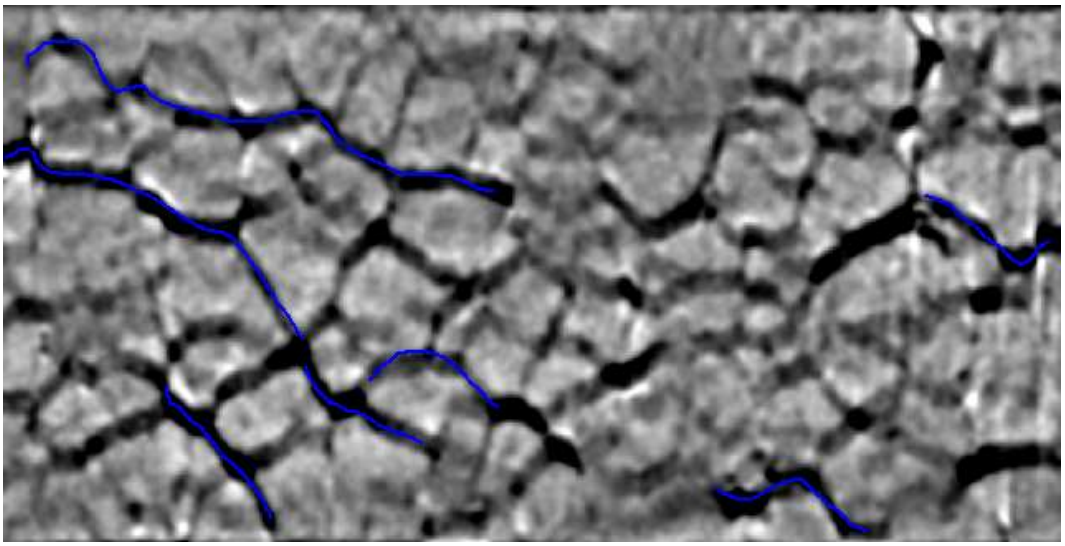

**Figure 29 Tx2 Y direction Sample with filter and traced cracks**

As you can see there are many cracks that have been left out that is because there are 2 sets of images and some cracks are visible in both direction of shearing in the images, the two images were opened side by side and then traced accordingly to avoid having overlapping of the cracks and keep repetition of cracks at zero, the following is the image of the same side but in the X direction with the filter applied and the cracks traced:

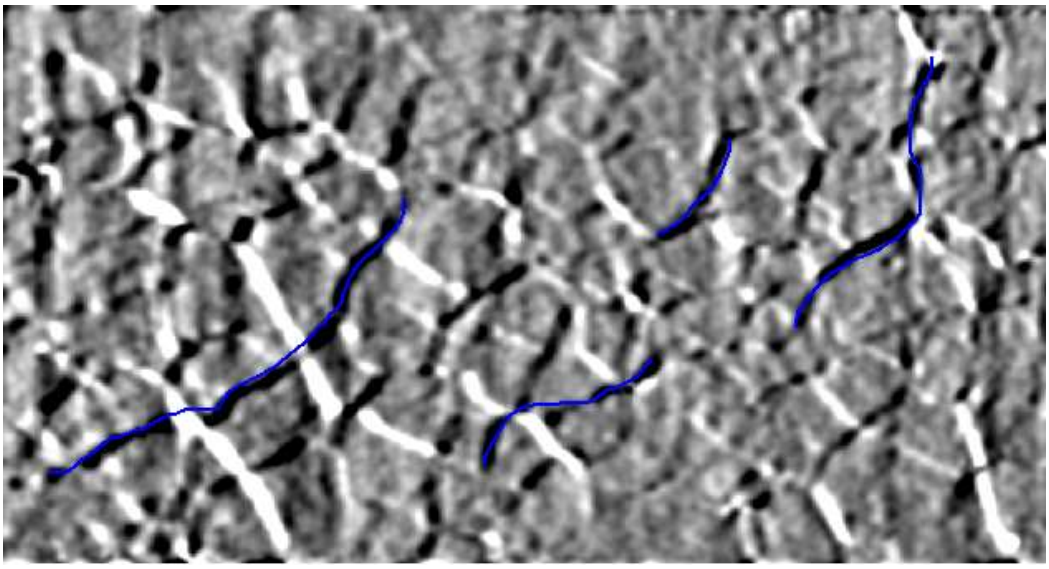

**Figure 30 Tx2 X direction sample with the tracing done**

There were many parts of the images that might look like cracks but are most probably undulations and irregularities on the images for which reason they were left out form the tracing process of the cracks.

After the tracings were done on both the images the calibration was applied and the measurements taken, then a mask of the images were created which is the tracing

taken on a black background to have output images that show us tracings done on a separate background.

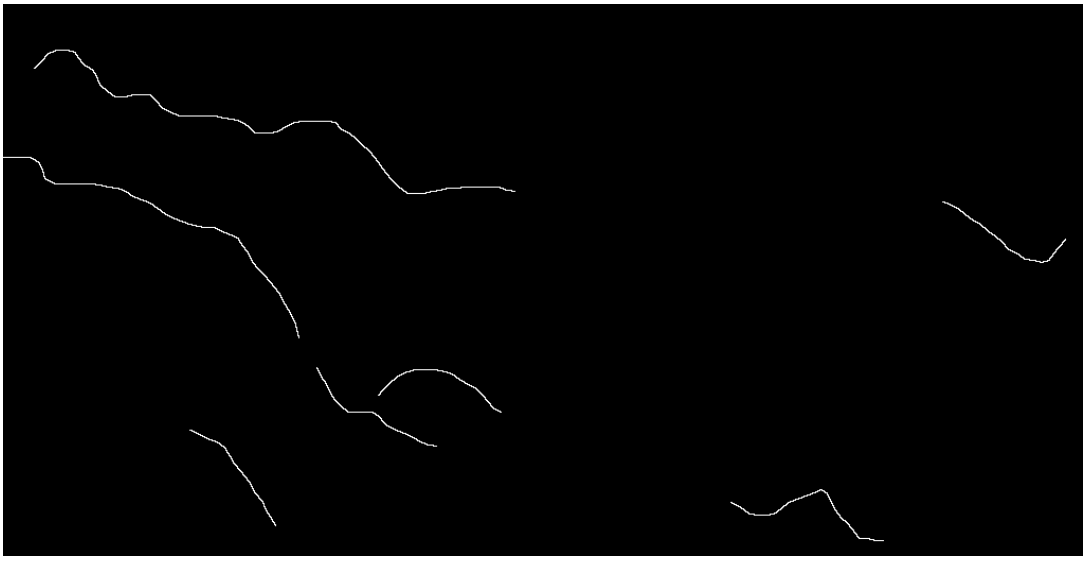

**Figure 31 Tx2 traced Crack Mask Image Y direction**

**Figure 32 Tx2 traced Crack Mask Image X direction**

Now using an image calculator feature of ImageJ (Open-source software) both the images can be combined to form one single output image, the image was also inverted to have the cracks on a white background.

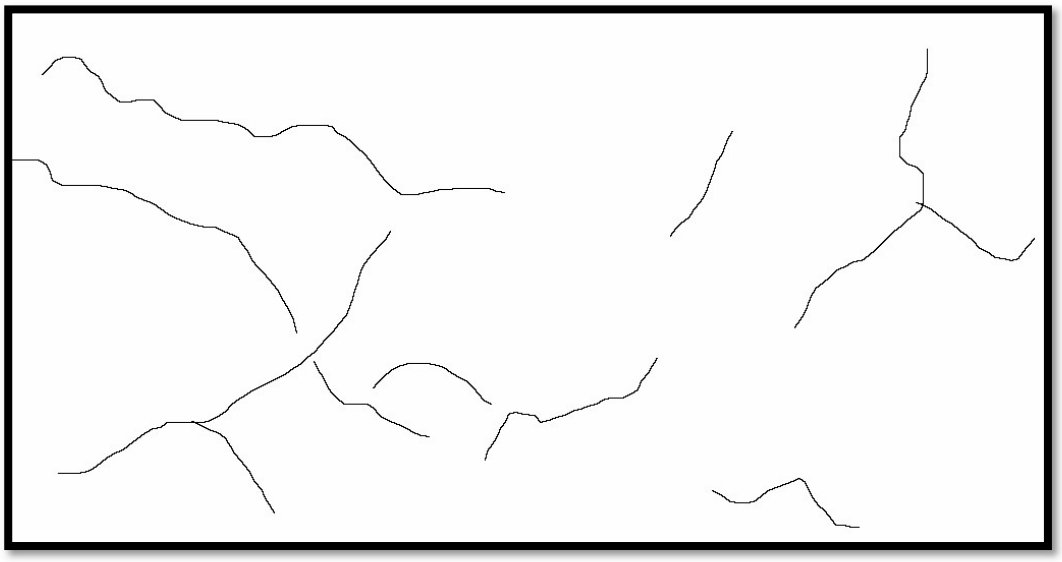

**Figure 33 Tx2 X+Y direction Combined Image with cracks traced and inverted colours**

The cracks now have been all traced and placed on a separate background making them easier to see.

### 5.7 Measurements from tracing

Using the available measurement tool from the data collector the number of cracks, length and angle form the horizontal from each of the traced cracks is taken as a measurement the units are kept in inches using the calibration that was described earlier, the measurements are recorded in the data table.

**Table 2 Measurement Table Tx2 side 1a_x-3-13-08_0001***

| Feature Name | Length(in) | Angle(deg) |
|---|---|---|
| PL1 | 2.44419573 | 36.0944468 |
| PL2 | 1.988294753 | 244.523575 |
| PL3 | 1.274353201 | 210.560843 |
| PL4 | 0.691547818 | 239.300276 |

| Feature Name | Length(in) | Angle(deg) |
|---|---|---|
| PL1 | 2.028388749 | 328.570437 |
| PL2 | 0.823537711 | 326.673723 |
| PL3 | 0.707317208 | 311.877859 |
| PL4 | 2.971050557 | 345.642131 |
| PL5 | 0.819665392 | 342.950962 |
| PL6 | 1.00816894 | 346.108815 |
| PL7 | 0.786428524 | 352.40537 |

## Chapter 6 Results and discussions

As discussed in Chapter 5, preliminary attempts to use a fully automated approach to processing the images failed because it generated too many artefacts. Hence it was necessary to use a manual approach to identify the cracks to find the crack trace. This significantly slowed down the overall processing. To keep within the available time and use every image that was available on all 4 dates, it was possible to analyse only 4 images per prism for each date. Two images each on opposite sides of the prism were selected. With 4 prisms imaged on 4 dates that amounted to 64 individual images being analysed.

In this Chapter only the summary crack statistics are presented. The individual shearography images and the resulting crack traces are provided for reference in appendix.

### 6.1 Crack Statistics

Once the crack trace has been obtained, ImagePro can calculate various statistics. The two most useful here are crack length and number of cracks per image It was not possible to estimate crack width because the software traced the crack as having a width of a single pixel.

ImagePro does not report the lengths of individual cracks. It does give the sum of the crack lengths for the image. It also gives the number of cracks. Hence it is possible to calculate an average crack length per image. In this section, these two data

items are presented at level of the individual side image for each prism over time. These are then averaged to give the mean crack length and number of cracks for the level of the entire prism.

### 6.1.1 Prism TX1

**Table 3 Crack Lengths TX1**

| Days | Side Average | | | | Prism Average | Std.dev. |
|---|---|---|---|---|---|---|
| | 1A | 1B | 2A | 2B | | |
| 45 | 0.8 | 1.1 | 1.3 | 1.4 | 1.1 | 0.2 |
| 97 | 0.7 | 0.7 | 1.2 | 1 | 0.9 | 0.2 |
| 367 | 1 | 1.4 | 1.2 | 1.4 | 1.3 | 0.2 |
| 548 | 1.3 | 1.2 | 1.7 | 1.3 | 1.4 | 0.2 |

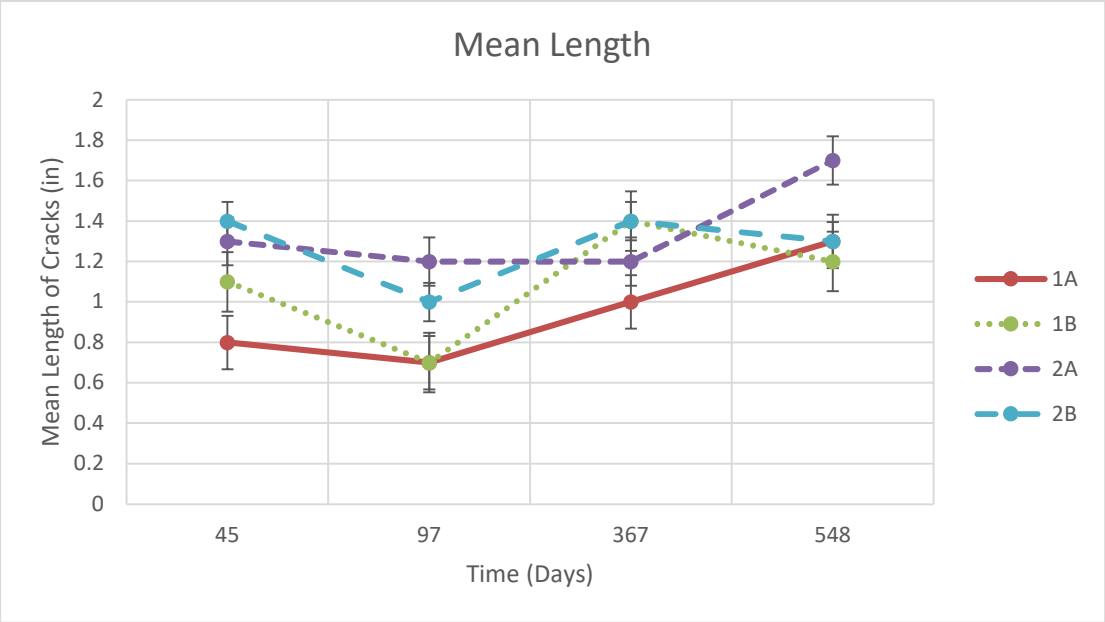


**Figure 34 Scatter plot of side average crack length vs time**

**Table 4 Number of Cracks TX1**

| | Number per Side | | | | Prism Average | Std.dev. |
|---|---|---|---|---|---|---|
| Days | 1A | 1B | 2A | 2B | | |
| 45 | 20 | 16 | 16 | 14 | 17 | 2 |
| 97 | 10 | 19 | 14 | 14 | 14 | 3 |
| 365 | 14 | 10 | 12 | 10 | 12 | 2 |
| 548 | 9 | 11 | 8 | 10 | 10 | 1 |

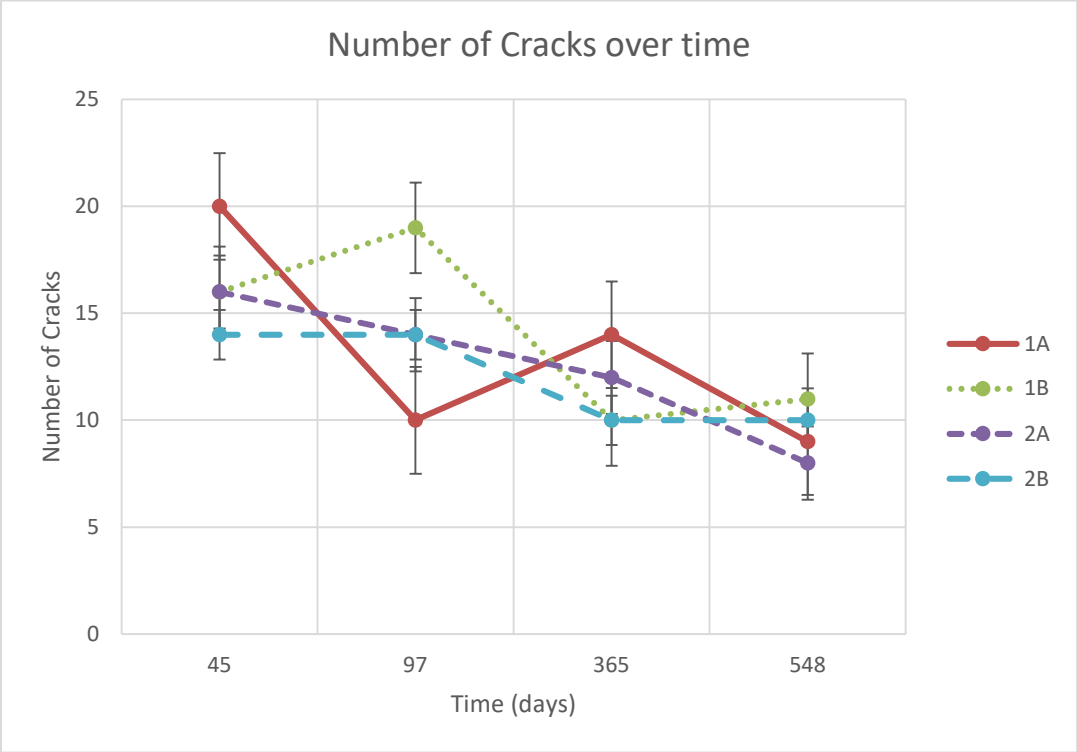


**Figure 35 Scatterplot of number of cracks TX1**

### 6.1.2. Prism TX2

**Table 5 Length of cracks per side TX2**

| | Side Average | | | | Prism Average | Std.dev. |
|---|---|---|---|---|---|---|
| Days | 1A | 1B | 2A | 2B | | |
| 45 | 1.4 | 1.7 | 1.2 | 1.1 | 1.4 | 0.2 |
| 97 | 1.1 | 0.9 | 1.2 | 0.8 | 1 | 0.2 |
| 367 | 1.1 | 1.1 | 1.6 | 0.7 | 1.1 | 0.3 |
| 548 | 1.9 | 1.3 | 1 | 2 | 1.6 | 0.4 |

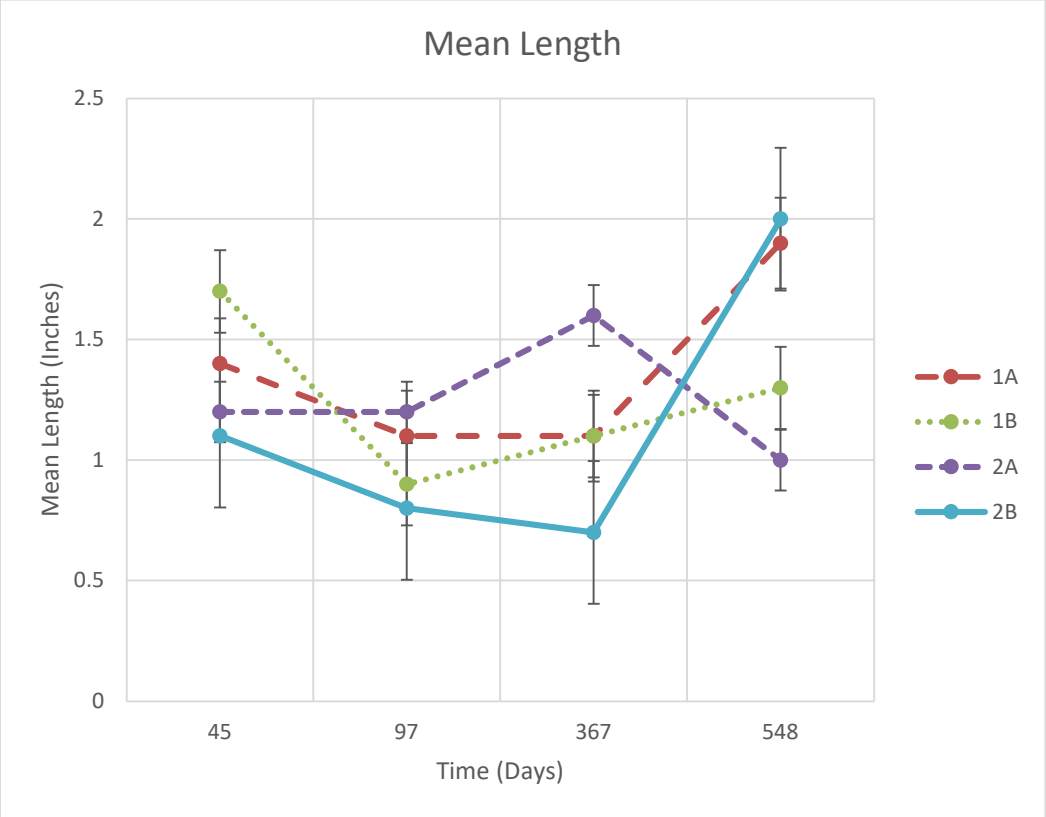


**Figure 36 Scatter plot of side average length of cracks vs time sample TX2**

**Table 6 Number of Cracks per side TX2**

| | Number per Side | | | | Prism Average | Std.dev. |
|---|---|---|---|---|---|---|
| Days | 1A | 1B | 2A | 2B | | |
| 45 | 11 | 8 | 10 | 13 | 11 | 2 |
| 97 | 10 | 7 | 4 | 12 | 8 | 3 |
| 365 | 10 | 10 | 4 | 5 | 7 | 3 |
| 548 | 6 | 3 | 5 | 2 | 4 | 2 |

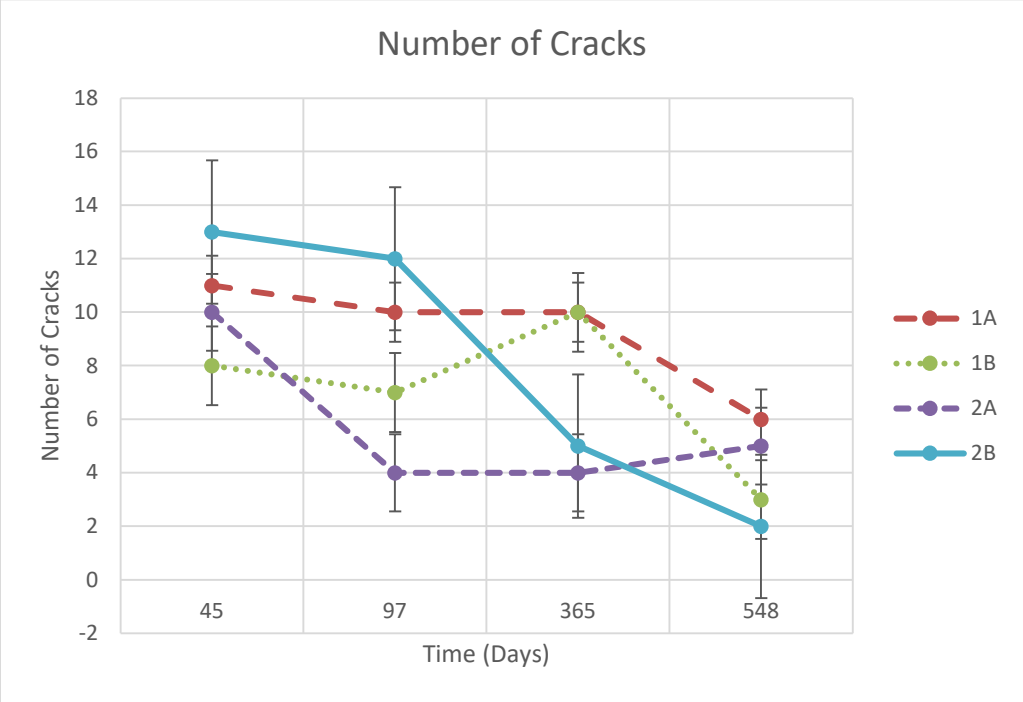


**Figure 37 Scatter plot of side Number of cracks vs time sample TX2**

### 6.1.3 Prism TX3

**Table 7 Cracks Lengths TX3**

| | Side Average (in) | | | | Prism Average | Std.dev. |
|---|---|---|---|---|---|---|
| Days | 1A | 1B | 2A | 2B | | |
| 33 | 0.9 | 1 | 0.9 | 0.8 | 0.9 | 0.1 |
| 272 | 1.1 | 1.3 | 0.7 | 1.1 | 1 | 0.2 |
| 453 | 2.4 | 1.1 | 1.1 | 0.9 | 1.4 | 0.6 |

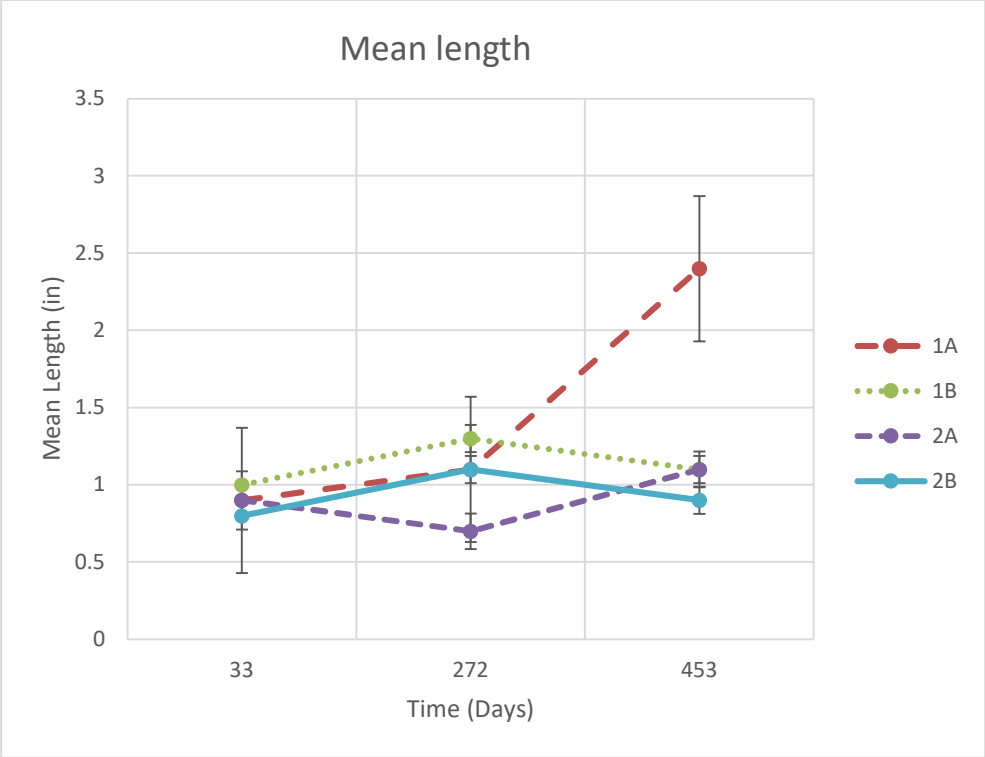


**Figure 38 Scatter plot of side average crack length vs time sample TX3**

**Table 8 Number of cracks TX3**

| | Number per Side | | | | Prism Average | Std.dev. |
|---|---|---|---|---|---|---|
| Days | 1A | 1B | 2A | 2B | | |
| 33 | 11 | 10 | 7 | 6 | 9 | 2 |
| 272 | 9 | 9 | 9 | 7 | 9 | 1 |
| 453 | 2 | 4 | 5 | 4 | 4 | 1 |

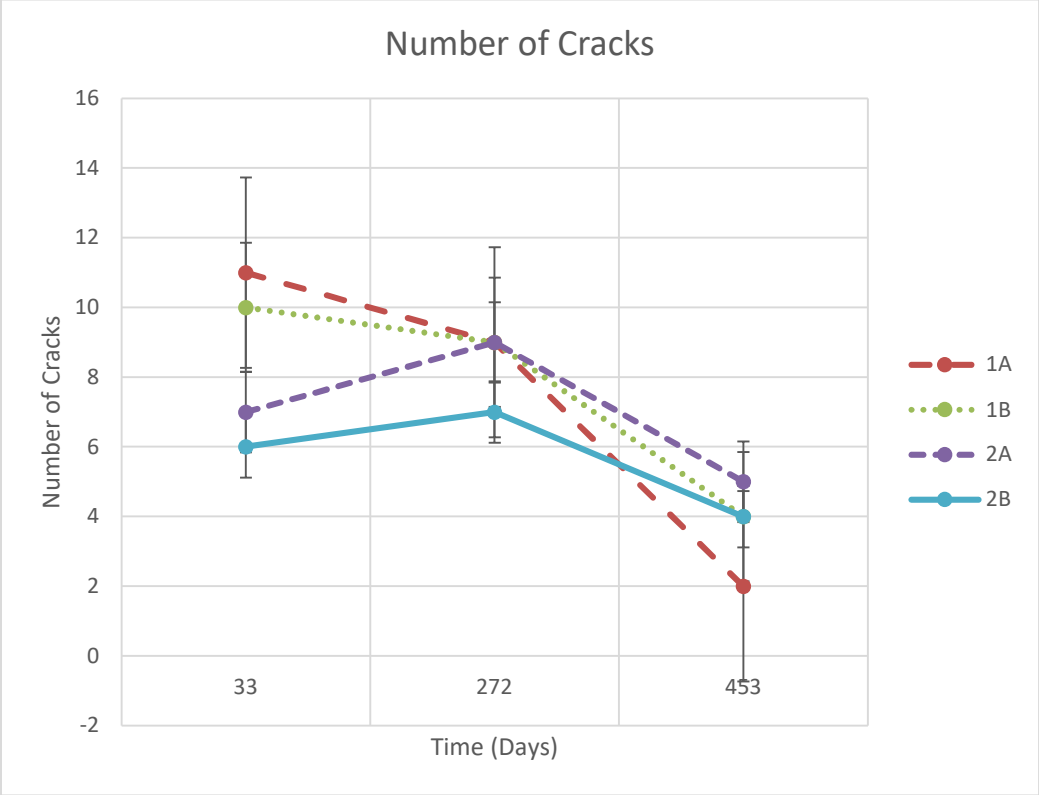


**Figure 39 Scatter plot of number of cracks vs time sample TX3 6.1.4. Prism TX4**

**Table 9 Cracks Lengths TX4**

| | Side Average (in) | | | | Prism Average | Std.dev. |
|---|---|---|---|---|---|---|
| Days | 1A | 1B | 2A | 2B | | |
| 33 | 0.4 | 0.4 | 0.7 | 0.8 | 0.6 | 0.2 |
| 272 | 0.6 | 0.4 | 0.8 | 0.9 | 0.7 | 0.2 |
| 453 | 0.8 | 0.5 | 1 | 0.8 | 0.8 | 0.2 |

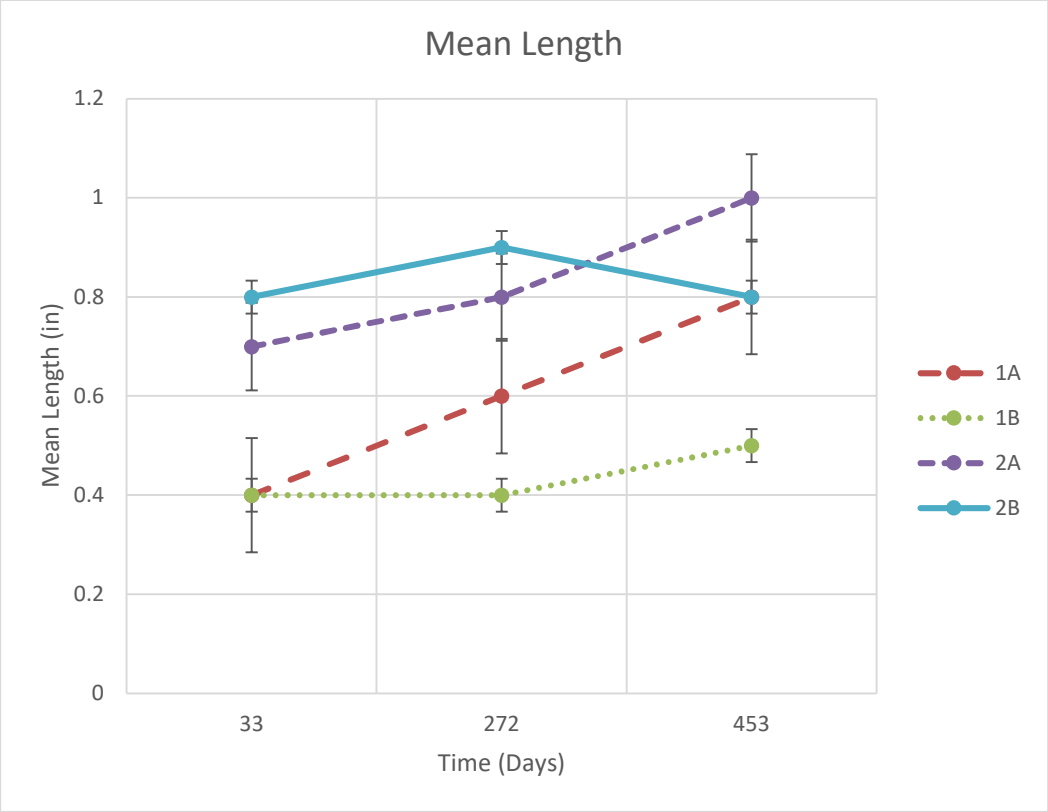


**Figure 40 Scatter plot of side average crack length vs time sample TX4**

**Table 10 Number of cracks TX4**

| | Number per Side | | | | Prism Average | Std.dev. |
|---|---|---|---|---|---|---|
| Days | 1A | 1B | 2A | 2B | | |
| 33 | 6 | 8 | 4 | 10 | 7 | 2 |
| 272 | 5 | 7 | 10 | 11 | 8 | 2 |
| 453 | 4 | 4 | 6 | 6 | 5 | 1 |

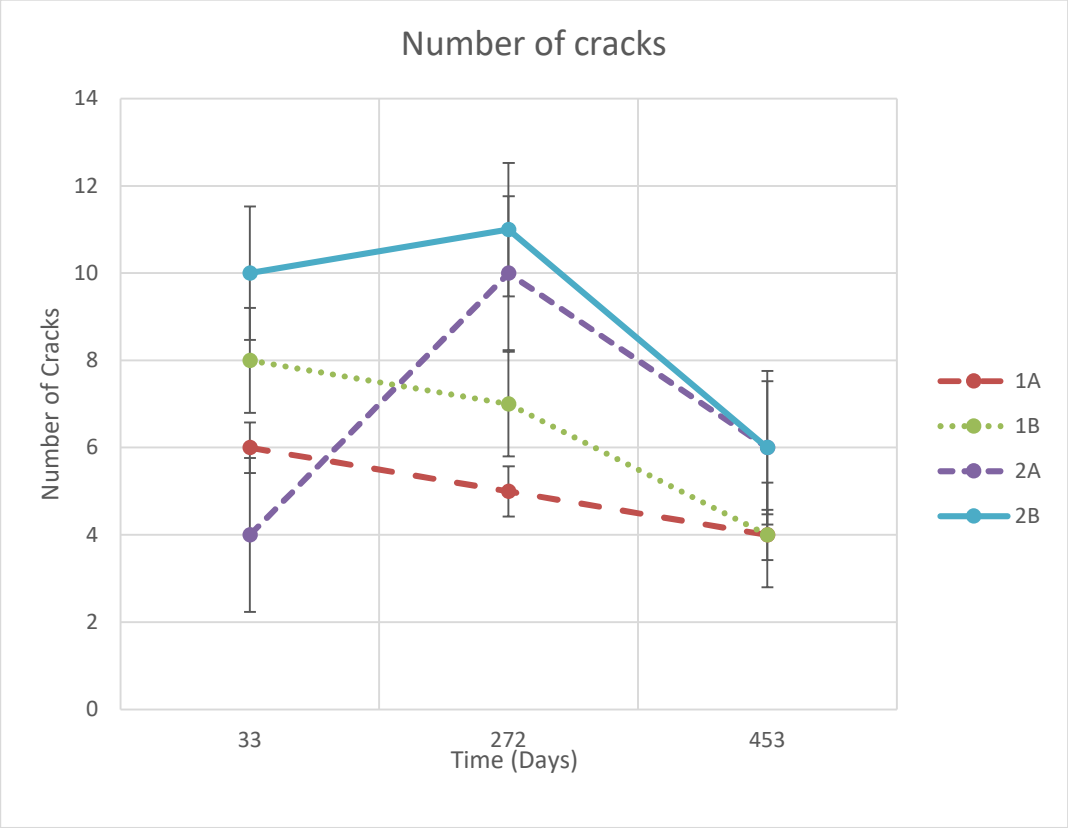


**Figure 41 Scatter plot of side number of cracks vs time sample TX4**

## 6.2 Discussion

### 6.2.1 Average Crack Length

The average crack length for the entire prisms is plotted in Figure 40. It shows a positive correlation with the measured amount of expansion with the prism that had both elevated potassium and heat cycles having the highest mean crack length and the controls having the lowest. The number of cracks did not increase for any of the prisms indicating that DEF did not generate expansive stresses strong enough to nucleate new cracks. This implies that the cracks were initiated by the high temperatures during the early curing. This is consistent with the results of temperature history modelling studies of D.E.F. in actual bridges.

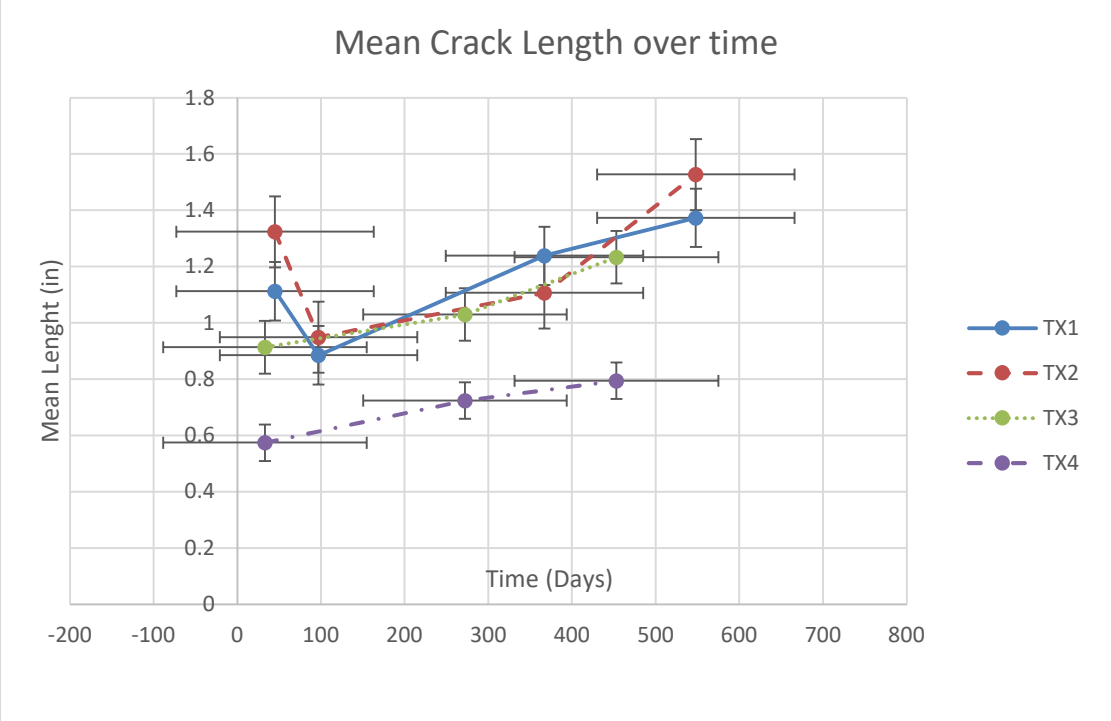


**Figure 42 Results from all samples over all the available times, Mean crack length over time**

### 6.2.2 Number of Cracks

The number of cracks for the entire prisms is plotted in Figure. 10. This is higher for the prims with elevated potassium which suggests that this element made the concrete more susceptible to cracking, possibly by making it more brittle. The number of cracks decreased with time for all the prisms. However, in the high potassium cases this was due to individual cracks joining up to make longer cracks, while for the control cases it was due to superficial cracks healing or being covered by a layer of precipitated calcium hydroxide or carbonate. During immersion in the limewater baths.

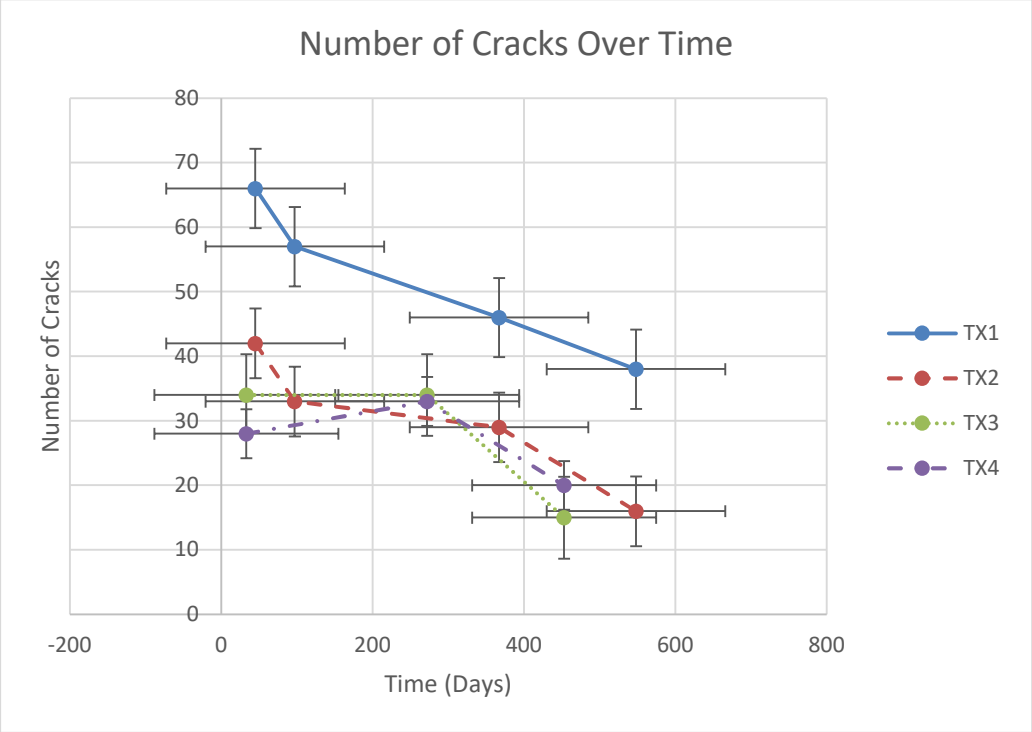


**Figure 43 Results from all samples over all the available times, Number of Cracks over time**

### 6.3 Software improvements

Software designed specifically for processing laser shearography needs to be developed. This includes replacing the current manual method of crack identification with a fully automated one. This could take advantage of the fact that the laser shearography image is the first derivative of the surface topography. Also, artificial intelligence techniques could use be for crack recognition and tracing. The software should also calculate crack width, again possibly making use of the spatial first derivative information contained in the laser shearography image. Finally, the software should be capable of calculating statistics at the crack network level such as branching and fractal ratios which can be used to characterise crack network morphology that may be useful for investigating D.E.F. damage mechanics.

# Chapter 7 Conclusion and Future Research

## 7.1 Application of Image Processing Software to Laser Shearography Images

Laser Shearography images of cracks in concrete have been successfully quantified using the commercially available automated image processing software ImagePro. This made it possible to measure the development of the cracks over time as the D.E.F. damage progressed. However, the crack statistics that were obtained were limited to crack length and number. It was not possible to estimate crack width because the software traced the crack as having a width of a single pixel.

The image processing was only semi-automated because the identification and tracing of an individual crack had to be done manually. This labour-intensive step slowed down the analysis process to the point where only about 10 cracks per image be quantified. Moreover, only 4 images out of a total of 12 per prism could be analysed due to the lack of data for the other sides for all the available dates. This inability to make use of all the information in the images reduced the robustness of the statistics. Also, the manual step introduced the possibility of human error in detecting cracks.

## 7.2 D.E.F. damage Mechanics

The average crack length showed a positive correlation with the measured amount of expansion with the prism that had both elevated potassium and heat

cycles having the highest mean crack length and the controls having the lowest. The number of cracks did not increase for any of the prisms indicating that D.E.F. did not generate expansive stresses strong enough to nucleate new cracks. This implies that the cracks were initiated by the high temperatures during the early curing. This is consistent with the results of temperature history modelling studies of D.E.F. in actual bridges.

The number of cracks was higher for the prims with elevated potassium which suggests that this element made the concrete more susceptible to cracking, possibly by making it more brittle. The number of cracks decreased with time for all the prisms. However, in the high potassium cases this was due to individual cracks joining up to make longer cracks, while for the control cases it was due to superficial cracks healing or being covered by a layer of precipitated calcium hydroxide or carbonate. During immersion in the limewater baths.

### 7.3 Future Research

Software designed specifically for processing Laser Shearography needs to be developed. This includes replacing the current manual method of crack identification with a fully automated one. This could take advantage of the fact that the laser shearography image is the first derivative of the surface topography. Also, artificial intelligence techniques could be used for crack recognition and tracing. The software should also calculate crack width, again possibly making

use of the spatial first derivative information contained in the laser shearography image. Finally, the software should be capable of calculating statistics at the crack network level such as branching and fractal ratios which can be used to characterize crack network morphology that may be useful for investigating D.E.F. damage mechanics.

With this specialized software laser shearography can then be applied to further investigate D.E.F. damage mechanics using the accelerated test method described here. One important issue is the effect of temperature during early age curing on crack development and subsequent D.E.F. progress. This would require taking laser shearography images immediately after curing and before the application of heat cycles. Another important fact is the potassium content of the mix and also the ratio of sodium to potassium. Another research area is the role of aggregate mineralogy and size. The ultimate goal is the development of a predictive model of the risk of D.E.F. given knowledge of concrete mix design and environmental conditions. The combination of the accelerated test method and laser shearography could also be applied to investigate alkali-silicate reaction (A.S.R.) damage mechanics.

As an outcome of this proposed laboratory research program laser shearography can then be applied as a nondestructive test method in the field to diagnose D.E.F. in concrete structures and to predict the remaining service life.

## Appendices

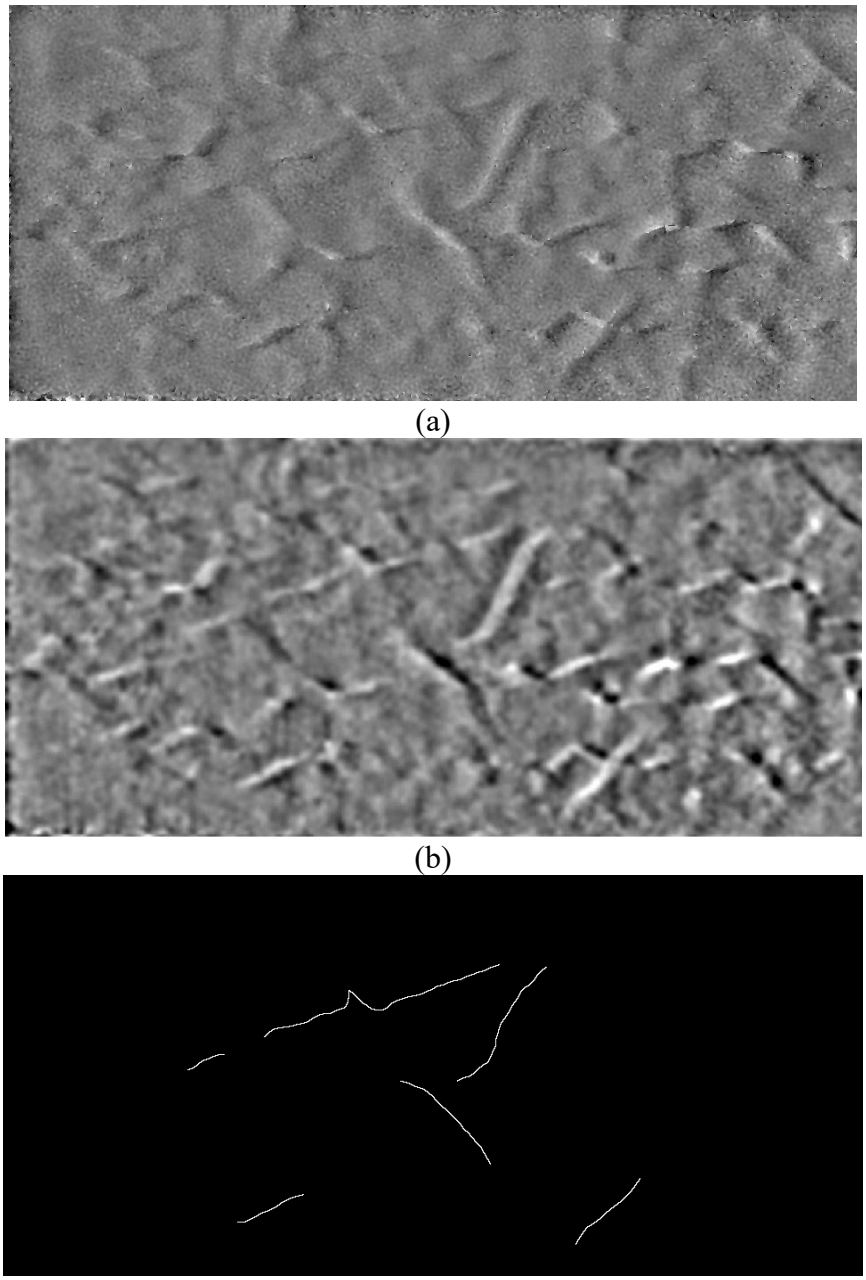

(a)

(b)

(c)

Figure A.1 Tx3 Section 1 A-X at 33 days after cast (a) original image (b) Image after filtering (c) Image after tracing and Mask

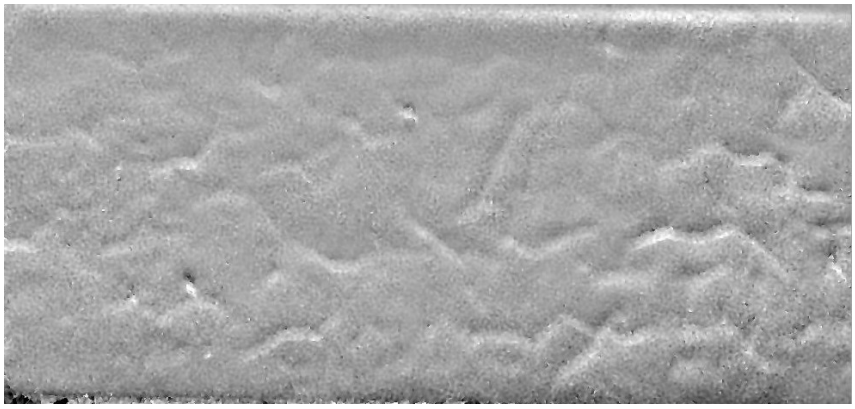

(a)

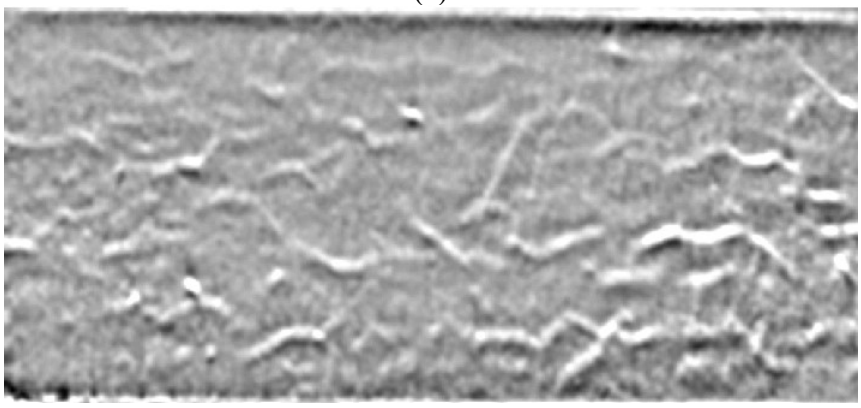

(b)

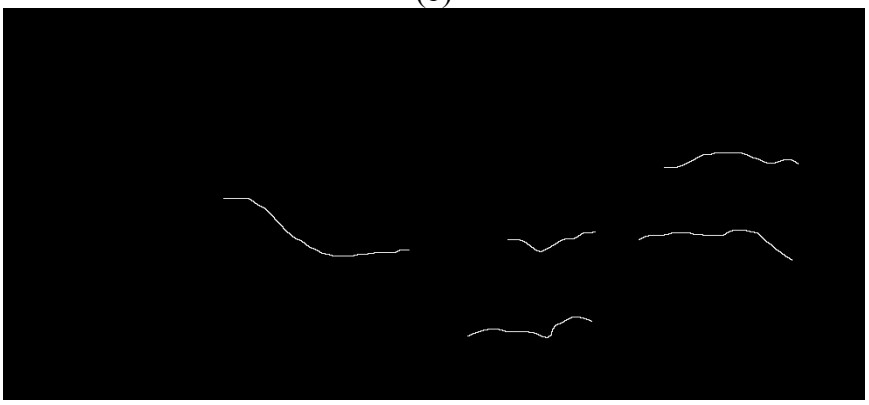

(c)

Figure A.2 Tx3 Section 1 A-Y at 33 days after cast (a) original image (b) Image after filtering (c) Image after tracing and Mask

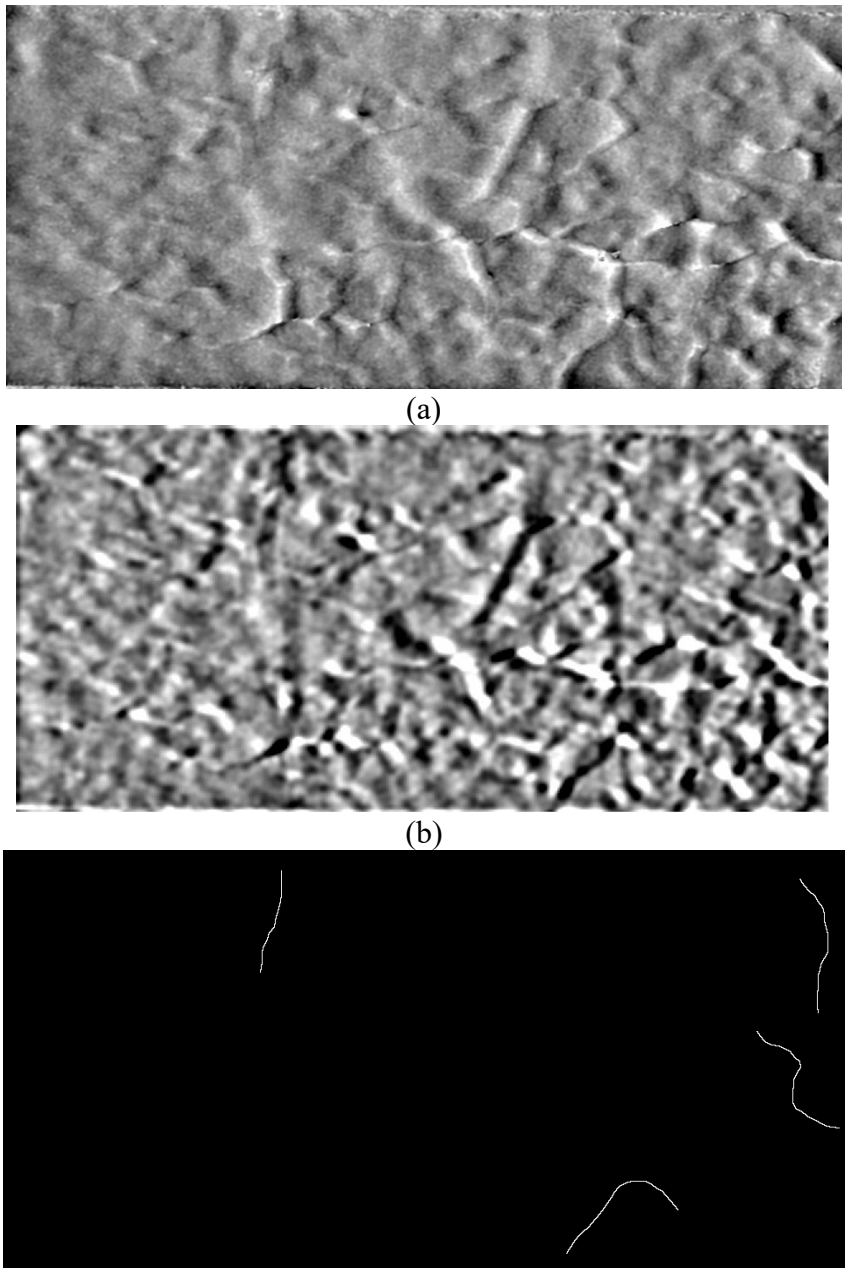

Figure A.3 Tx3 Section 1 A-X at 272 days after cast (a) original image (b) Image after filtering (c) Image after tracing and Mask

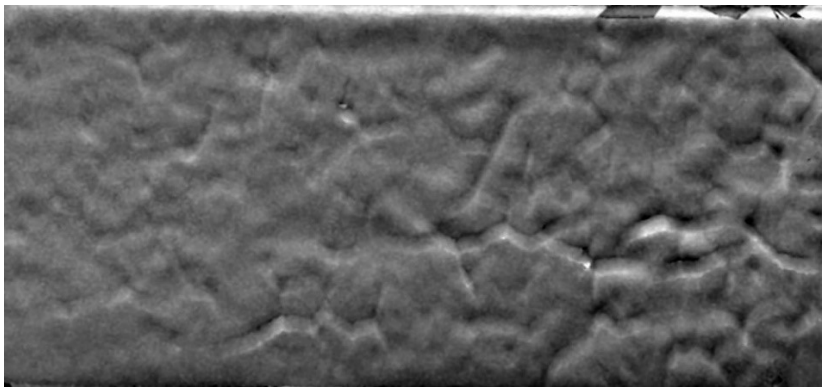

(a)

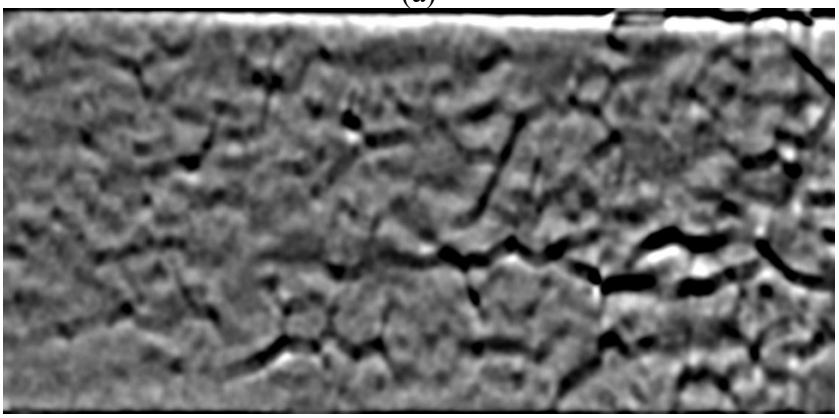

(b)

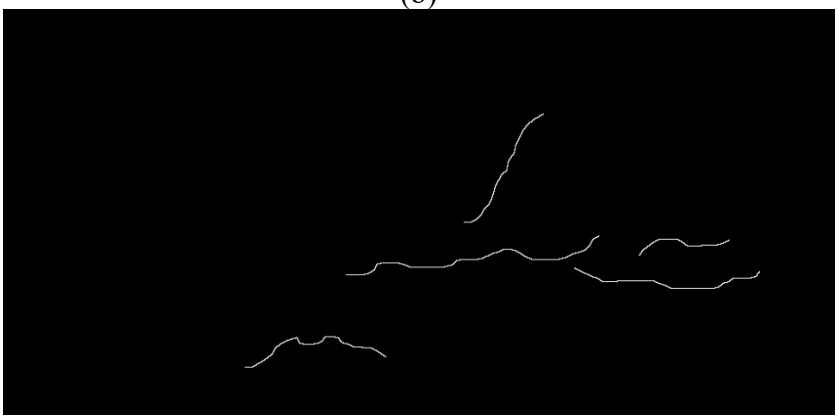

(c)

Figure A.4 Tx3 Section 1 A-Y at 272 days after cast (a) original image (b) Image after filtering (c) Image after tracing and Mask

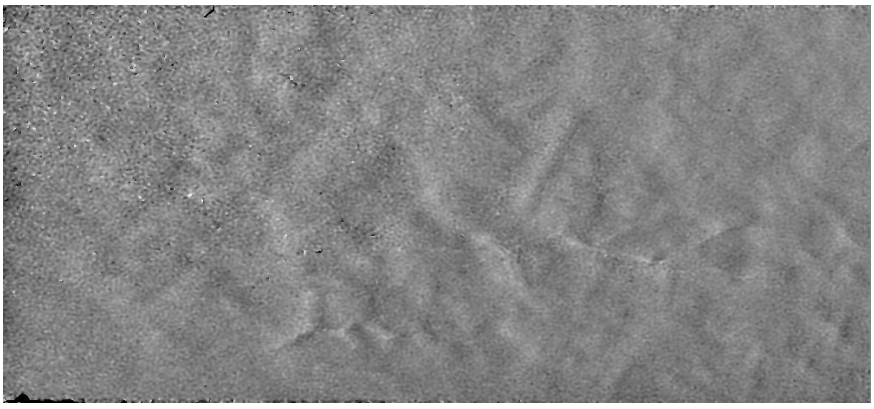

(a)

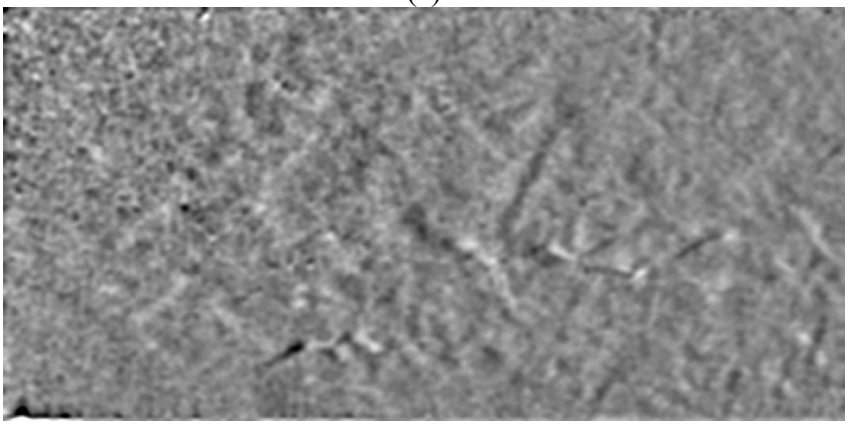

(b)

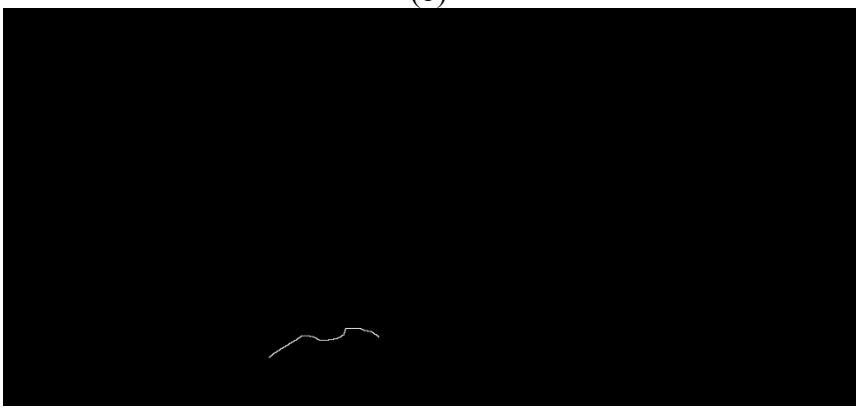

(c)

Figure A.5 Tx3 Section 1 A-X at 453 days after cast (a) original image (b) Image after filtering (c) Image after tracing and Mask

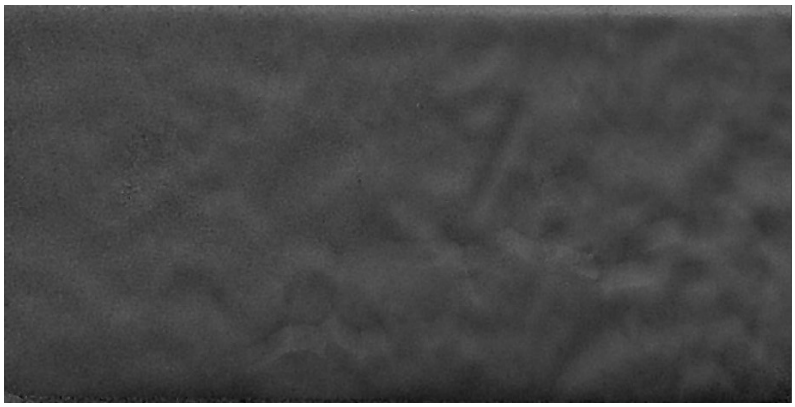

(a)

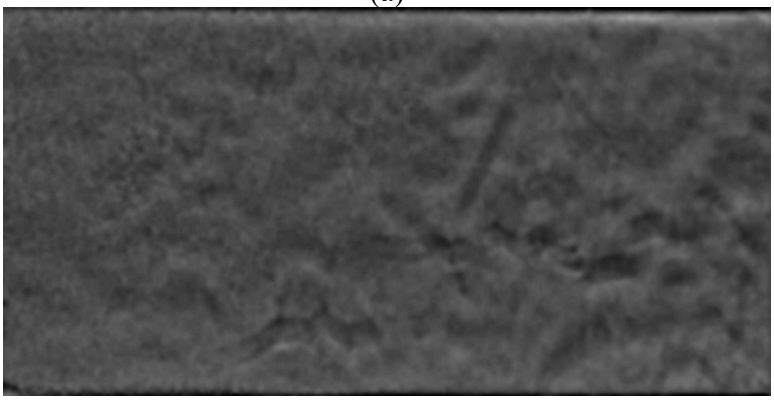

(b)

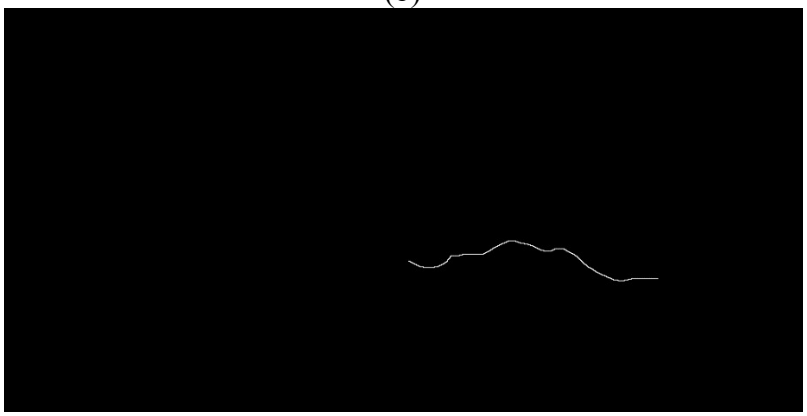

(c)

Figure A.6 Tx3 Section 1 A-X at 453 days after cast (a) original image (b) Image after filtering (c) Image after tracing and Mask

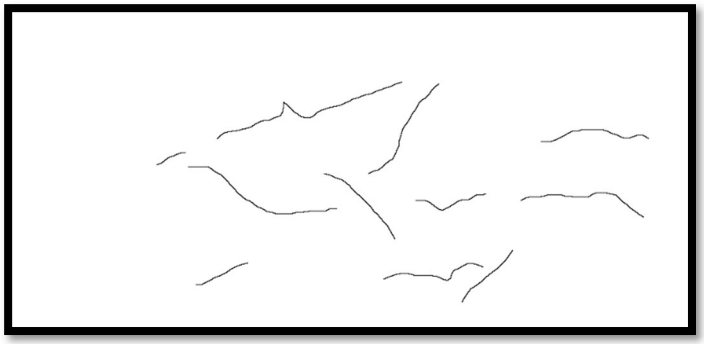

(a)

(b)

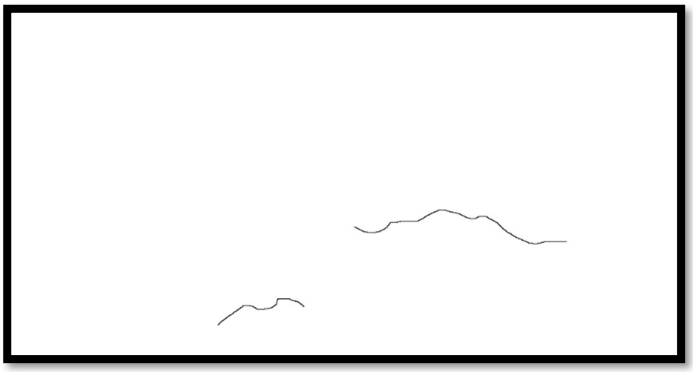

(c)

Figure A.7 Section 1A Tx3 Mask X and Y shear direction combined traced cracks and inverted (a) 45 Days (b) 272 Days (c) 453 Days

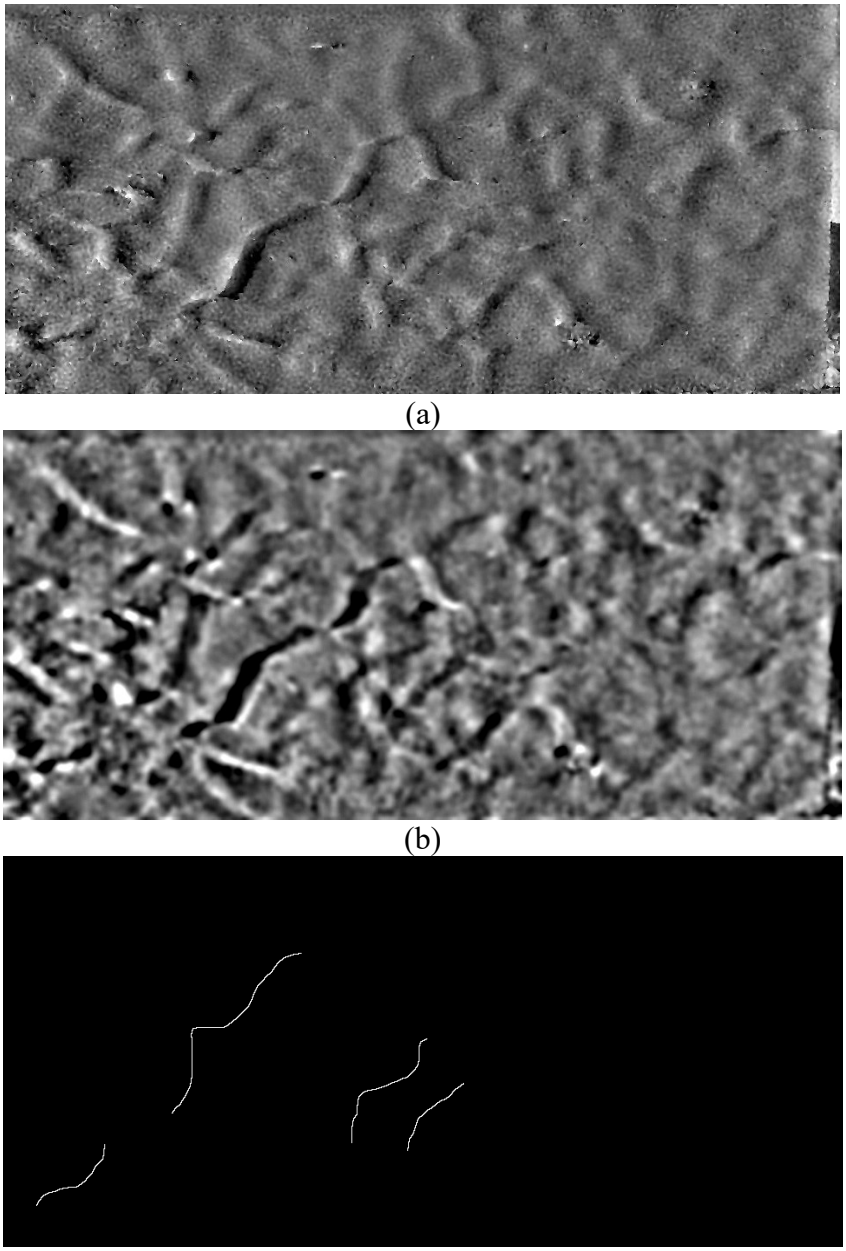

(a)

(b)

(c)

Figure A.9 TX3 Section 1 B-X at 33 days after cast (a) original image (b) Image after filtering (c) Image after tracing and Mask

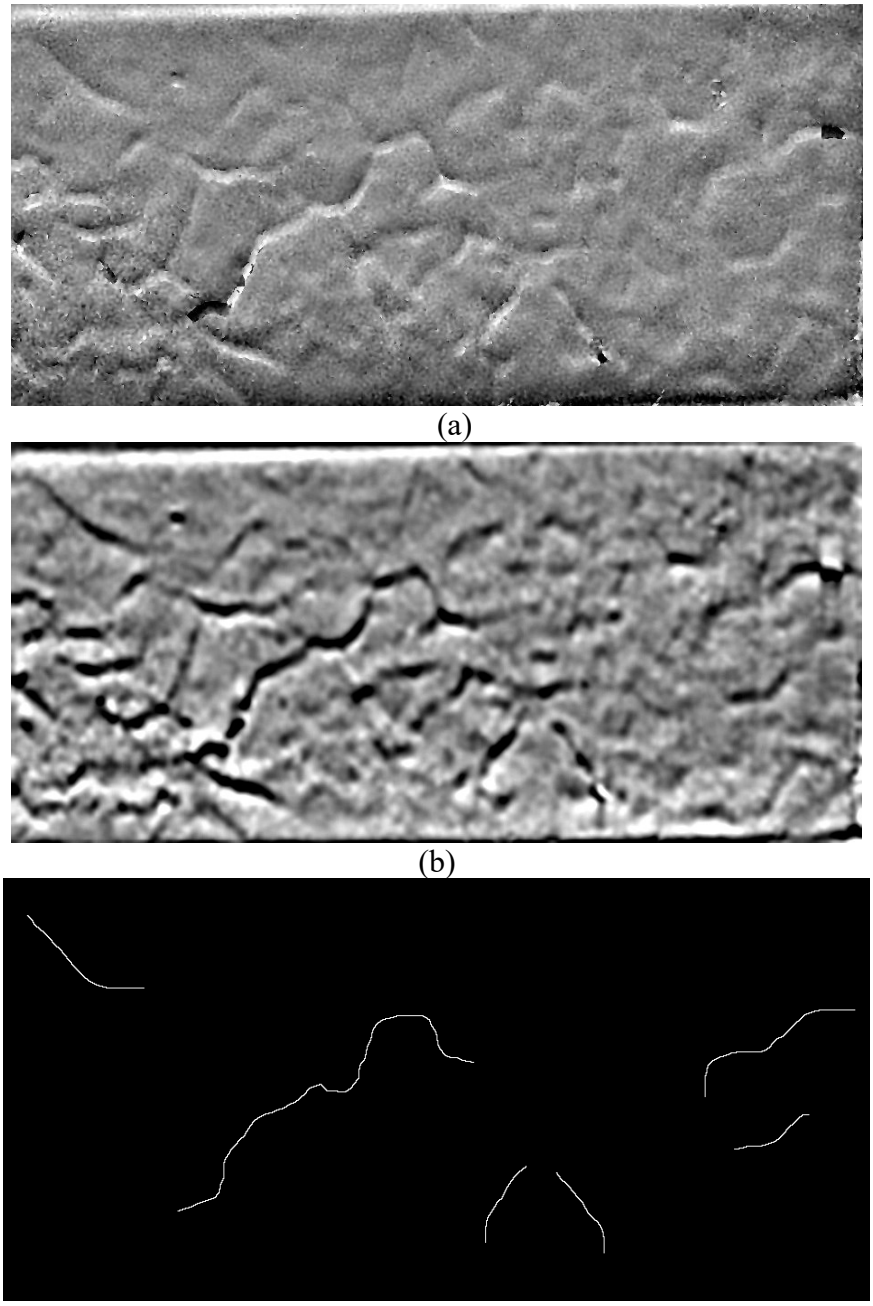

(a)

(b)

(c)

Figure A.10 TX3 Section 1 B-Y at 33 days after cast (a) original image (b) Image after filtering (c) Image after tracing and Mask

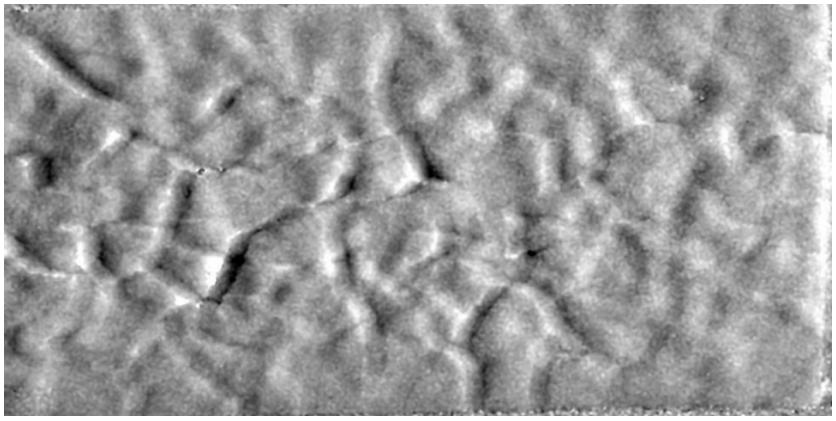

(a)

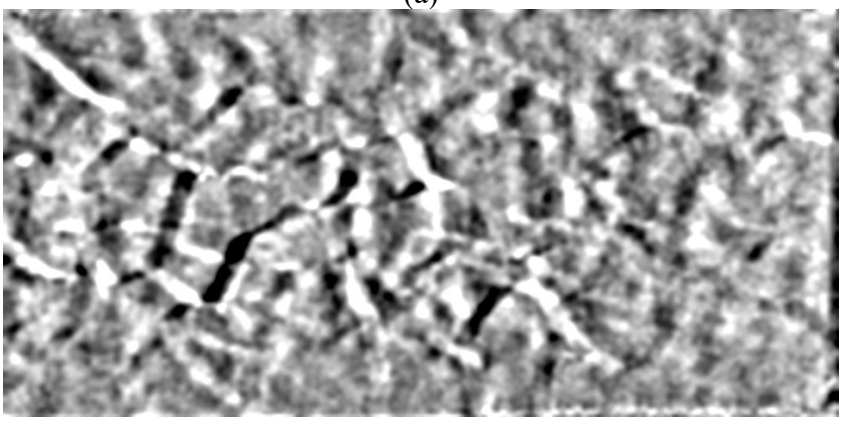

(b)

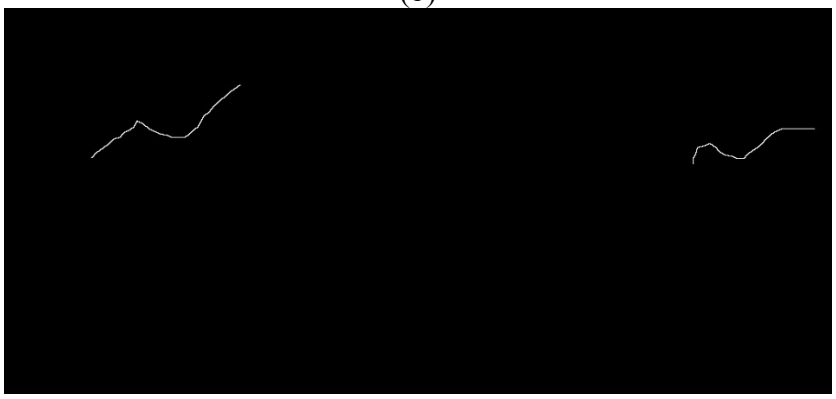

(c)

Figure A.11 TX3 Section 1 B-X at 272 days after cast (a) original image (b) Image after filtering (c) Image after tracing and Mask

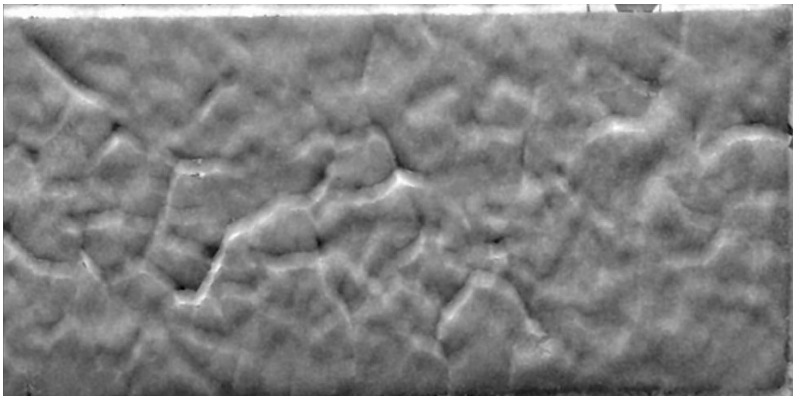

(a)

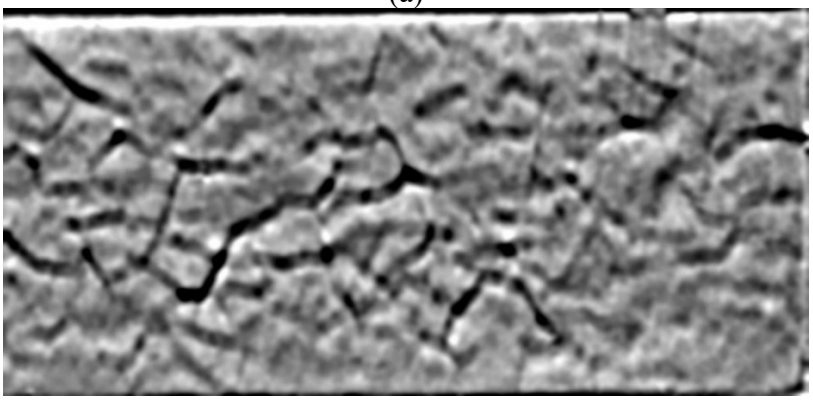

(b)

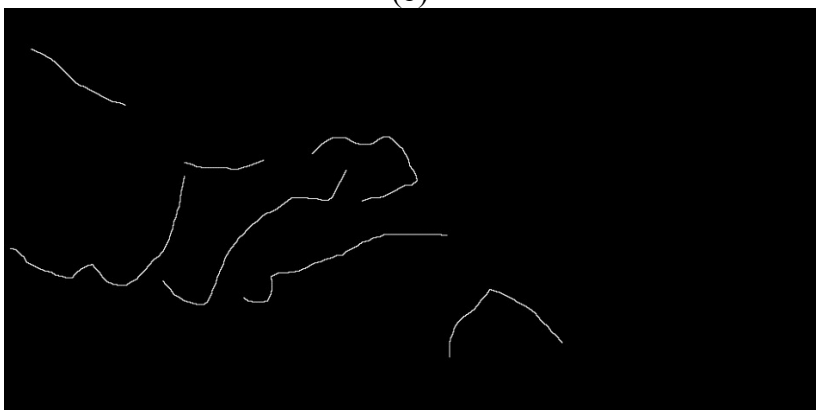

(c)

Figure A.12 TX3 Section 1 B-Y at 272 days after cast (a) original image (b) Image after filtering (c) Image after tracing and Mask

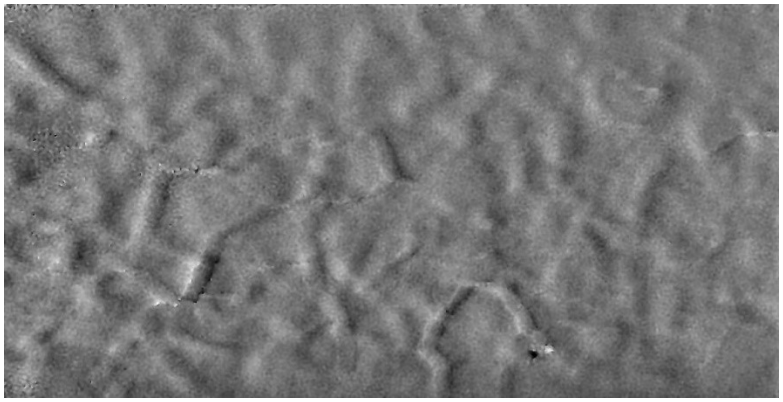

Tx3 Section 1 B-X, 453 Days from casting

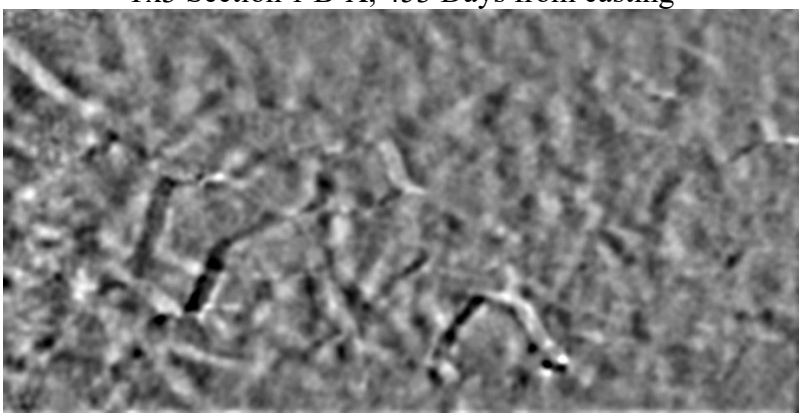

Tx3 Section 1 B-X, 453 Days after filtering

Tx3 Mask of the traced cracks after manual tracing

Figure A.13 TX3 Section 1 B-X at 453 days after cast (a) original image (b) Image after filtering (c) Image after tracing and Mask

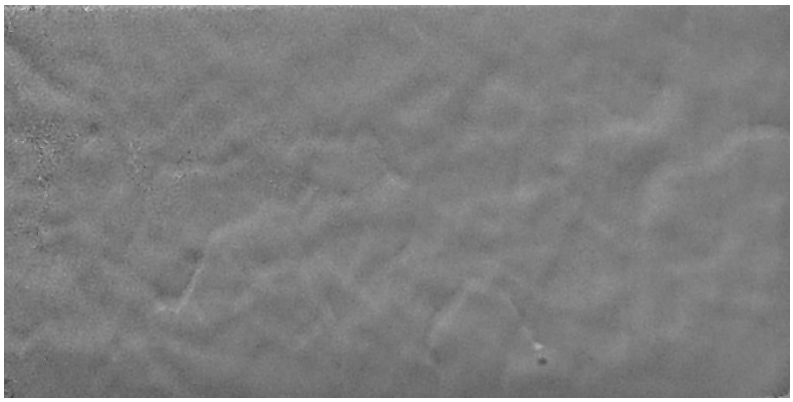

Tx3 Section 1 B-Y, 453 Days from casting

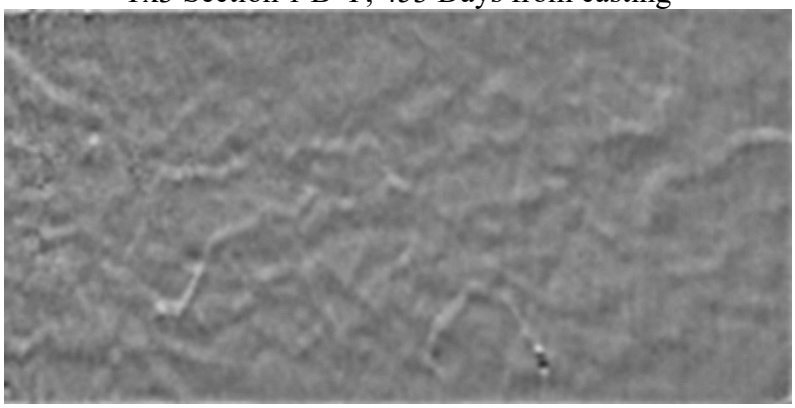

Tx3 Section 1 B-Y, 453 Days after filtering

Tx3 Mask of the traced cracks after manual tracing

Figure A.14 TX3 Section 1 B-Y at 453 days after cast (a) original image (b) Image after filtering (c) Image after tracing and Mask

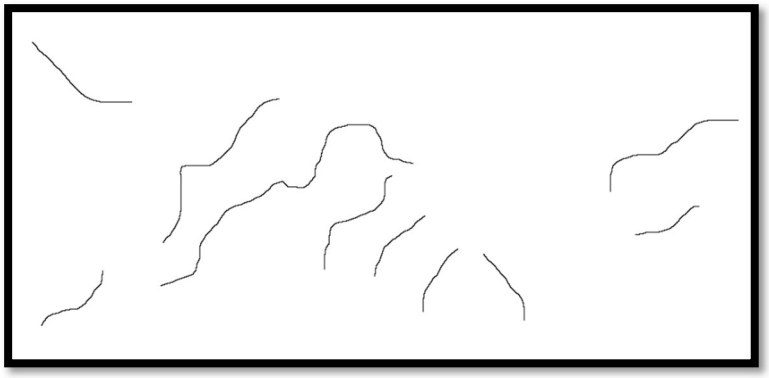

(a)

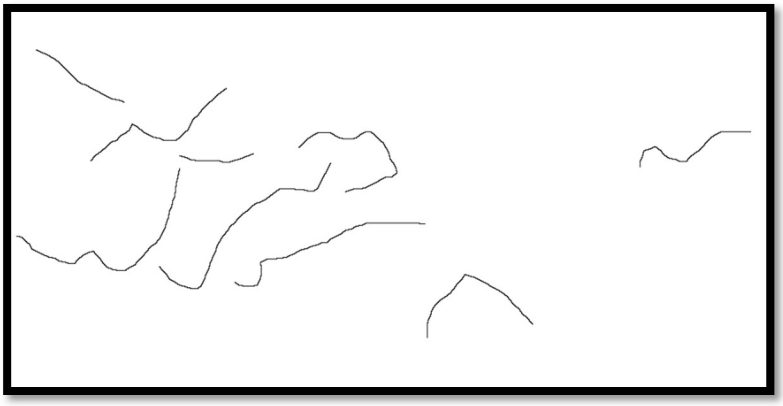

(b)

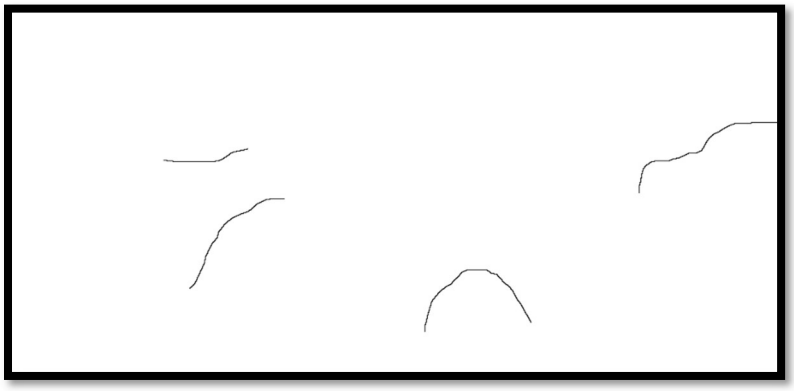

(c)

Figure A.15 Section 1B Tx3 Mask X and Y shear direction combined traced cracks and inverted (a) 45 Days (b) 272 Days (c) 453 Days

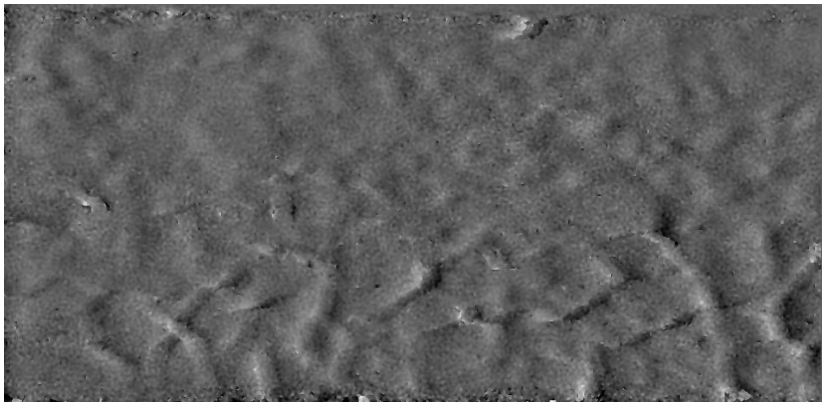

(a)

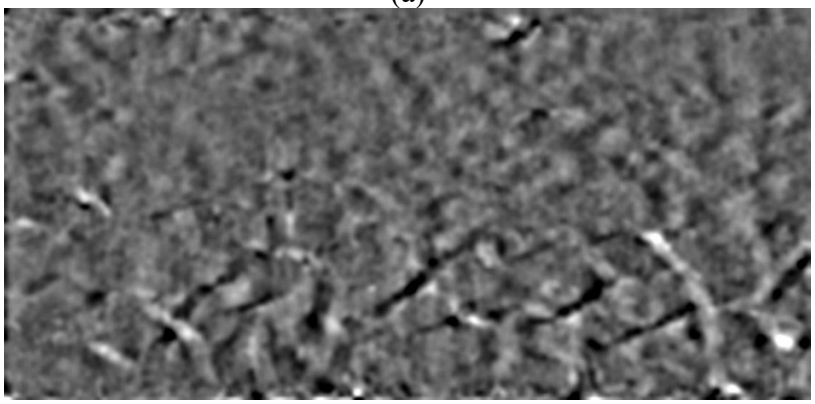

(b)

(c)

Figure A.17 TX3 Section 2 A-X at 33 days after cast (a) original image (b) Image after filtering (c) Image after tracing and Mask

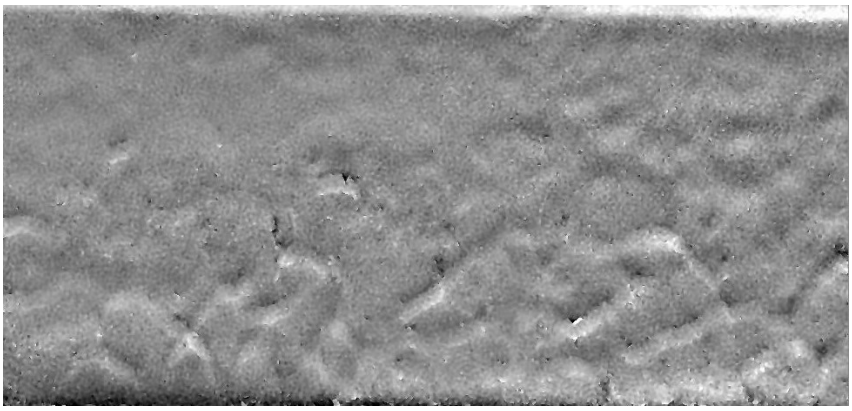

(a)

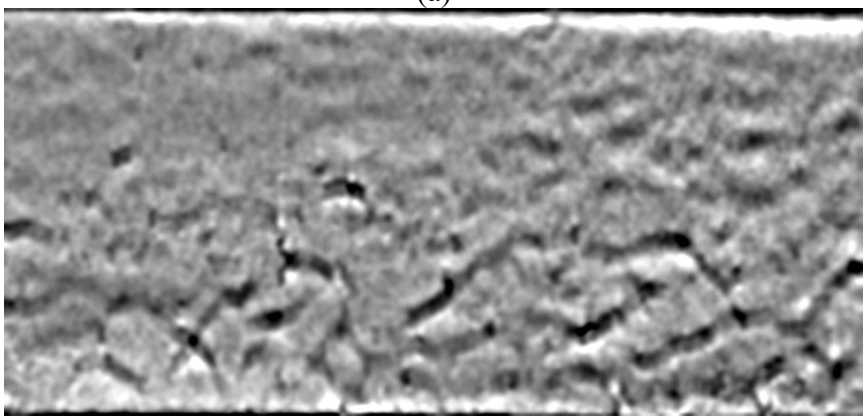

(b)

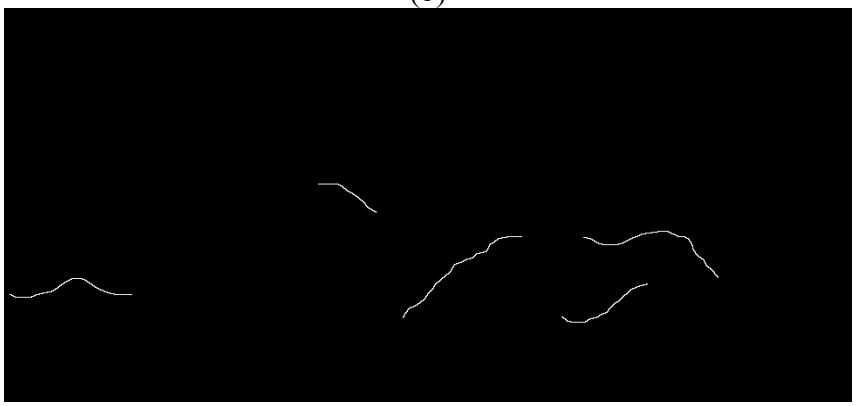

(c)

Figure A.18 TX3 Section 2 A-Y at 33 days after cast (a) original image (b) Image after filtering (c) Image after tracing and Mask

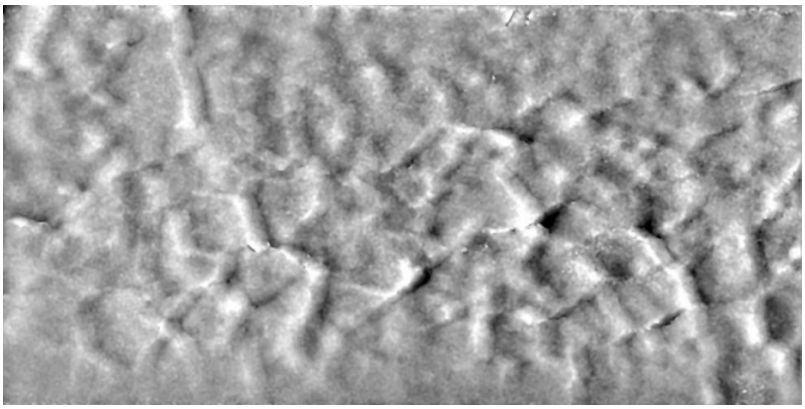

(a)

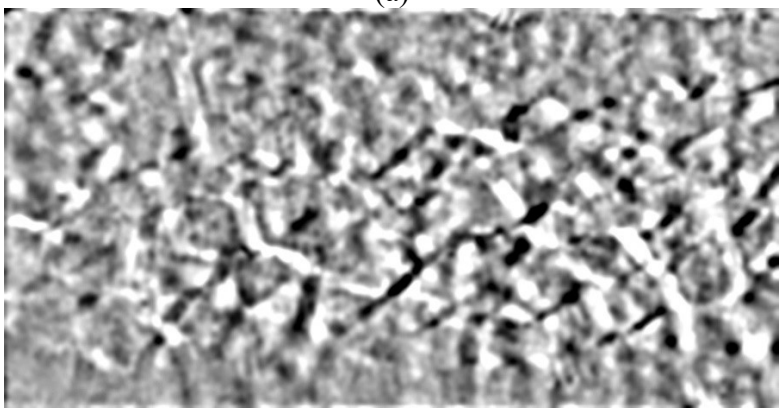

(b)

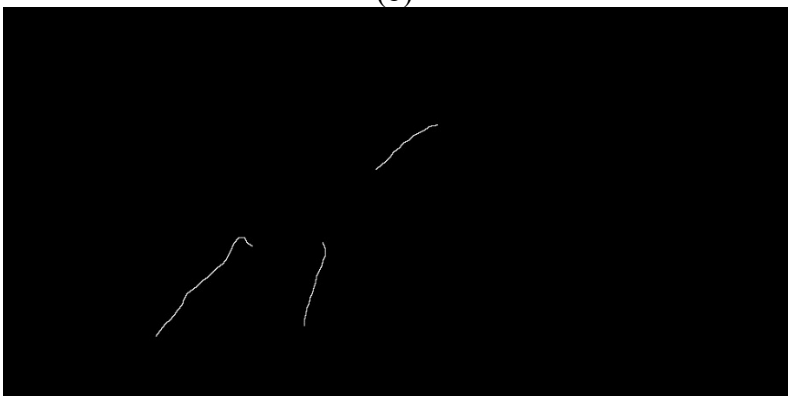

(c)

Figure A.19 TX3 Section 2 A-X at 272 days after cast (a) original image (b) Image after filtering (c) Image after tracing and Mask

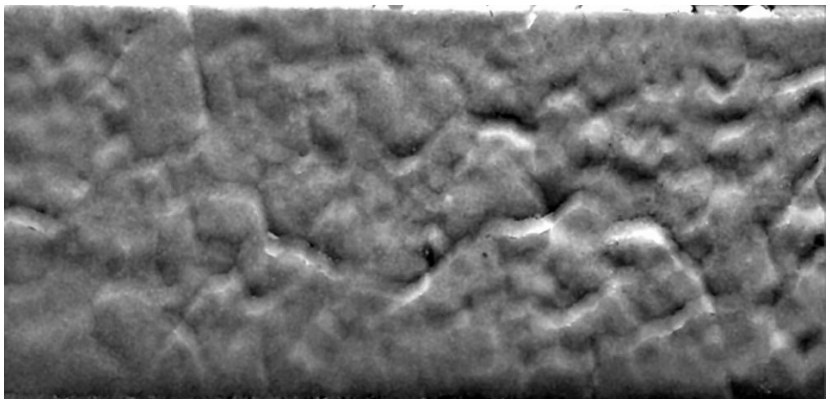

(a)

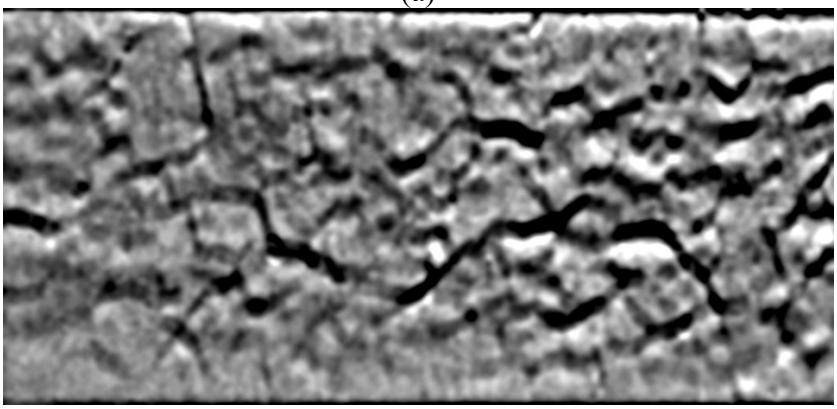

(b)

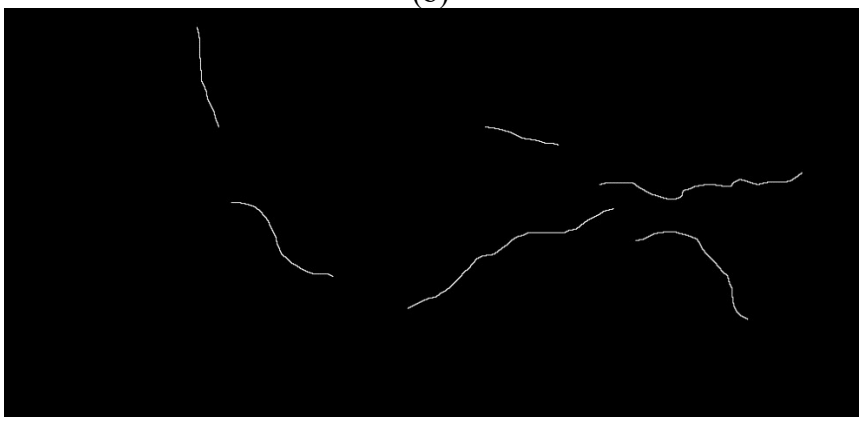

(c)

Figure A.20 TX3 Section 2 A-Y at 272 days after cast (a) original image (b) Image after filtering (c) Image after tracing and Mask

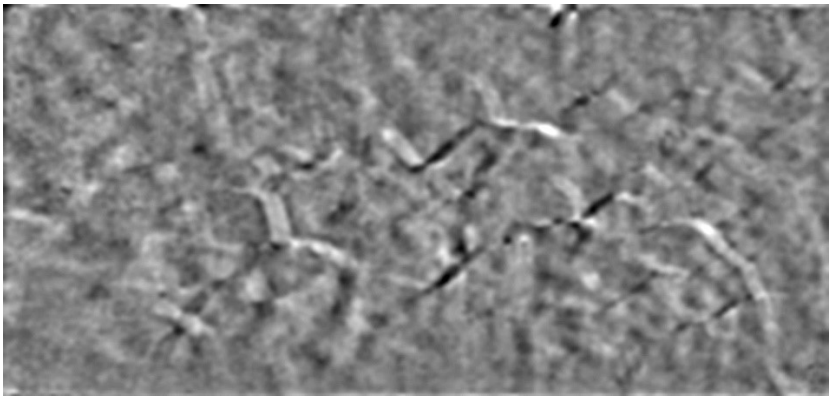

(a)

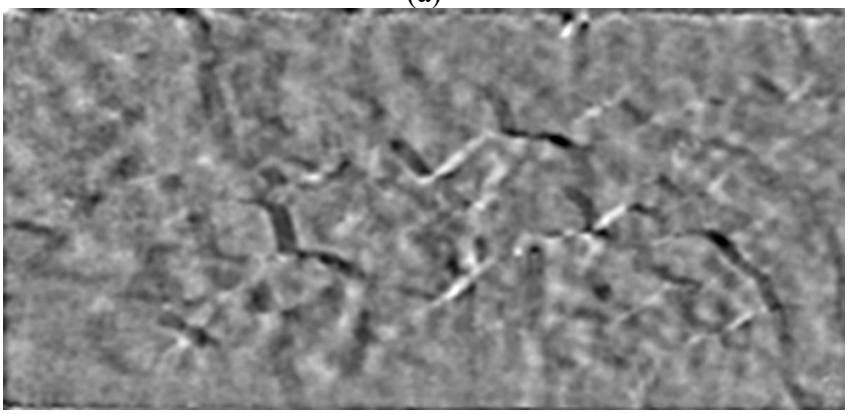

(b)

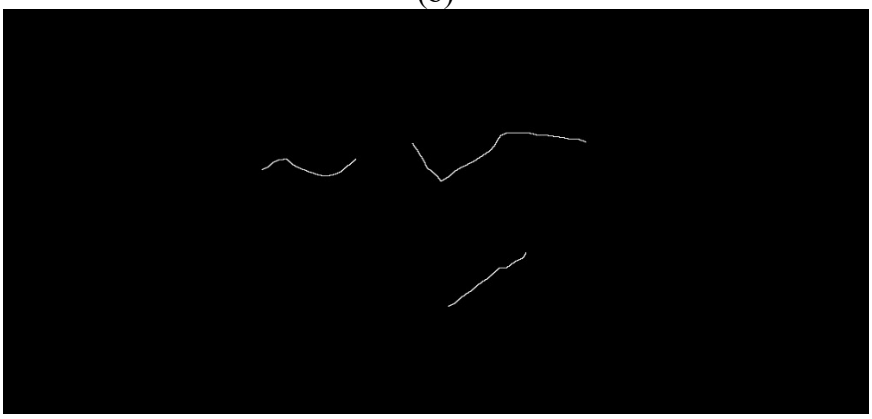

(c)

Figure A.21 TX3 Section 2 A-X at 453 days after cast (a) original image (b) Image after filtering (c) Image after tracing and Mask

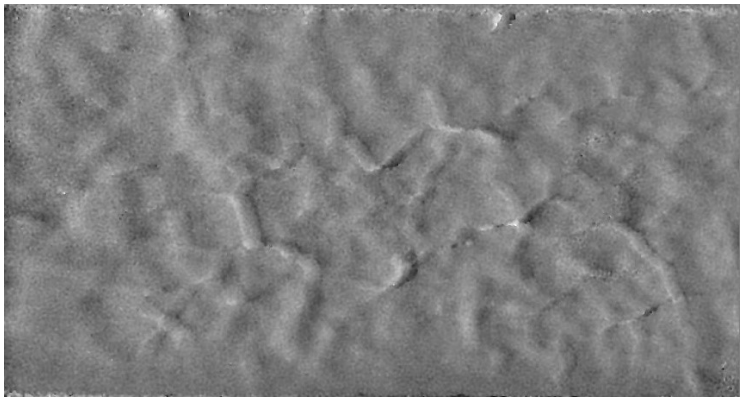

(a)

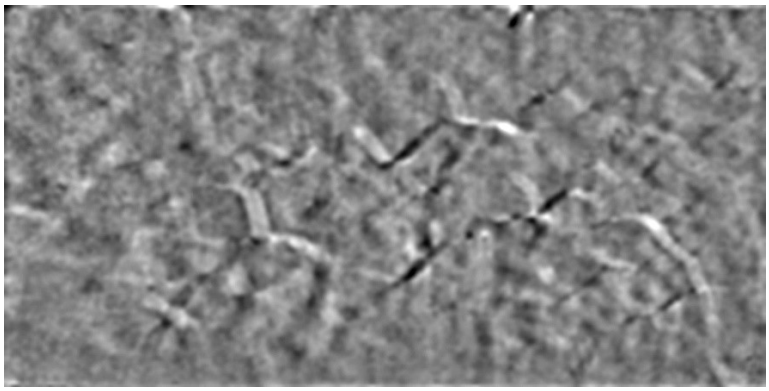

(b)

(c)

Figure A.22 TX3 Section 2 A-Y at 453 days after cast (a) original image (b) Image after filtering (c) Image after tracing and Mask

(a)

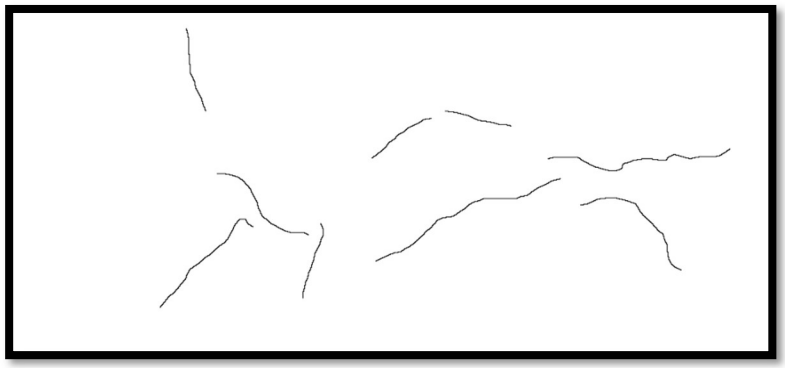

(b)

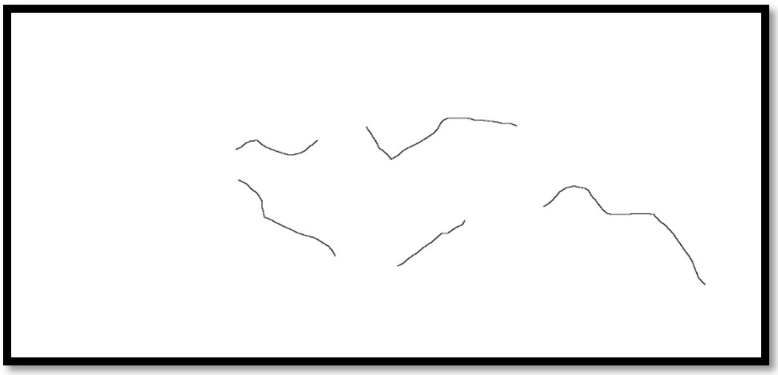

(c)

Figure A.23 Section 2A Tx3 Mask X and Y shear direction combined traced cracks and inverted (a) 45 Days (b) 272 Days (c) 453 Days

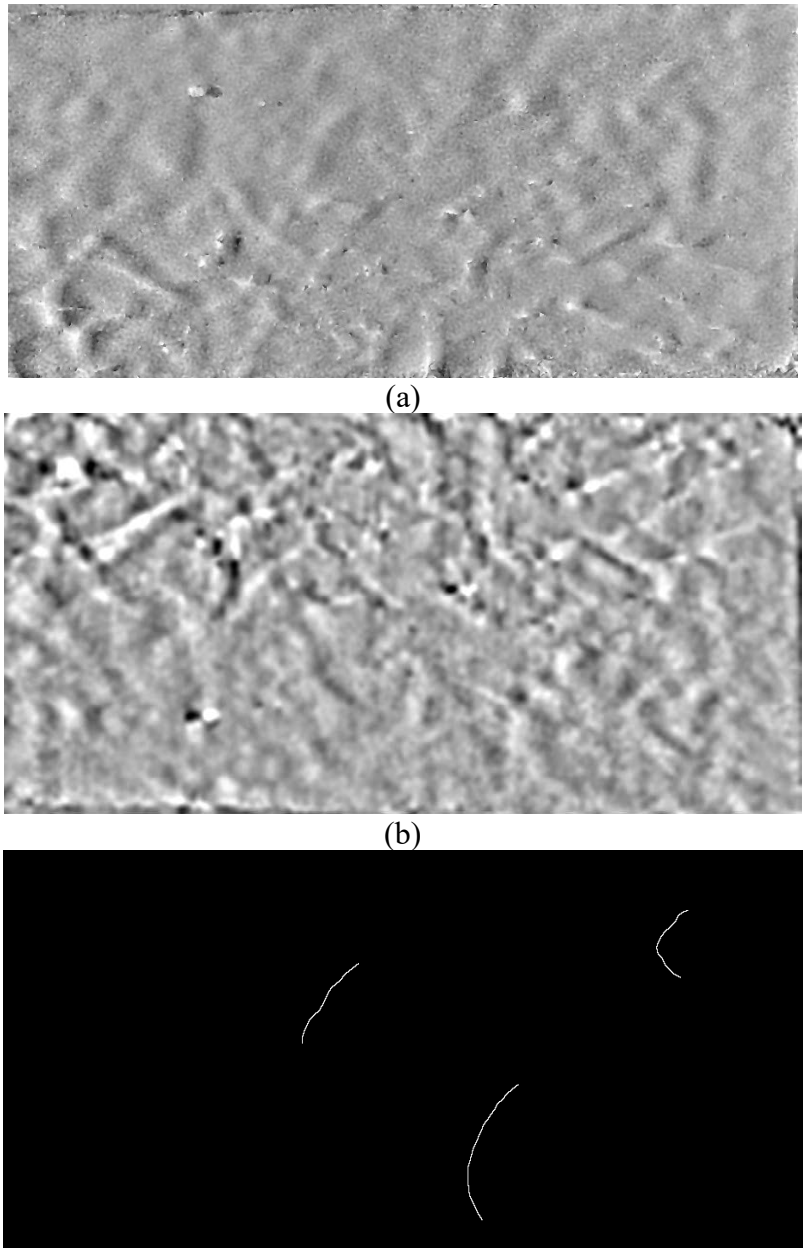

(a)

(b)

(c)

Figure A.25 TX3 Section 2 B-X at 33 days after cast (a) original image (b) Image after filtering (c) Image after tracing and Mask

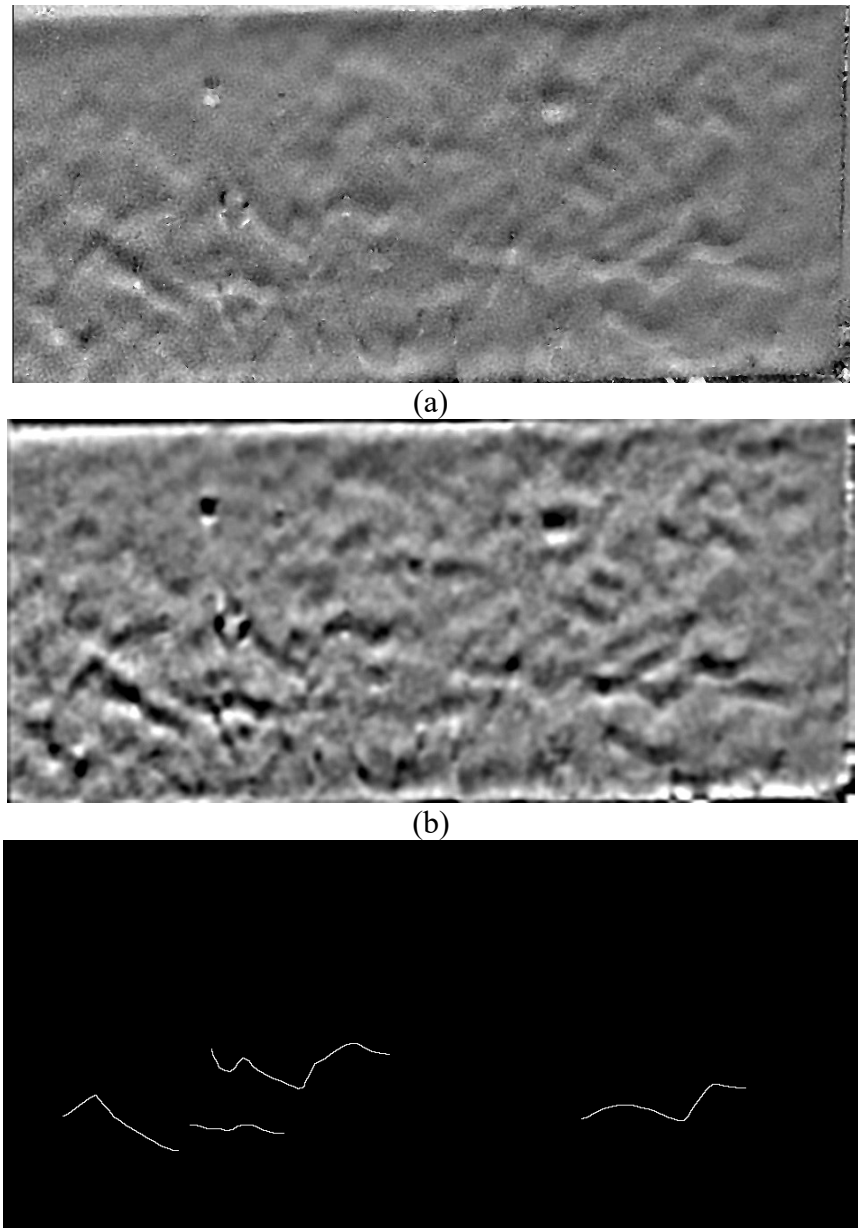

Figure A.26 TX3 Section 2 B-Y at 33 days after cast (a) original image (b) Image after filtering (c) Image after tracing and Mask

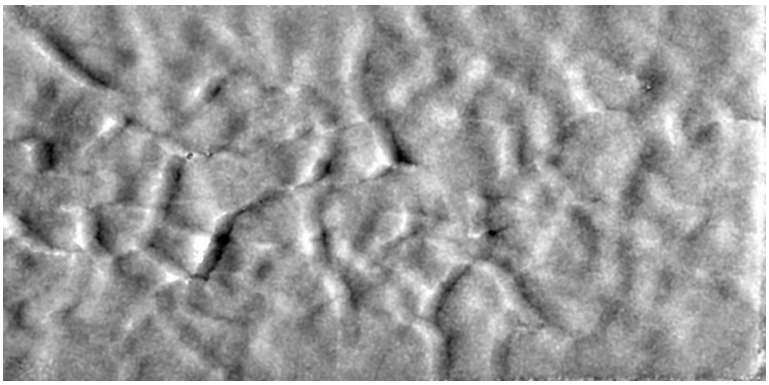

(a)

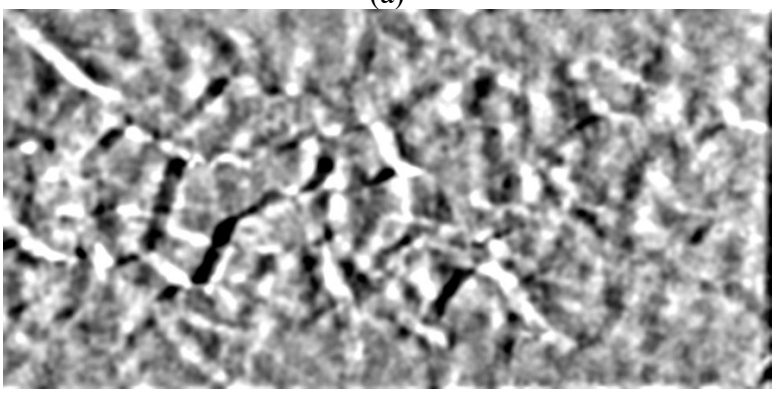

(b)

(c)

Figure A.27 TX3 Section 2 B-X at 272 days after cast (a) original image (b) Image after filtering (c) Image after tracing and Mask

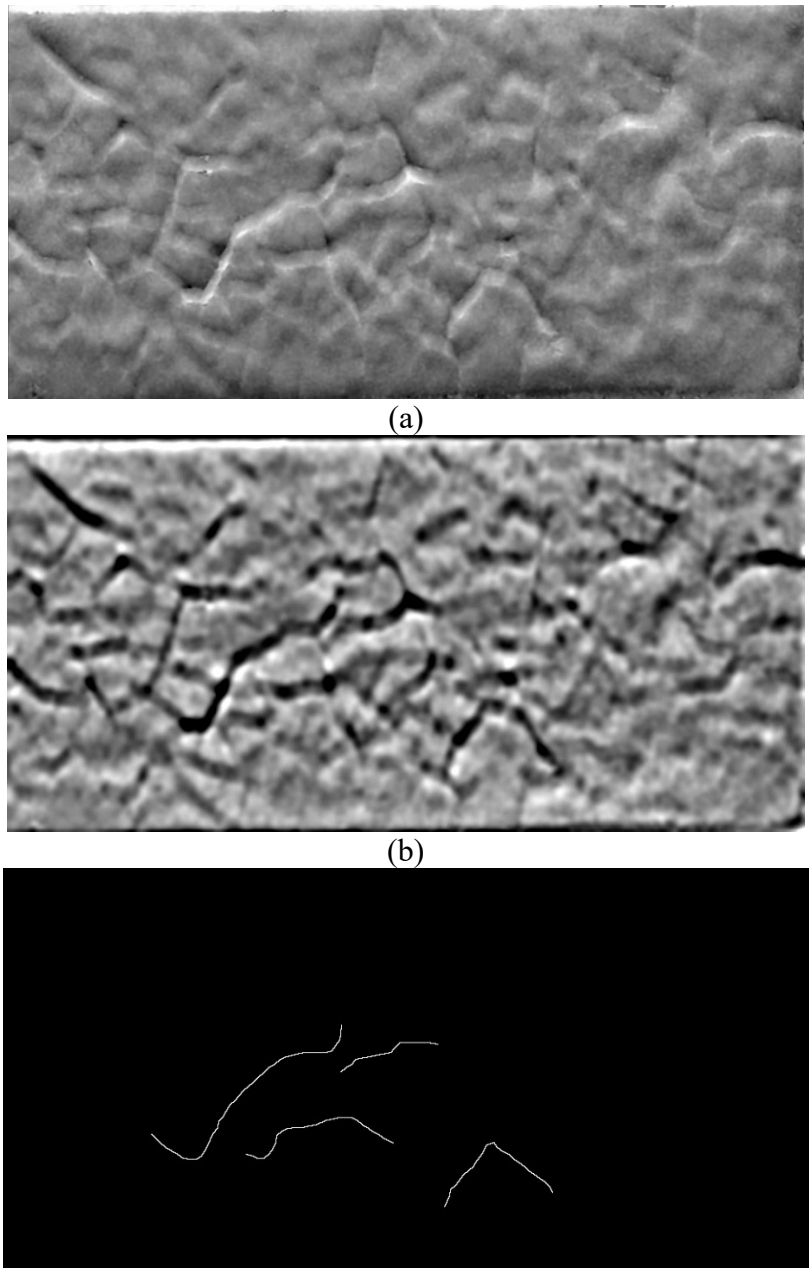

(a)

(b)

(c)

Figure A.28 TX3 Section 2 B-Y at 272 days after cast (a) original image (b) Image after filtering (c) Image after tracing and Mask

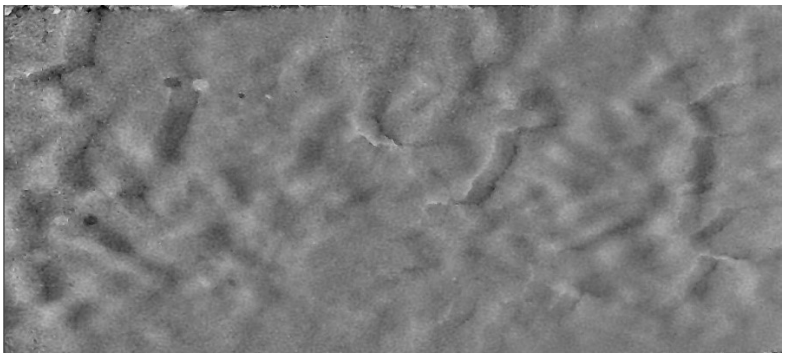

(a)

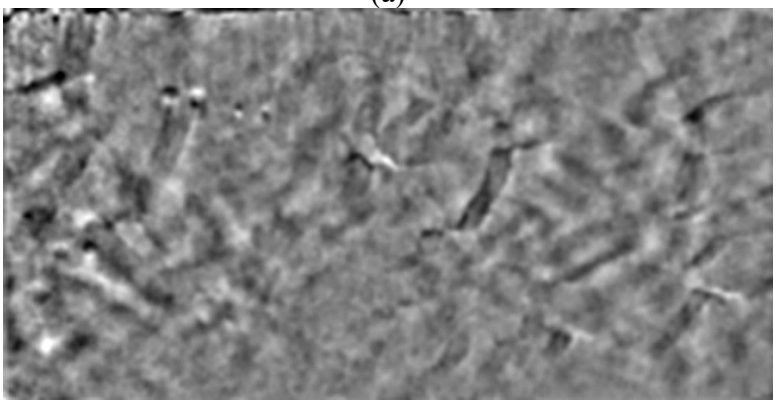

(b)

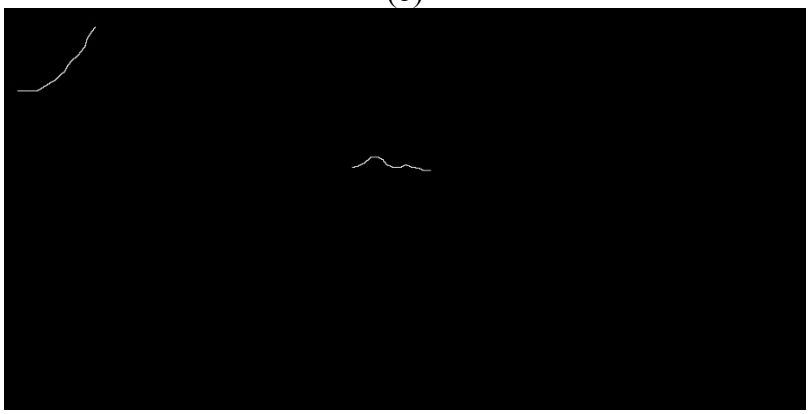

(c)

Figure A.29 TX3 Section 2 B-X at 453 days after cast (a) original image (b) Image after filtering (c) Image after tracing and Mask

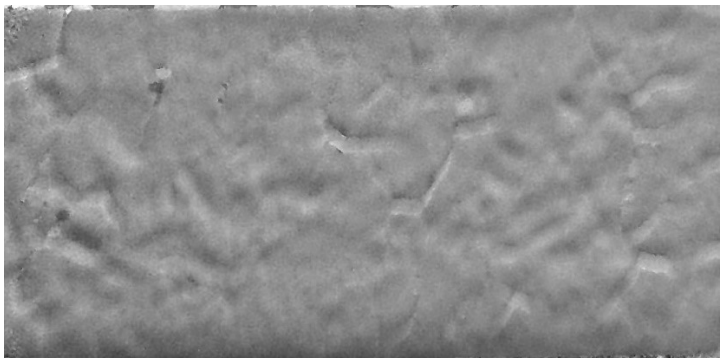

(a)

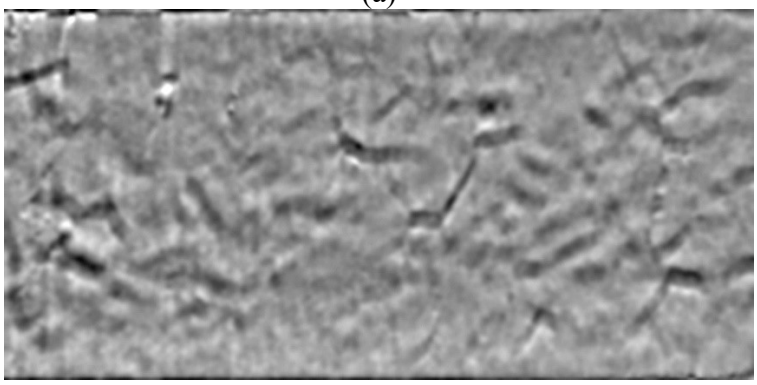

(b)

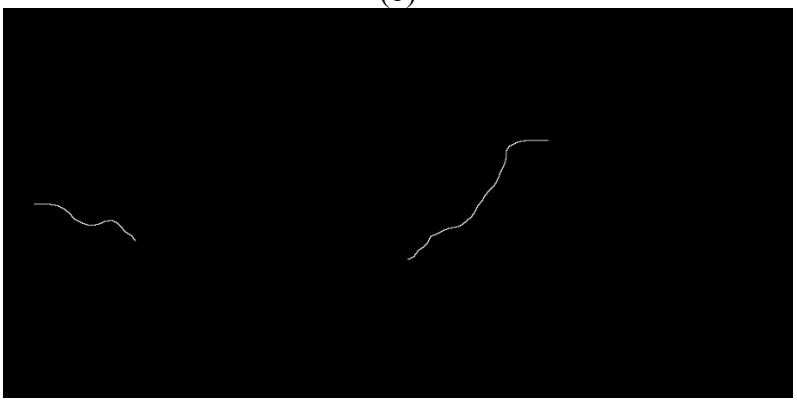

(c)

Figure A.30 TX3 Section 2 B-Y at 453 days after cast (a) original image (b) Image after filtering (c) Image after tracing and Mask

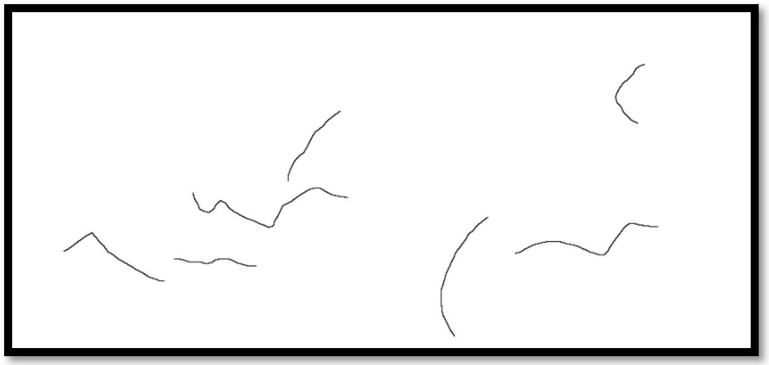

(a)

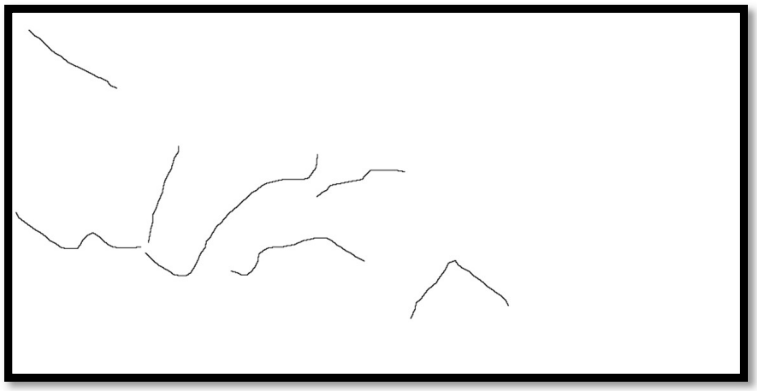

(b)

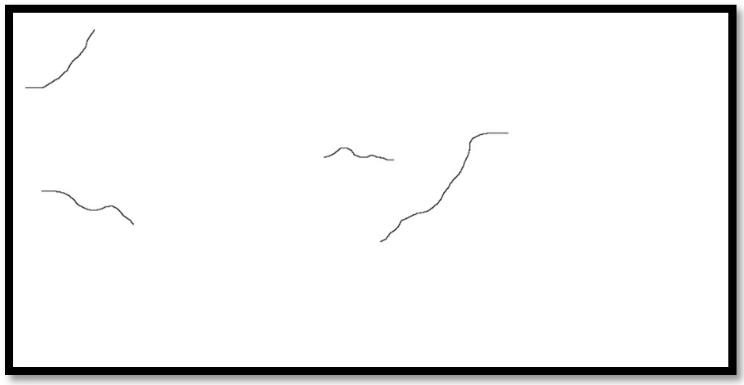

(c)

Figure A.31 Section 2B Tx3 Mask X and Y shear direction combined traced cracks and inverted (a) 45 Days (b) 272 Days (c) 453 Days

Sample Tx4: -

Since only 2 sides of the Prism were used for taking reading throughout all the dates, the images from only 2 sides have been used for this part, the 2 parts were divided into 2 sections A and B.

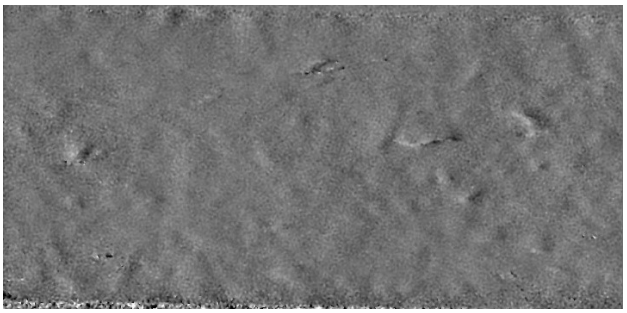

(a)

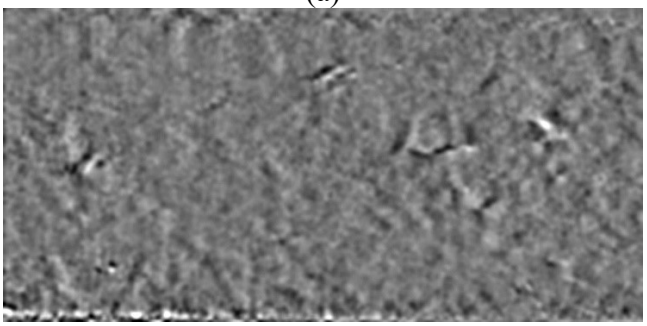

(b)

(c)

Figure A.33 TX4 Section 1A-X at 33 days after cast (a) original image (b) Image after filtering (c) Image after tracing and Mask

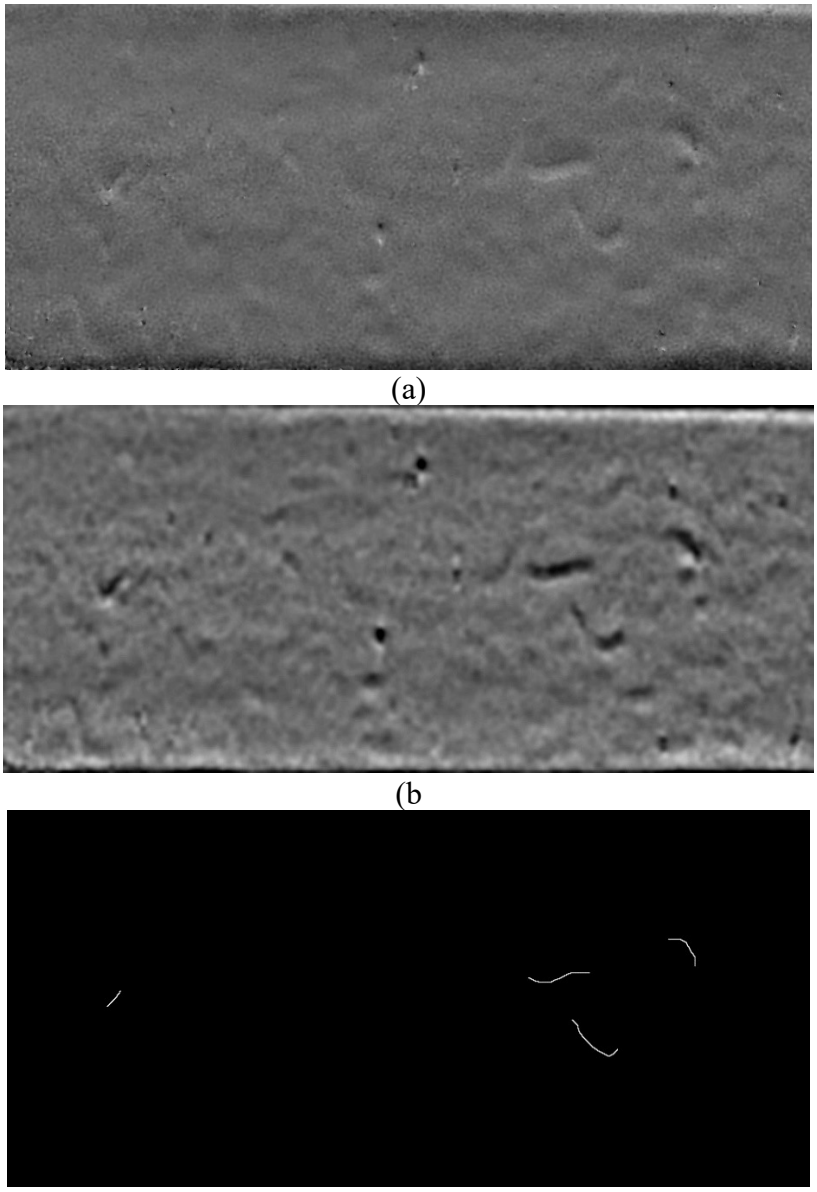

Figure A.34 TX4 Section 1A-Y at 33 days after cast (a) original image (b) Image after filtering (c) Image after tracing and Mask

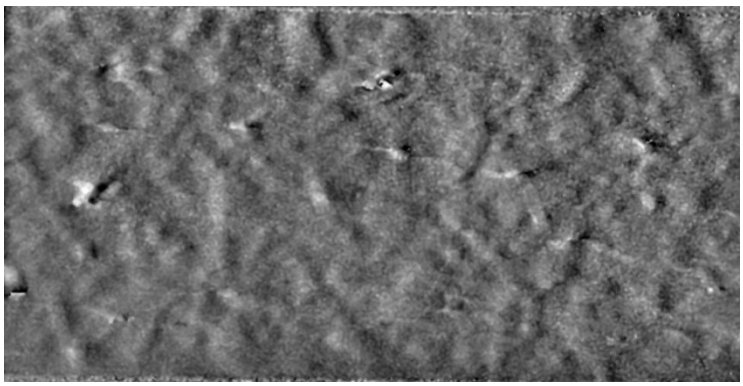

(a)

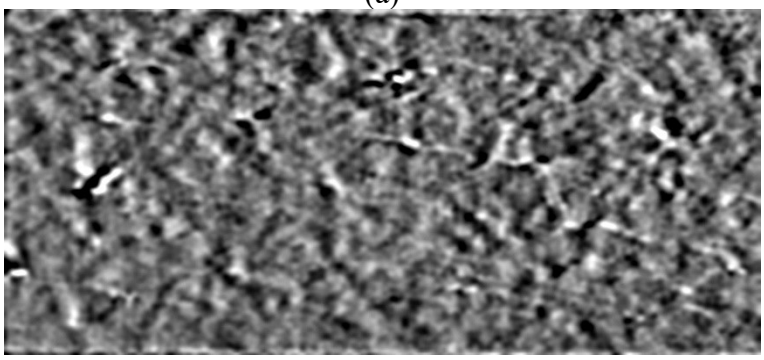

(b)

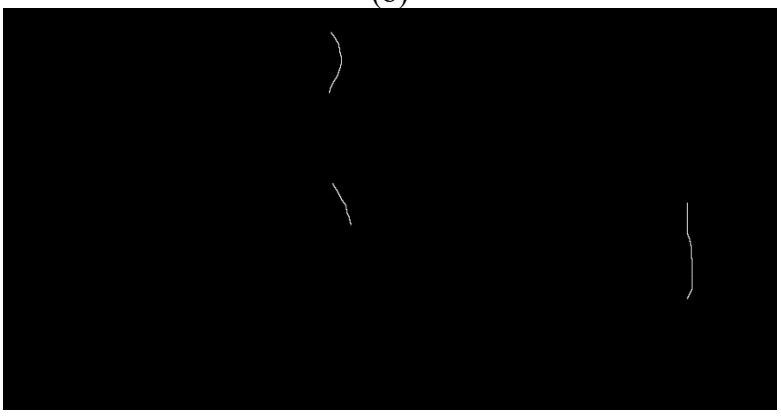

(c)

Figure A.35 TX4 Section 1A-X at 272 days after cast (a) original image (b) Image after filtering (c) Image after tracing and Mask

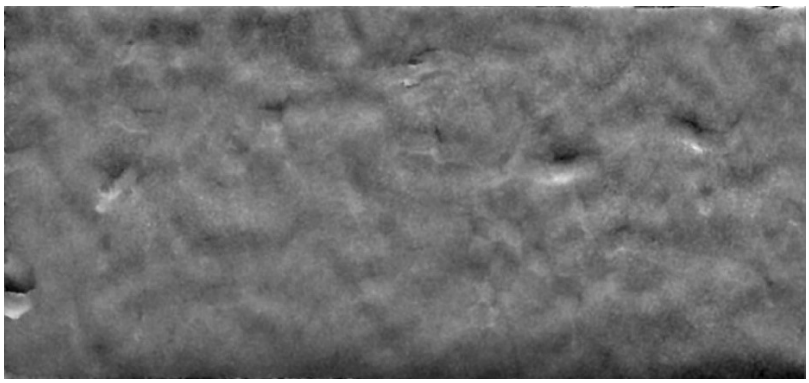

(a)

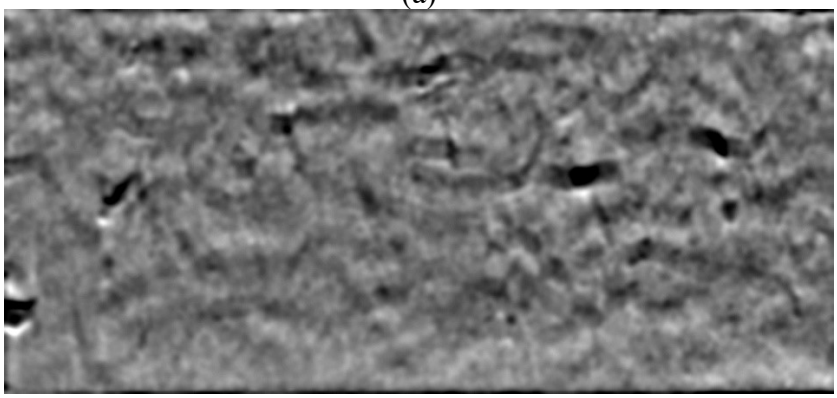

(b)

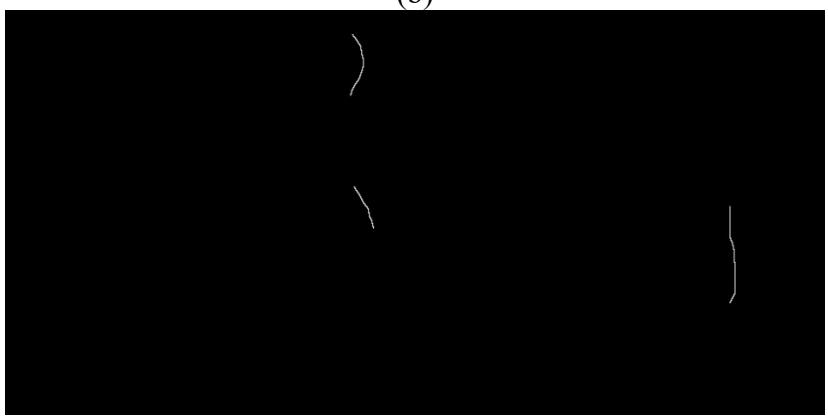

(c)

Figure A.36 TX4 Section 1A-X at 272 days after cast (a) original image (b) Image after filtering (c) Image after tracing and Mask

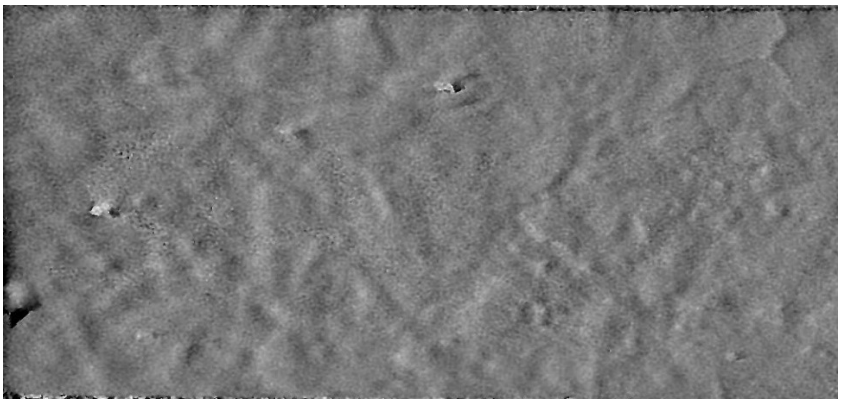

(a)

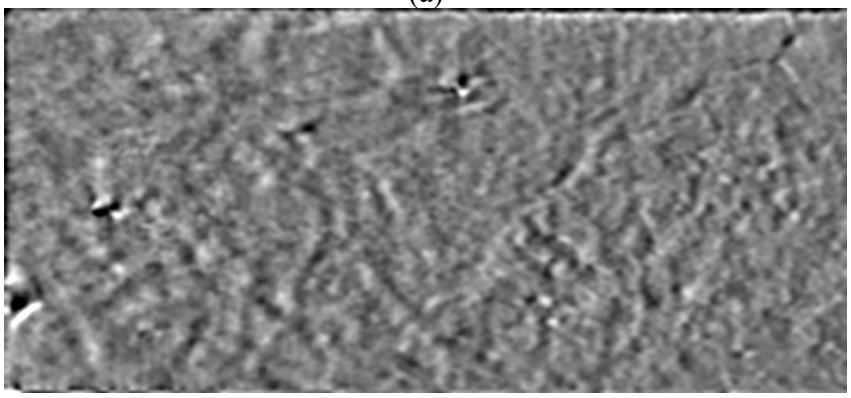

(b)

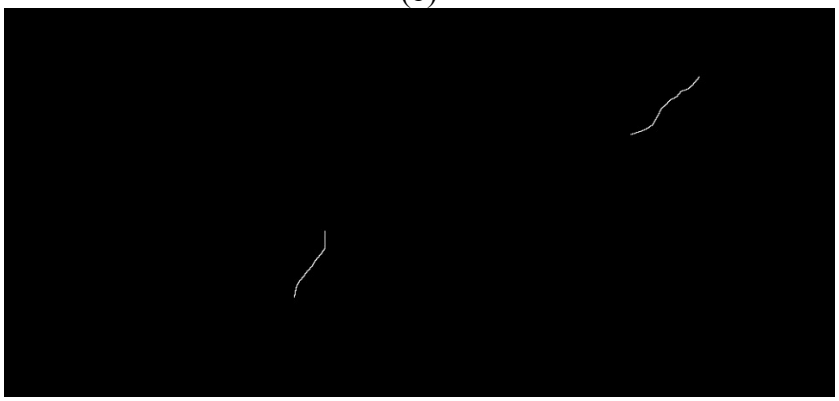

(c)

Figure A.37 TX4 Section 1A-X at 453 days after cast (a) original image (b) Image after filtering (c) Image after tracing and Mask

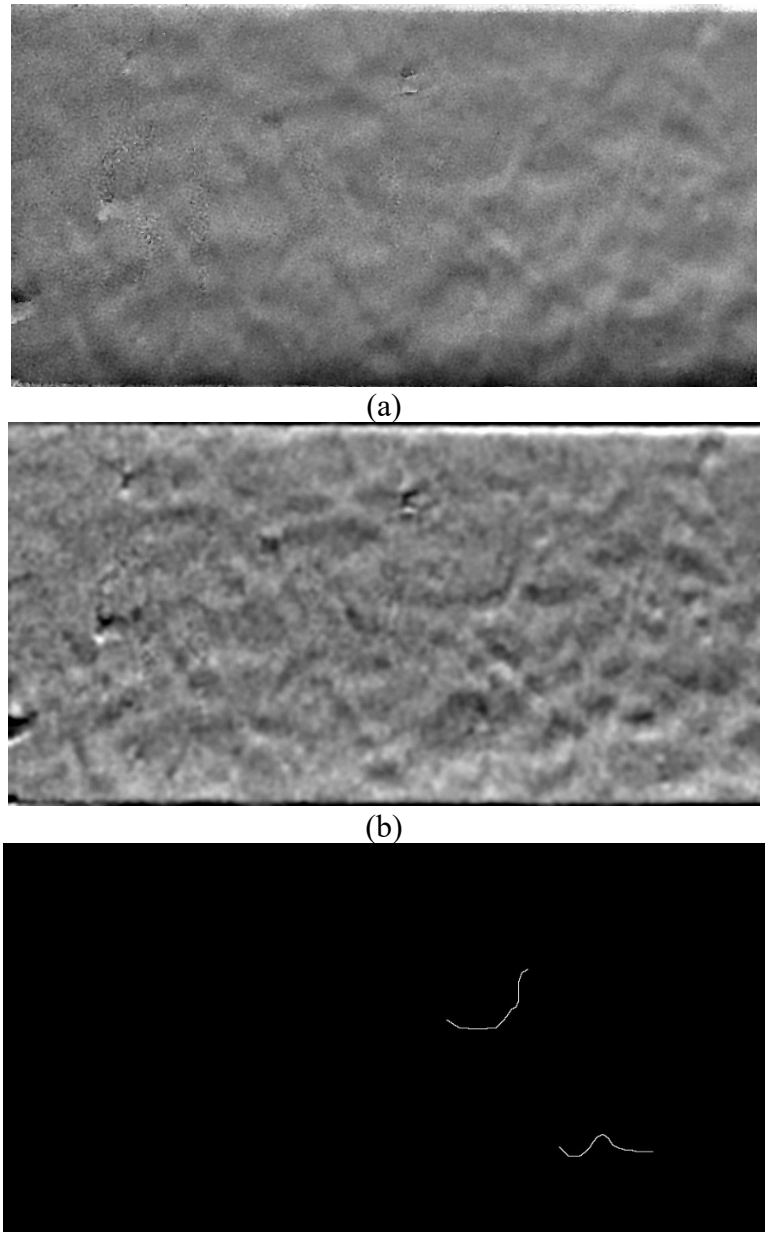

(a)

(b)

(c)

Figure A.38 TX4 Section 1A-Y at 453 days after cast (a) original image (b) Image after filtering (c) Image after tracing and Mask

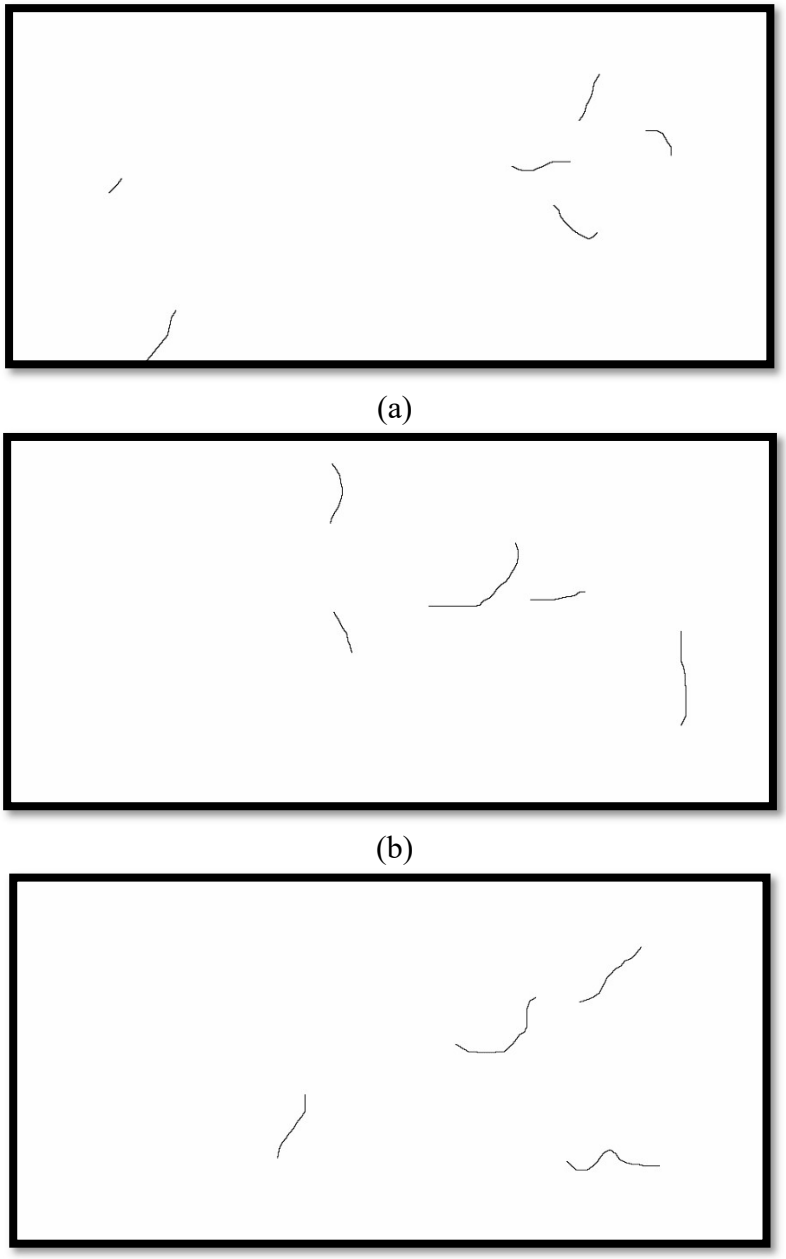

(a)

(b)

(c)

Figure A.39 Section 1A Tx4 Mask X and Y shear direction combined traced cracks and inverted (a) 45 Days (b) 272 Days (c) 453 Days

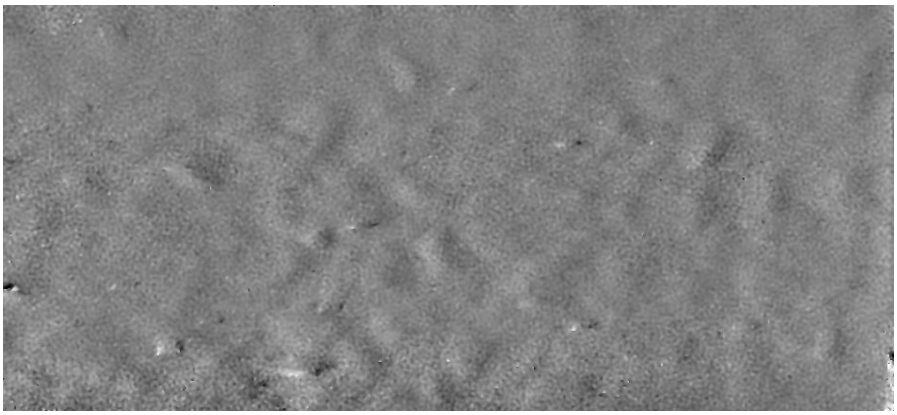

(a)

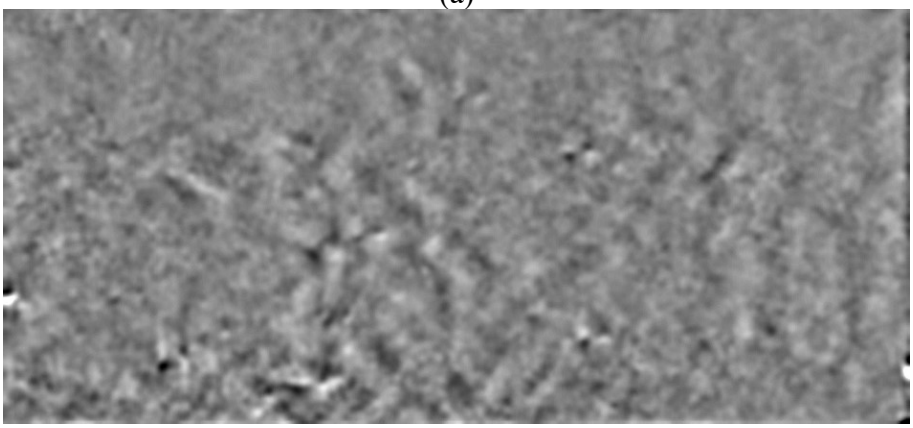

(b)

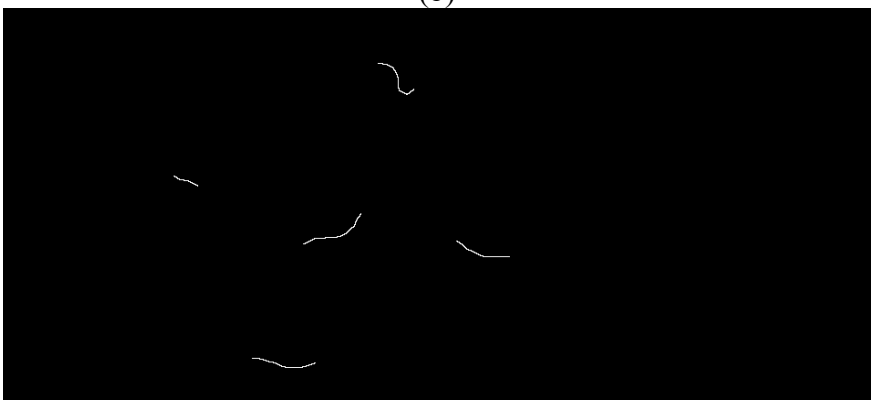

(c)

Figure A.41 TX4 Section 1B-X at 33 days after cast (a) original image (b) Image after filtering (c) Image after tracing and Mask

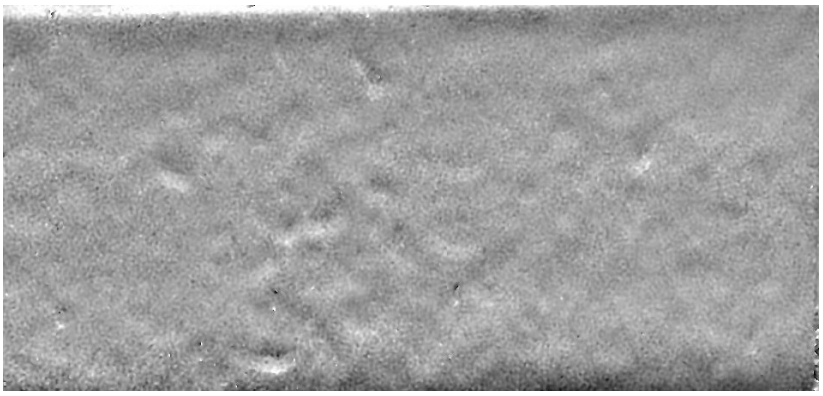

(a)

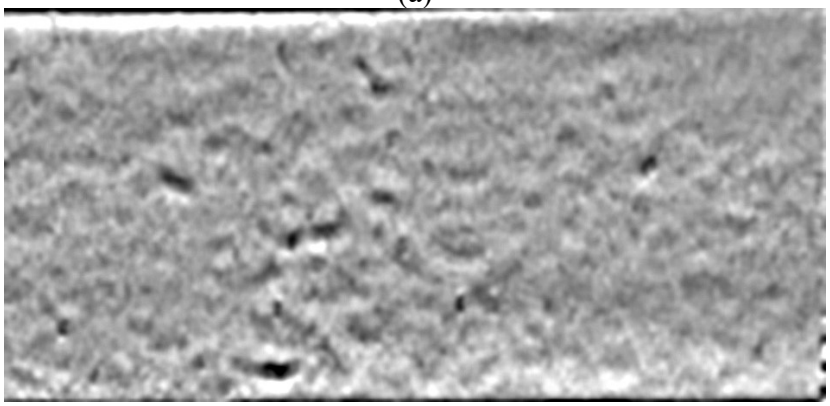

(b)

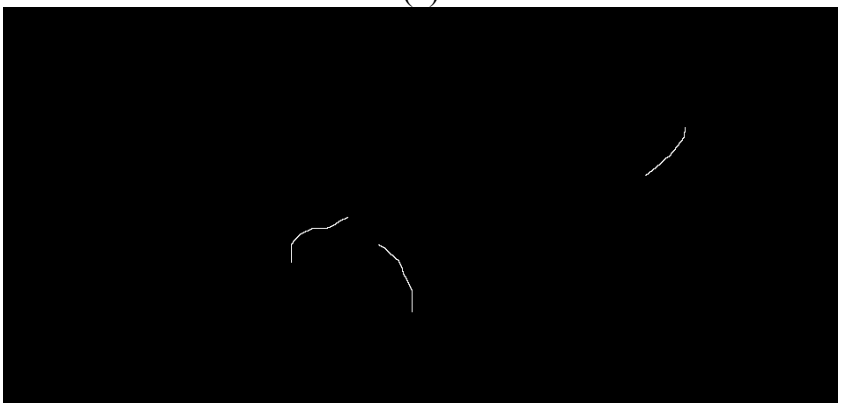

(c)

Figure A.42 TX4 Section 1B-Y at 33 days after cast (a) original image (b) Image after filtering (c) Image after tracing and Mask

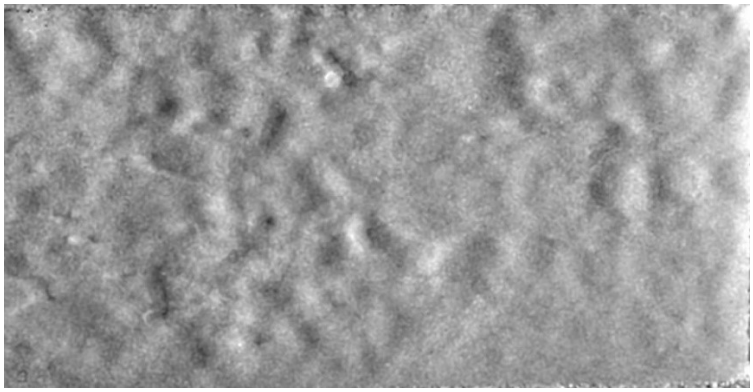

(a)

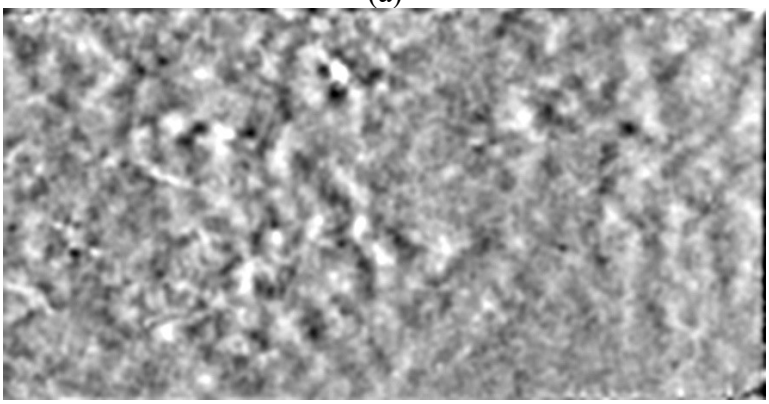

(b)

(c)

Figure A.43 TX4 Section 1B-X at 272 days after cast (a) original image (b) Image after filtering (c) Image after tracing and Mask

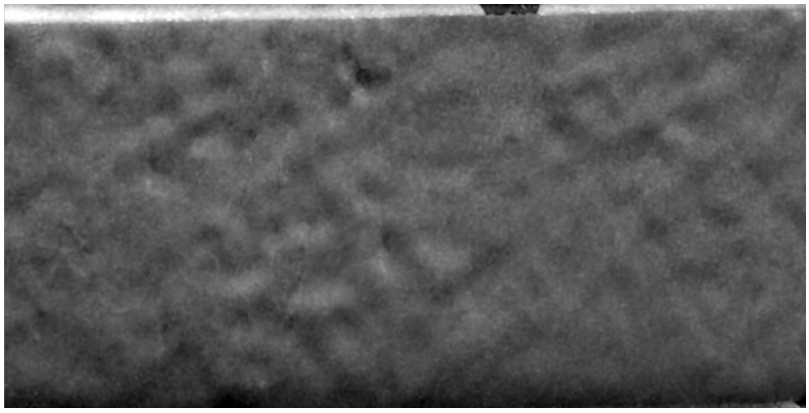

(a)

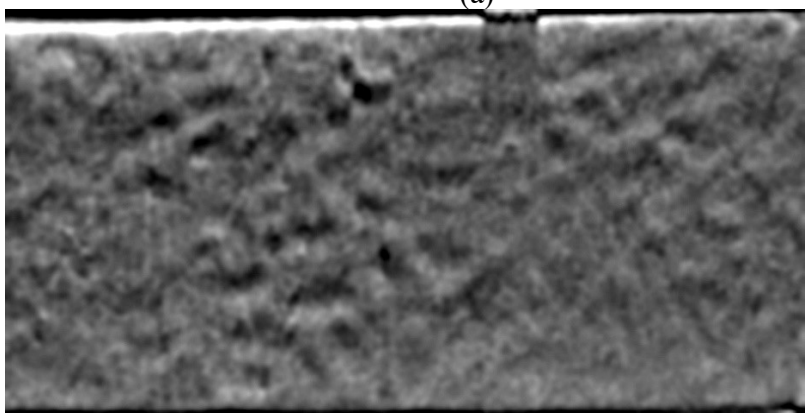

(b)

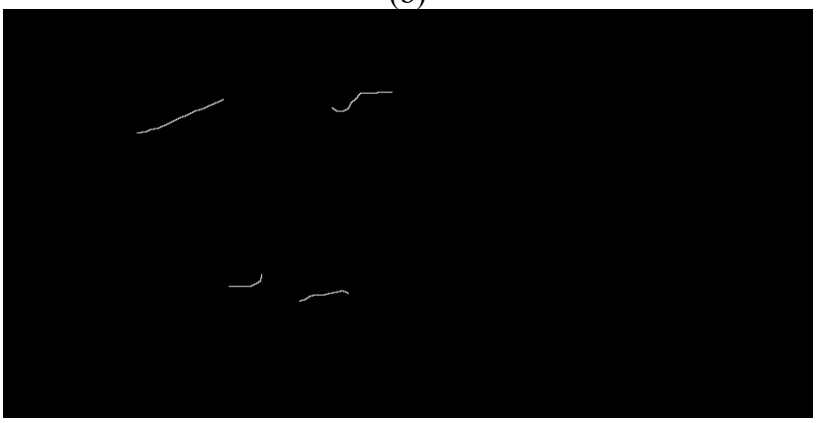

(c)

Figure A.44 TX4 Section 1B-Y at 272 days after cast (a) original image (b) Image after filtering (c) Image after tracing and Mask

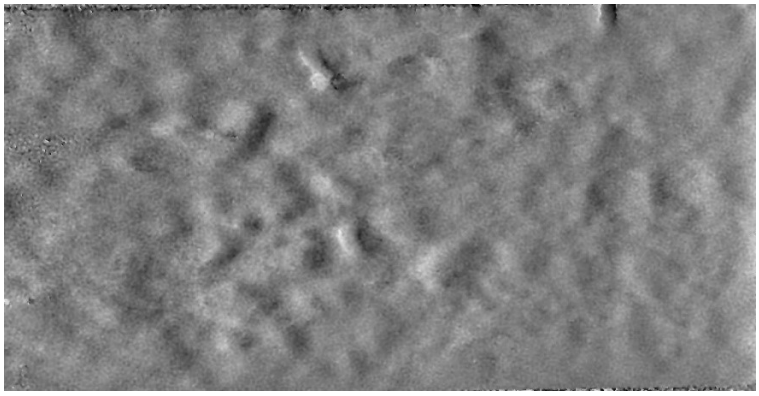

(a)

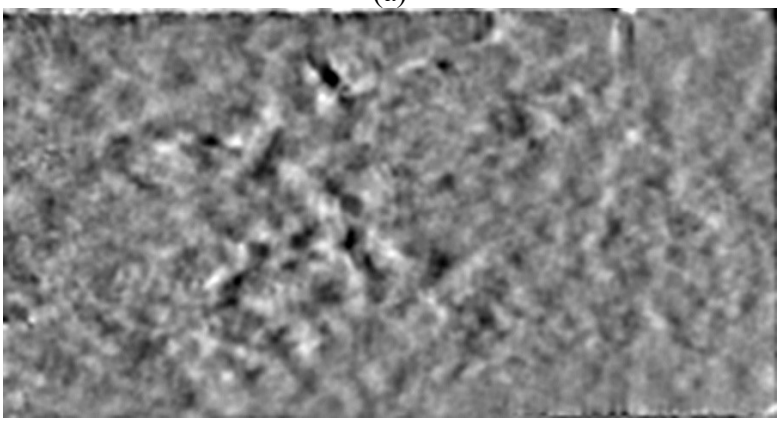

(b)

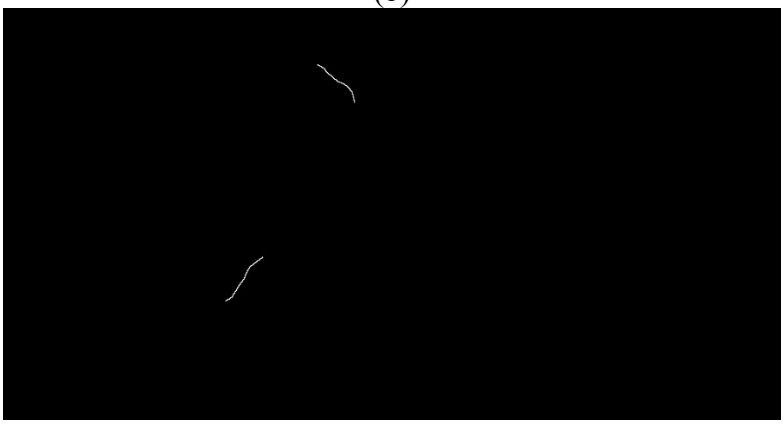

(c)

Figure A.45 TX4 Section 1B-X at 453 days after cast (a) original image (b) Image after filtering (c) Image after tracing and Mask

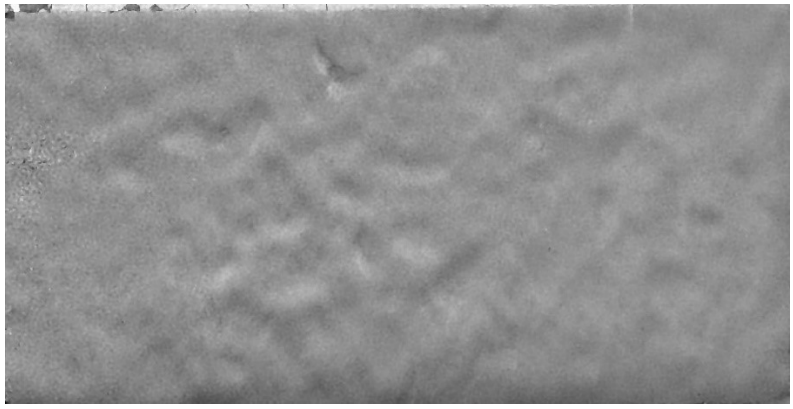

(a)

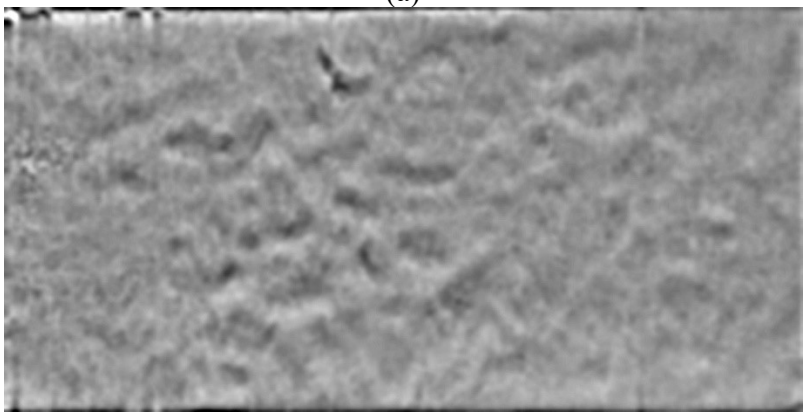

(b)

(c)

Figure A.46 TX4 Section 1B-Y at 453 days after cast (a) original image (b) Image after filtering (c) Image after tracing and Mask

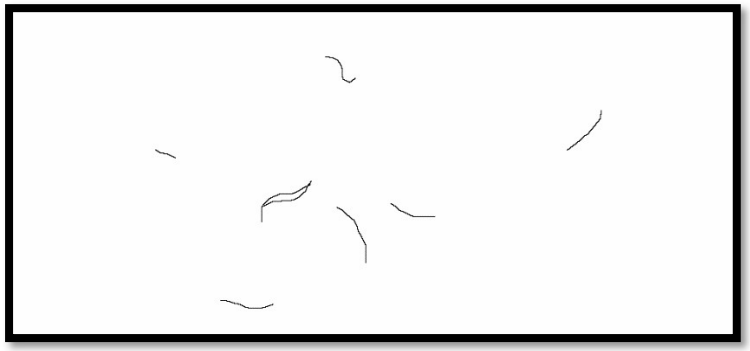

(a)

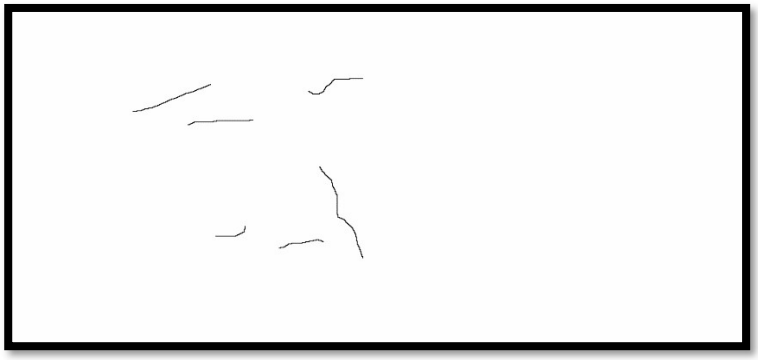

(b)

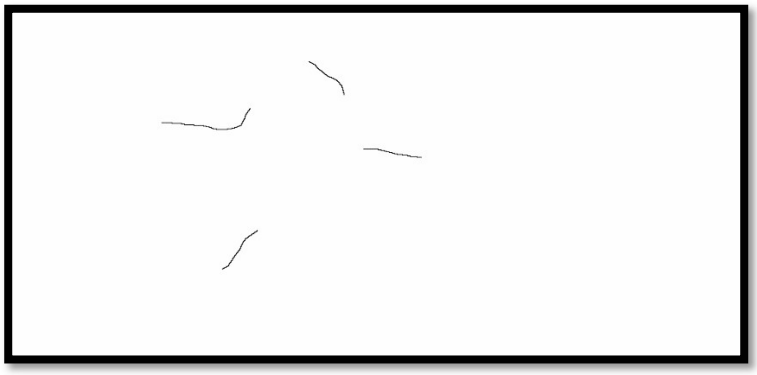

(c)

Figure A.47 Section 1B Tx4 Mask X and Y shear direction combined traced cracks and inverted (a) 45 Days (b) 272 Days (c) 453 Days

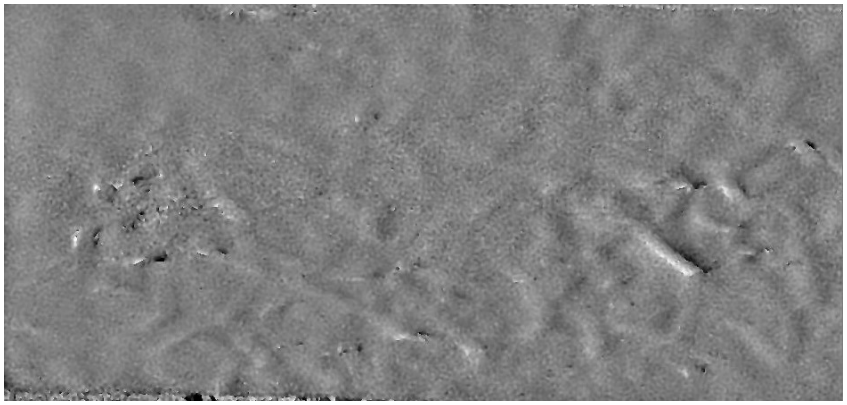

(a)

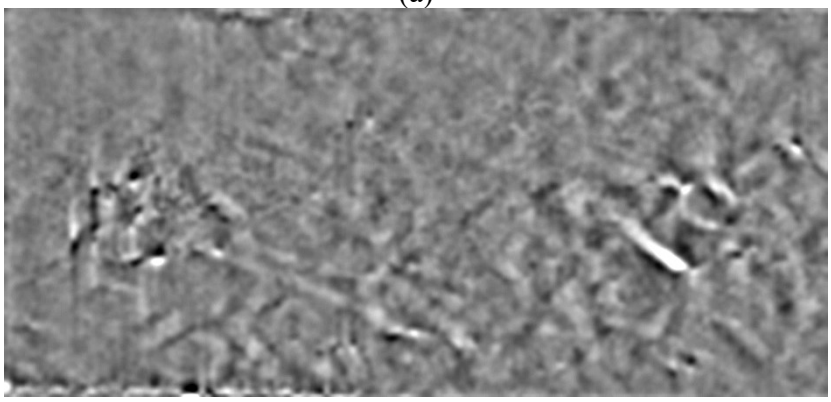

(b)

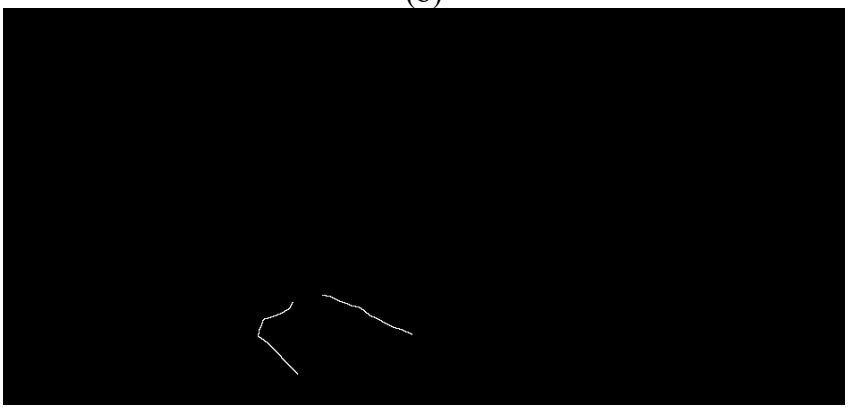

(c)

Figure A.49 TX4 Section 2A-X at 33 days after cast (a) original image (b) Image after filtering (c) Image after tracing and Mask

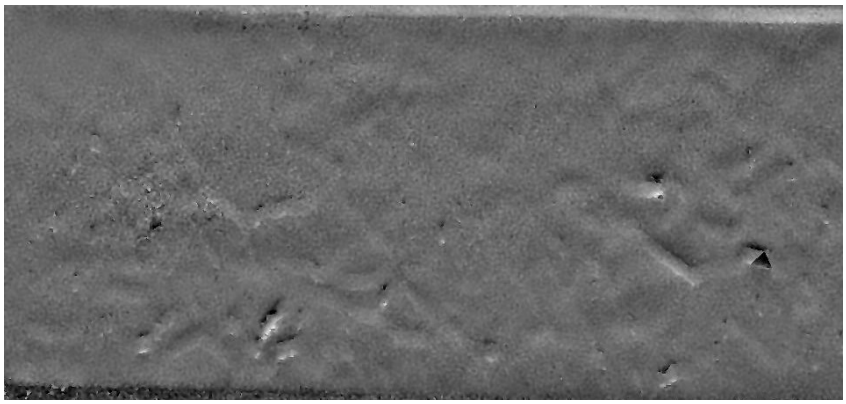

(a)

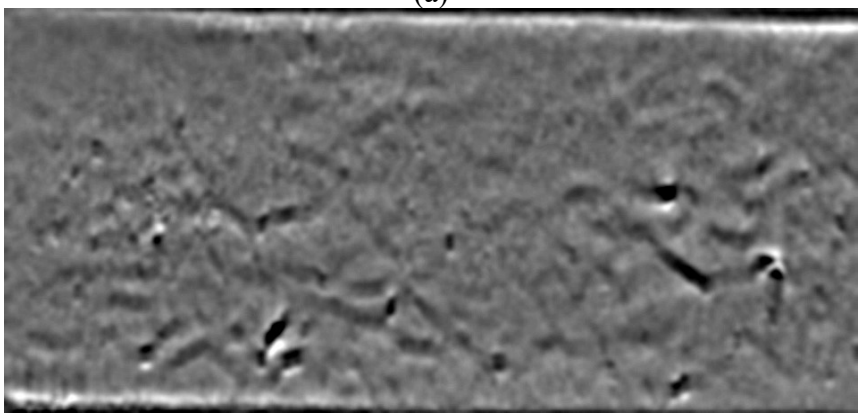

(b)

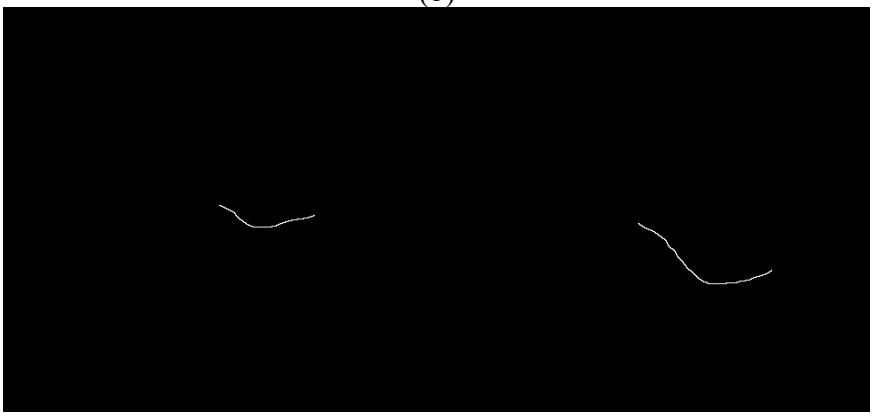

(c)

Figure A.50 TX4 Section 2A-Y at 33 days after cast (a) original image (b) Image after filtering (c) Image after tracing and Mask

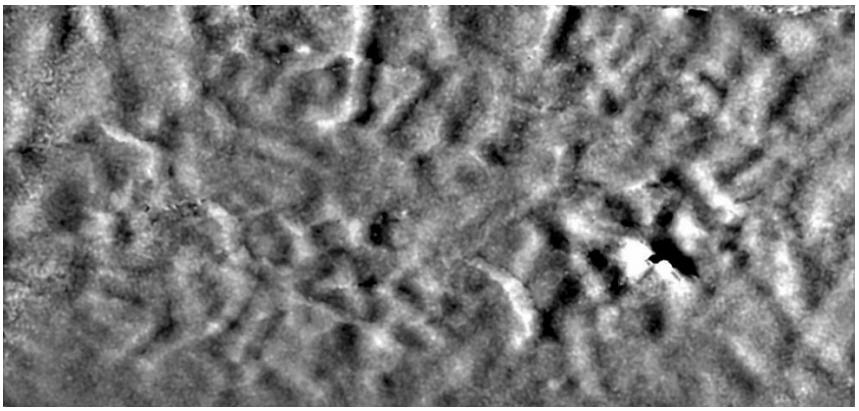

(a)

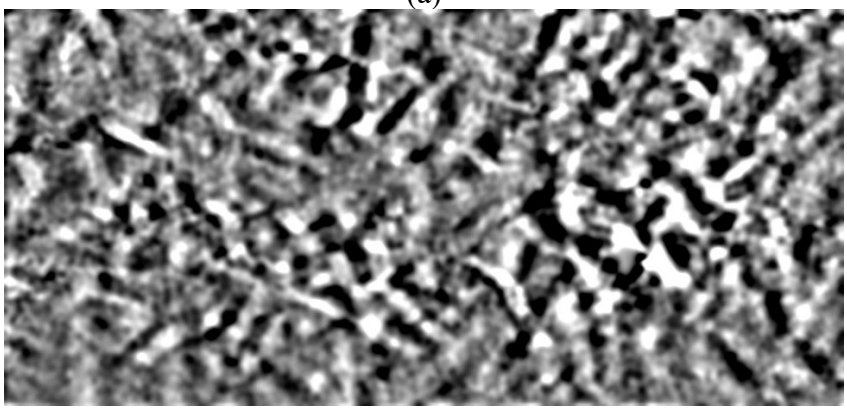

(b)

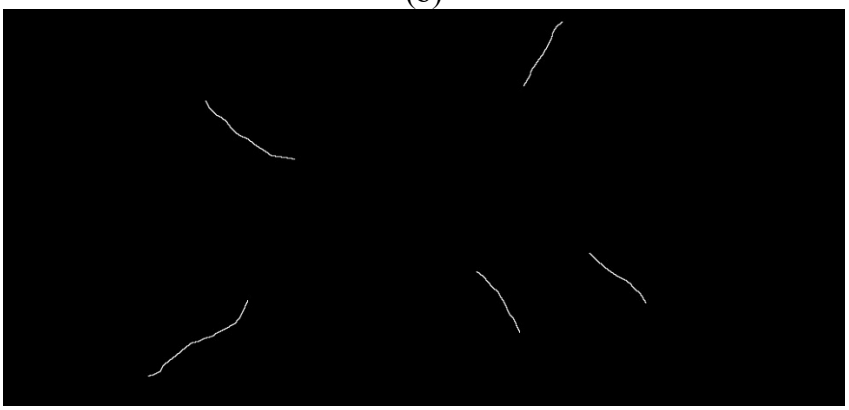

(c)

Figure A.51 TX4 Section 2A-X at 272 days after cast (a) original image (b) Image after filtering (c) Image after tracing and Mask

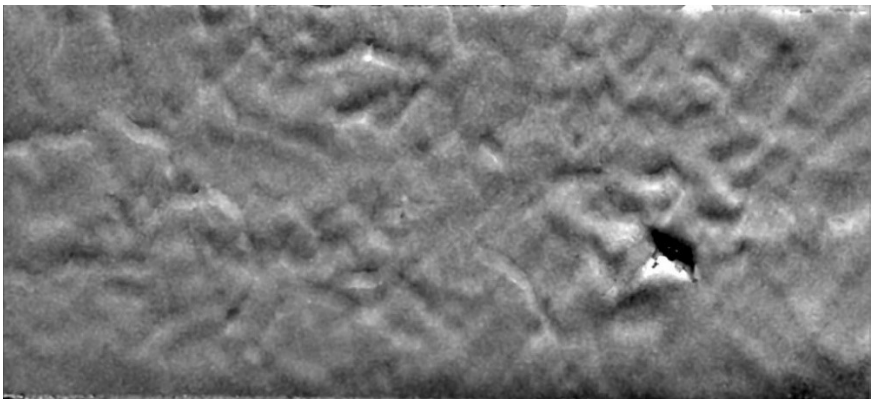

(a)

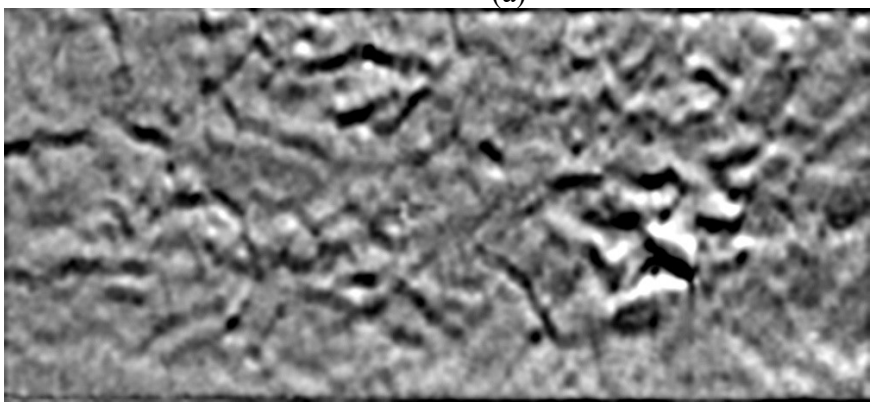

(b)

(c)

Figure A.52 TX4 Section 2A-Y at 272 days after cast (a) original image (b) Image after filtering (c) Image after tracing and Mask

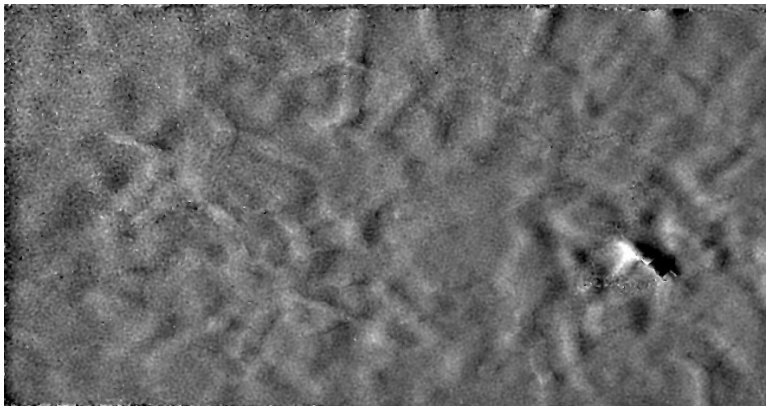

(a)

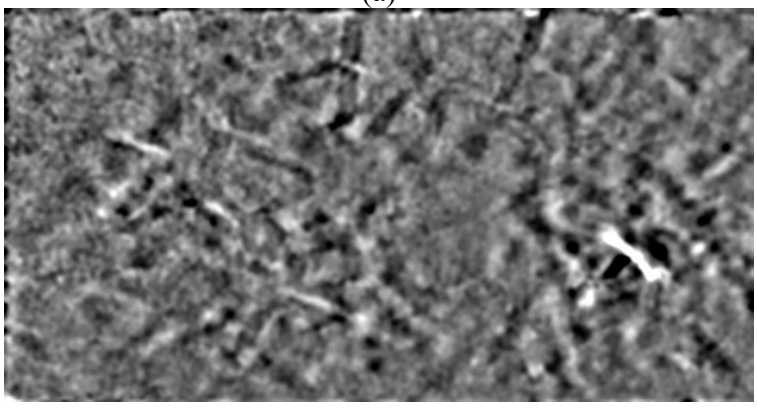

(b)

(c)

Figure A.53 TX4 Section 2A-X at 453 days after cast (a) original image (b) Image after filtering (c) Image after tracing and Mask

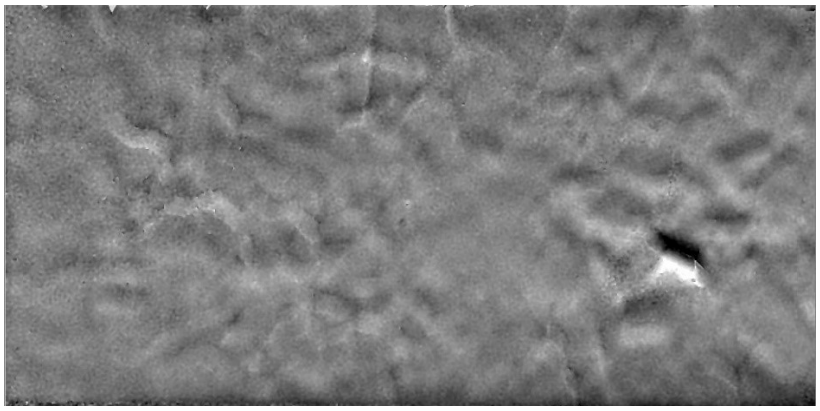

(a)

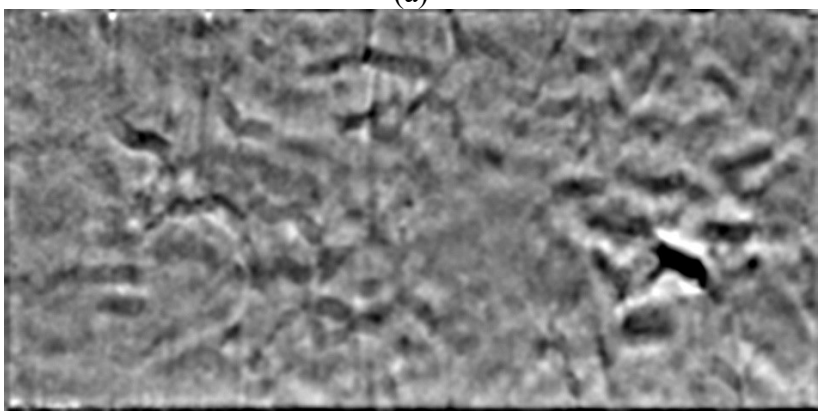

(b)

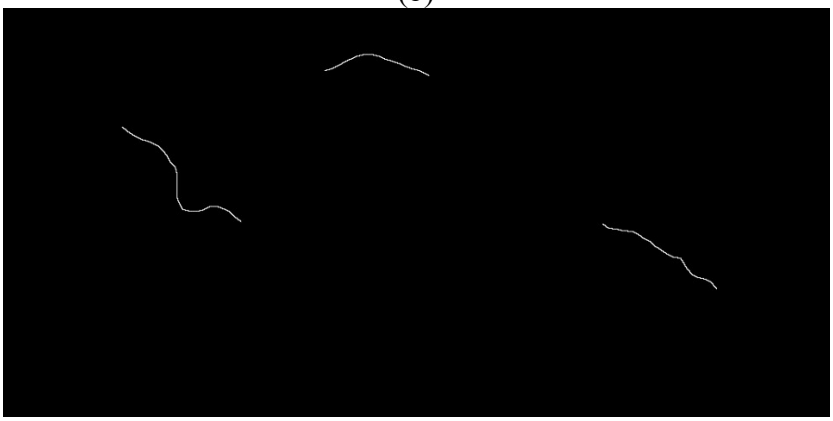

(c)

Figure A.54 TX4 Section 2A-Y at 453 days after cast (a) original image (b) Image after filtering (c) Image after tracing and Mask

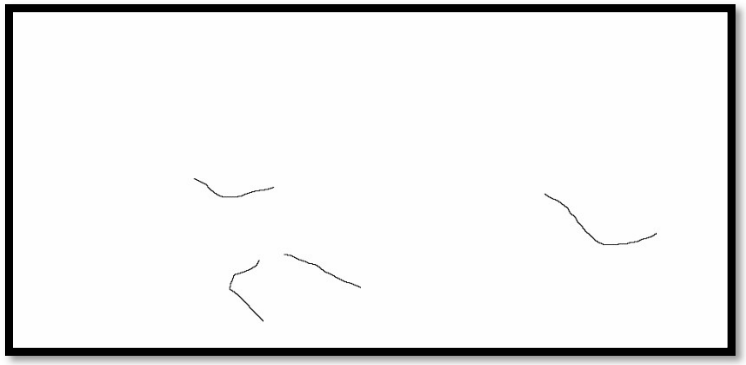

(a)

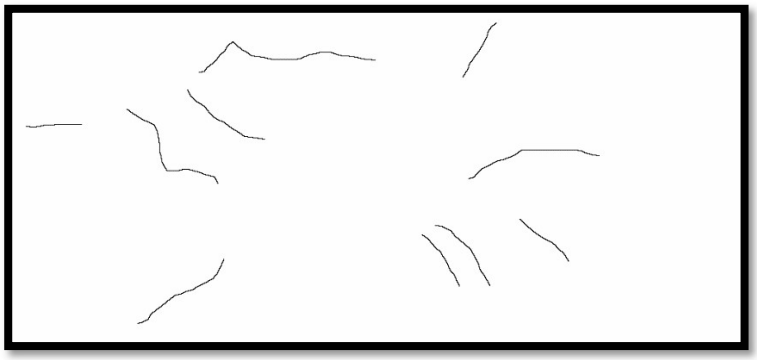

(b)

(c)

Figure A.55 Section 2A Tx4 Mask X and Y shear direction combined traced cracks and inverted (a) 45 Days (b) 272 Days (c) 453 Days

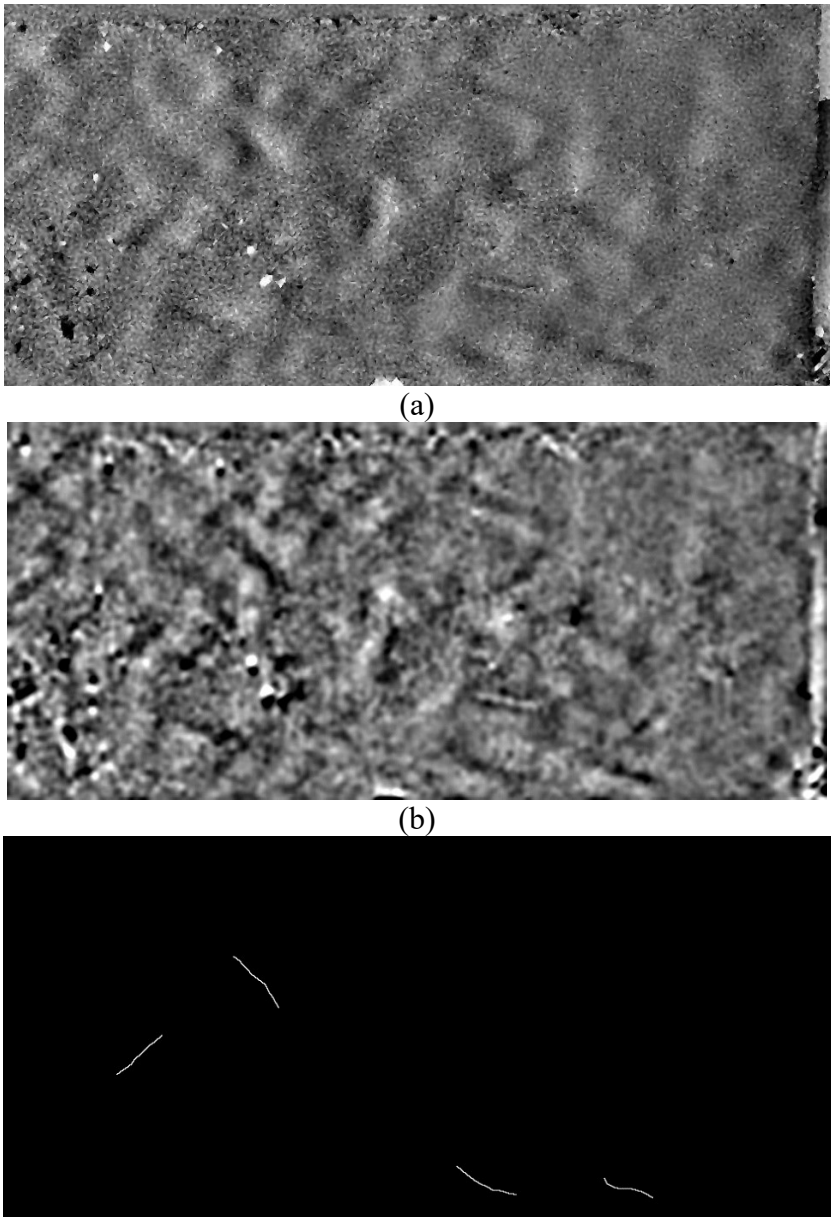

Figure A.57 TX4 Section 2B-X at 33 days after cast (a) original image (b) Image after filtering (c) Image after tracing and Mask

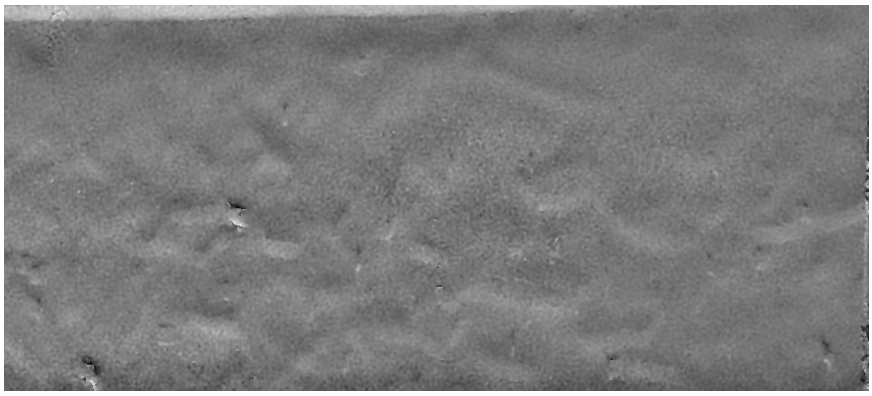

(a)

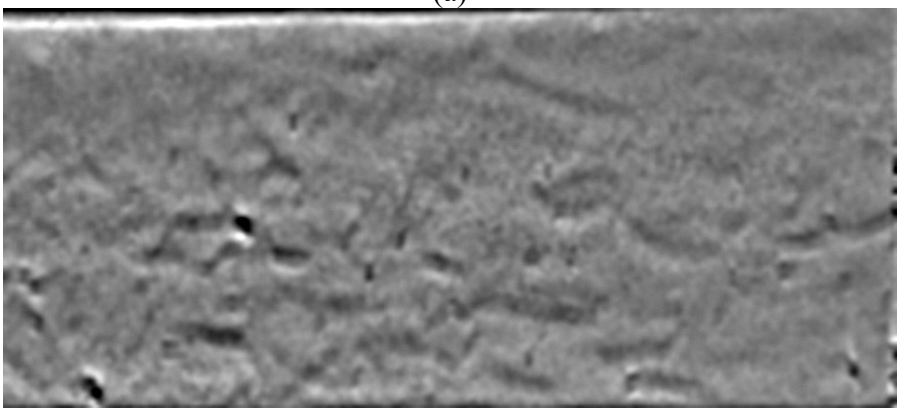

(b)

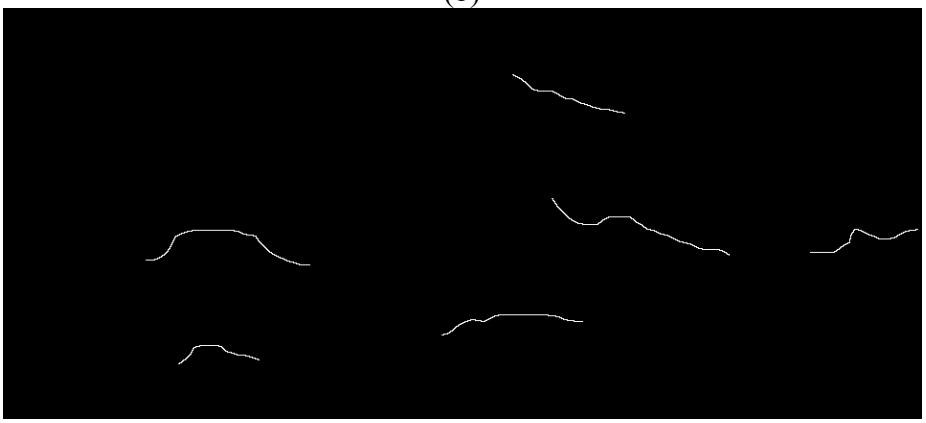

(c)

Figure A.58 TX4 Section 2B-Y at 33 days after cast (a) original image (b) Image after filtering (c) Image after tracing and Mask

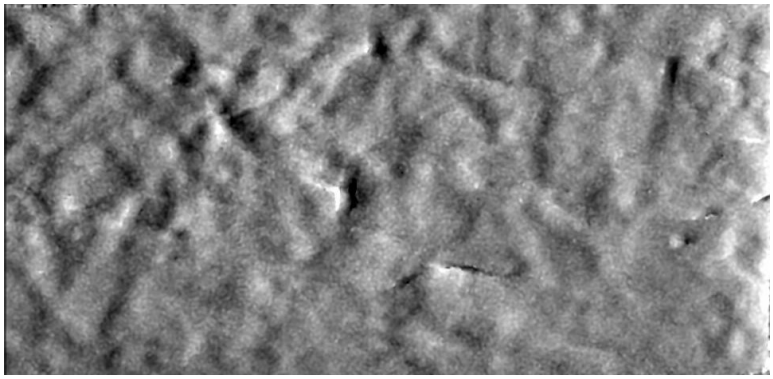

(a)

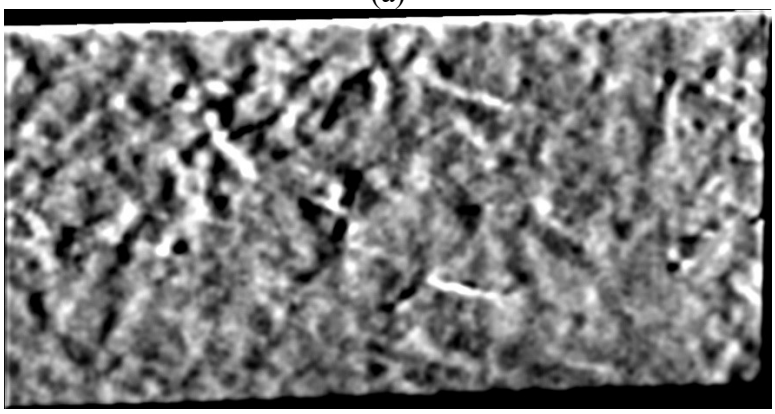

(b)

(c)

Figure A.59 TX4 Section 2B-X at 272 days after cast (a) original image (b) Image after filtering (c) Image after tracing and Mask

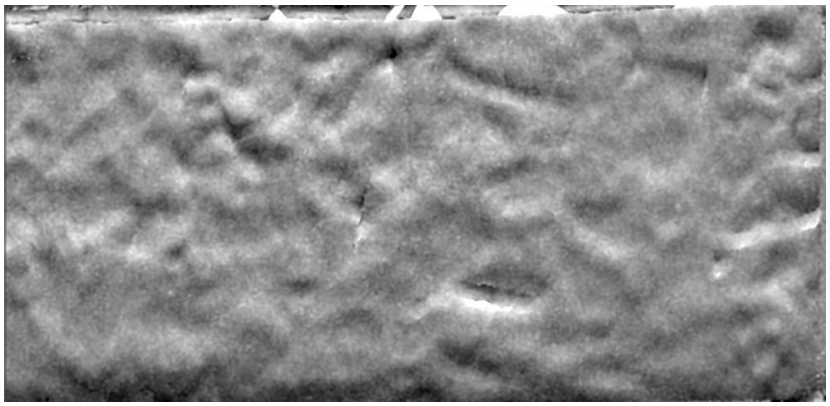

(a)

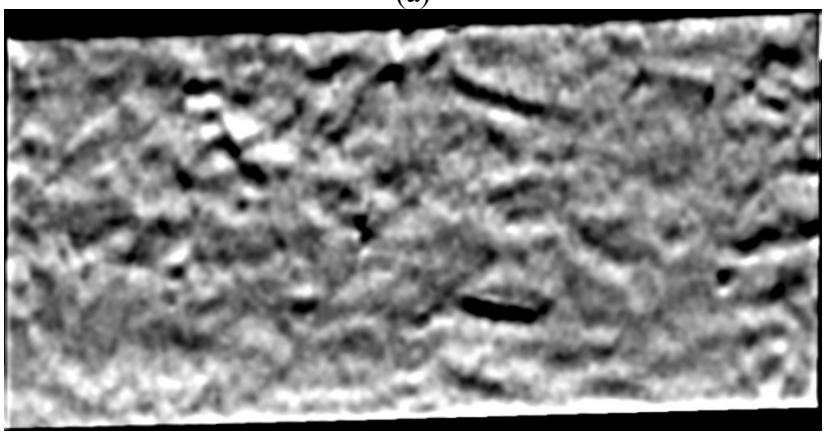

(b)

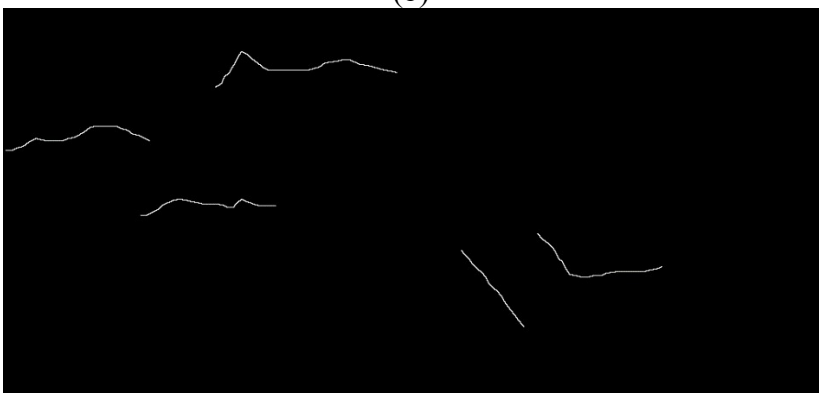

(c)

Figure A.60 TX4 Section 2B-Y at 272 days after cast (a) original image (b) Image after filtering (c) Image after tracing and Mask

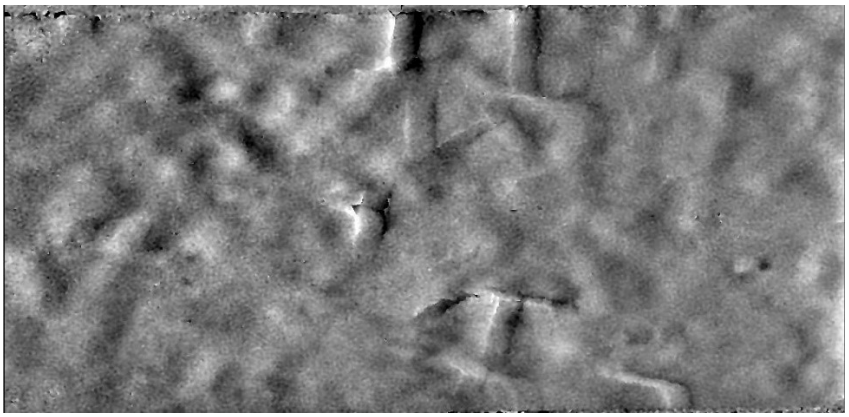

Tx4 Section 2 B-X, 453 Days from casting

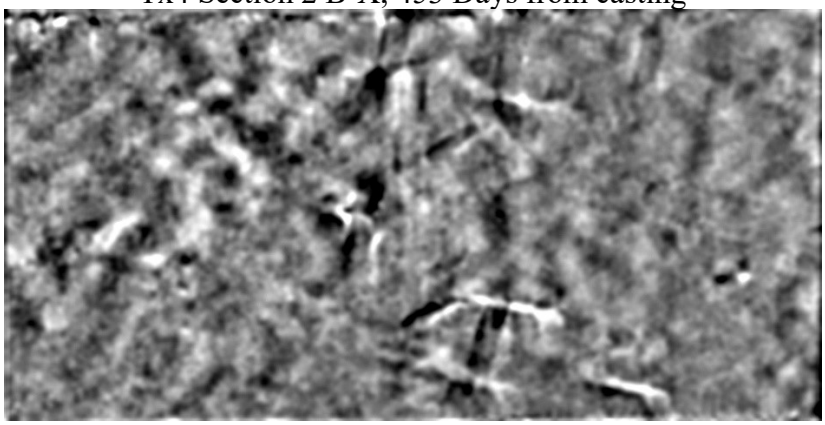

Tx4 Section 2 B-X, 453 Days from casting after filtering

Tx4 Section 2 B-X, 453 Days from casting after filtering and mask

Figure A.61 TX4 Section 2B-X at 453 days after cast (a) original image (b) Image after filtering (c) Image after tracing and Mask

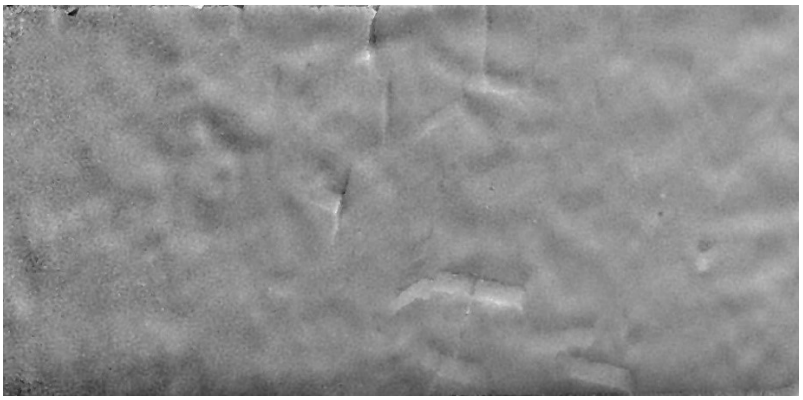

(a)

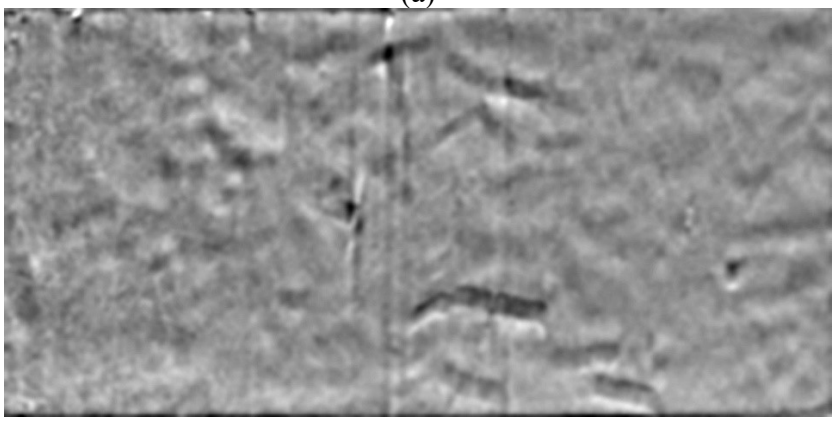

(b)

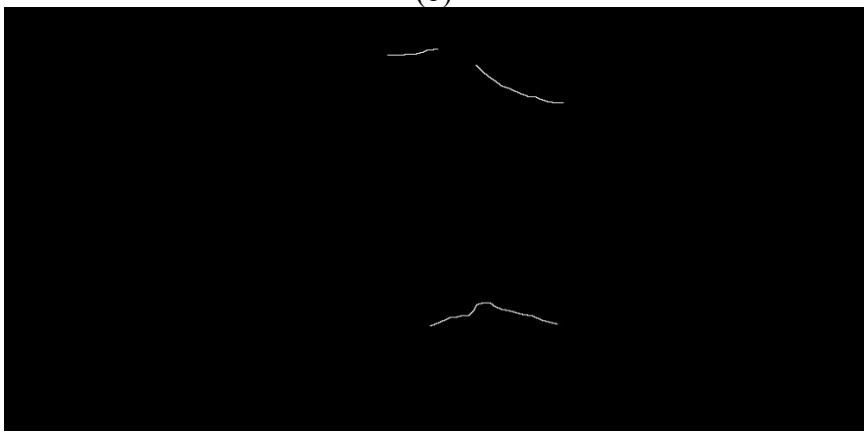

(c)

Figure A.62 TX4 Section 2B-Y at 453 days after cast (a) original image (b) Image after filtering (c) Image after tracing and Mask

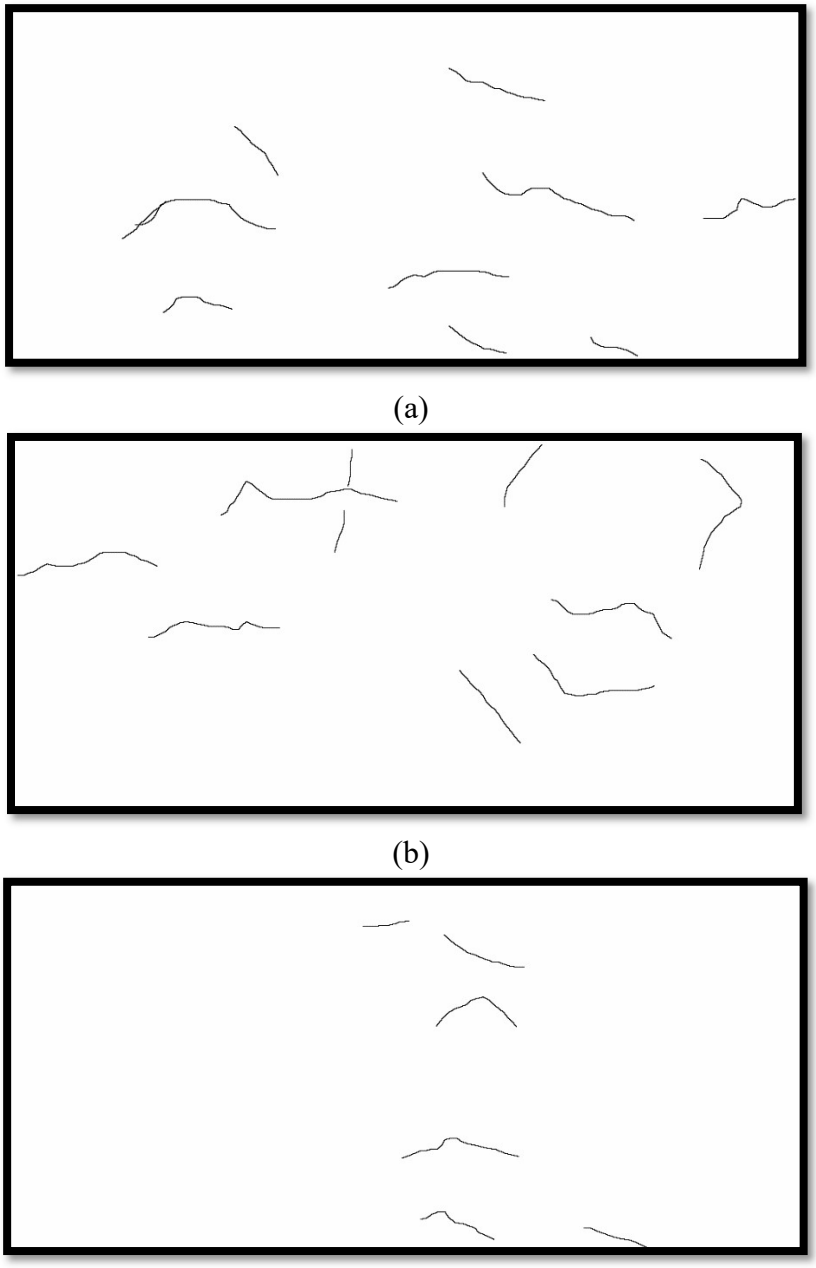

(a)

(b)

(c)

Figure A.63 Section 2B TX4 Mask X and Y shear direction combined traced cracks and inverted (a) 45 Days (b) 272 Days (c) 453 Days

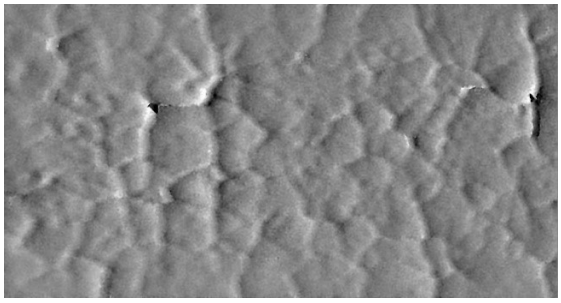

(a)

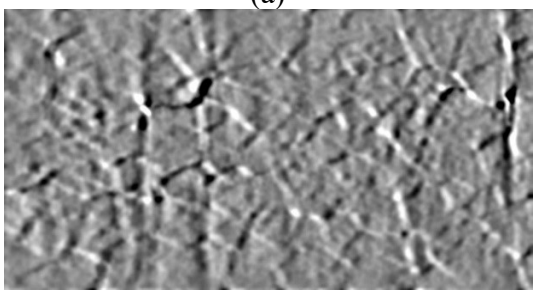

(b)

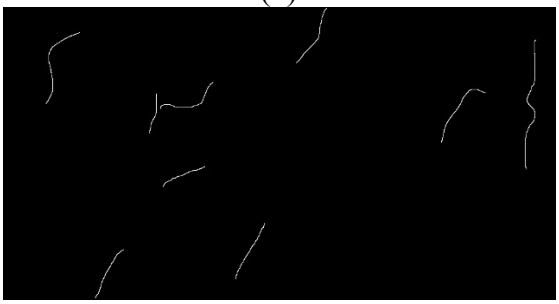

(c)

Figure A.65 TX1 Section 1A-X at 45 days after cast (a) original image (b) Image after filtering (c) Image after tracing and Mask

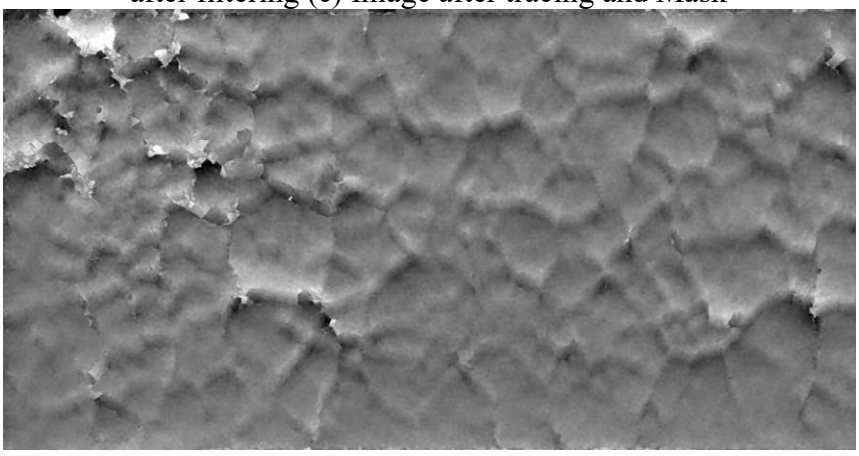

(a)

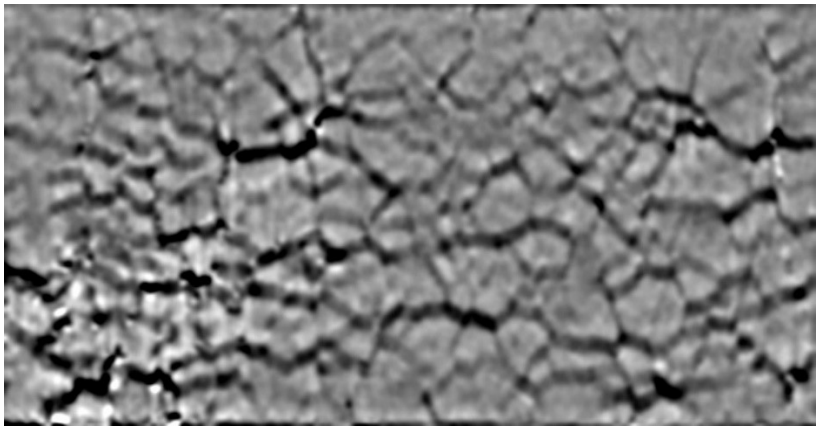

(b)

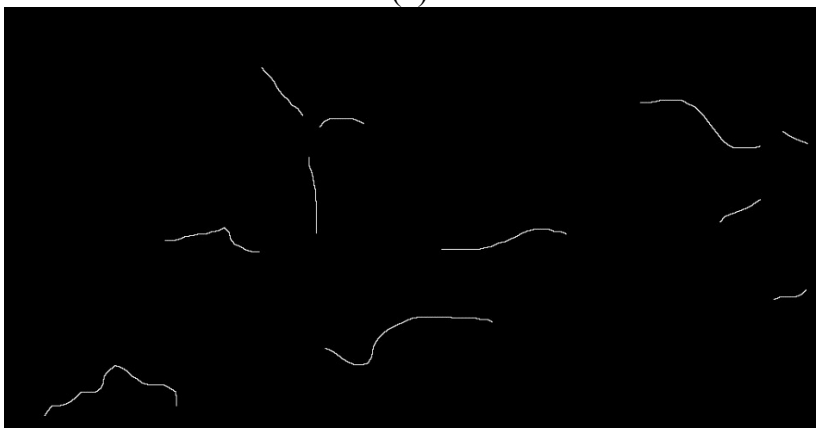

(c)

Figure A.66 TX1 Section 1A-Y at 45 days after cast (a) original image (b) Image after filtering (c) Image after tracing and Mask

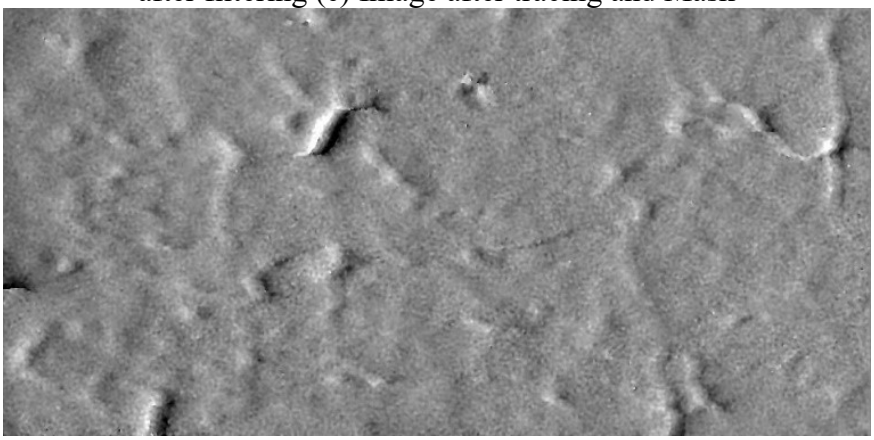

(a)

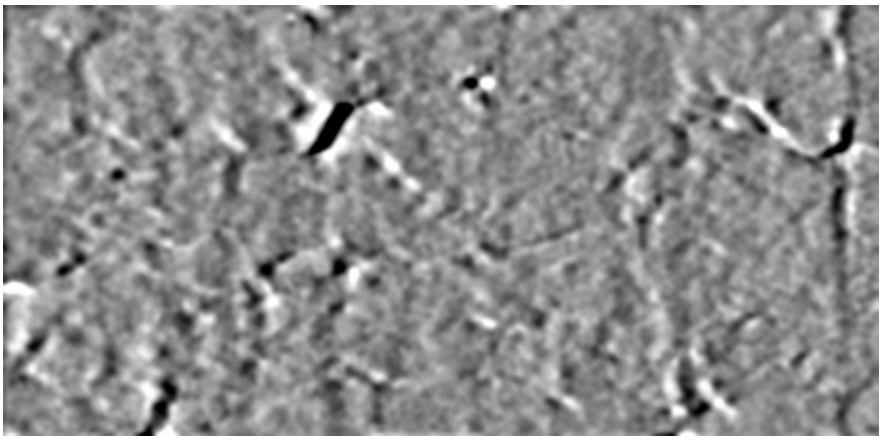

(b)

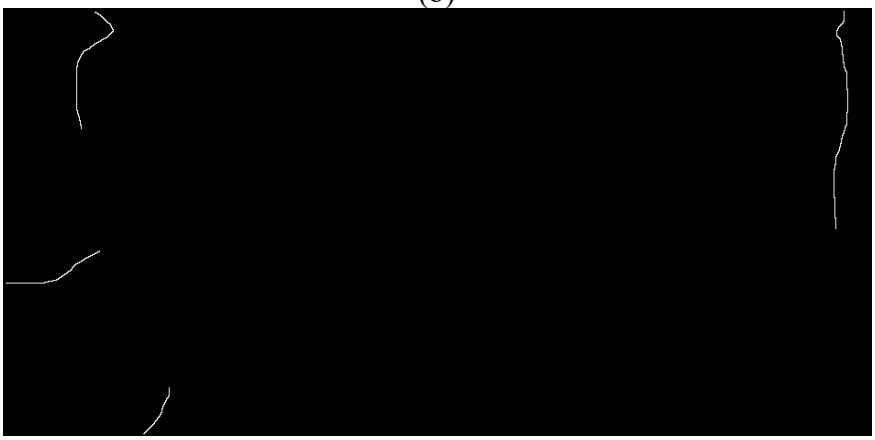

(c)

Figure A.67 TX1 Section 1A-X at 97 days after cast (a) original image (b) Image after filtering (c) Image after tracing and Mask

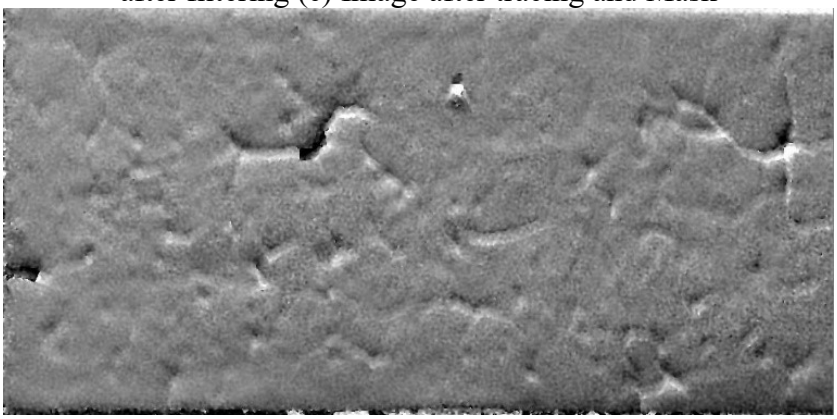

(a)

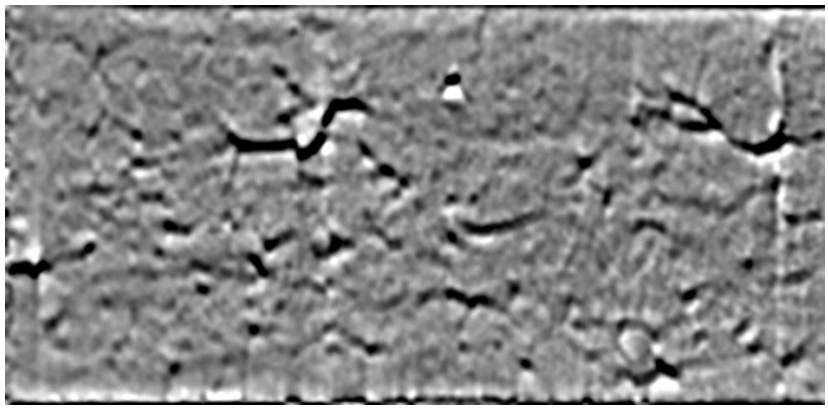

(b)

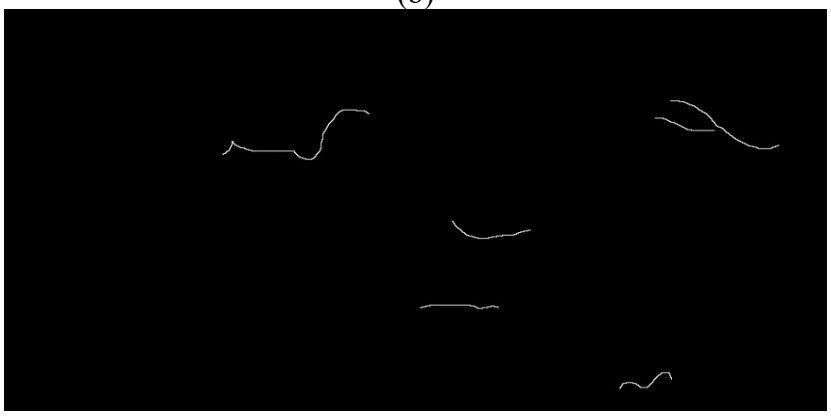

(c)

Figure A.68 TX1 Section 1A-Y at 97 days after cast (a) original image (b) Image after filtering (c) Image after tracing and Mask

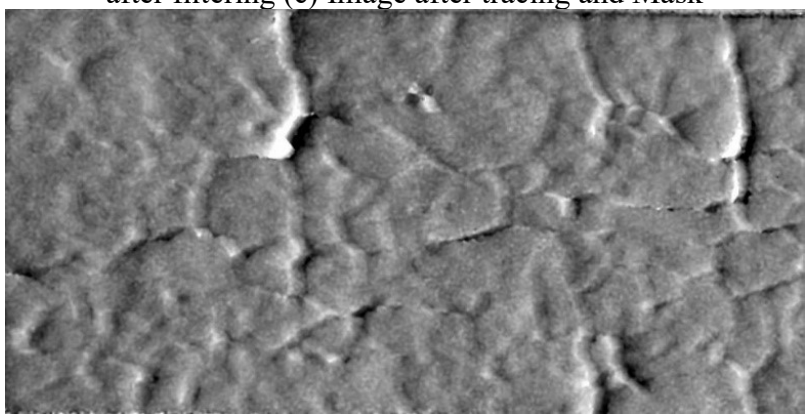

(a)

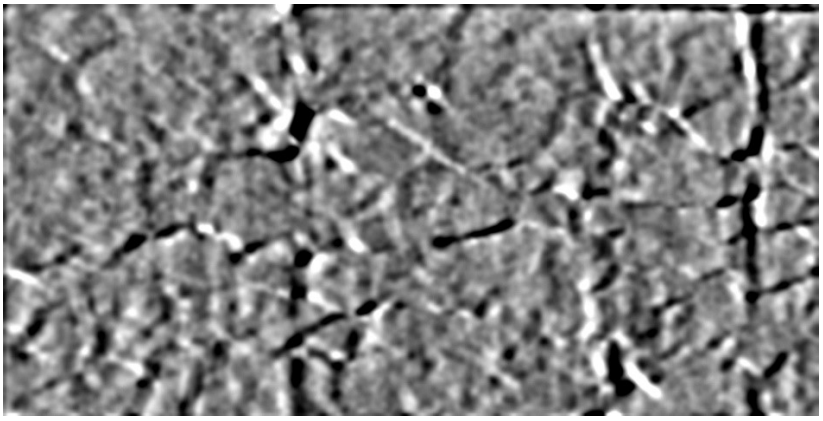

(b)

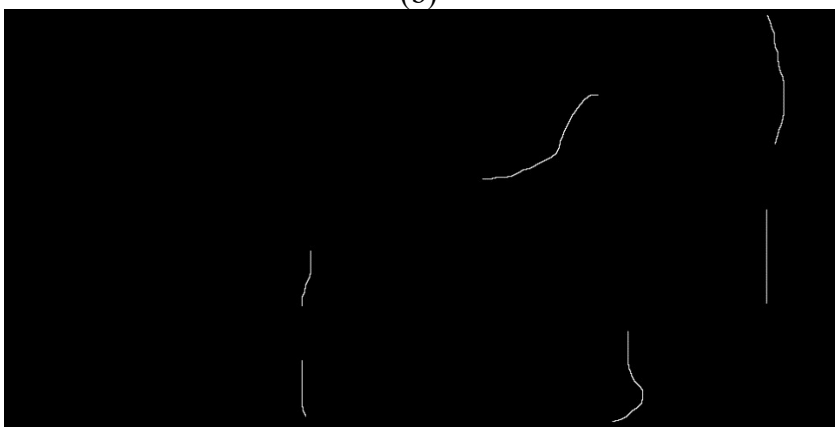

(c)

Figure A.69 TX1 Section 1A-X at 367 days after cast (a) original image (b) Image after filtering (c) Image after tracing and Mask

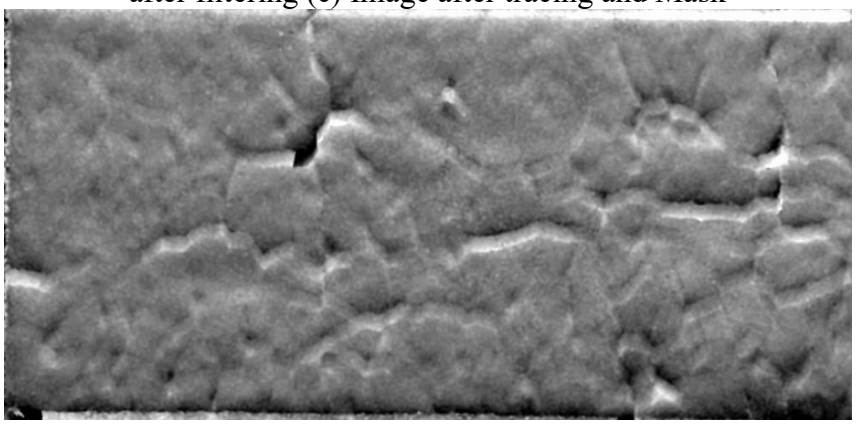

(a)

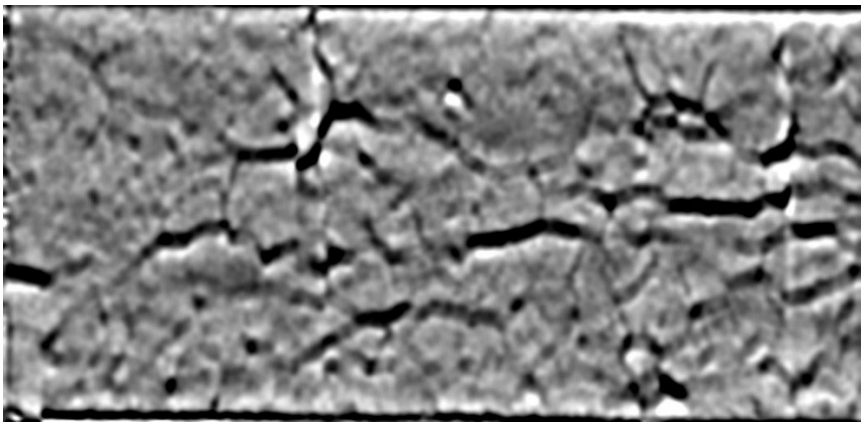

(b)

(c)

Figure A.70 TX1 Section 1A-Y at 367 days after cast (a) original image (b) Image after filtering (c) Image after tracing and Mask

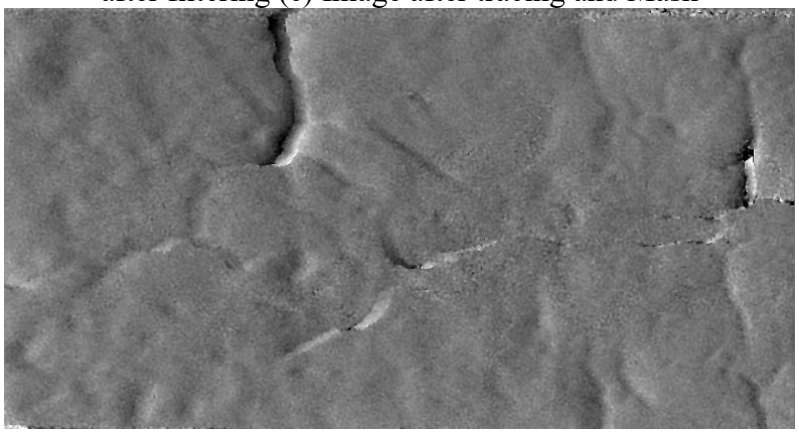

(a)

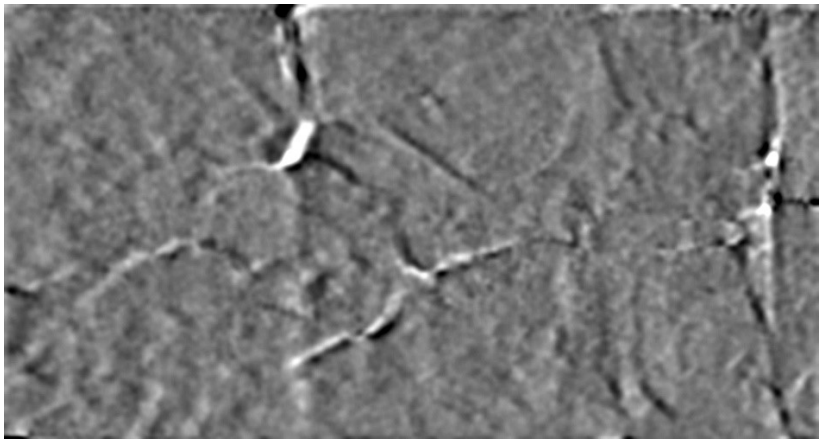

(b)

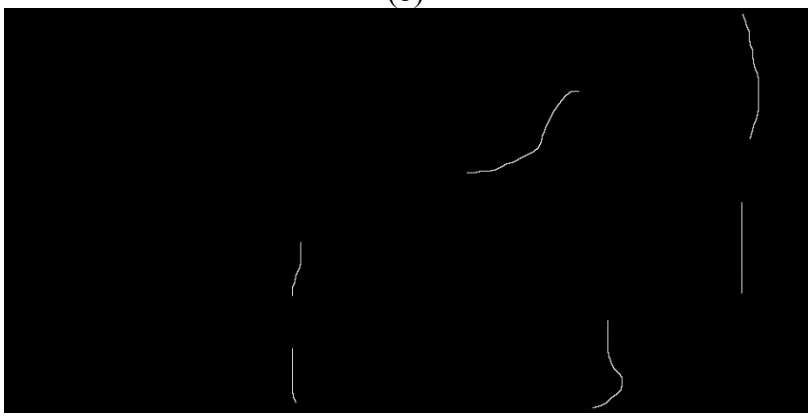

(c)

Figure A.71 TX1 Section 1A-X at 548 days after cast (a) original image (b) Image after filtering (c) Image after tracing and Mask

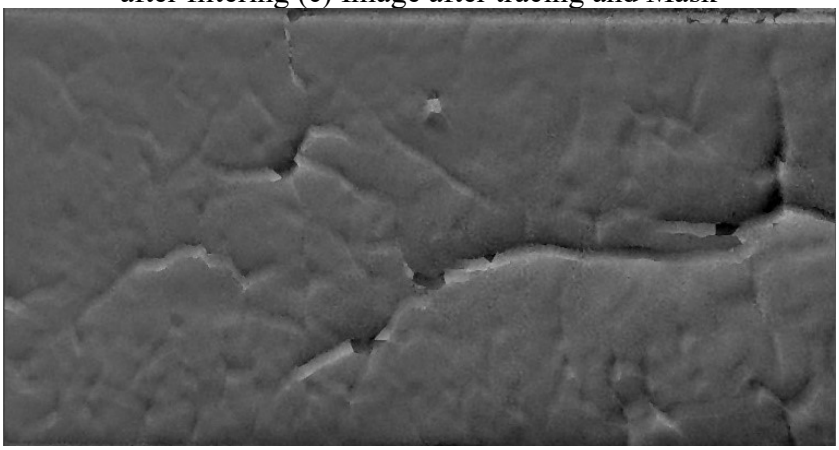

(a)

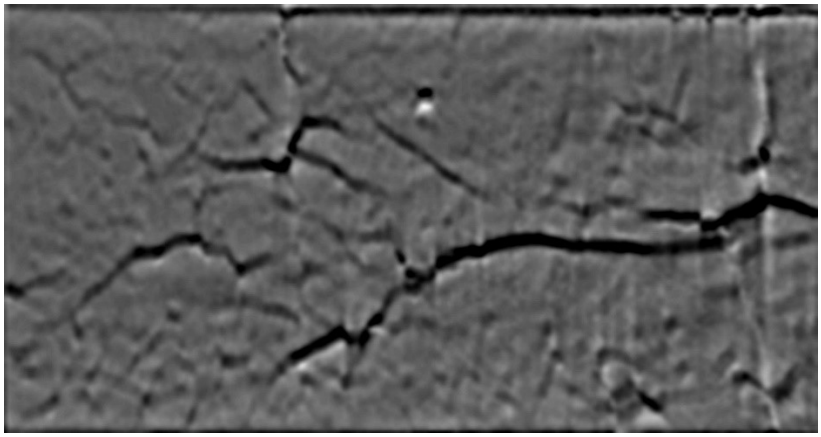

(b)

(c)

Figure A.72 TX1 Section 1A-Y at 548 days after cast (a) original image (b) Image after filtering (c) Image after tracing and Mask

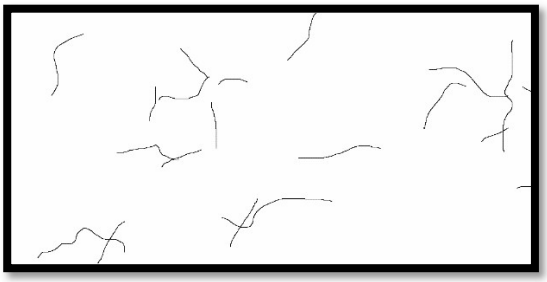

(a)

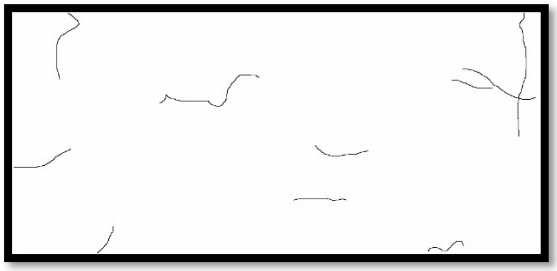

(b)

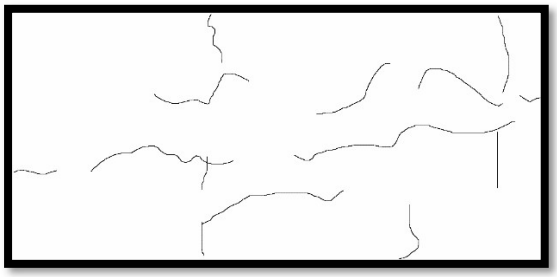

(c)

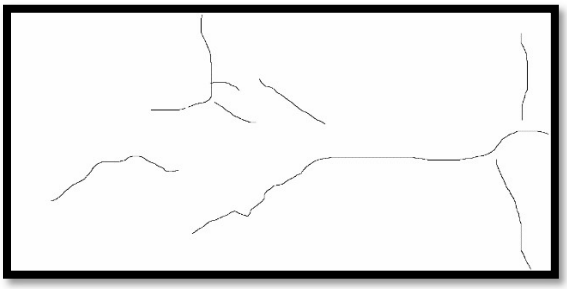

(d)

Figure A.73 Section 1A TX1 Mask X and Y shear direction combined traced cracks and inverted (a) 45 Days (b) 97 Days (c) 467 Days (d) 548 Days

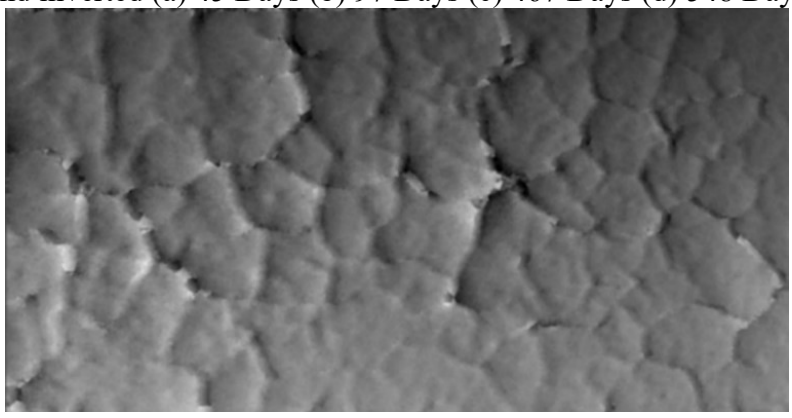

(a)

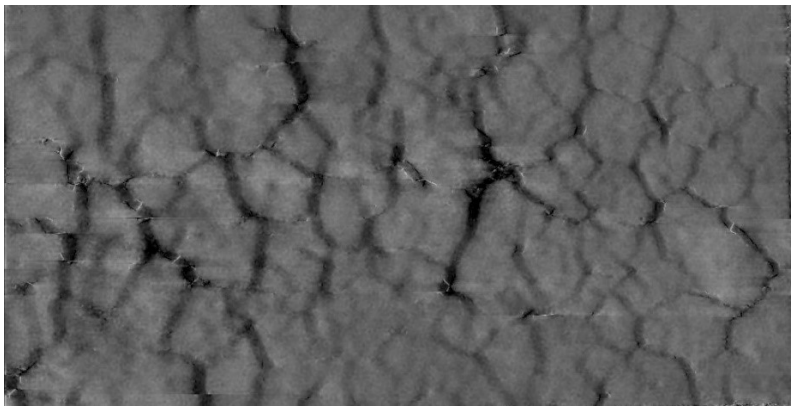

(b)

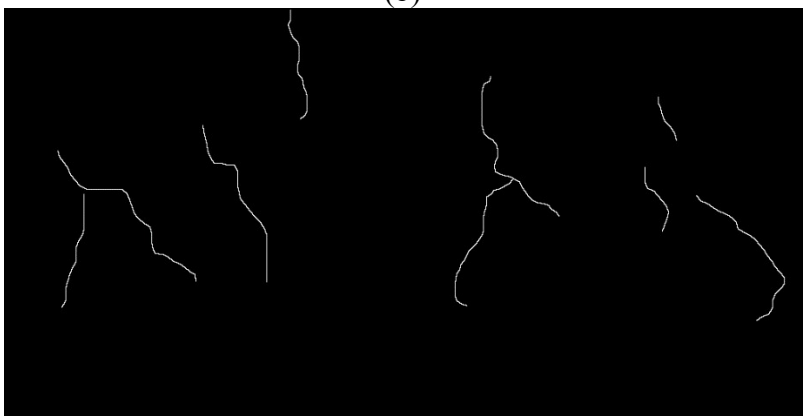

(c)

Figure A.75 TX1 Section 1B-X at 45 days after cast (a) original image (b) Image after filtering (c) Image after tracing and Mask

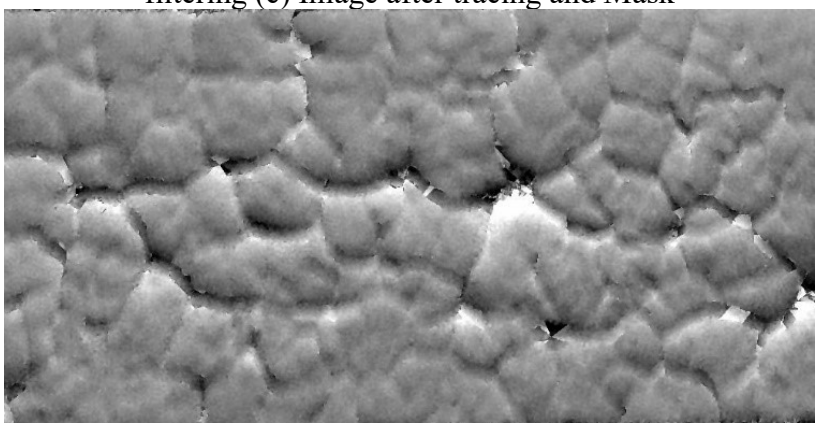

(a)

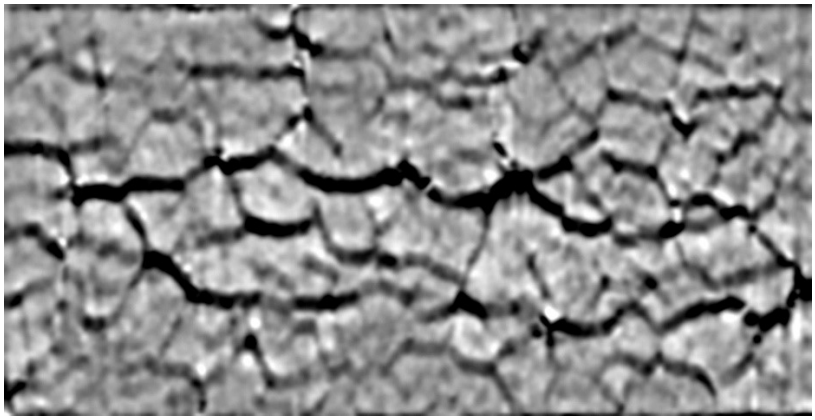

(b)

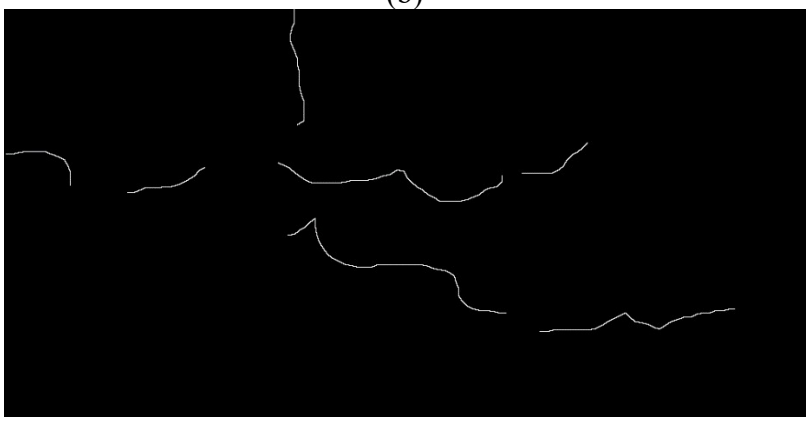

(c)

Figure A.76 TX1 Section 1B-Y at 45 days after cast (a) original image (b) Image after filtering (c) Image after tracing and Mask

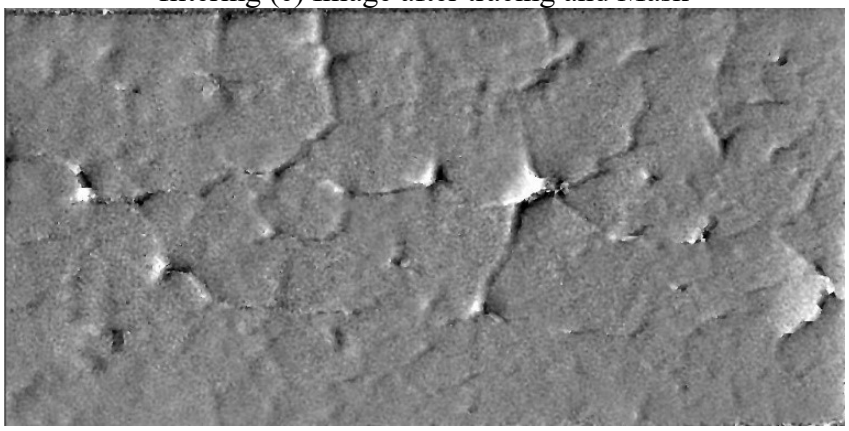

(a)

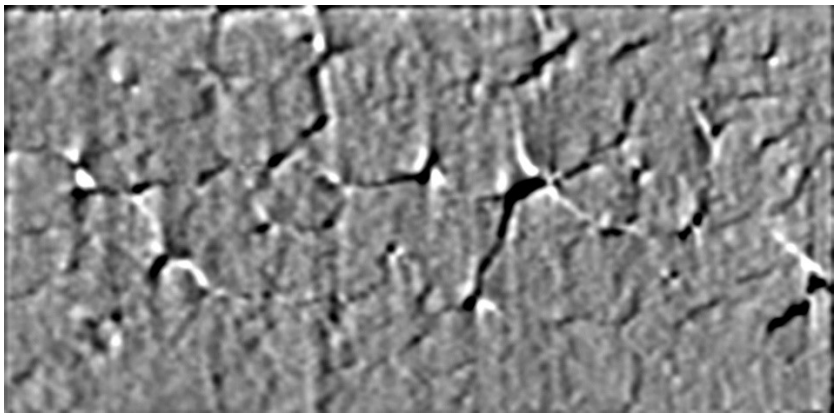

(b)

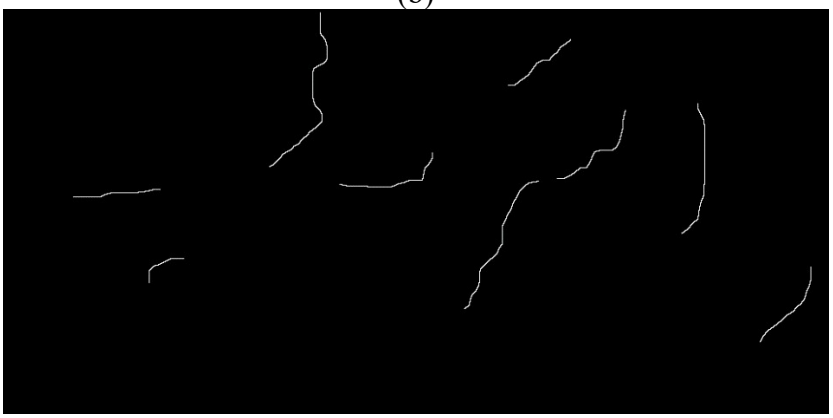

(c)

Figure A.77 TX1 Section 1B-X at 97 days after cast (a) original image (b) Image after filtering (c) Image after tracing and Mask

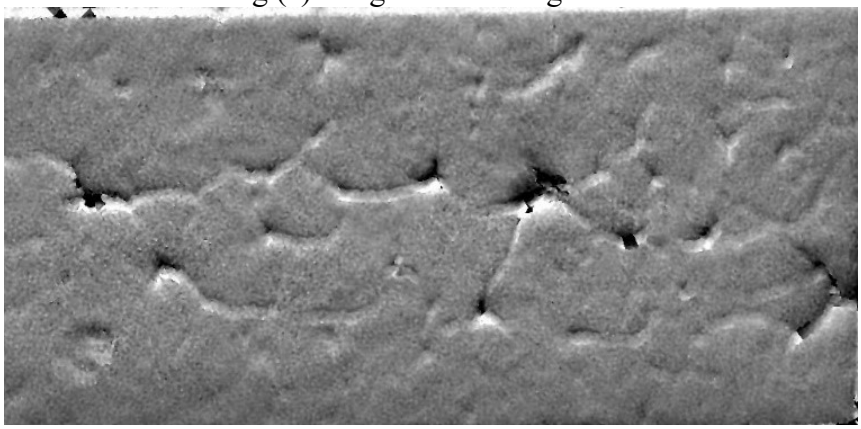

(a)

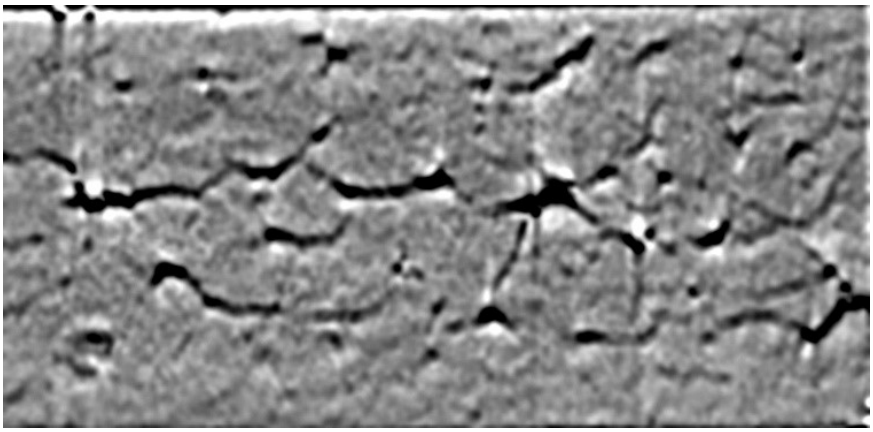

(b)

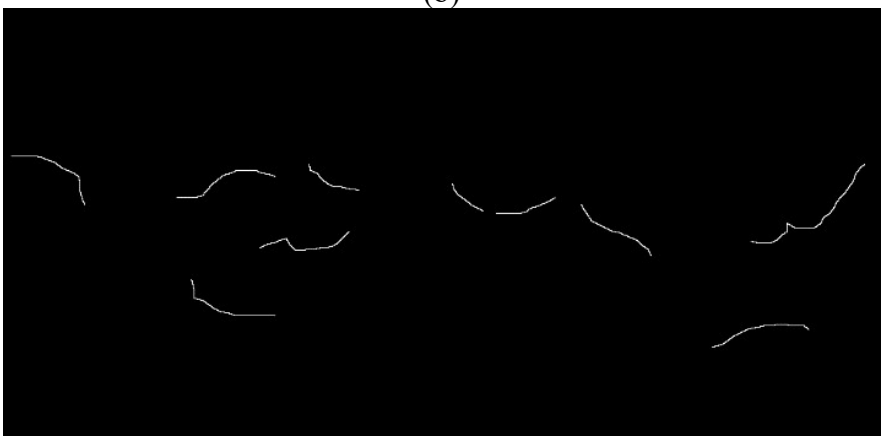

(c)

Figure A.78 TX1 Section 1B-Y at 97 days after cast (a) original image (b) Image after filtering (c) Image after tracing and Mask

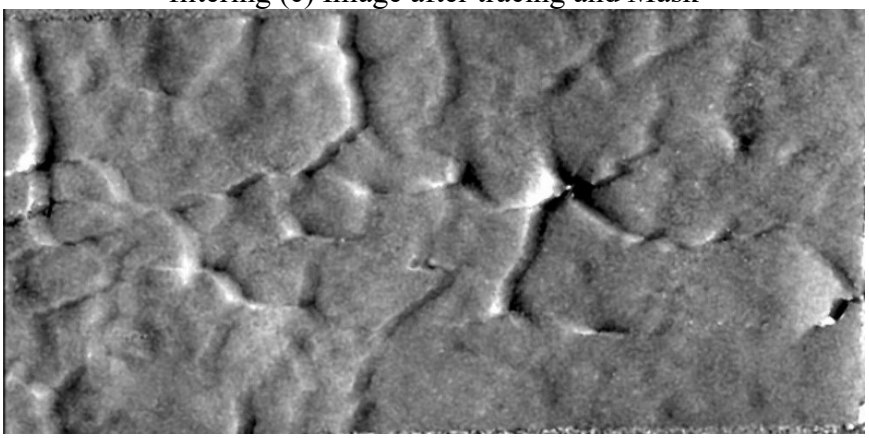

(a)

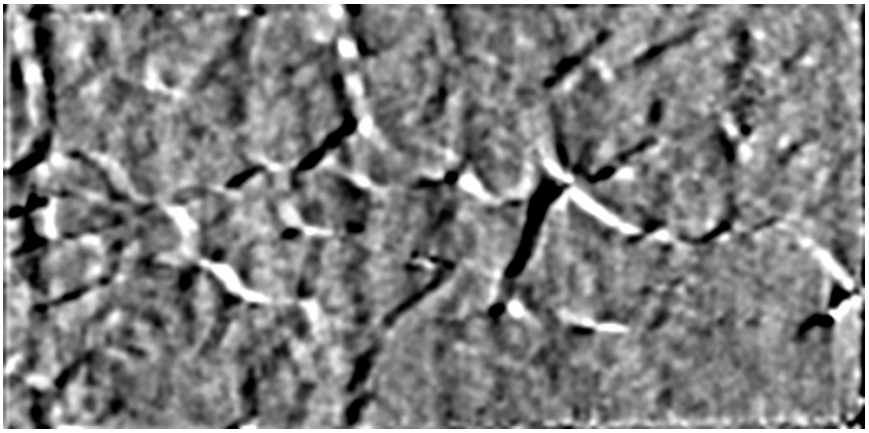

(b)

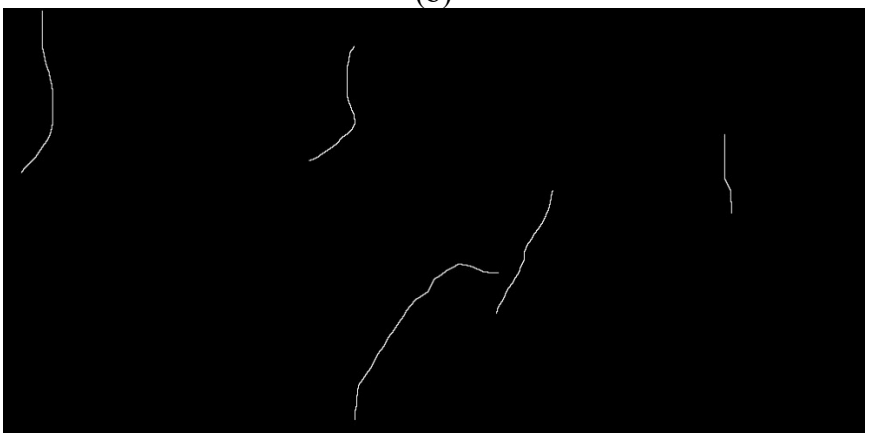

(c)

Figure A.79 TX1 Section 1B-X at 367 days after cast (a) original image (b) Image after filtering (c) Image after tracing and Mask

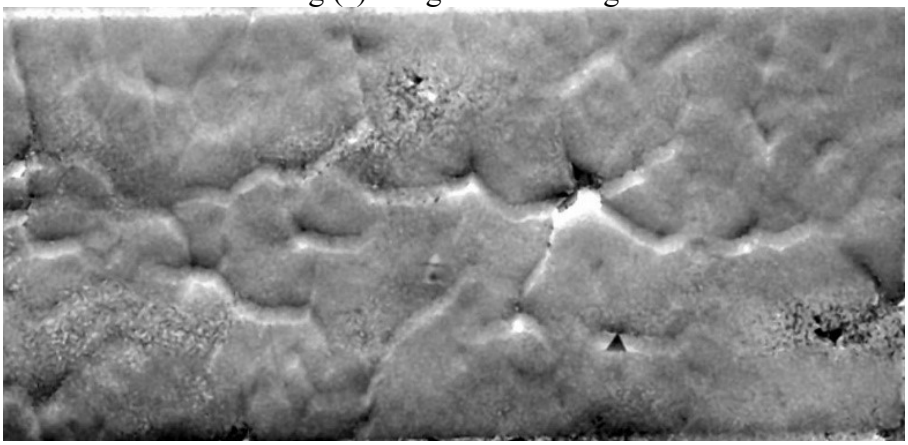

(a)

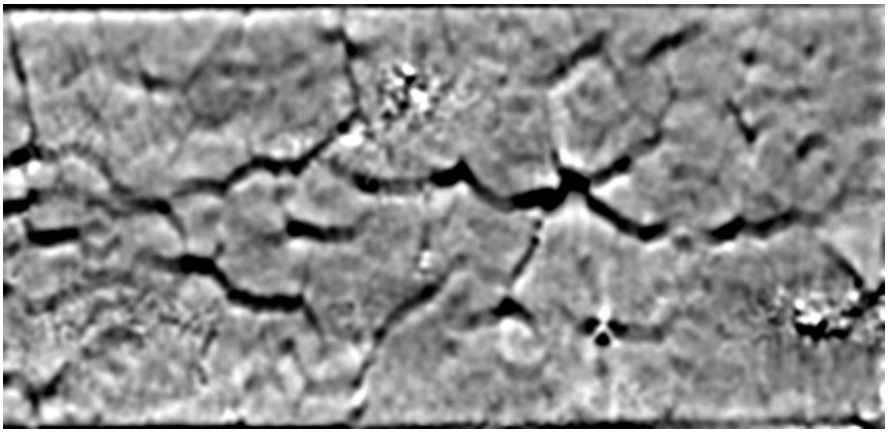

(b)

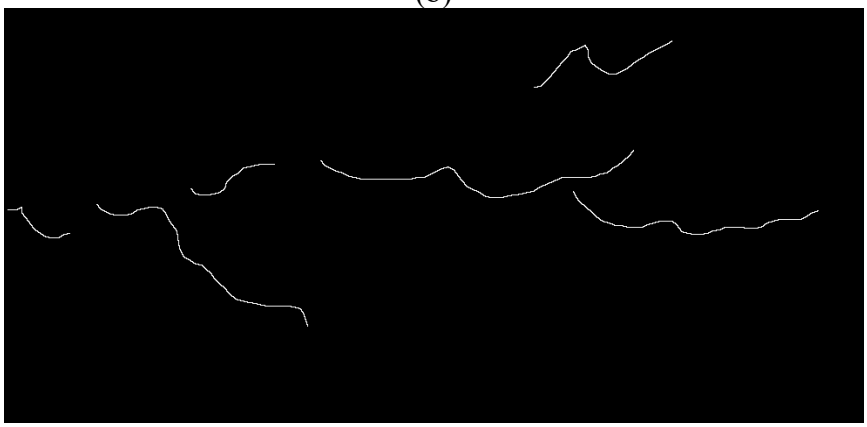

(c)

Figure A.80 TX1 Section 1B-Y at 367 days after cast (a) original image (b) Image after filtering (c) Image after tracing and Mask

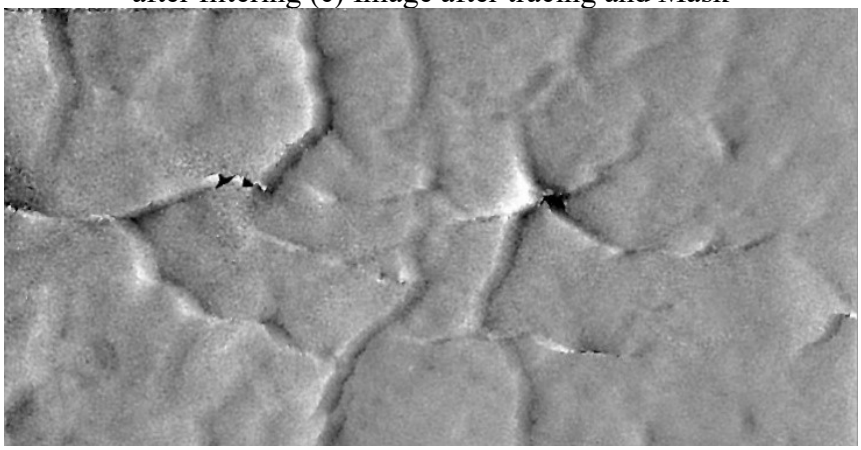

(a)

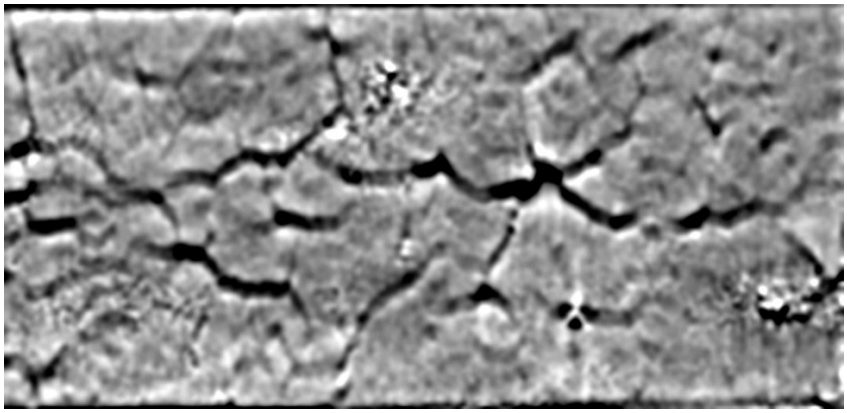

(b)

(c)

Figure A.81 TX1 Section 1B-X at 548 days after cast (a) original image (b) Image after filtering (c) Image after tracing and Mask

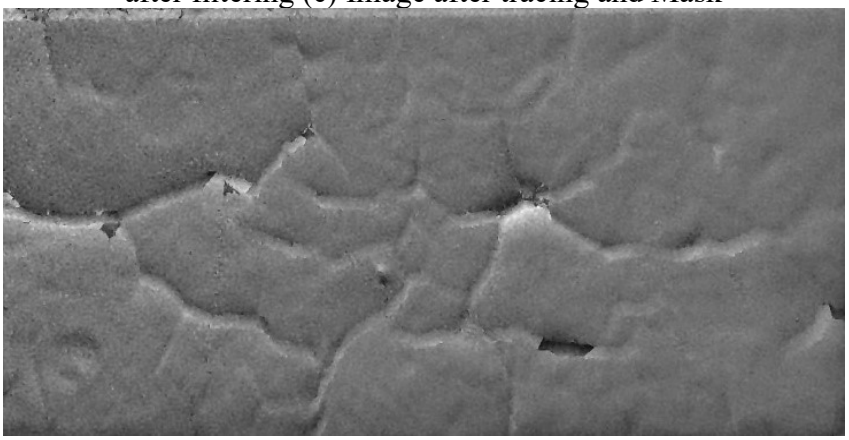

(a)

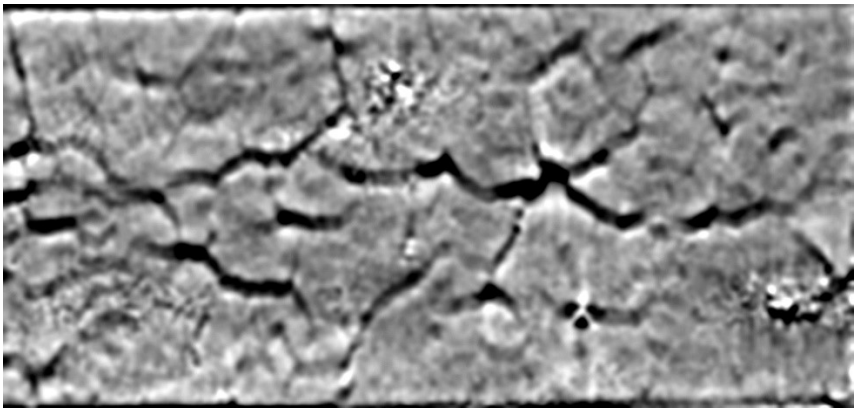

(b)

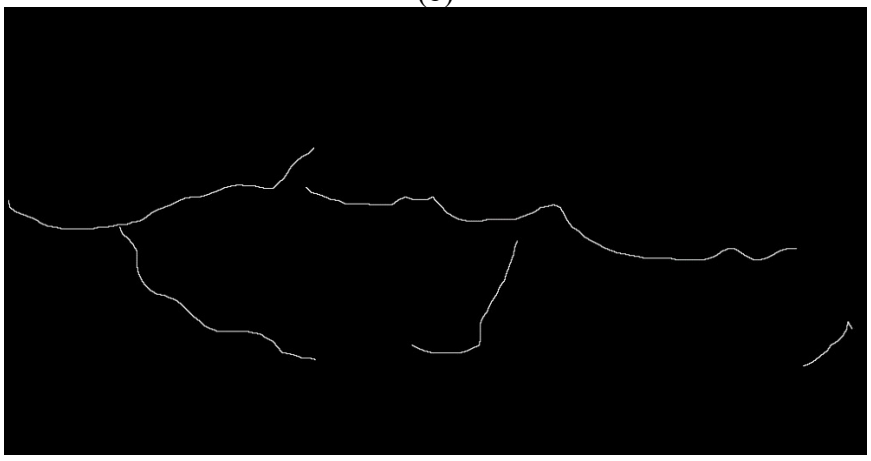

(c)

Figure A.82 TX1 Section 1B-Y at 548 days after cast (a) original image (b) Image after filtering (c) Image after tracing and Mask

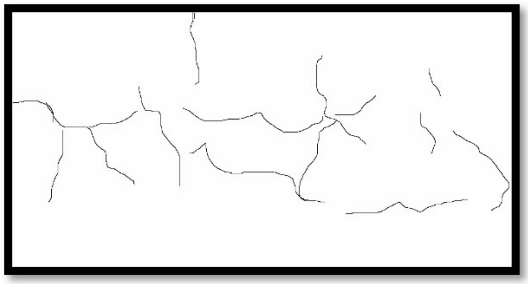

(a)

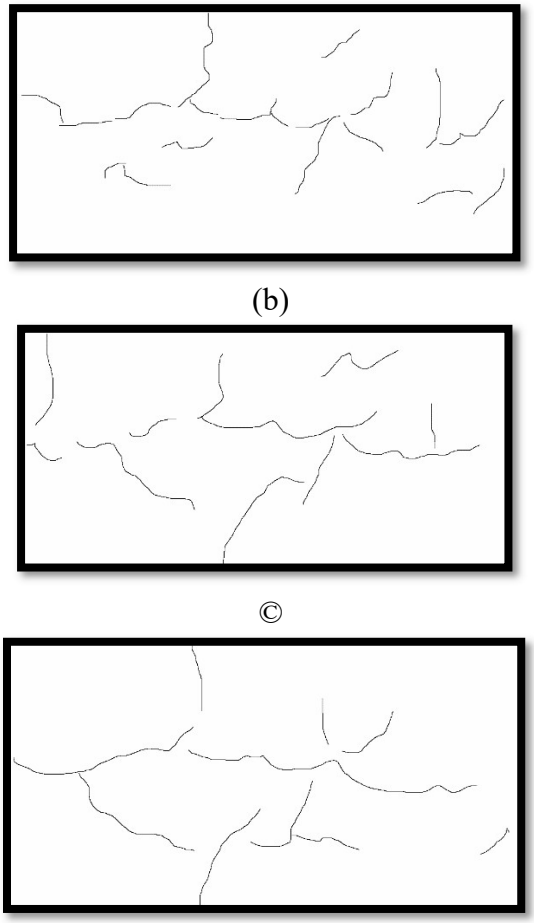

(b)

©

(d)

Figure A.83 Section 1B TX1 Mask X and Y shear direction combined traced cracks and inverted (a) 45 Days (b) 97 Days (c) 467 Days (d) 548 Days

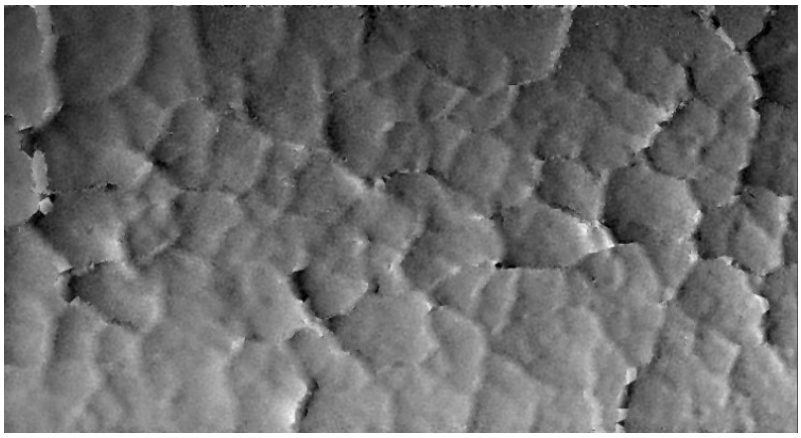

(a)

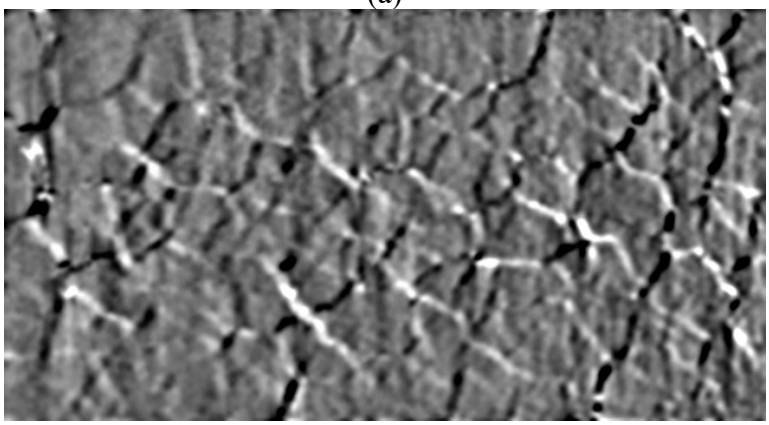

(b)

(c)

Figure A.85 TX1 Section 2A-X at 45 days after cast (a) original image (b) Image after filtering (c) Image after tracing and Mask

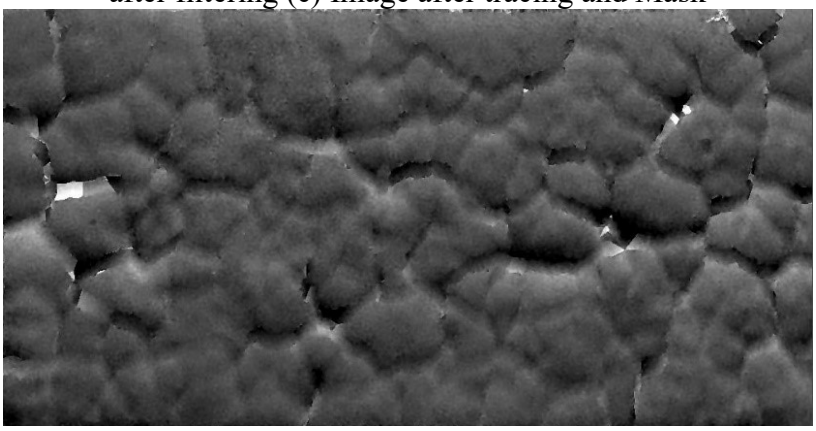

(a)

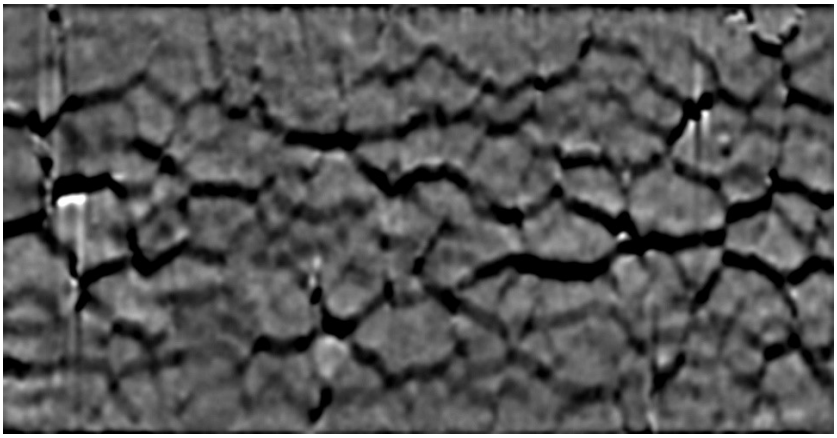

(b)

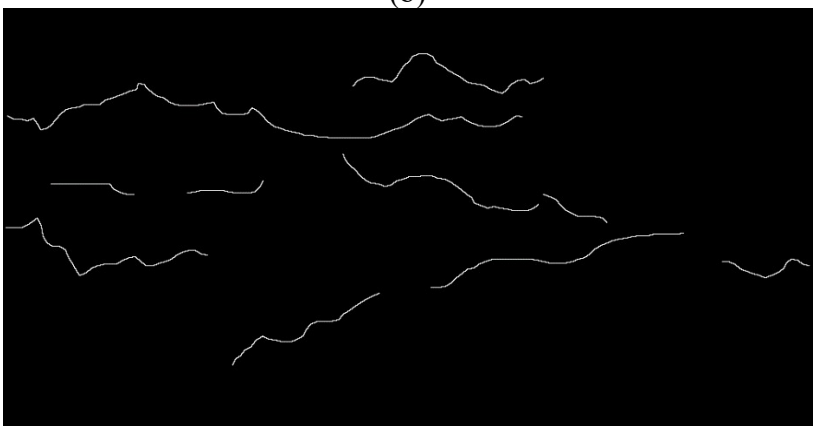

(c)

Figure A.86 TX1 Section 2A-Y at 45 days after cast (a) original image (b) Image after filtering (c) Image after tracing and Mask

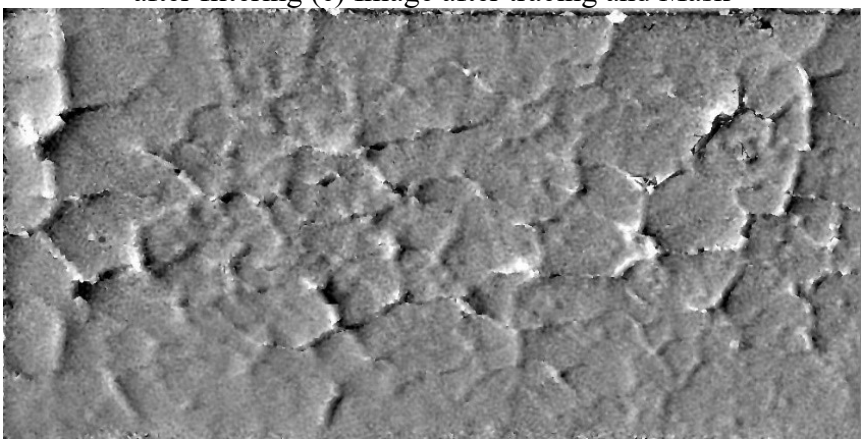

(a)

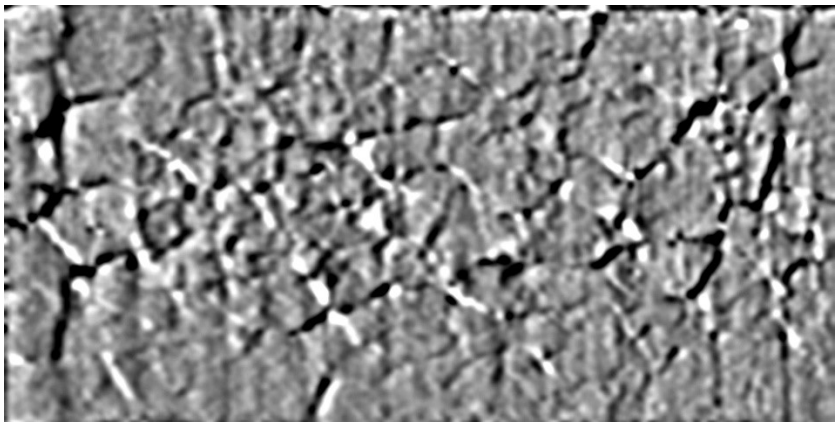

(b)

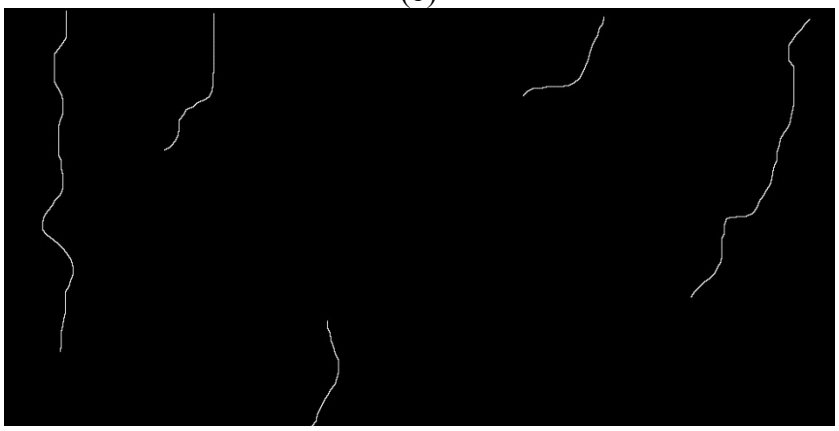

(c)

Figure A.87 TX1 Section 2A-X at 97 days after cast (a) original image (b) Image after filtering (c) Image after tracing and Mask

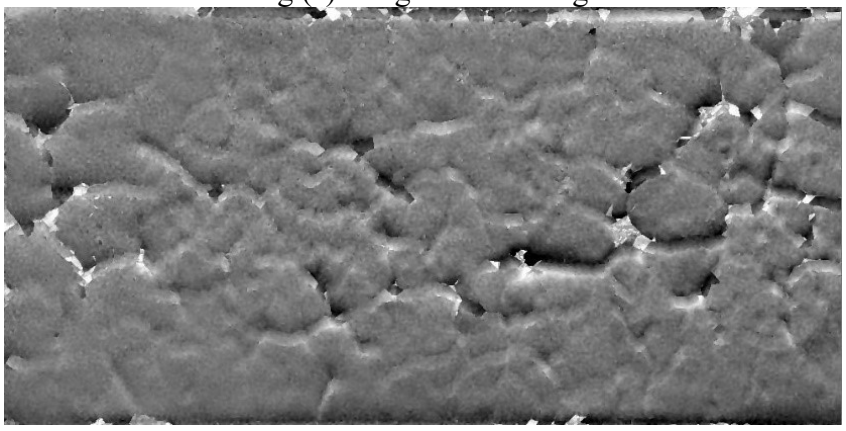

(a)

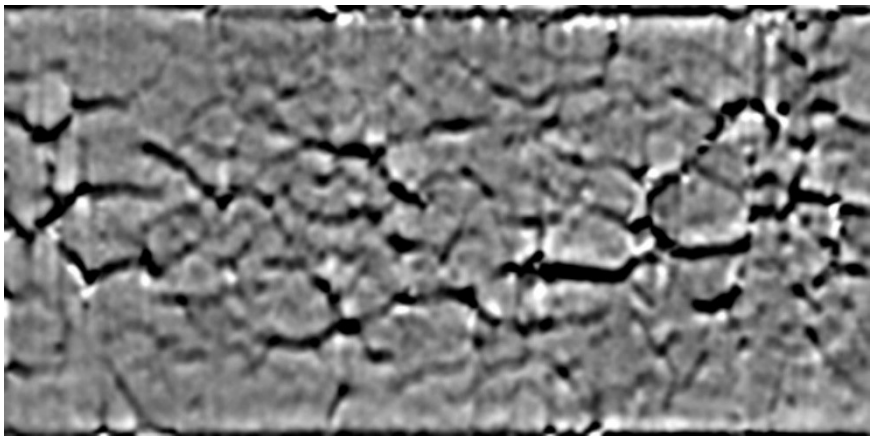

(b)

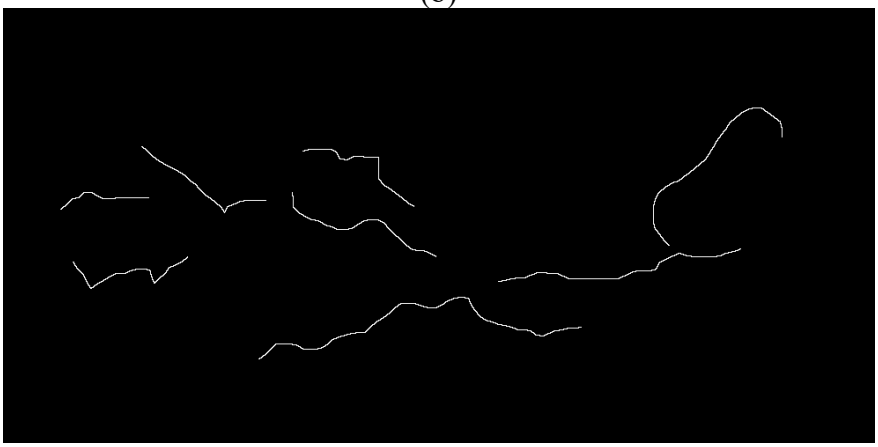

(c)

Figure A.88 TX1 Section 2A-Y at 97 days after cast (a) original image (b) Image after filtering (c) Image after tracing and Mask

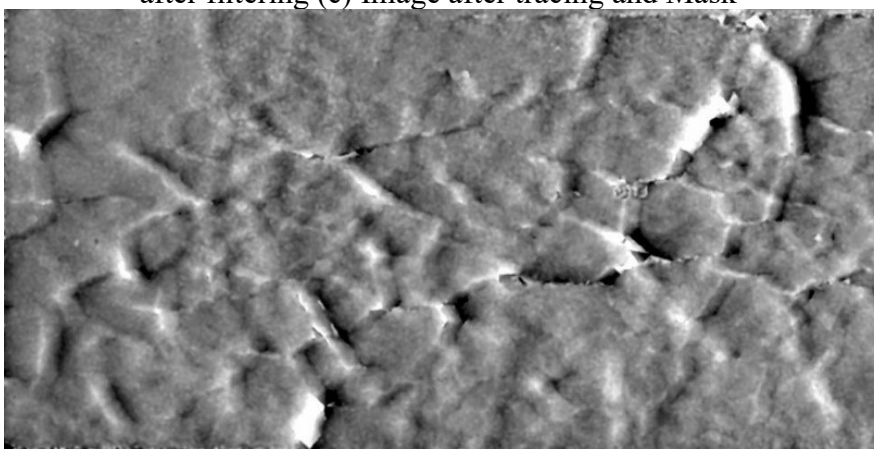

(a)

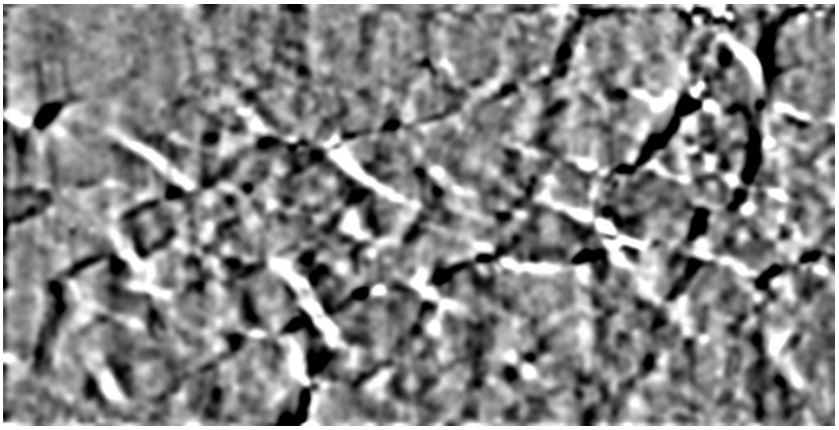

(b)

(c)

Figure A.89 TX1 Section 2A-X at 367 days after cast (a) original image (b) Image after filtering (c) Image after tracing and Mask

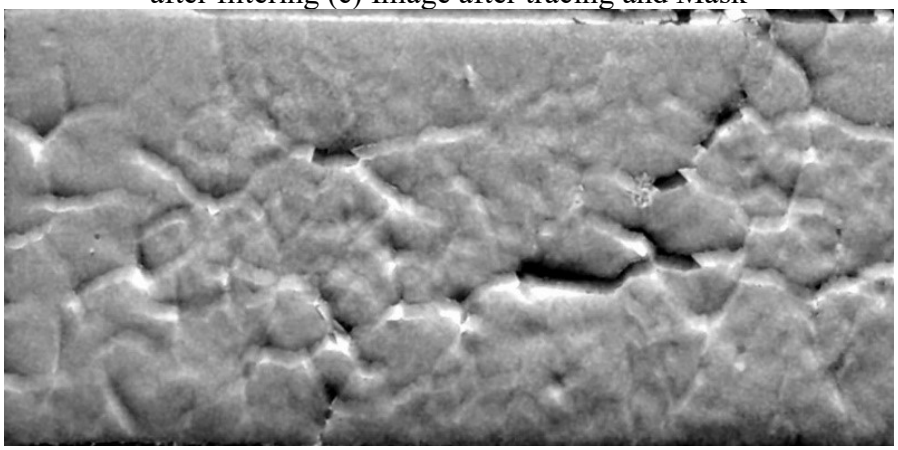

(a)

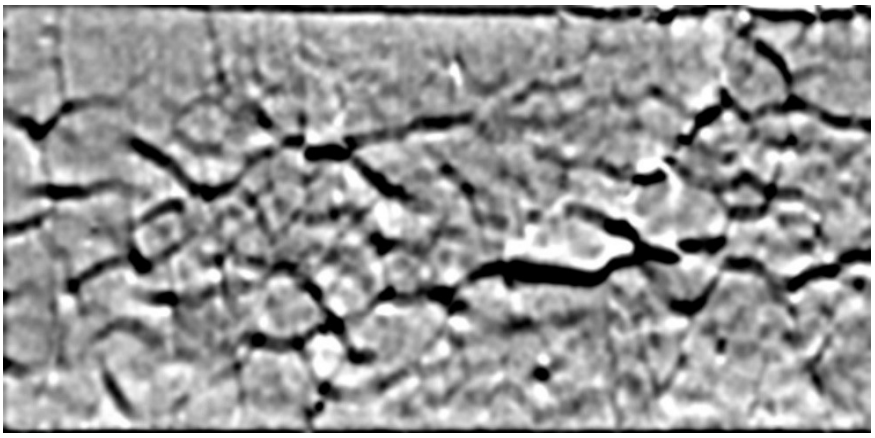

(b)

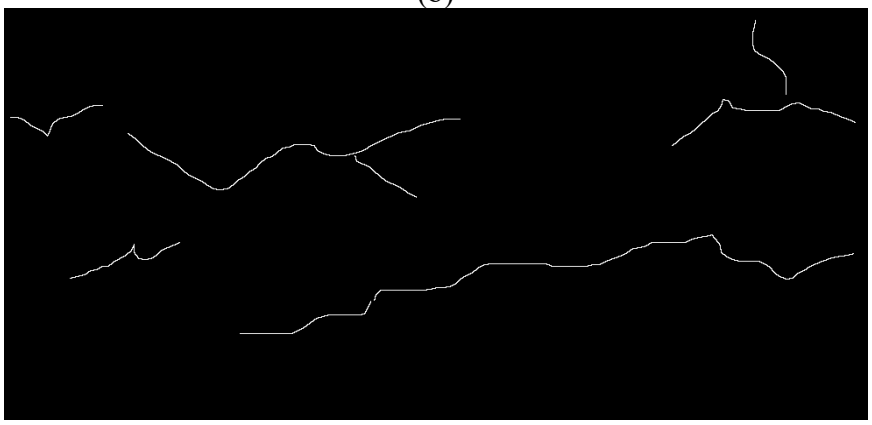

(c)

Figure A.90 TX1 Section 2A-Y at 367 days after cast (a) original image (b) Image after filtering (c) Image after tracing and Mask

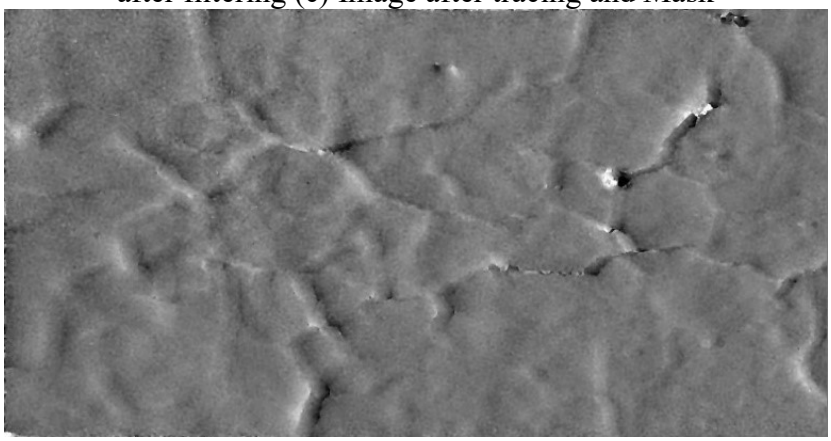

(a)

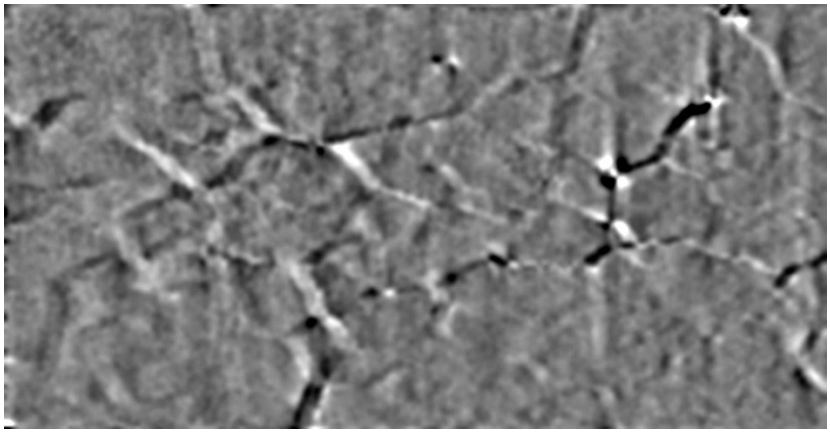

(b)

(c)

Figure A.91 TX1 Section 2A-X at 548 days after cast (a) original image (b) Image after filtering (c) Image after tracing and Mask

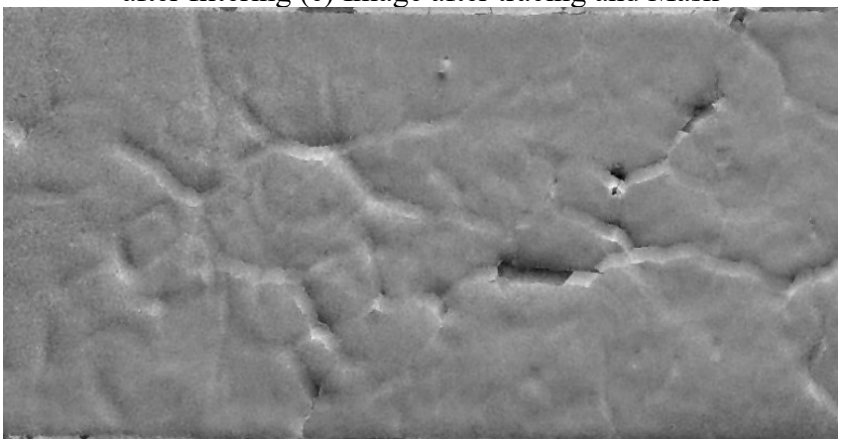

(a)

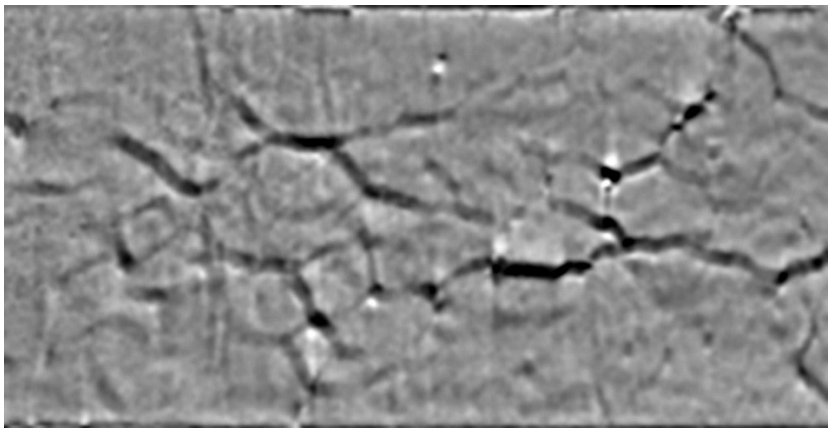

(b)

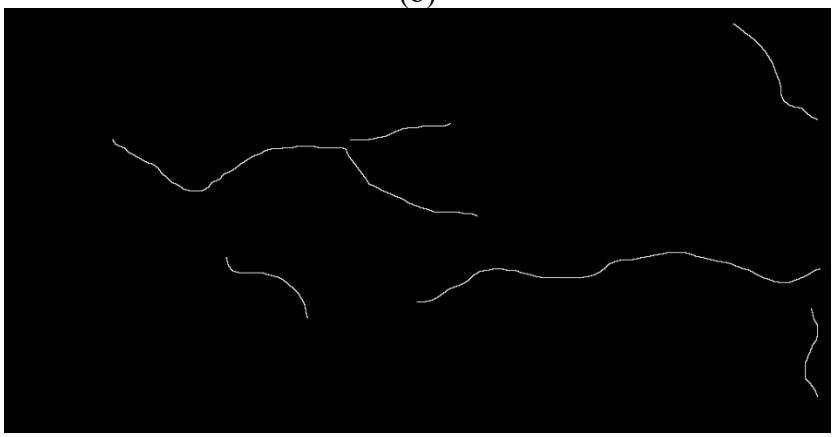

(c)

Figure A.92 TX1 Section 2A-Y at 548 days after cast (a) original image (b) Image after filtering (c) Image after tracing and Mask

(a)

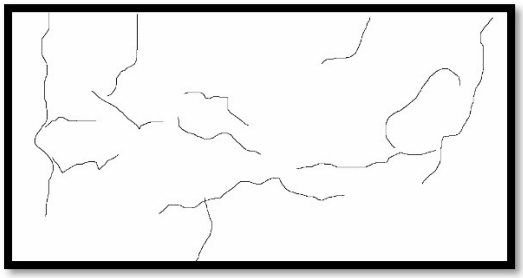

(b)

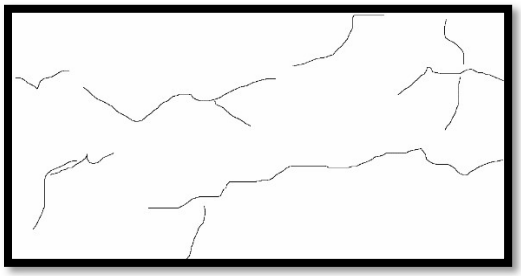

(c)

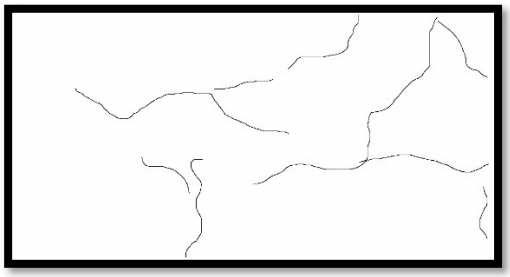

(d)

Figure A.93 Section 2A TX1 Mask X and Y shear direction combined traced cracks and inverted (a) 45 Days (b) 97 Days (c) 467 Days (d) 548 Days

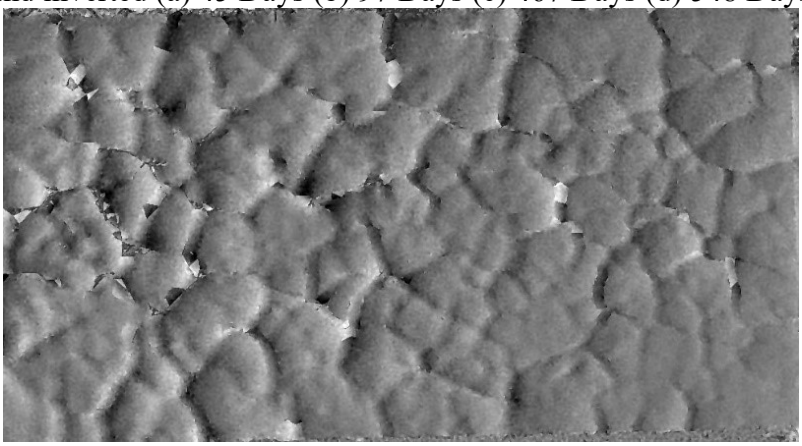

(a)

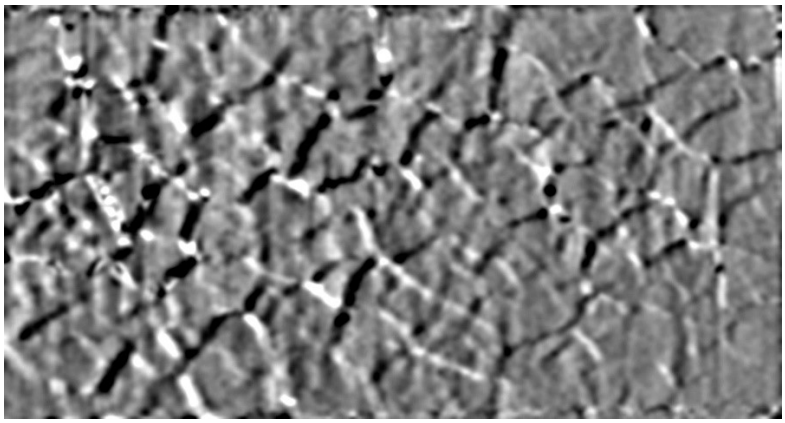

(b)

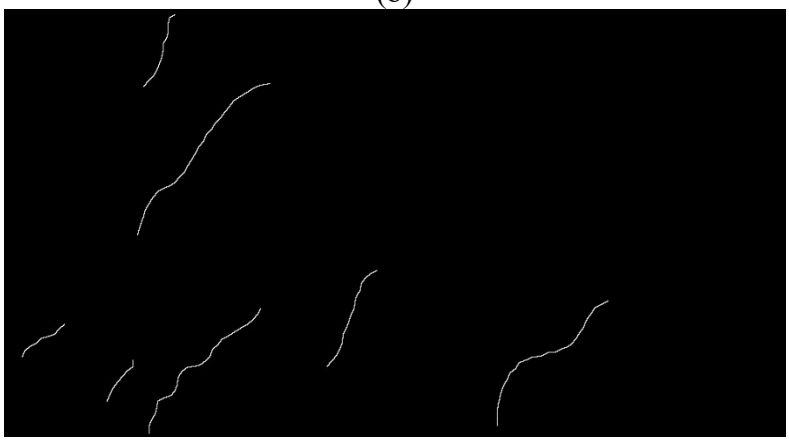

(c)

Figure A.95 TX1 Section 2B-X at 45 days after cast (a) original image (b) Image after filtering (c) Image after tracing and Mask

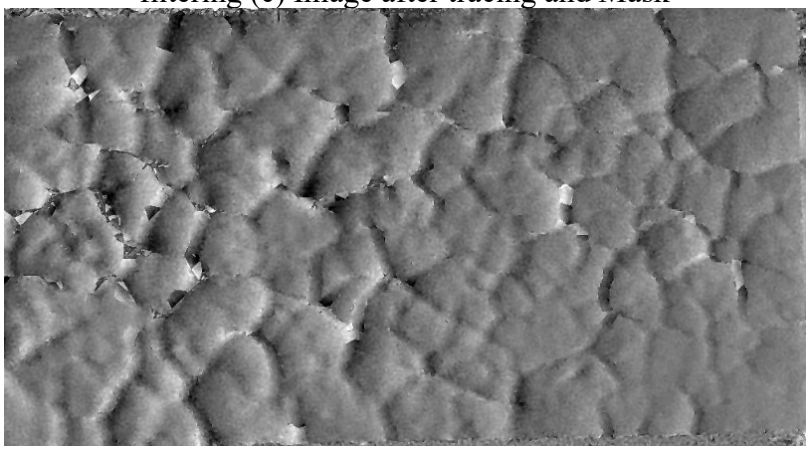

(a)

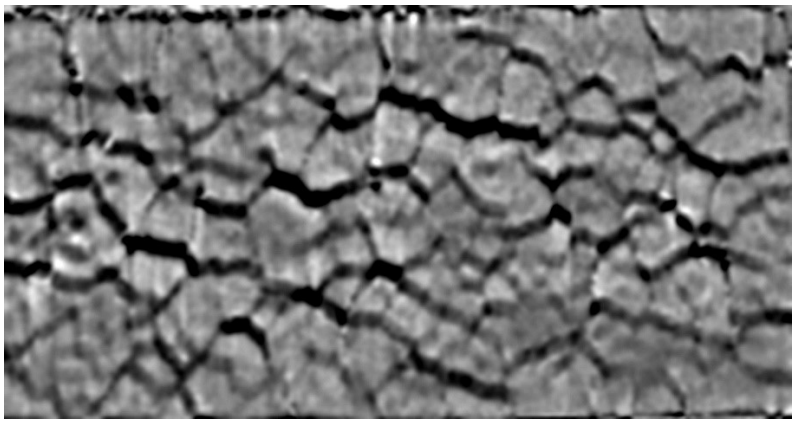

(b)

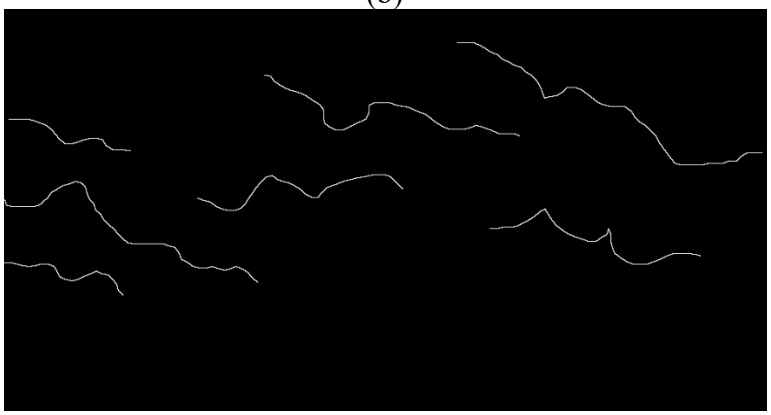

(c)

Figure A.96 TX1 Section 2B-Y at 45 days after cast (a) original image (b) Image after filtering (c) Image after tracing and Mask

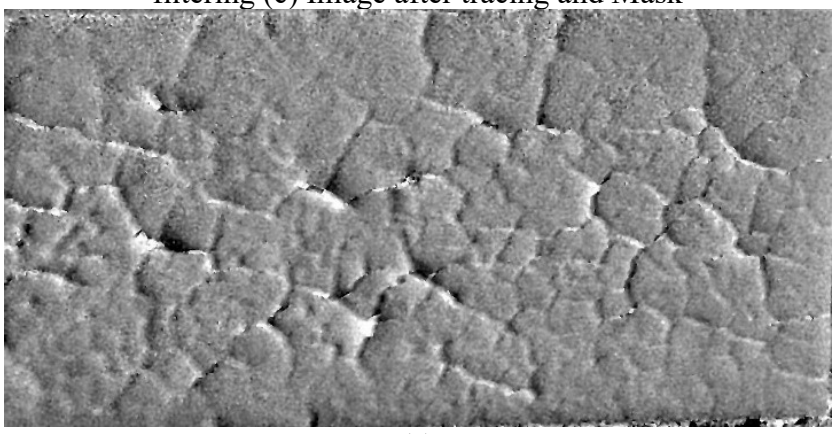

(a)

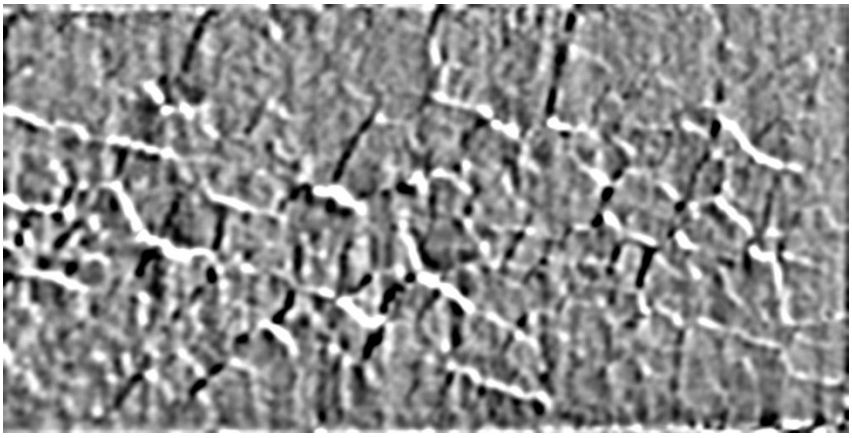

(b)

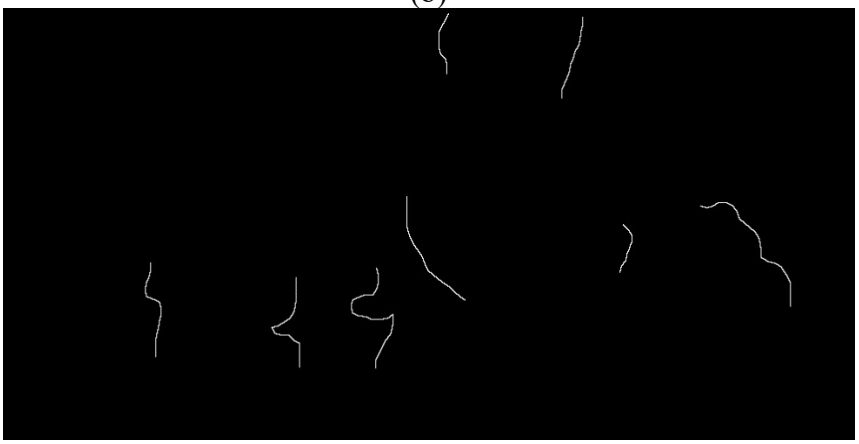

(c)

Figure A.97 TX1 Section 2B-X at 97 days after cast (a) original image (b) Image after filtering (c) Image after tracing and Mask

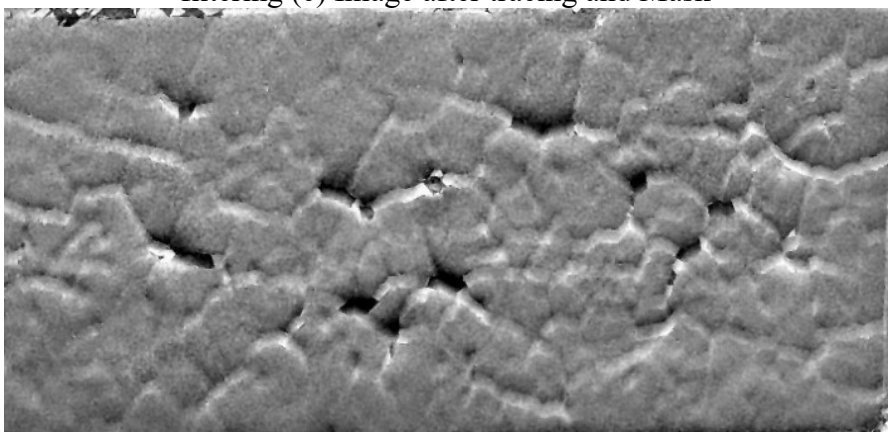

(a)

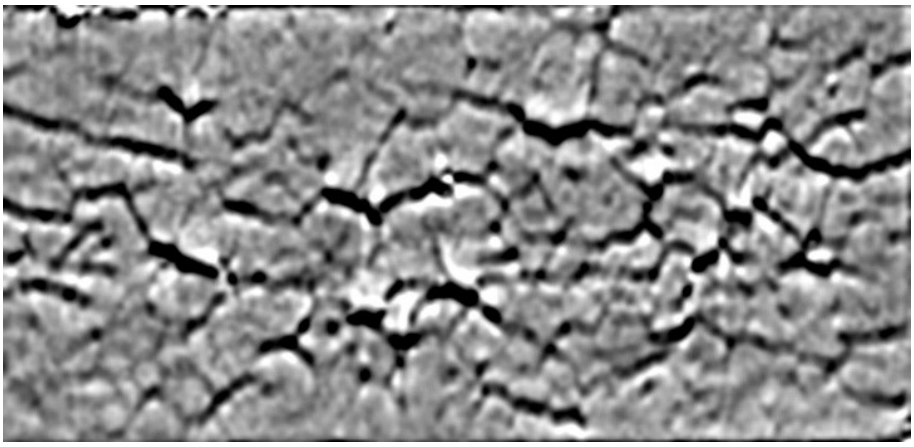

(b)

(c)

Figure A.98 TX1 Section 2B-Y at 97 days after cast (a) original image (b) Image after filtering (c) Image after tracing and Mask

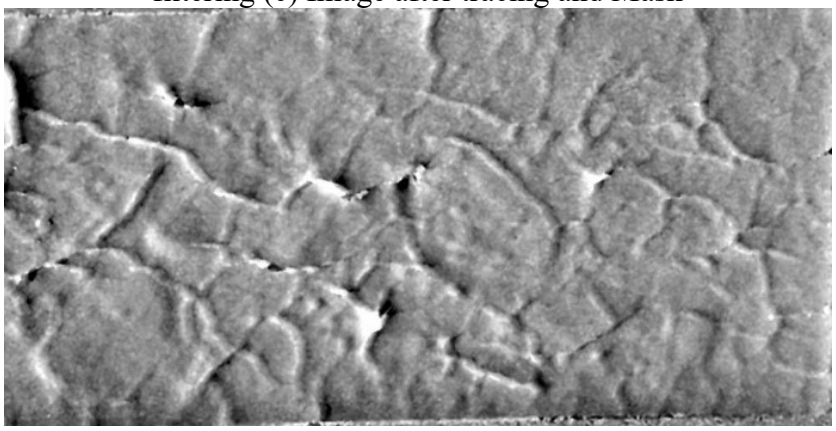

(a)

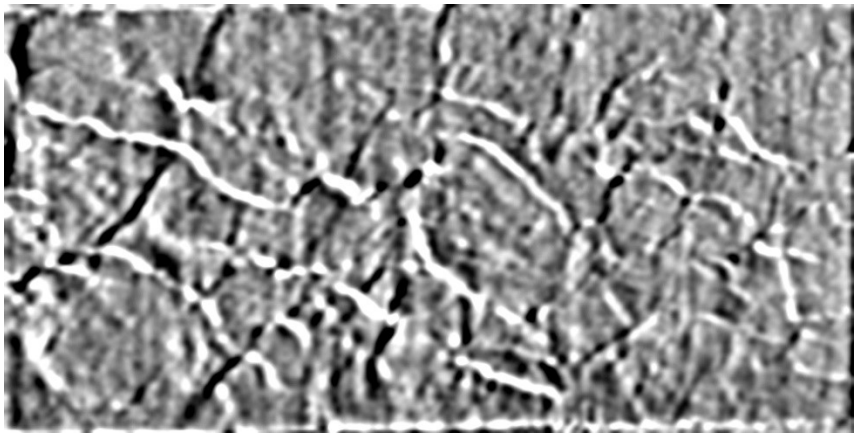

(b)

(c)

Figure A.99 TX1 Section 2B-X at 367 days after cast (a) original image (b) Image after filtering (c) Image after tracing and Mask

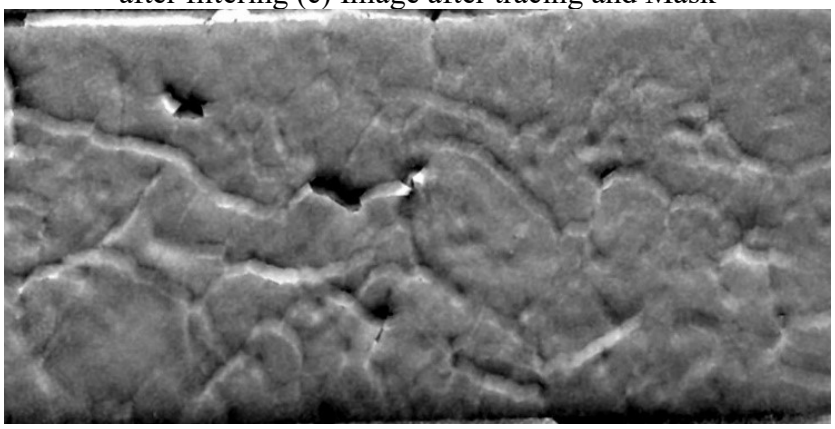

(a)

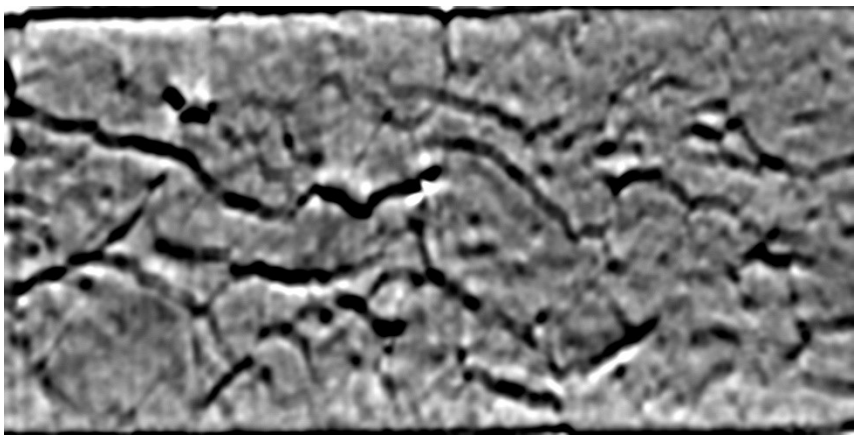

(b)

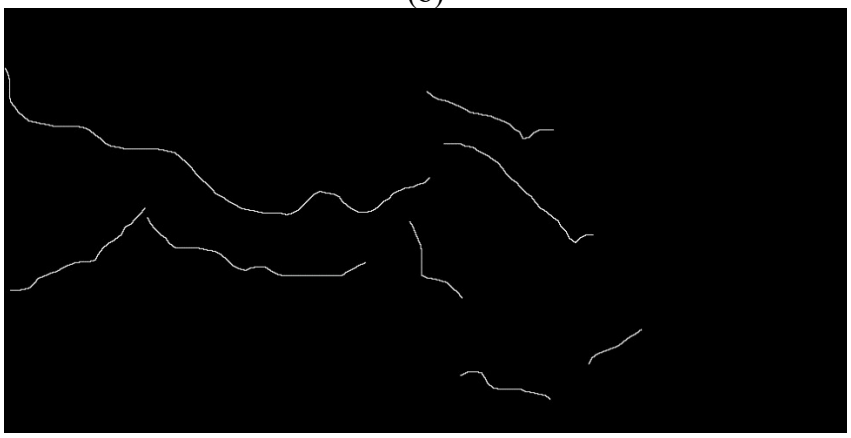

(c)

Figure A.100 TX1 Section 2B-Y at 367 days after cast (a) original image (b) Image after filtering (c) Image after tracing and Mask

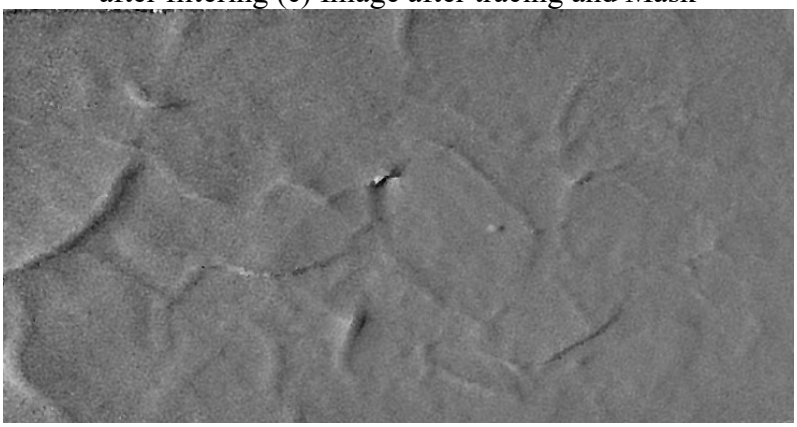

(a)

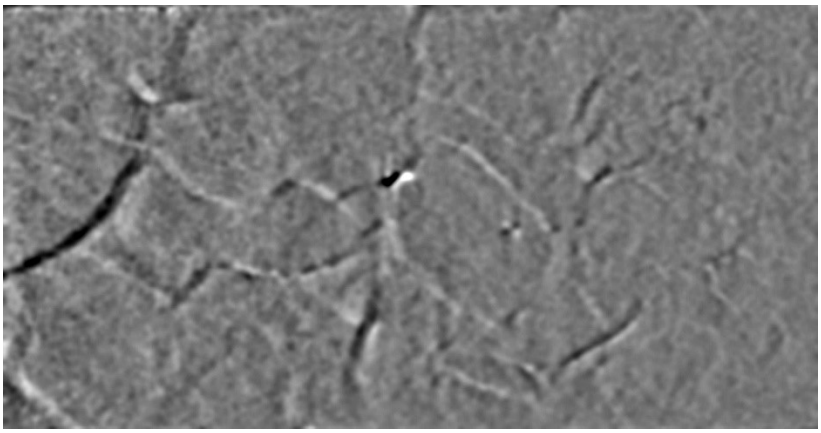

(b)

(c)

Figure A.101 TX1 Section 2B-X at 548 days after cast (a) original image (b) Image after filtering (c) Image after tracing and Mask

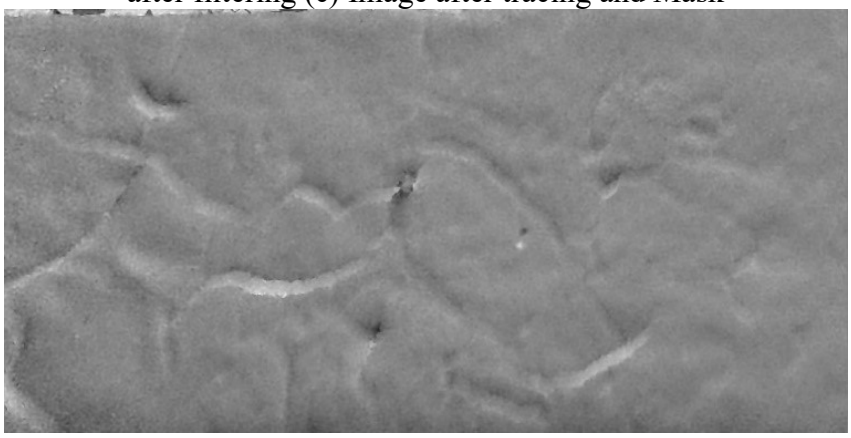

(a)

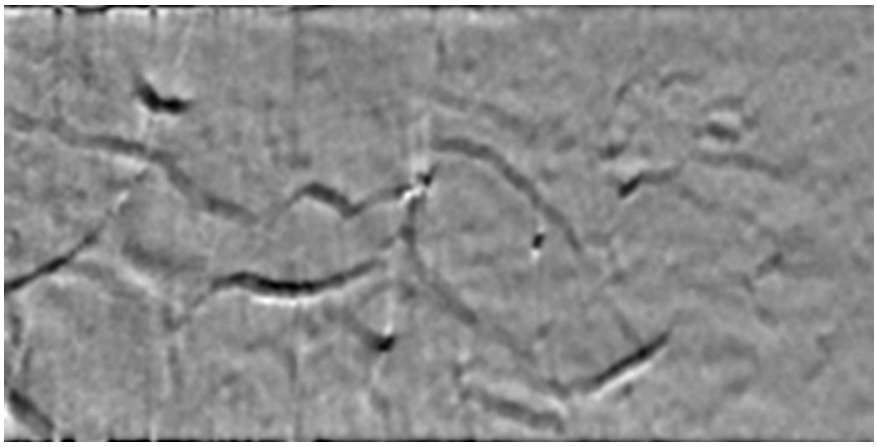

(b)

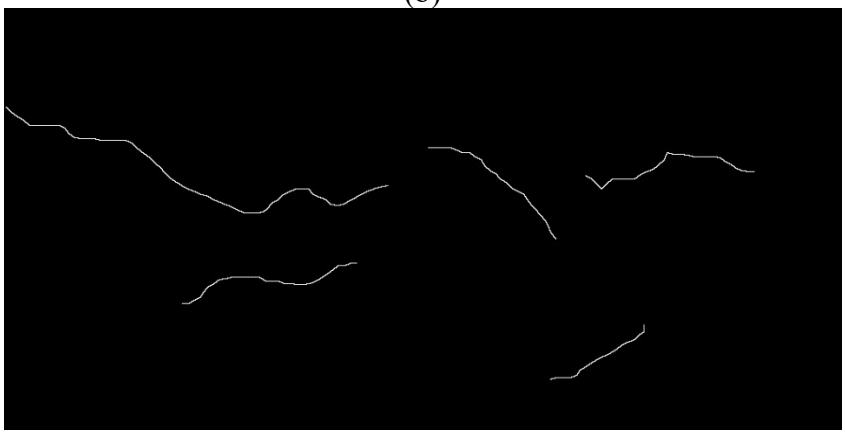

(c)

Figure A.102 TX1 Section 2B-Y at 548 days after cast (a) original image (b) Image after filtering (c) Image after tracing and Mask

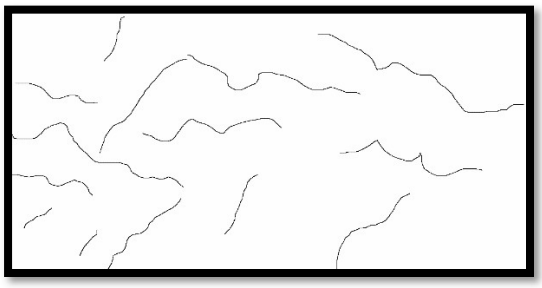

(a)

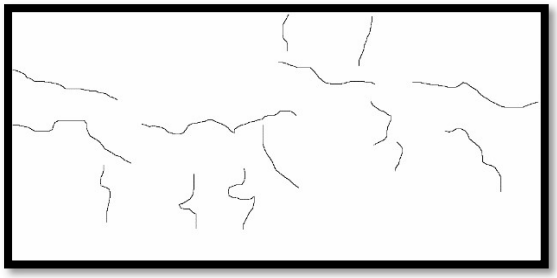

(b)

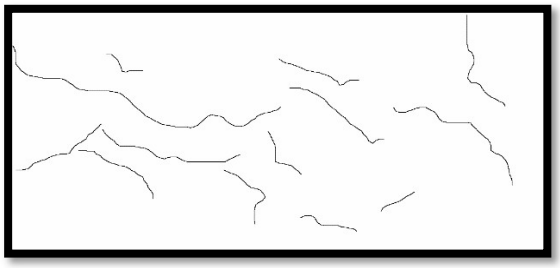

(c)

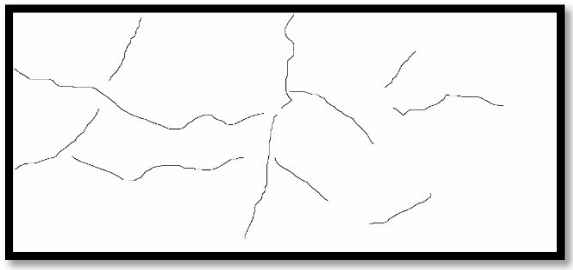

(d)

Figure A.103 Section 2B TX1 Mask X and Y shear direction combined traced cracks and inverted (a) 45 Days (b) 97 Days (c) 467 Days (d) 548 Days

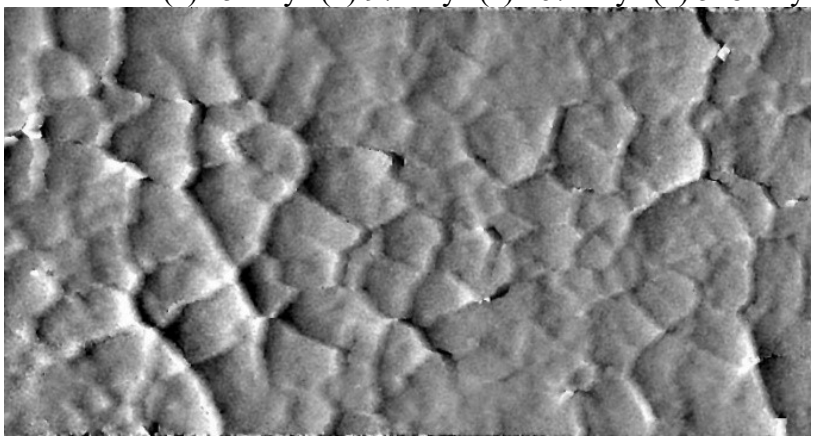

(a)

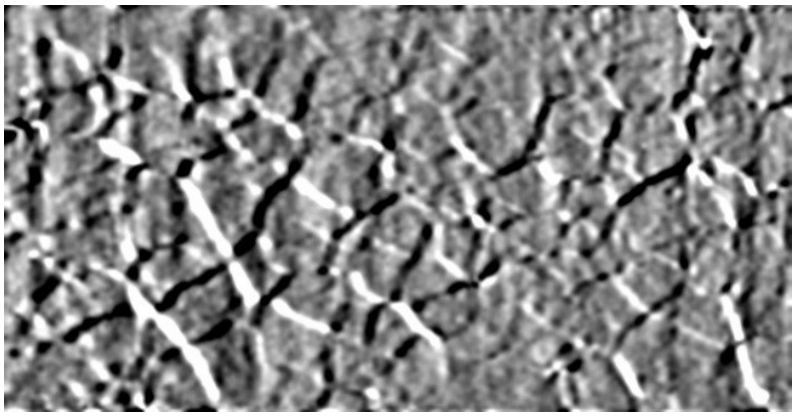

(b)

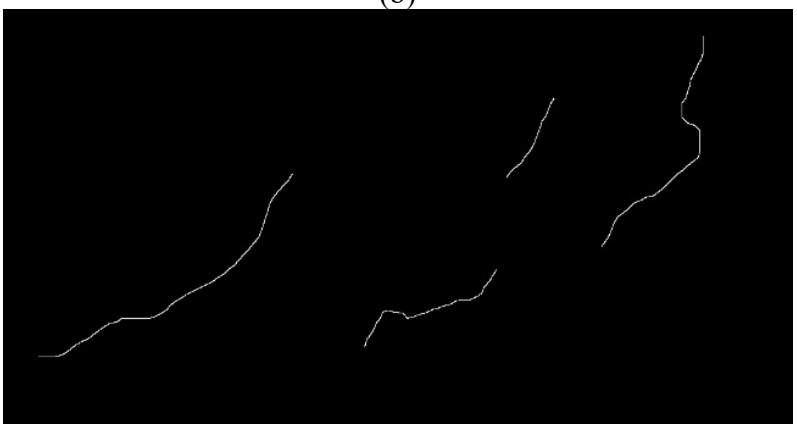

(c)

Figure A.105 TX2 Section 1A-X at 45 days after cast (a) original image (b) Image after filtering (c) Image after tracing and Mask

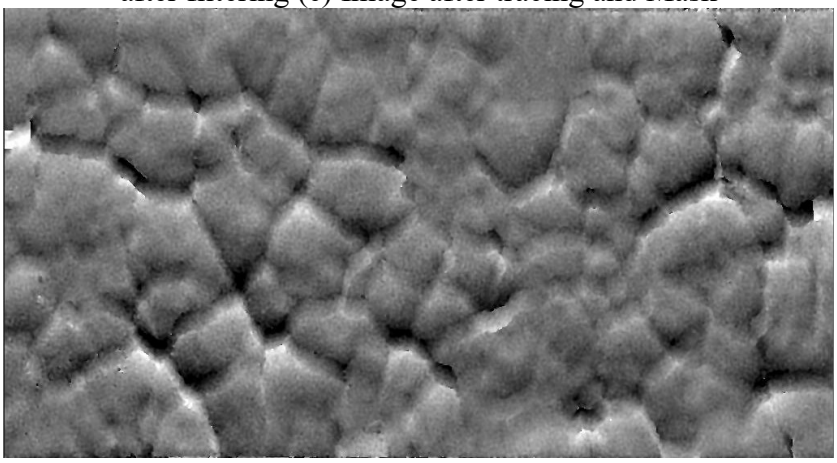

(a)

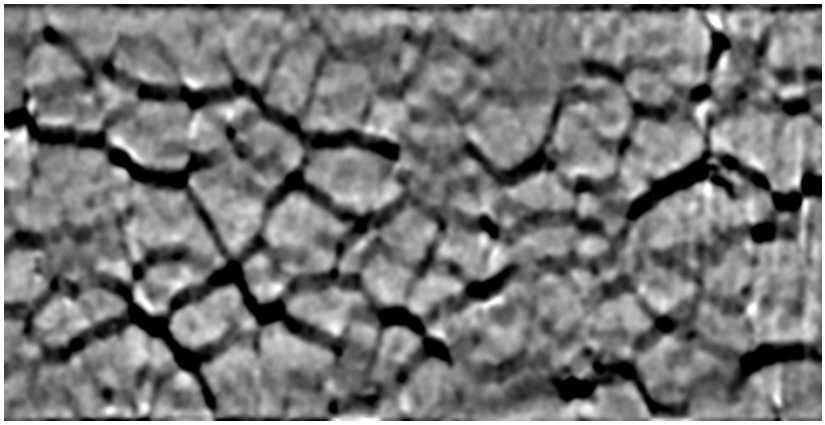

(b)

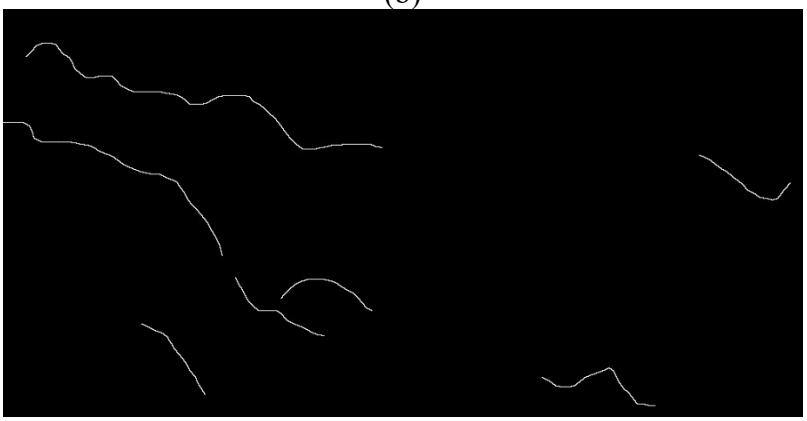

(c)

Figure A.106 TX2 Section 1A-Y at 45 days after cast (a) original image (b) Image after filtering (c) Image after tracing and Mask

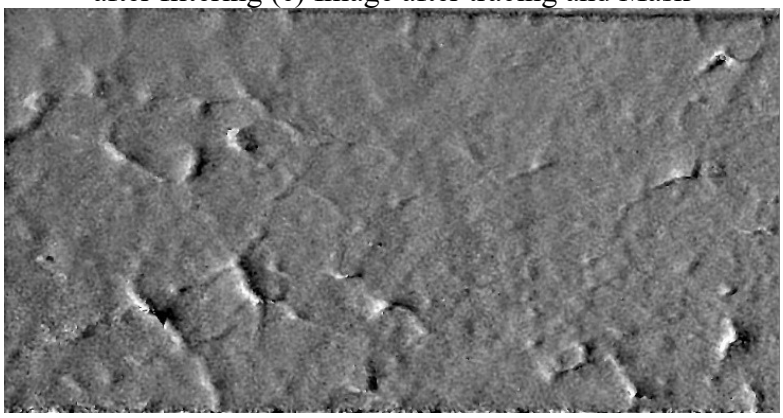

(a)

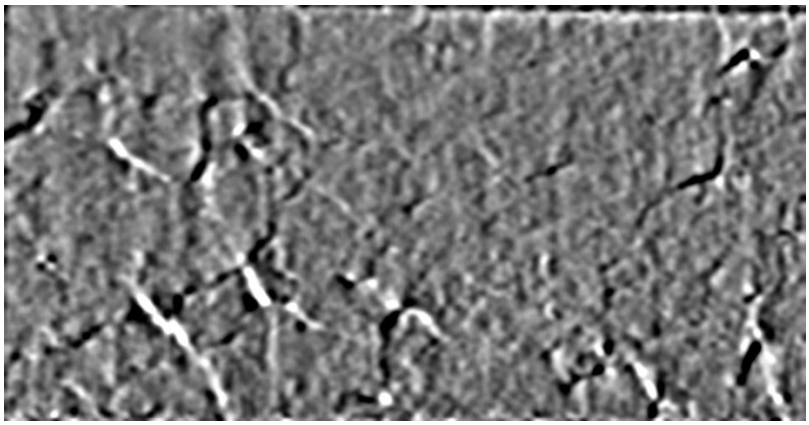

(b)

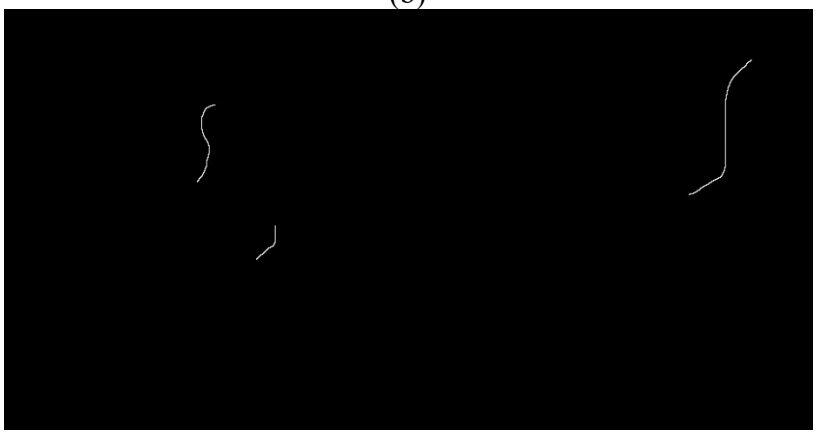

(c)

Figure A.107 TX2 Section 1A-X at 97 days after cast (a) original image (b) Image after filtering (c) Image after tracing and Mask

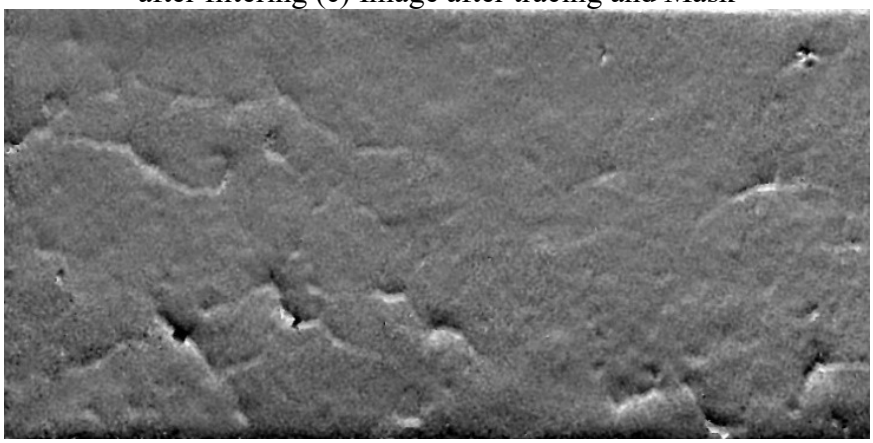

(a)

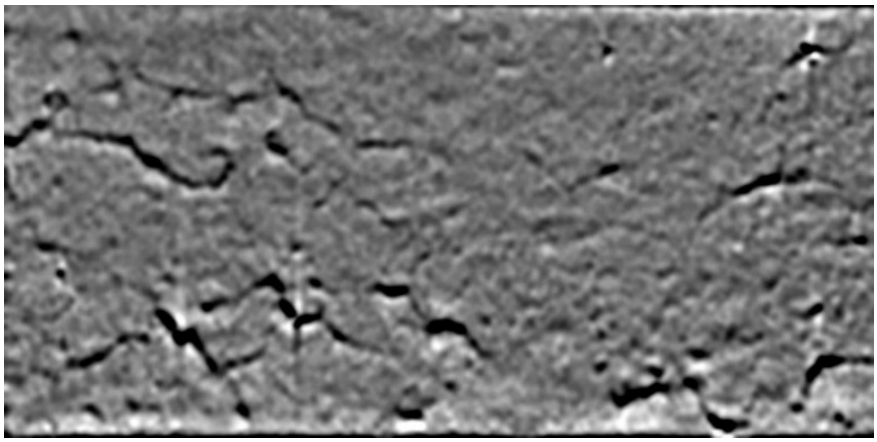

(b)

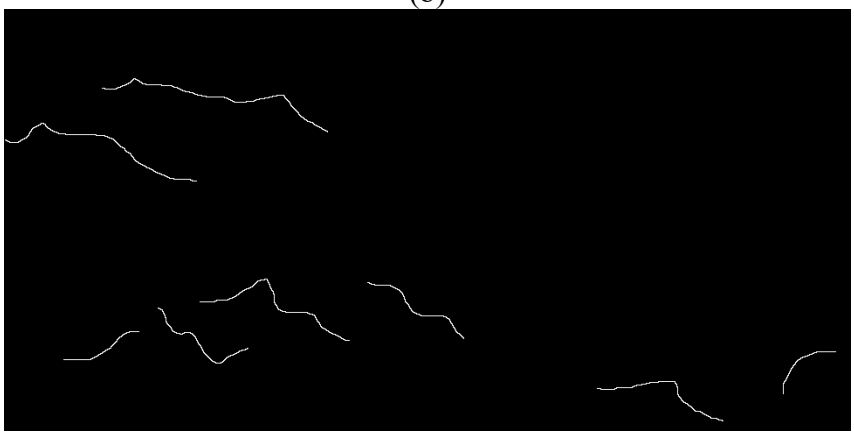

(c)

Figure A.108 TX2 Section 1A-Y at 97 days after cast (a) original image (b) Image after filtering (c) Image after tracing and Mask

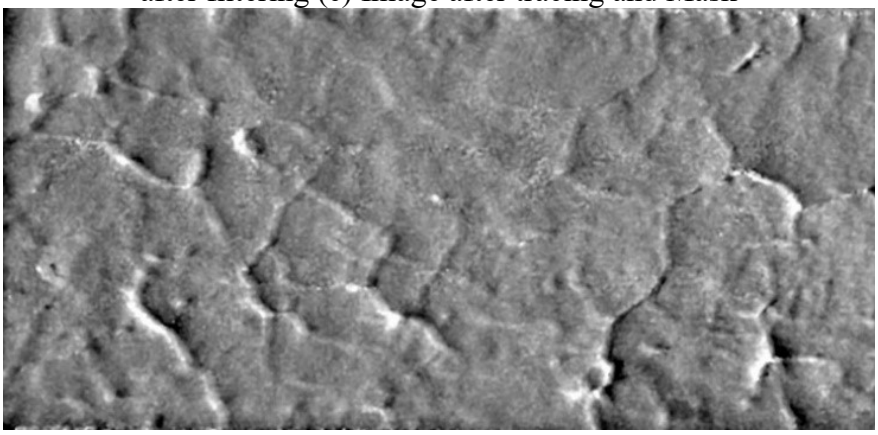

(a)

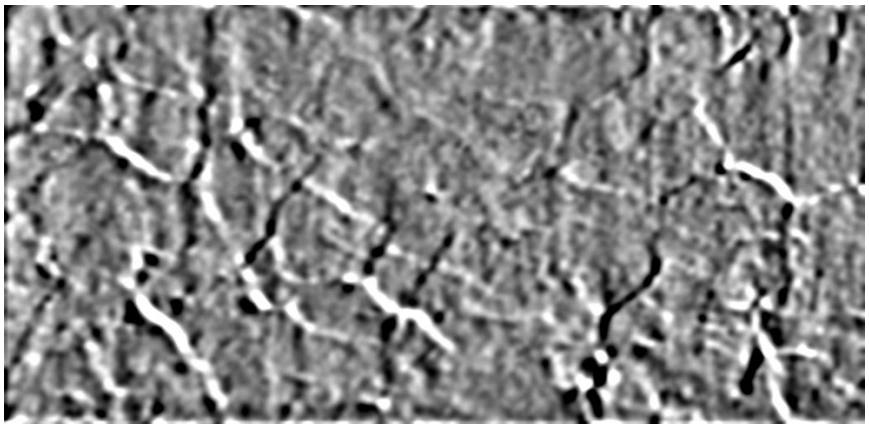

(b)

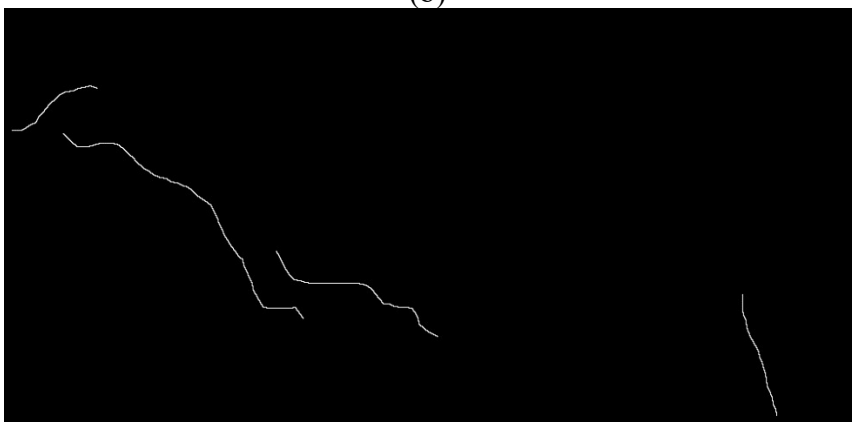

(c)

Figure A.109 TX2 Section 1A-X at 367 days after cast (a) original image (b) Image after filtering (c) Image after tracing and Mask

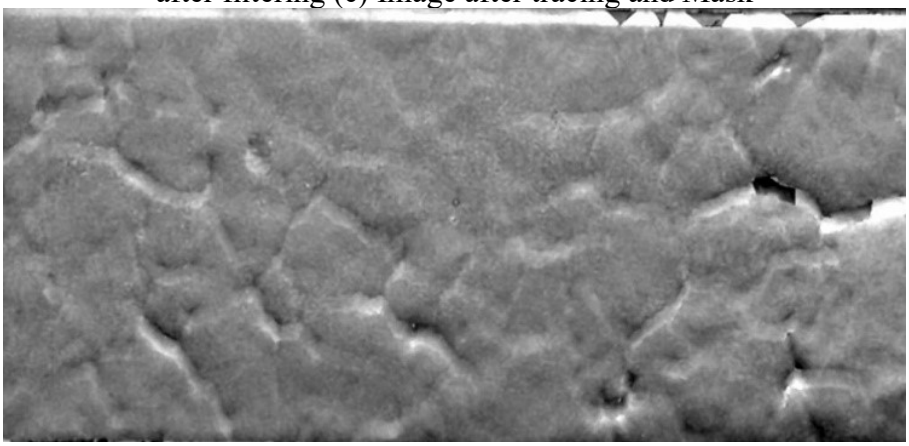

(a)

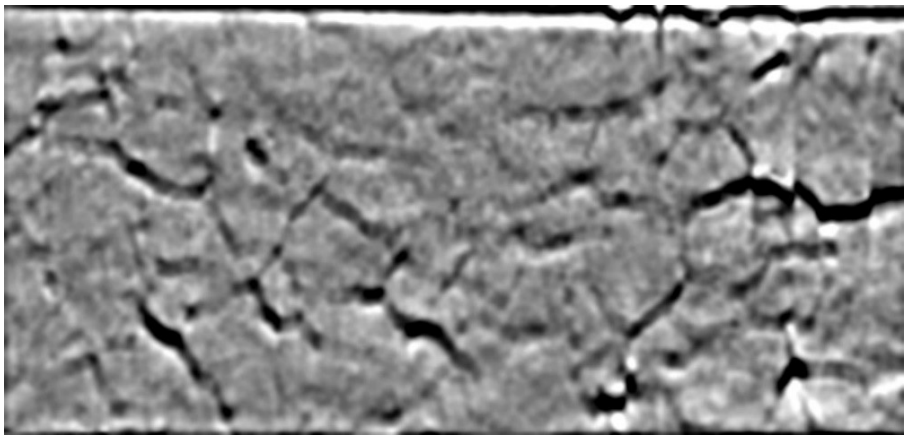

(b)

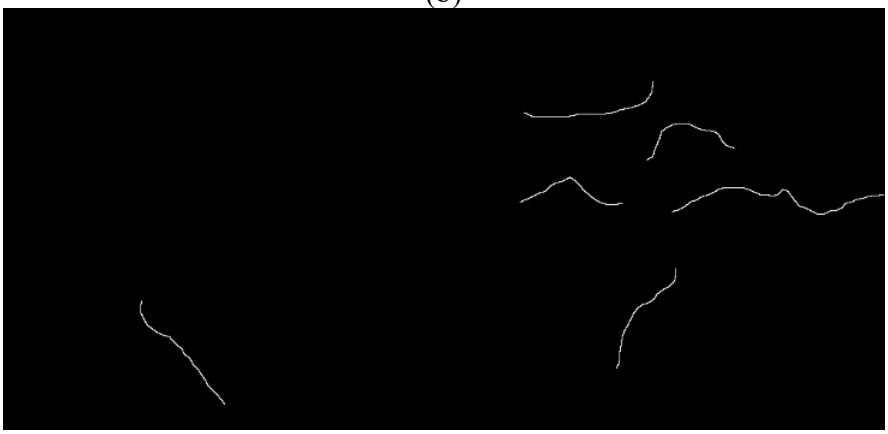

(c)

Figure A.110 TX2 Section 1A-Y at 367 days after cast (a) original image (b) Image after filtering (c) Image after tracing and Mask

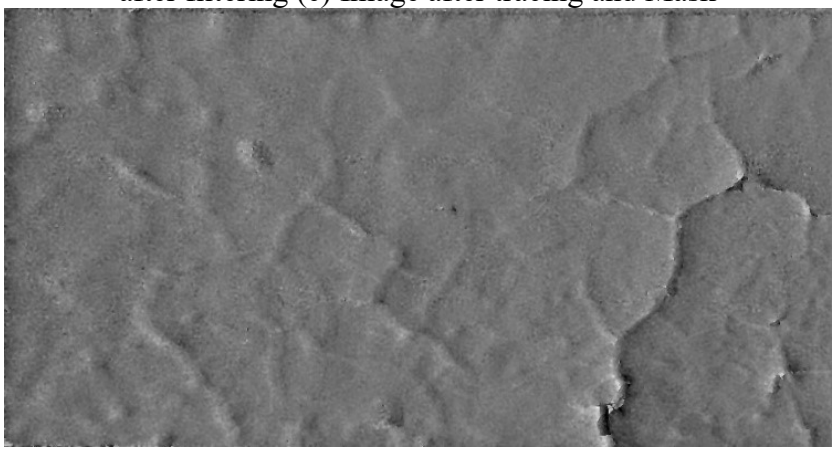

(a)

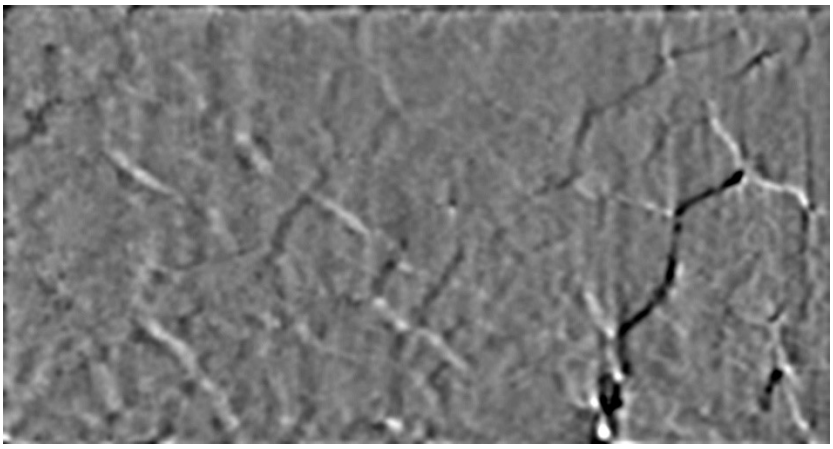

(b)

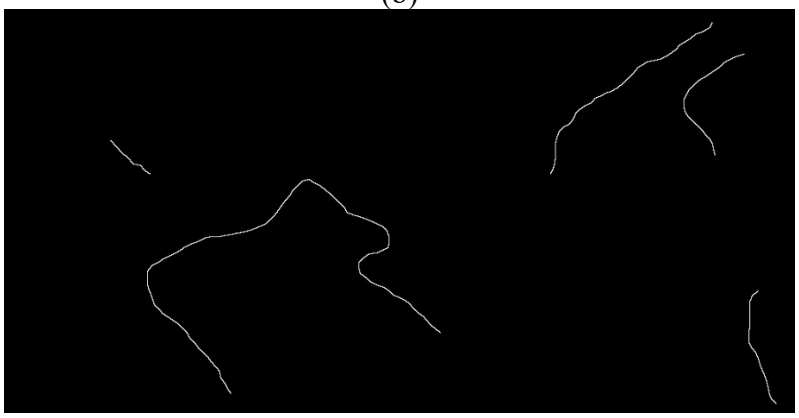

(c)

Figure A.111 TX2 Section 1A-X at 548 days after cast (a) original image (b) Image after filtering (c) Image after tracing and Mask

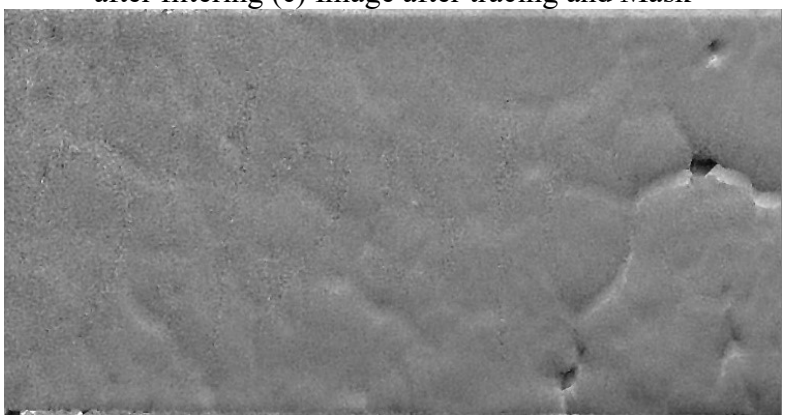

(a)

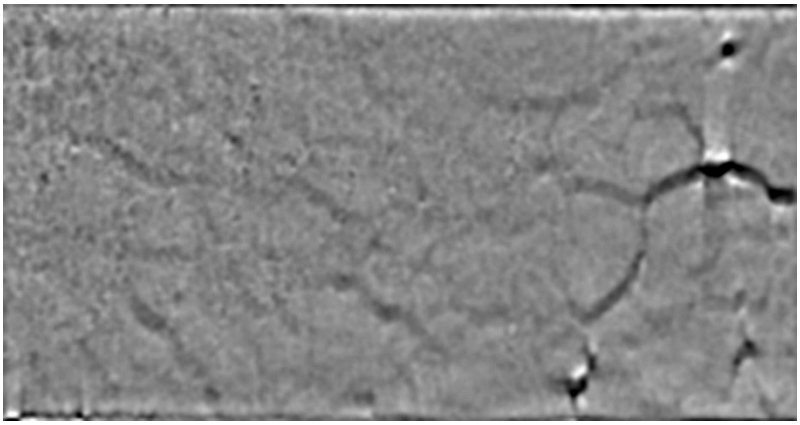

(b)

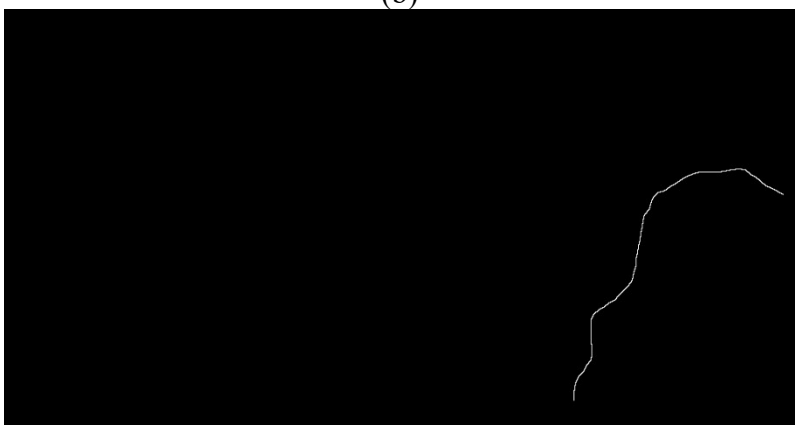

(c)

Figure A.112 TX2 Section 1A-Y at 548 days after cast (a) original image (b) Image after filtering (c) Image after tracing and Mask

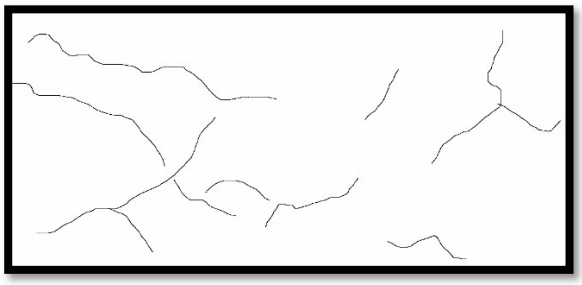

(a)

(b)

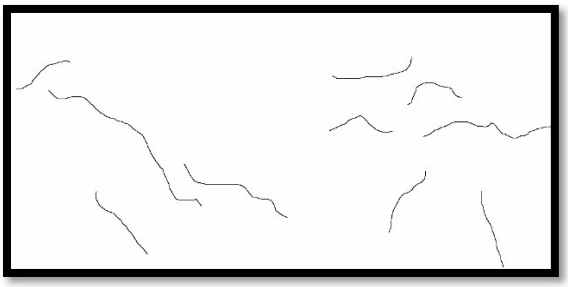

(c)

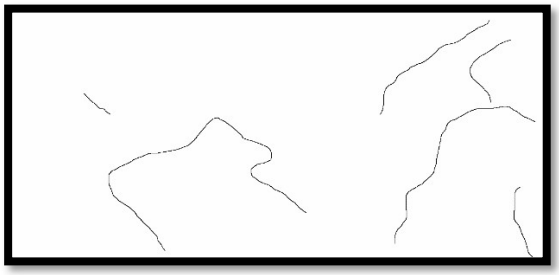

(d)

Figure A.114 Results from Side 2B TX1 (a) Average Length vs Number of Days (b) Number of Cracks vs Number of Days

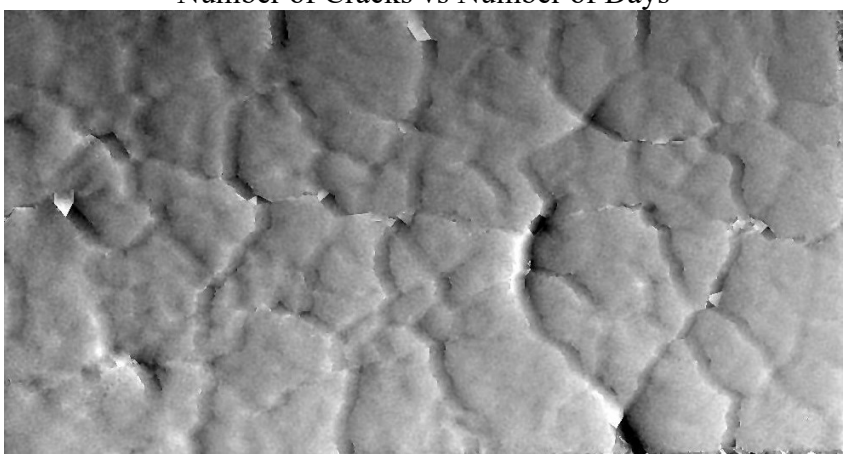

(a)

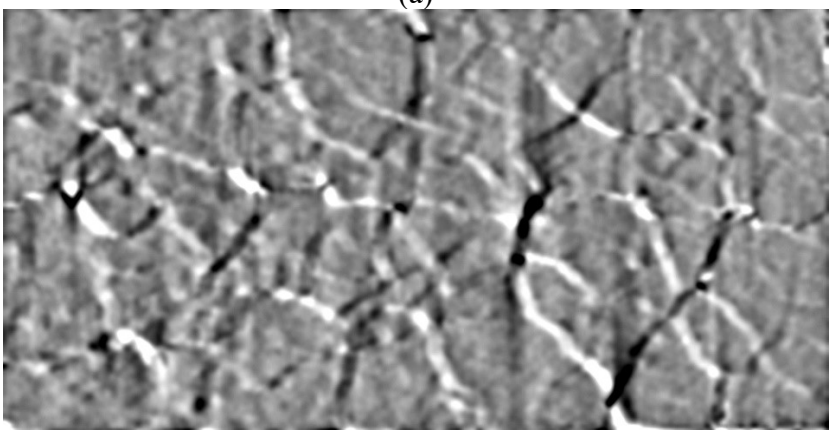

(b)

(c)

Figure A.115 TX2 Section 1B-X at 45 days after cast (a) original image (b) Image after filtering (c) Image after tracing and Mask

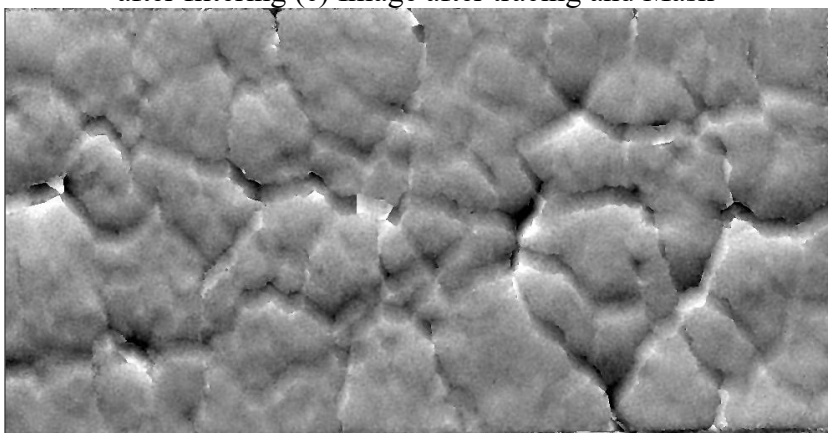

(a)

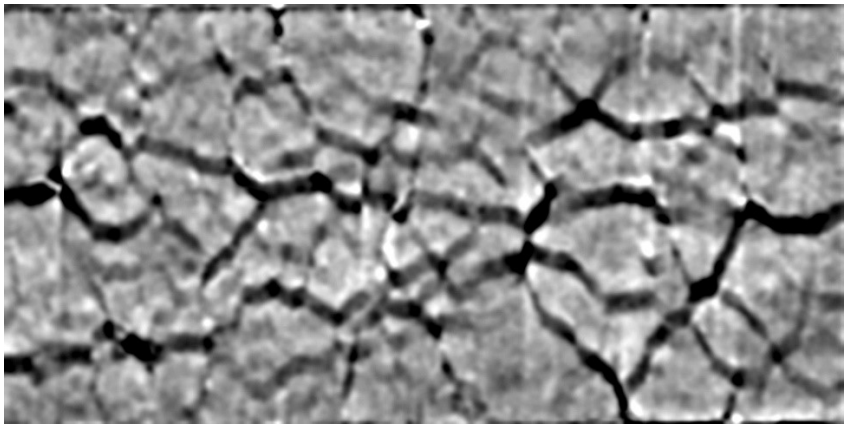

(b)

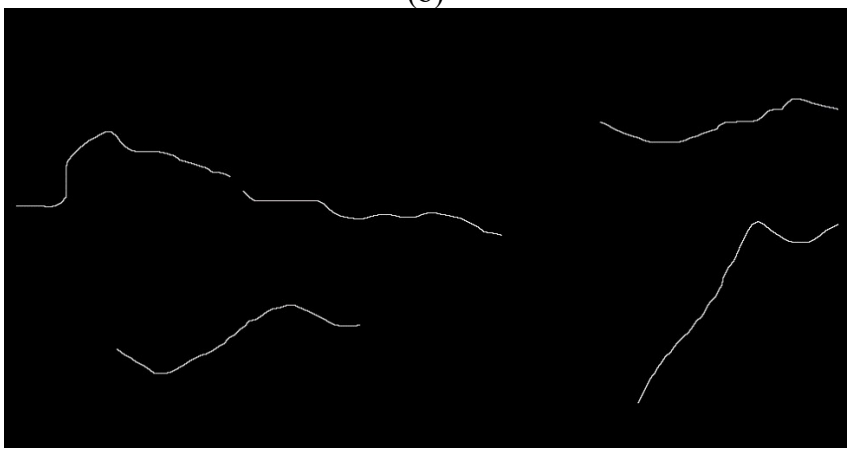

(c)

Figure A.116 TX2 Section 1B-Y at 45 days after cast (a) original image (b) Image after filtering (c) Image after tracing and Mask

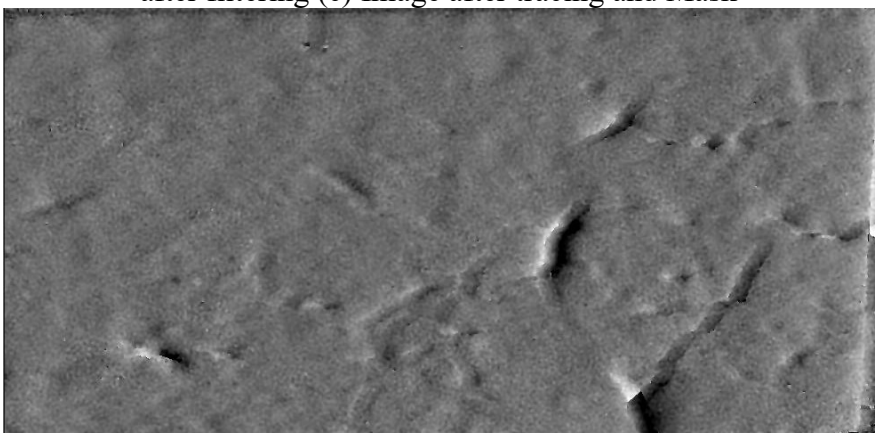

(a)

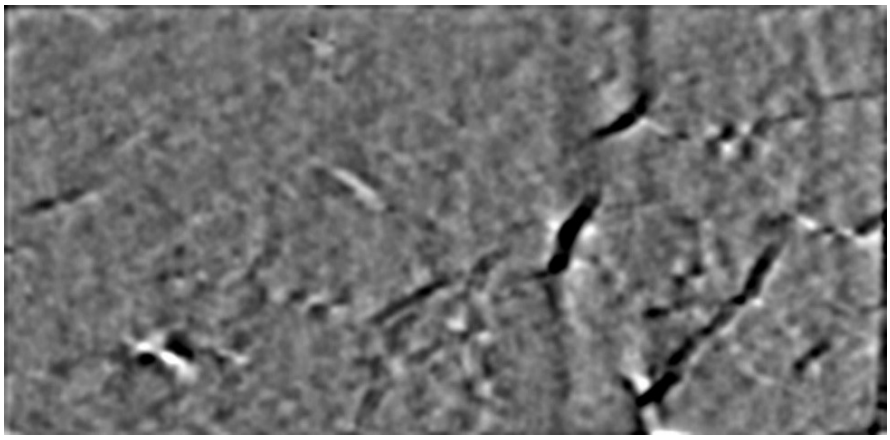

(b)

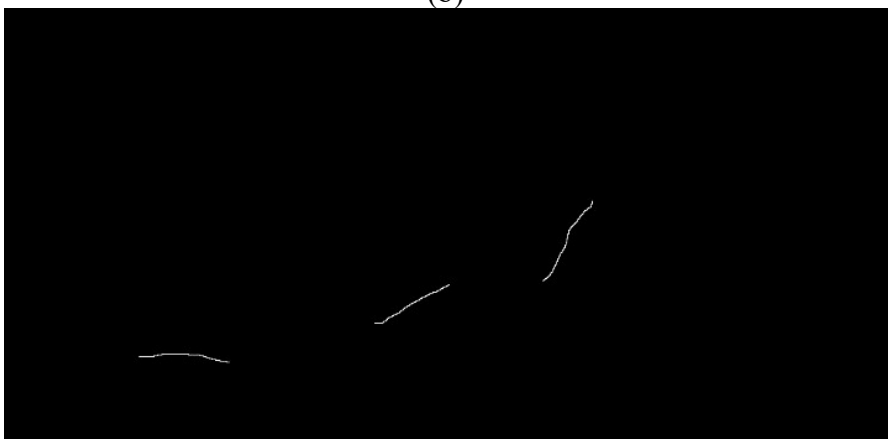

(c)

Figure A.117 TX2 Section 1B-X at 97 days after cast (a) original image (b) Image after filtering (c) Image after tracing and Mask

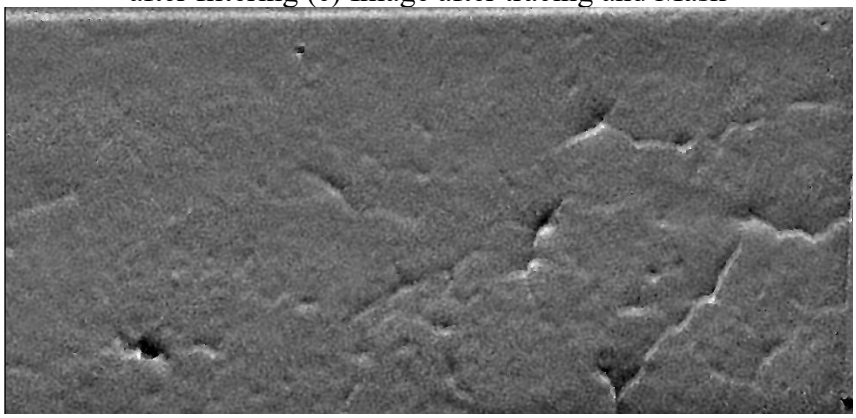

(a)

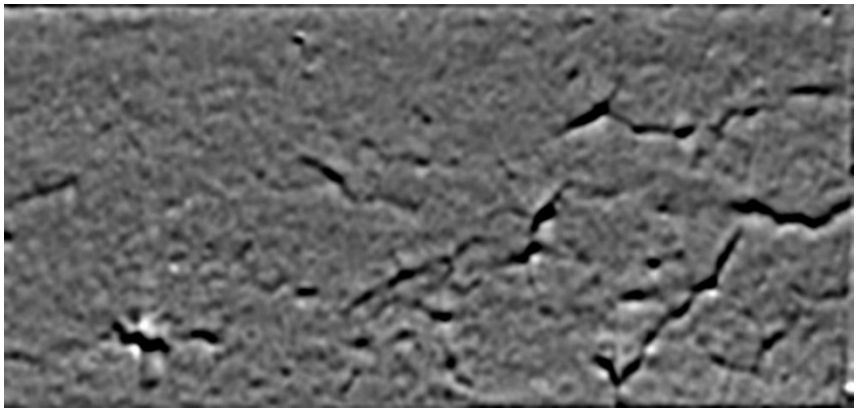

(b)

(c)

Figure A.118 TX2 Section 1B-Y at 97 days after cast (a) original image (b) Image after filtering (c) Image after tracing and Mask

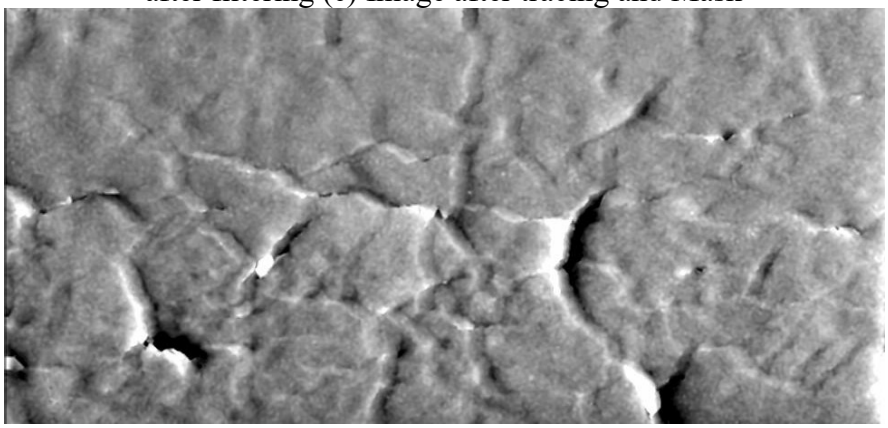

(a)

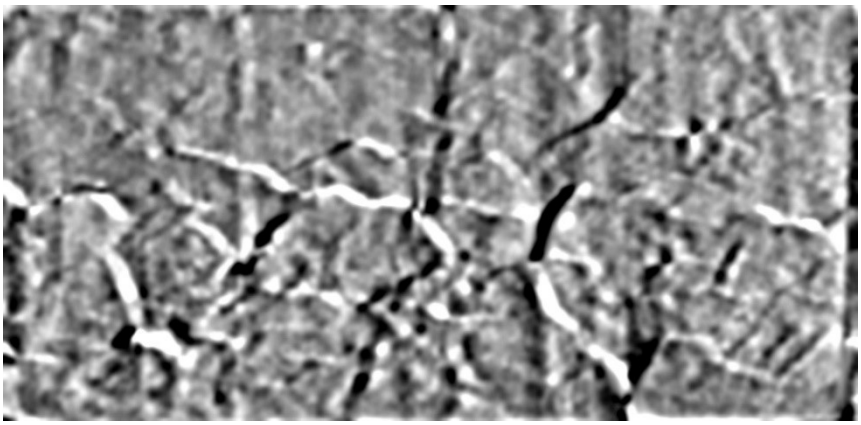

(b)

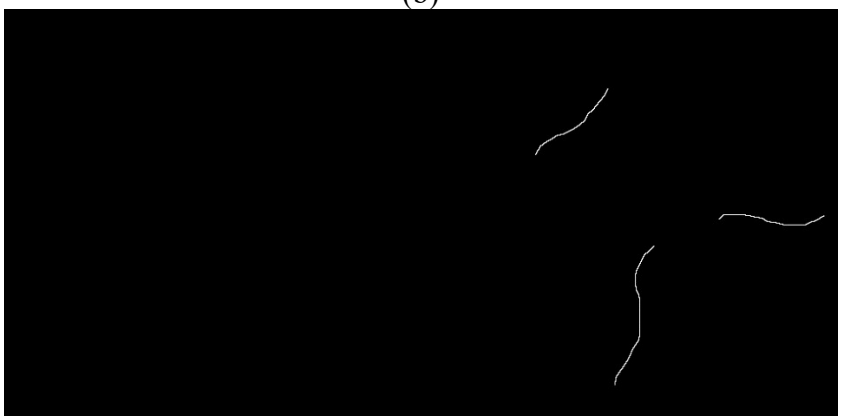

(c)

Figure A.119 TX2 Section 1B-X at 327 days after cast (a) original image (b) Image after filtering (c) Image after tracing and Mask

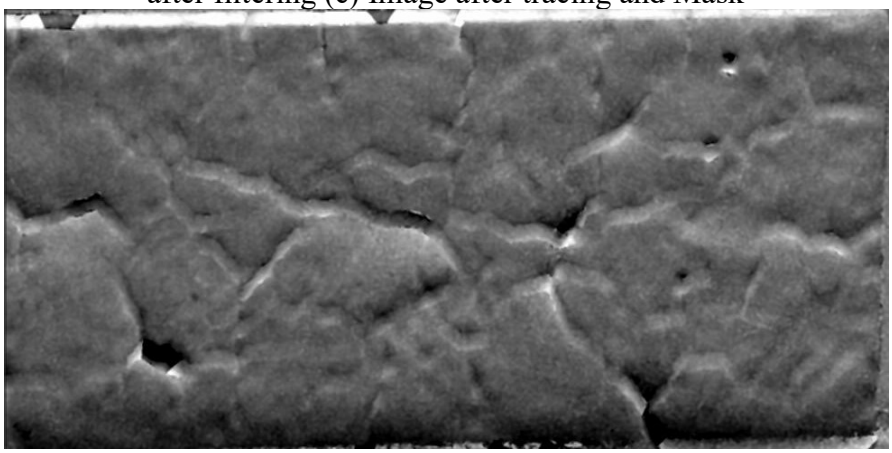

(a)

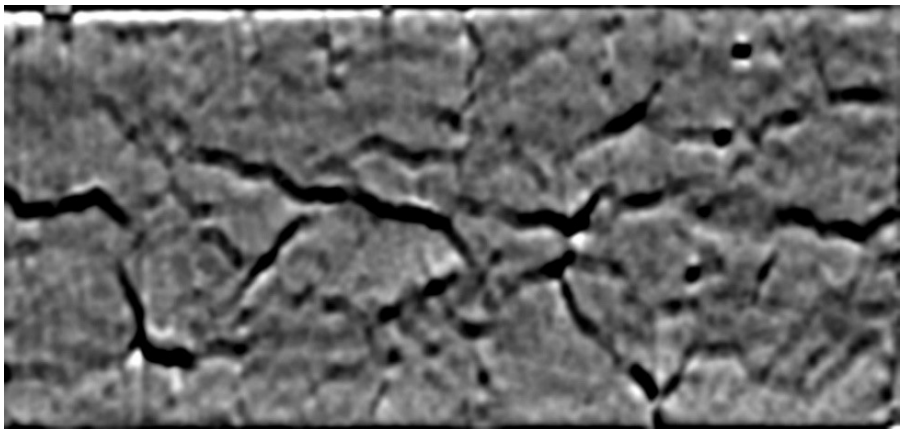

(b)

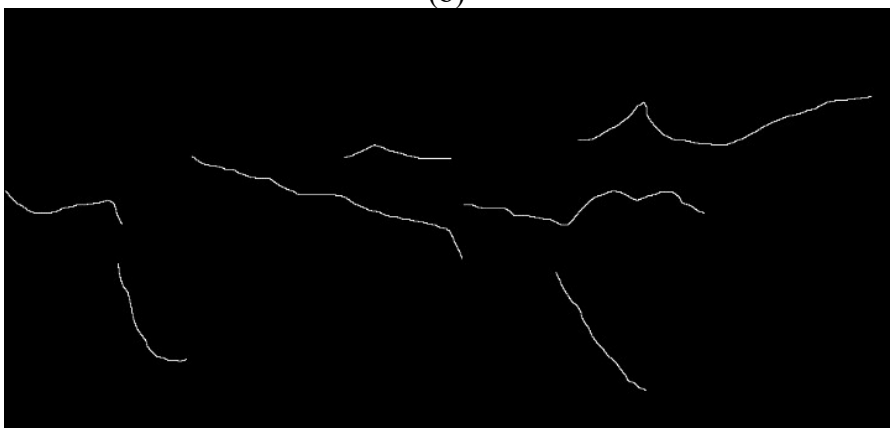

(c)

Figure A.120 TX2 Section 1B-Y at 327 days after cast (a) original image (b) Image after filtering (c) Image after tracing and Mask

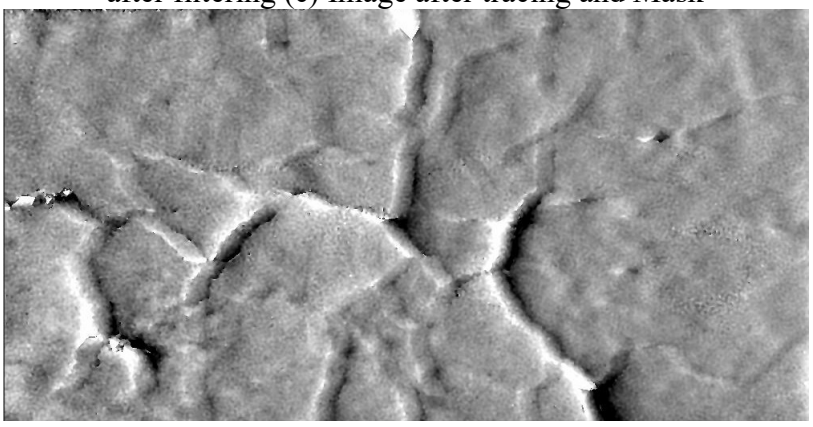

(a)

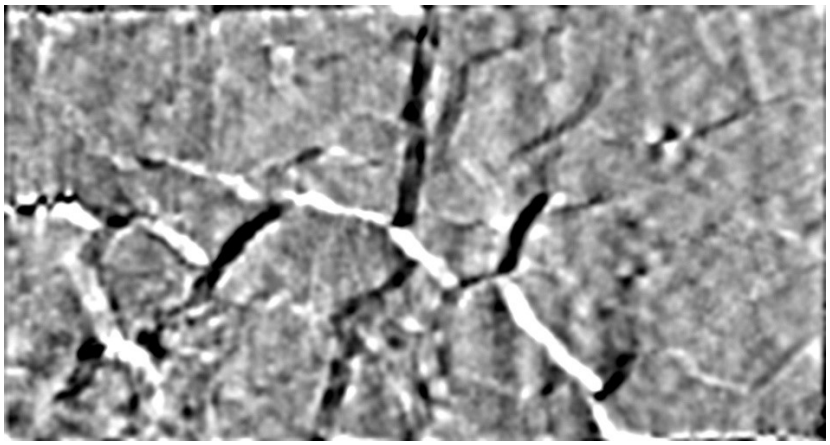

(b)

(c)

Figure A.121 TX2 Section 1B-X at 548 days after cast (a) original image (b) Image after filtering (c) Image after tracing and Mask

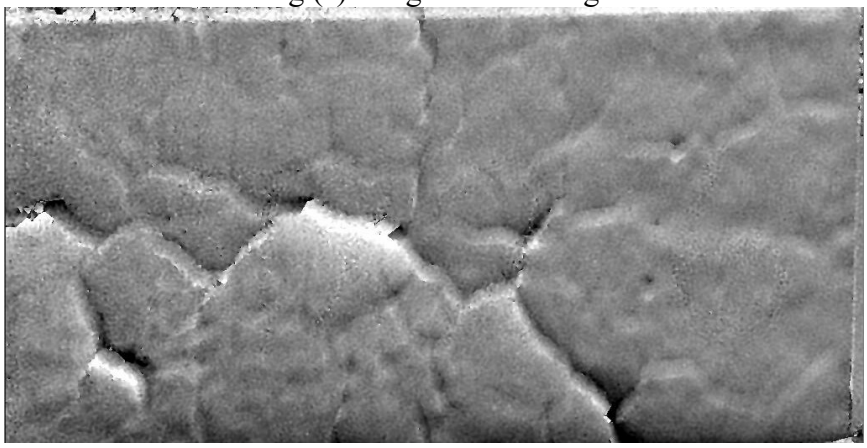

(a)

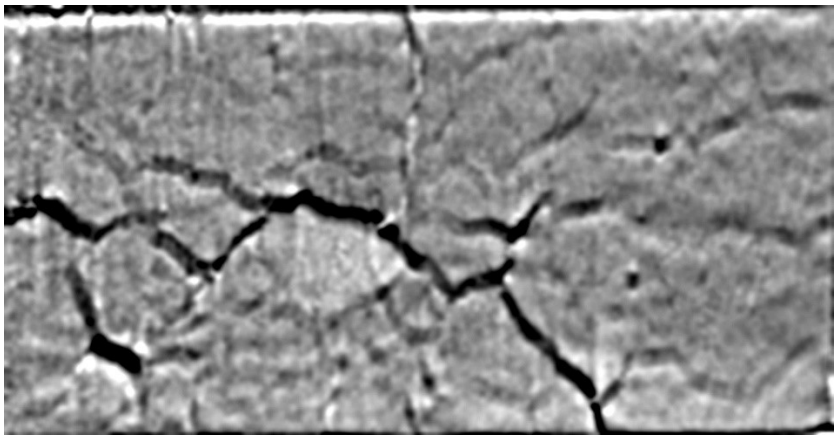

(B)

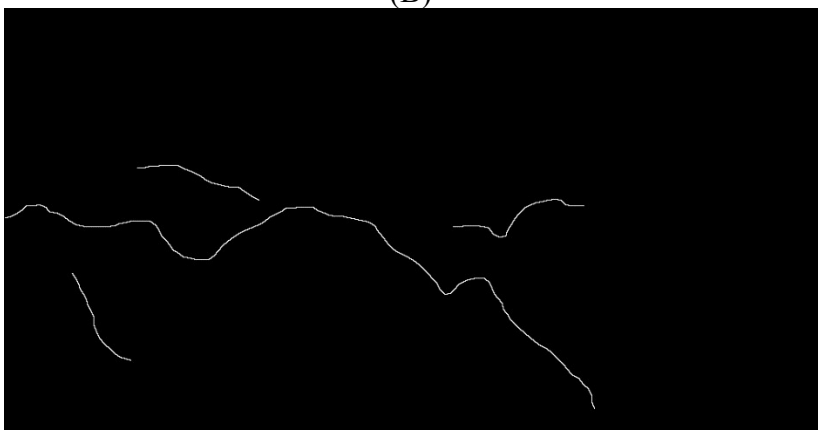

(C)

Figure A.122 TX2 Section 1B-Y at 548 days after cast (a) original image (b) Image after filtering (c) Image after tracing and Mask

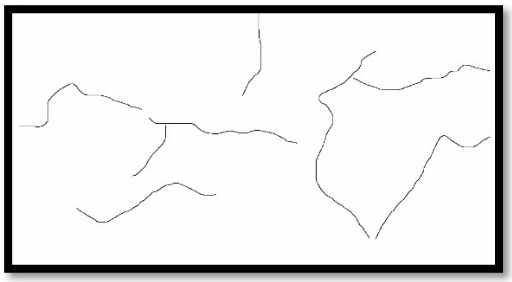

(a)

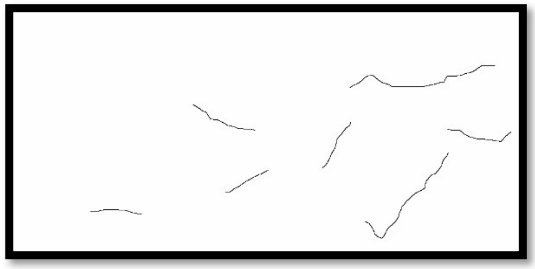

(b)

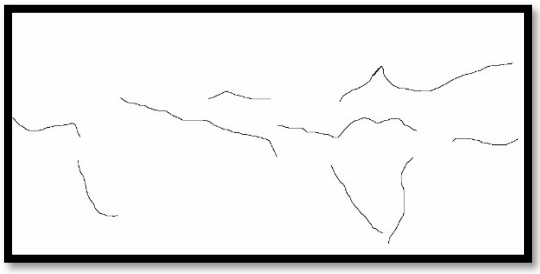

(c)

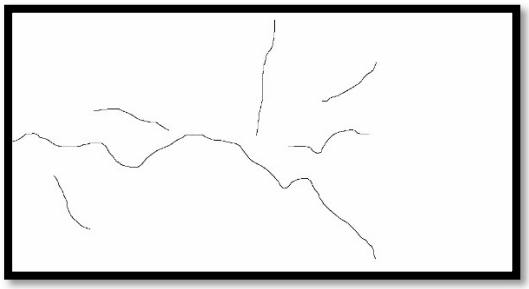

(d)

Figure A.123 Section 1B TX2 Mask X and Y shear direction combined traced cracks and inverted (a) 45 Days (b) 97 Days (c) 467 Days (d) 548 Days

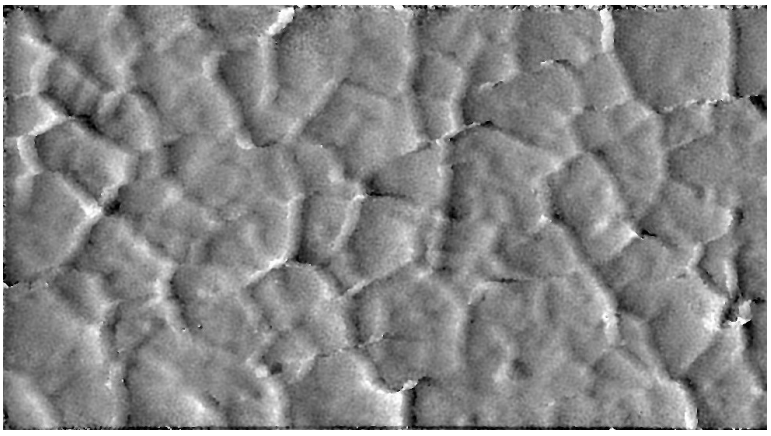

(a)

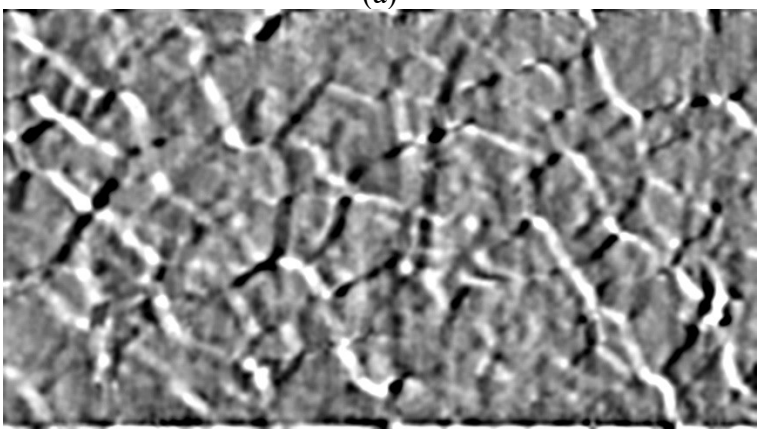

(b)

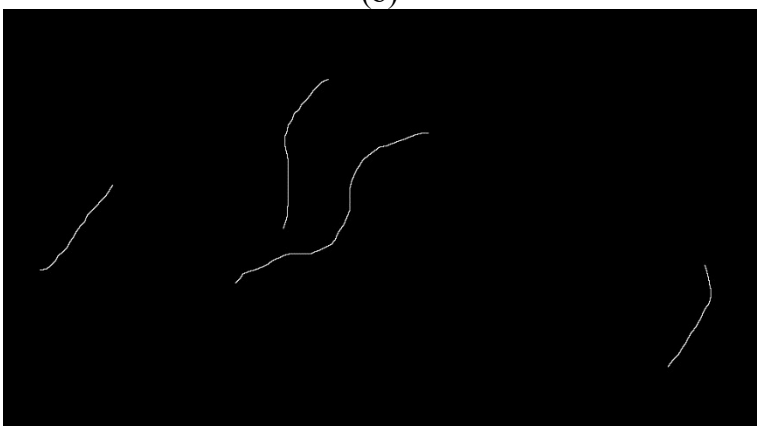

(c)

Figure A.125 TX2 Section 2A-X at 45 days after cast (a) original image (b) Image after filtering (c) Image after tracing and Mask

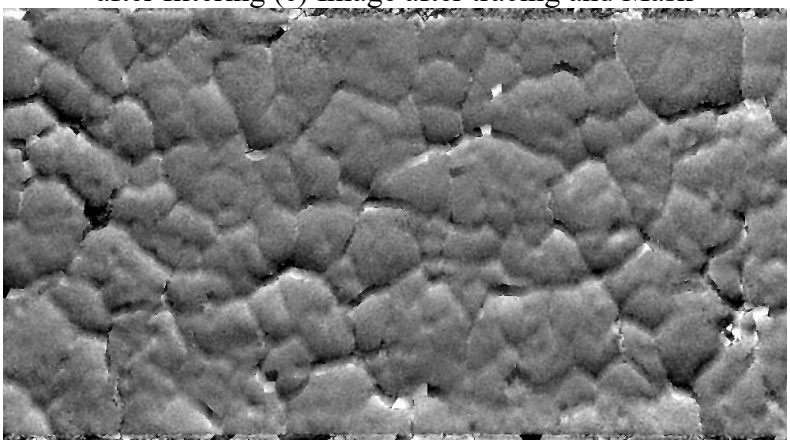

(a)

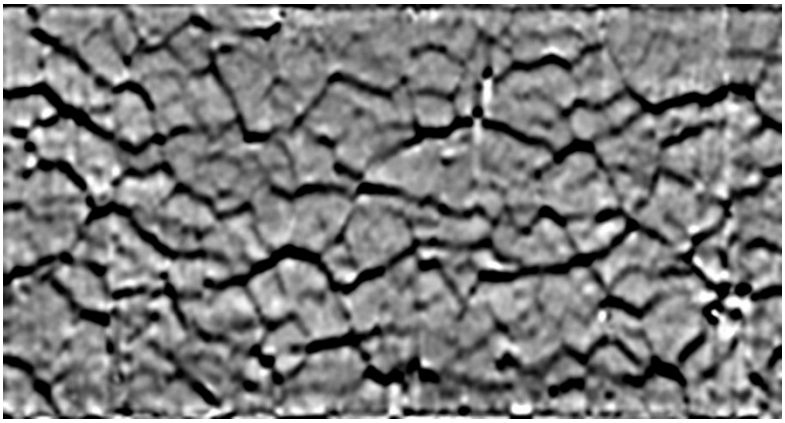

(b)

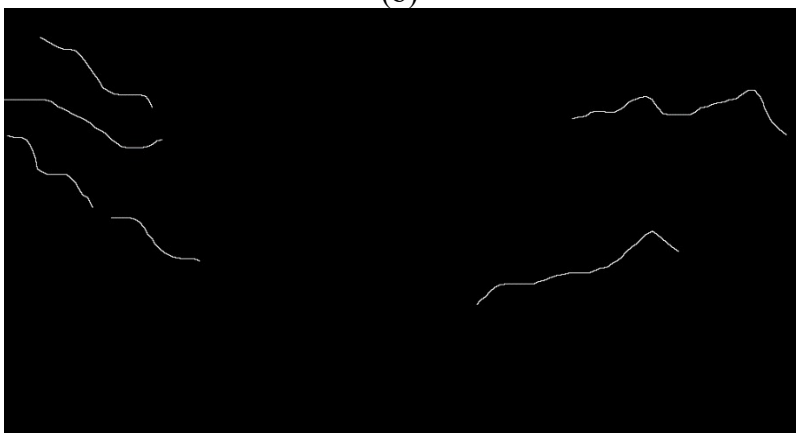

(c)

Figure A.126 TX2 Section 2A-Y at 45 days after cast (a) original image (b) Image after filtering (c) Image after tracing and Mask

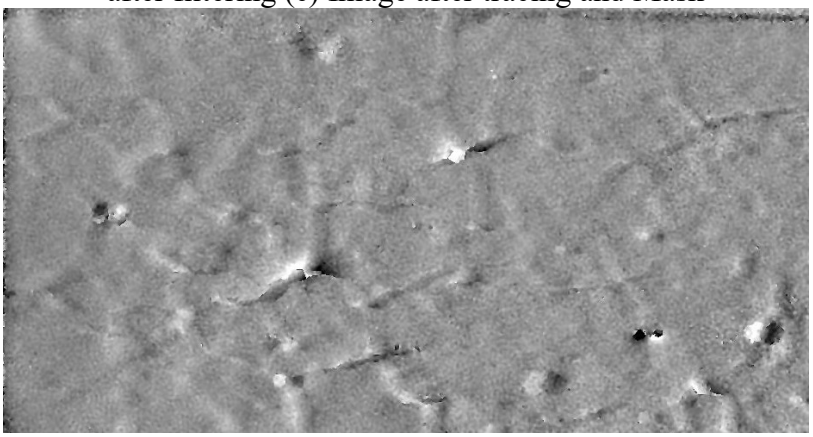

(a)

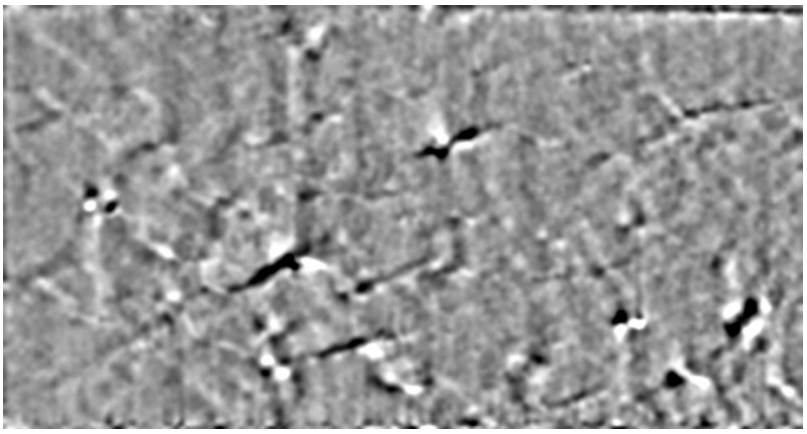

(b)

(c)

Figure A.127 TX2 Section 2A-X at 97 days after cast (a) original image (b) Image after filtering (c) Image after tracing and Mask

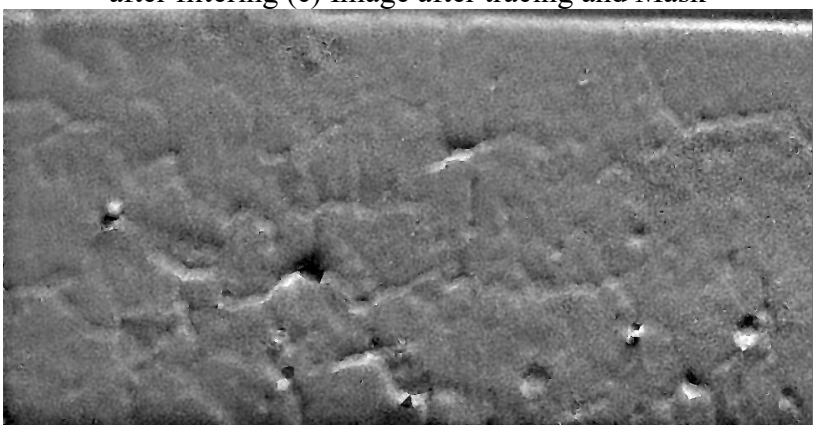

(a)

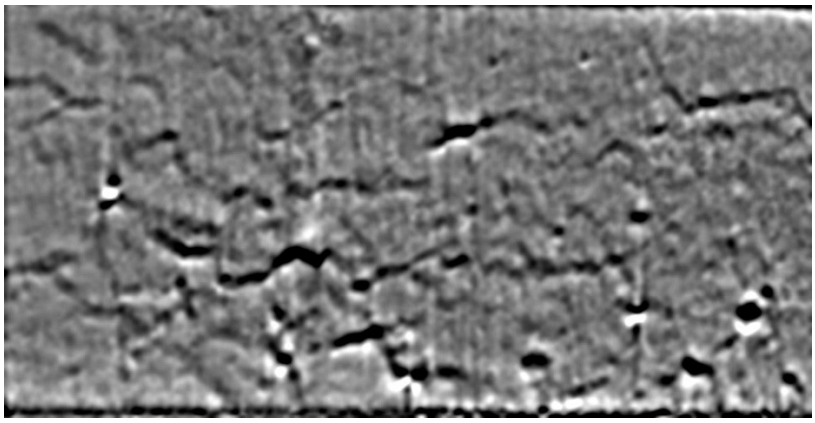

(b)

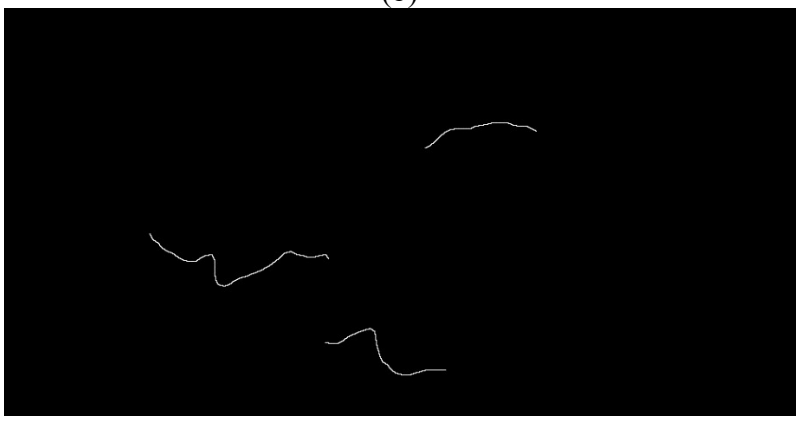

(c)

Figure A.128 TX2 Section 2A-Y at 97 days after cast (a) original image (b) Image after filtering (c) Image after tracing and Mask

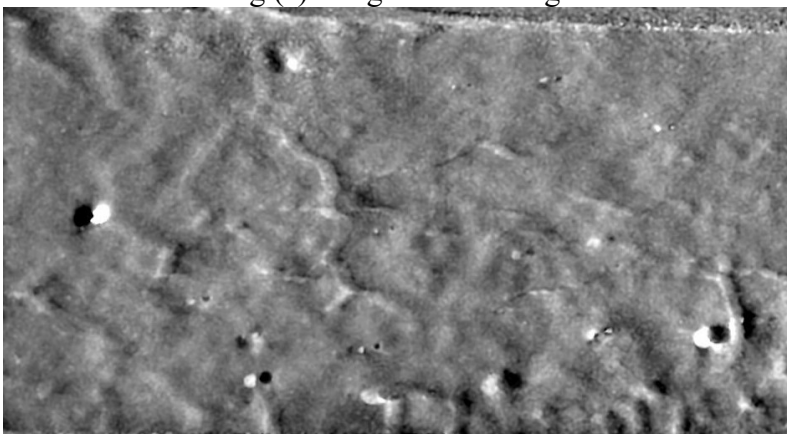

(a)

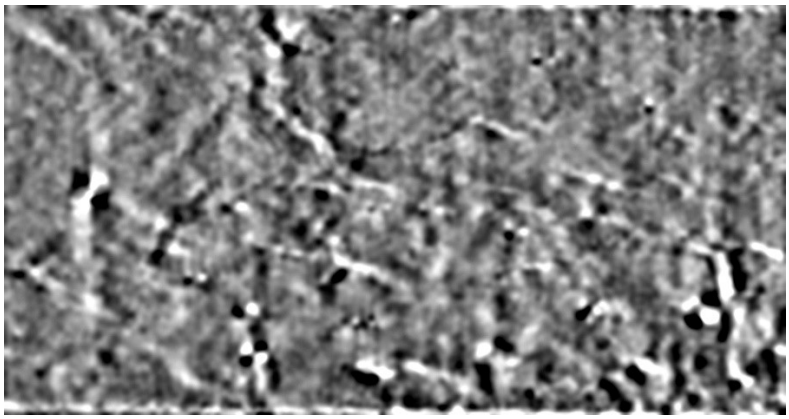

(b)

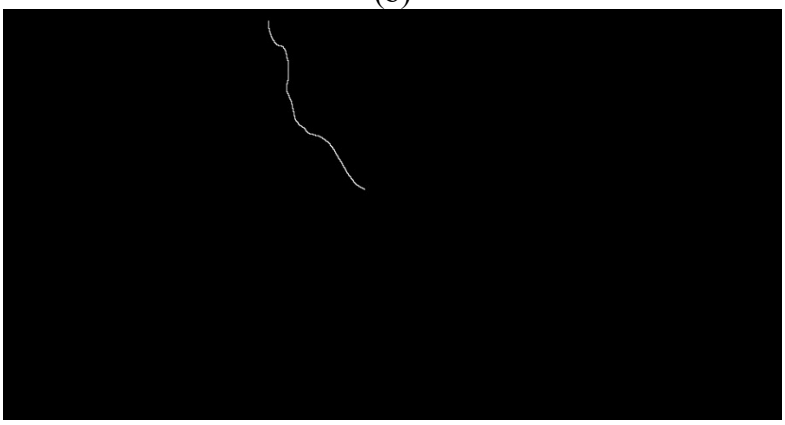

(c)

Figure A.129 TX2 Section 2A-X at 327 days after cast (a) original image (b) Image after filtering (c) Image after tracing and Mask

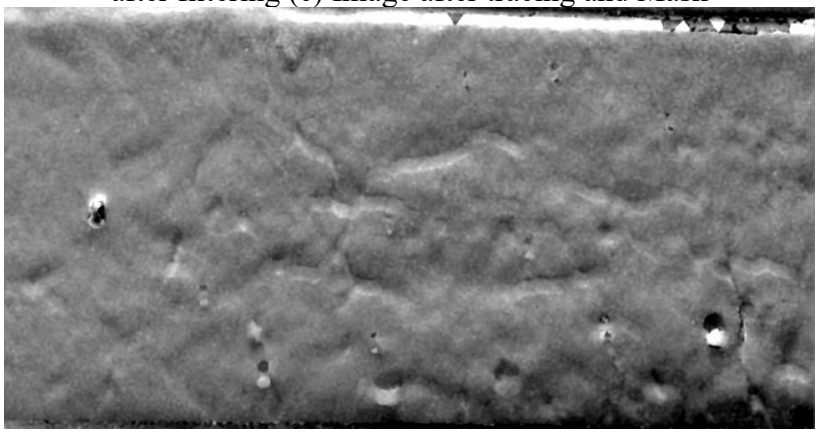

(a)

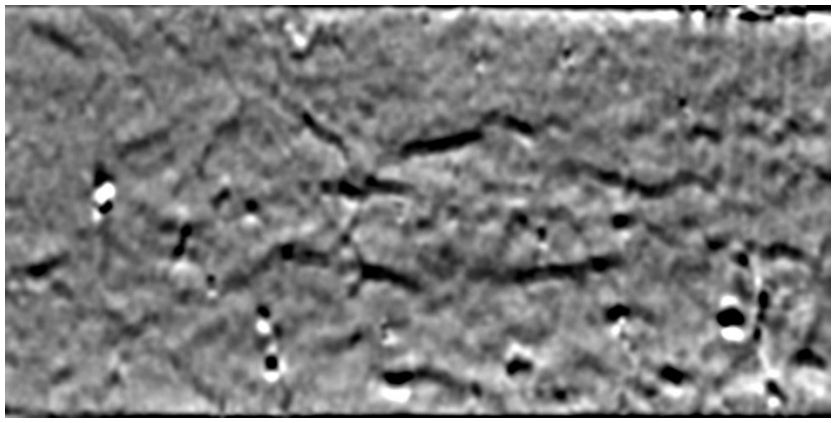

(b)

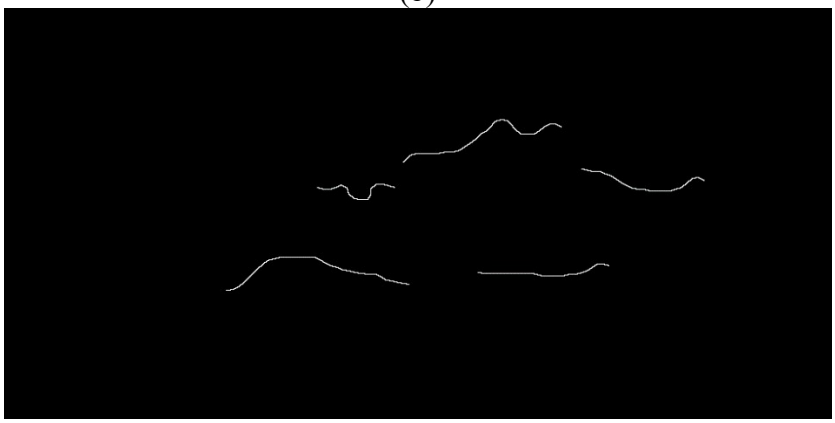

(c)

Figure A.130 TX2 Section 2A-Y at 327 days after cast (a) original image (b) Image after filtering (c) Image after tracing and Mask

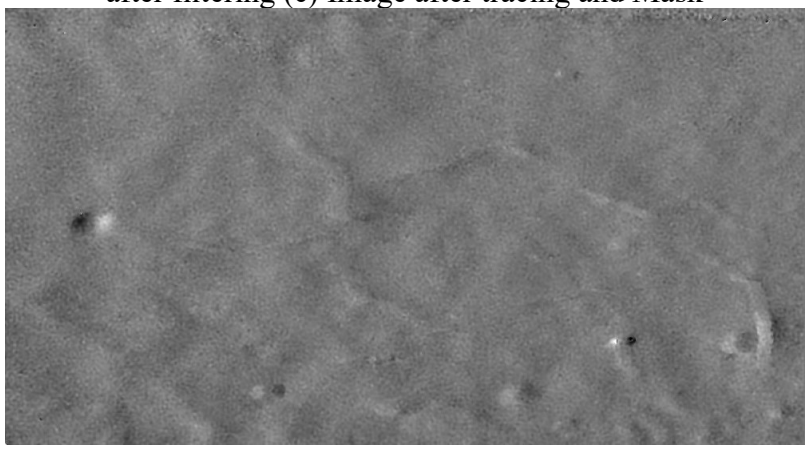

(a)

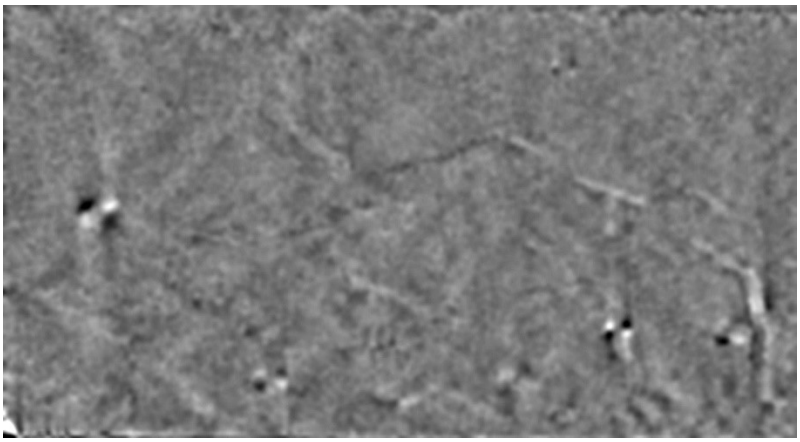

(b)

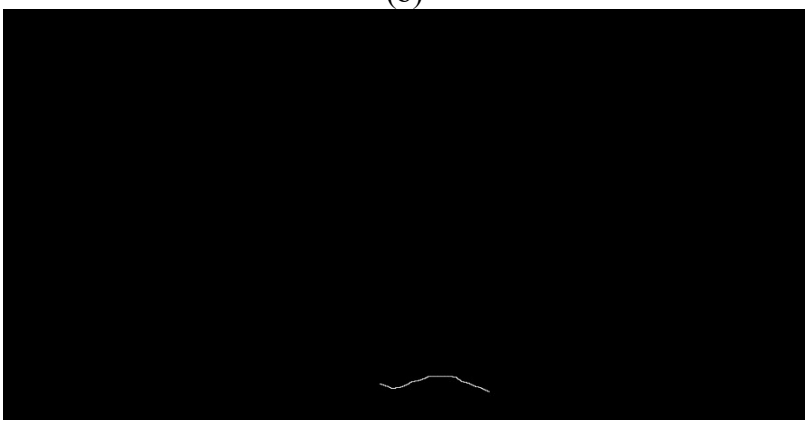

(c)

Figure A.131 TX2 Section 2A-X at 548 days after cast (a) original image (b) Image after filtering (c) Image after tracing and Mask

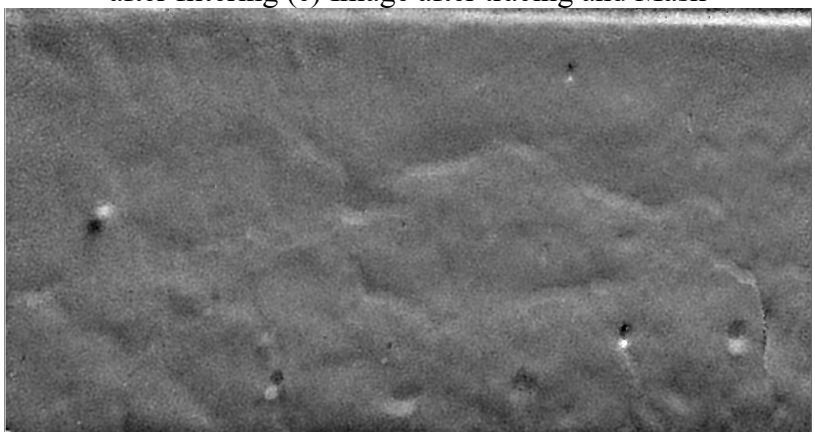

(a)

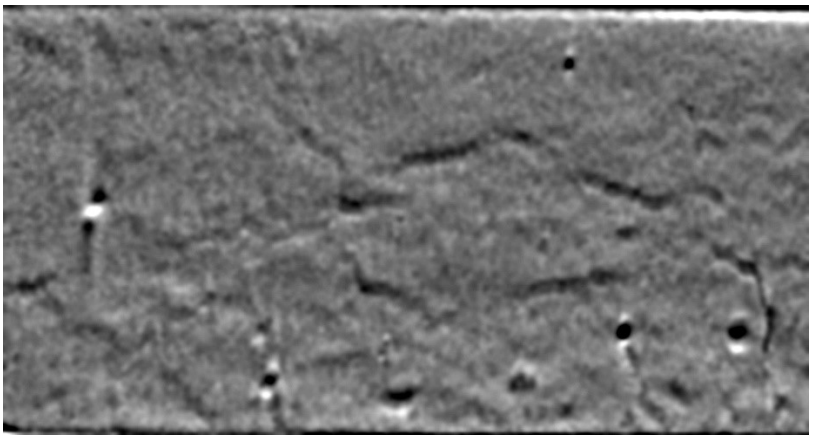

(b)

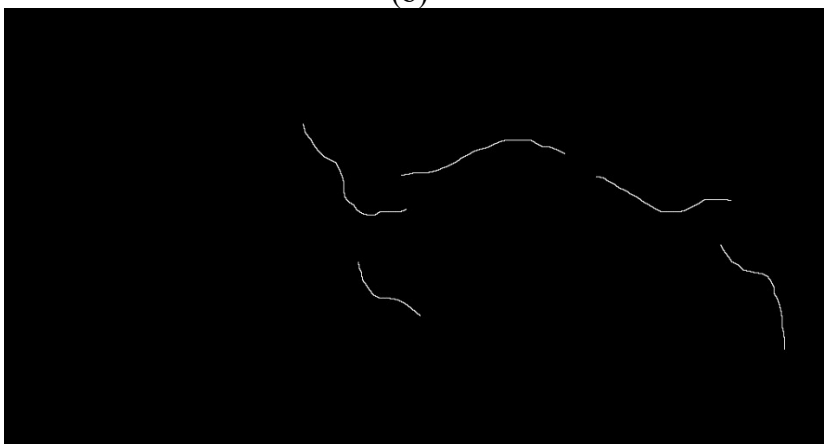

(c)

Figure A.132 TX2 Section 2A-Y at 548 days after cast (a) original image (b) Image after filtering (c) Image after tracing and Mask

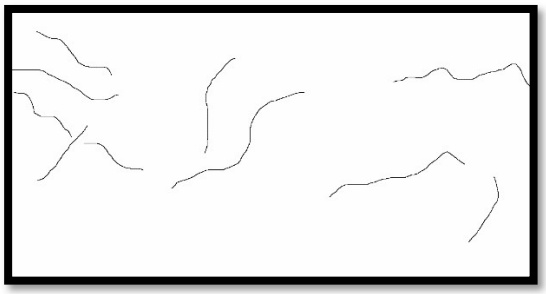

(a)

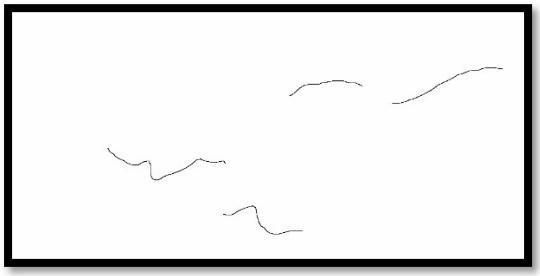

(b)

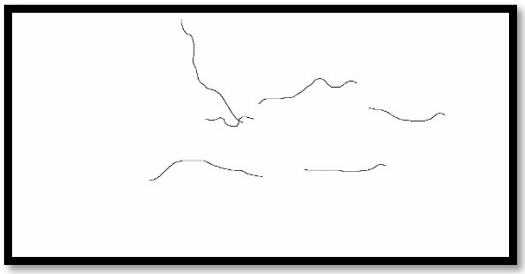

(c)

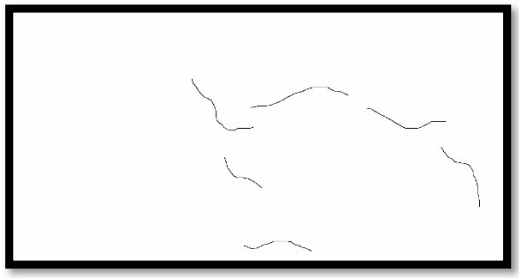

(d)

Figure A.133 Section 2A TX2 Mask X and Y shear direction combined traced cracks and inverted (a) 45 Days (b) 97 Days (c) 467 Days (d) 548 Days

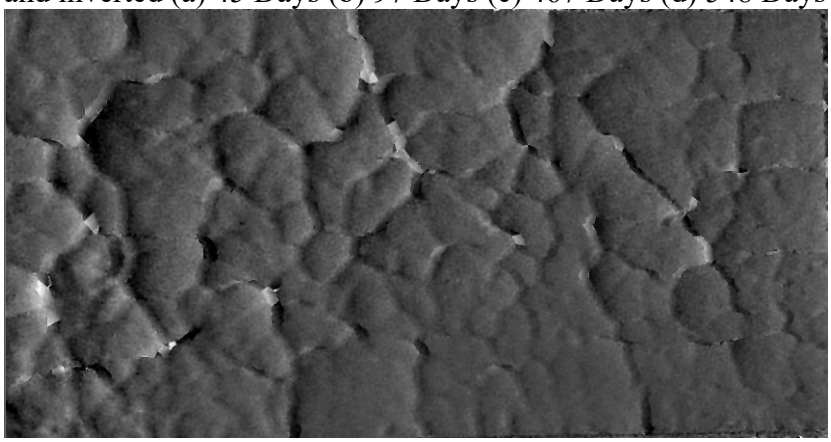

(a)

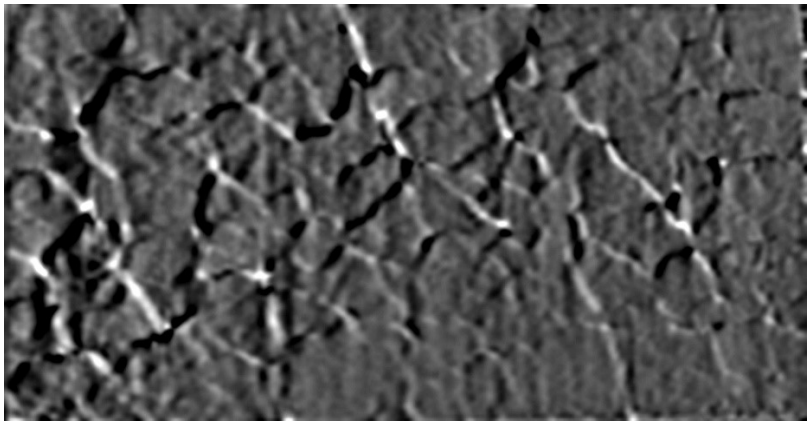

(b)

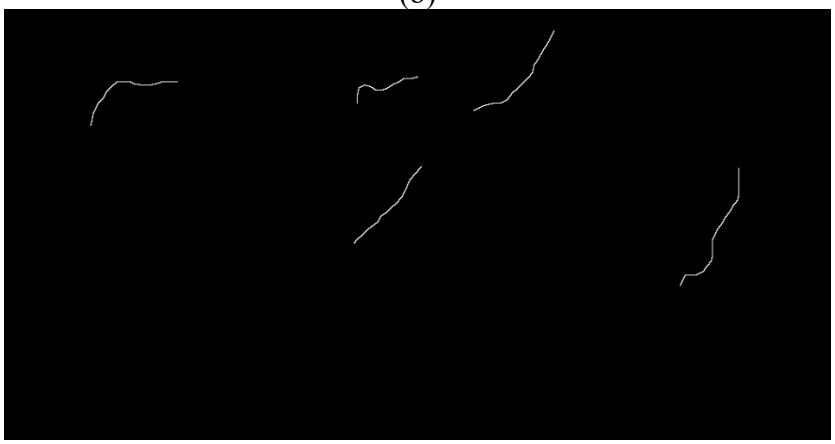

(c)

Figure A.135 TX2 Section 2B-X at 45 days after cast (a) original image (b) Image after filtering (c) Image after tracing and Mask

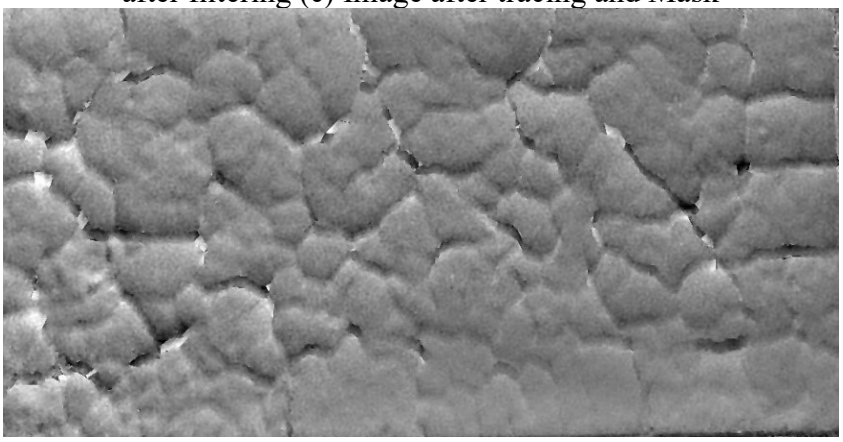

(a)

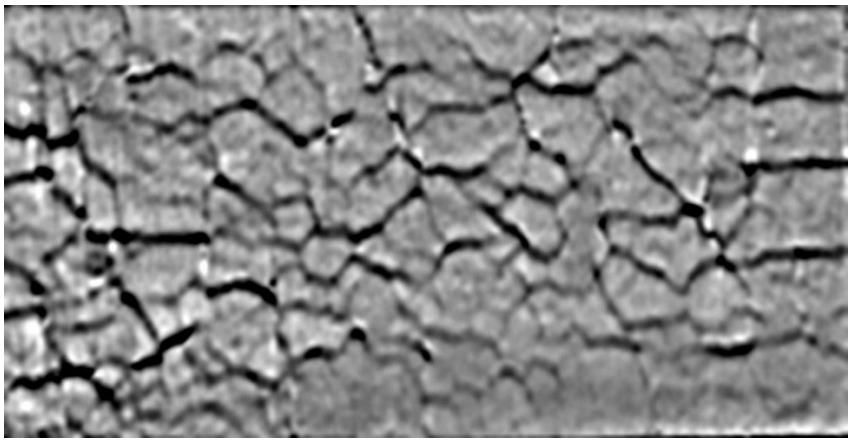

(b)

(c)

Figure A.136 TX2 Section 2B-X at 45 days after cast (a) original image (b) Image after filtering (c) Image after tracing and Mask

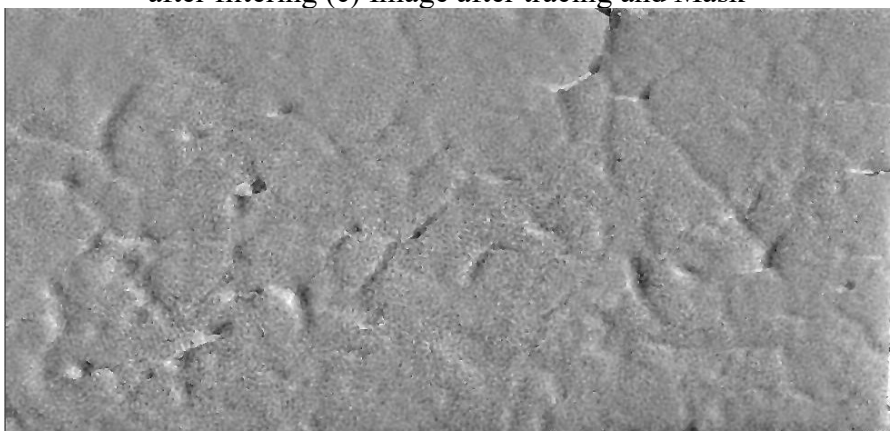

(a)

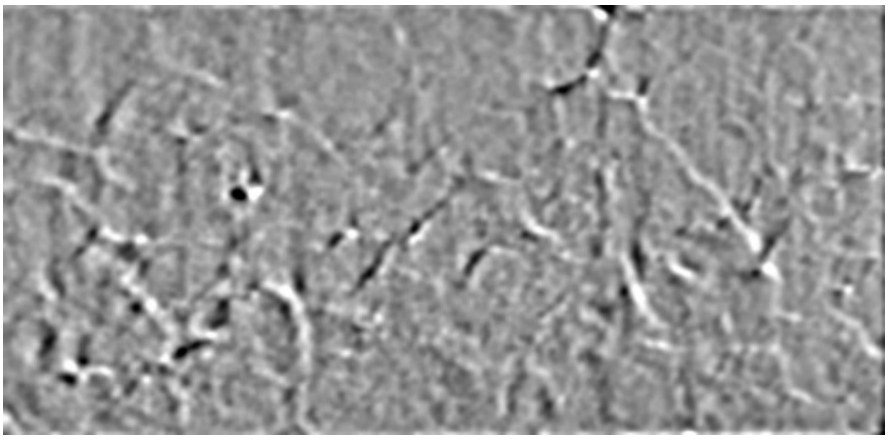

(b)

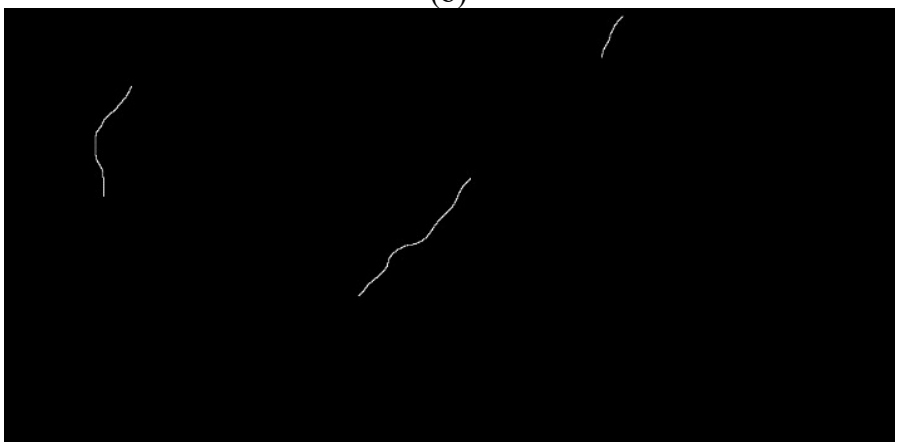

(c)

Figure A.137 TX2 Section 2B-X at 97 days after cast (a) original image (b) Image after filtering (c) Image after tracing and Mask

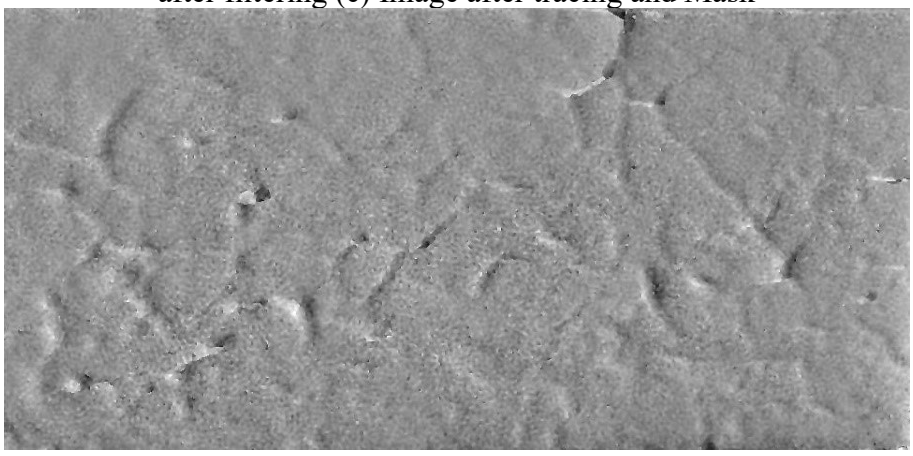

(a)

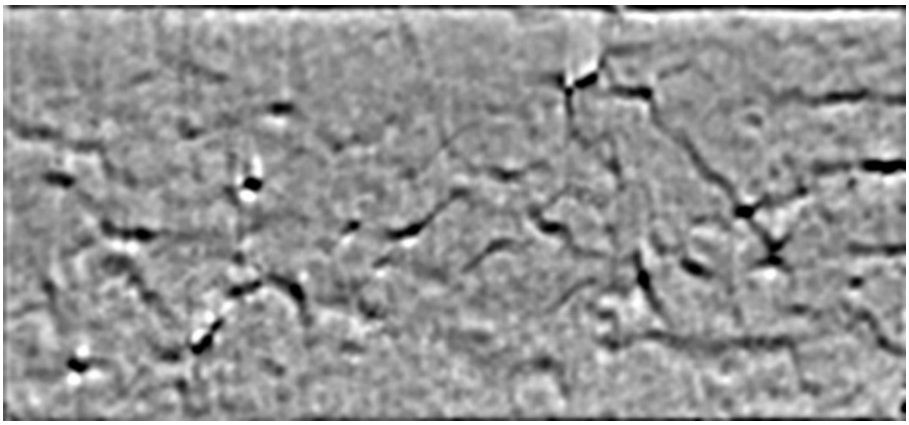

(b)

(c)

Figure A.138 TX2 Section 2B-Y at 97 days after cast (a) original image (b) Image after filtering (c) Image after tracing and Mask

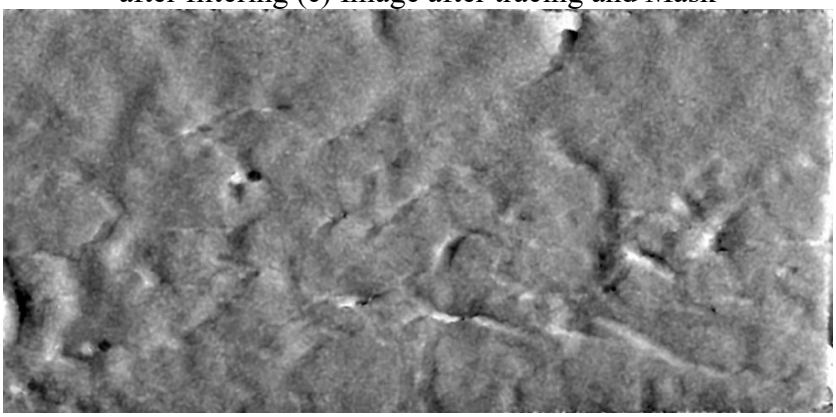

(a)

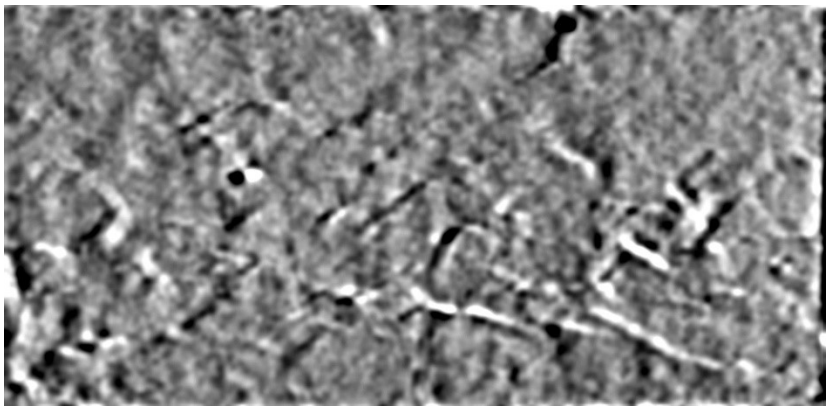

(b)

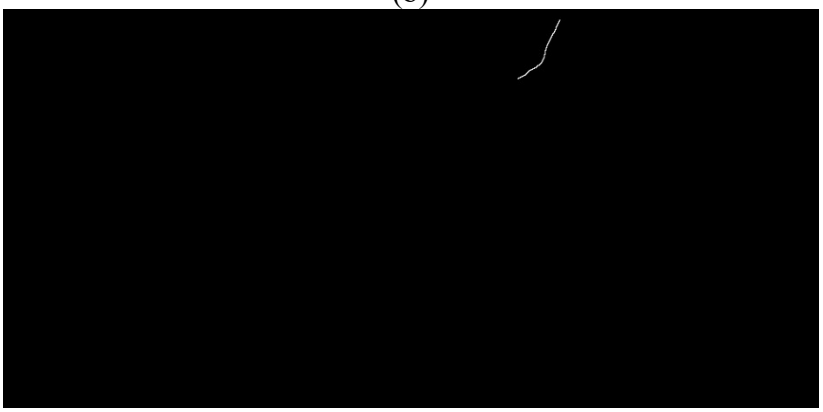

(c)

Figure A.139 TX2 Section 2B-X at 327 days after cast (a) original image (b) Image after filtering (c) Image after tracing and Mask

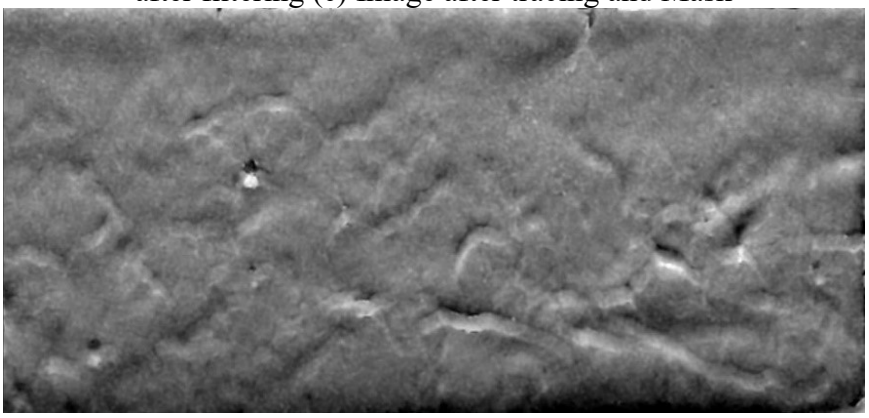

(a)

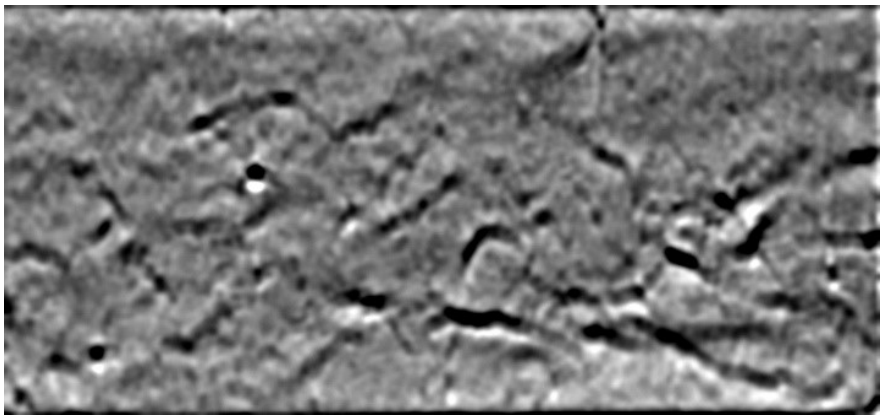

(b)

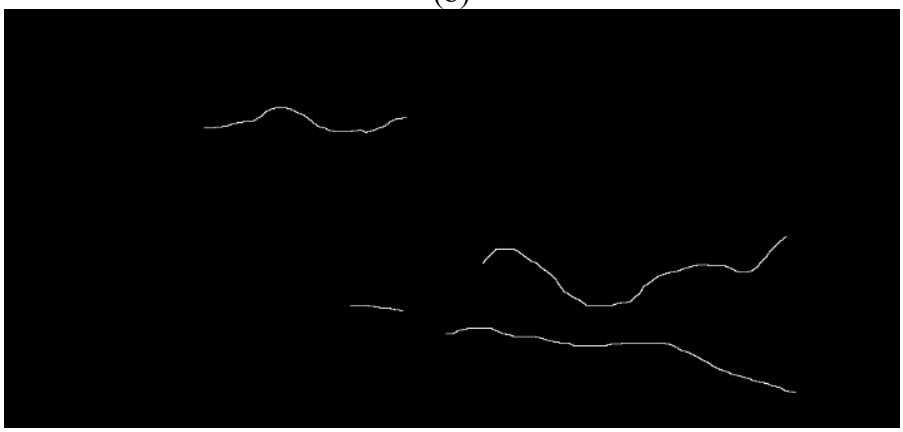

(c)

Figure A.140 TX2 Section 2B-Y at 327 days after cast (a) original image (b) Image after filtering (c) Image after tracing and Mask

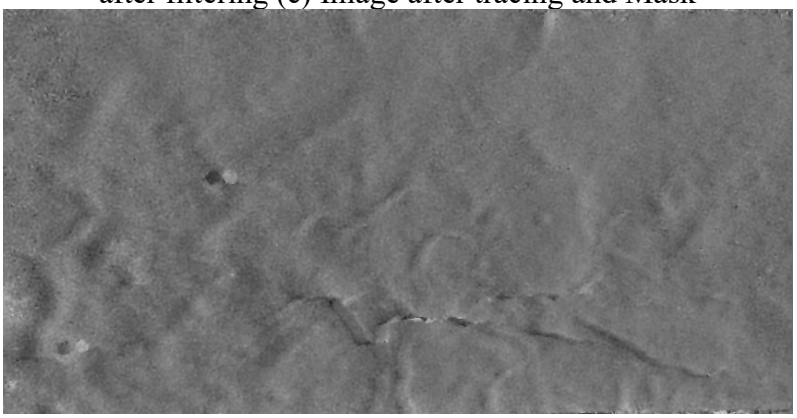

(a)

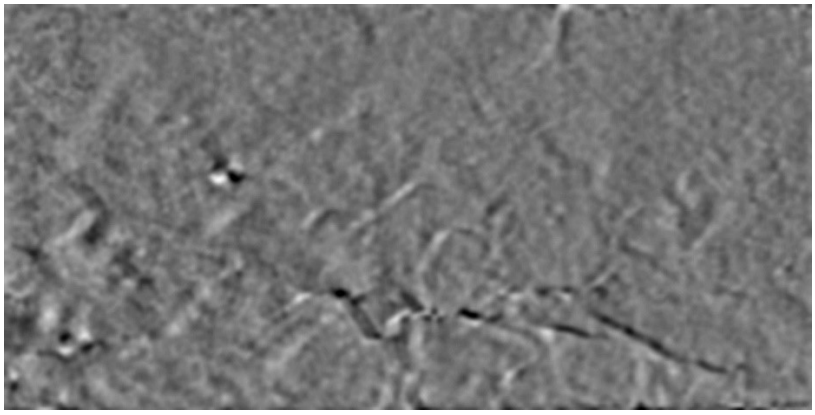

(b)

(c)

Figure A.141 TX2 Section 2B-X at 548 days after cast (a) original image (b) Image after filtering (c) Image after tracing and Mask

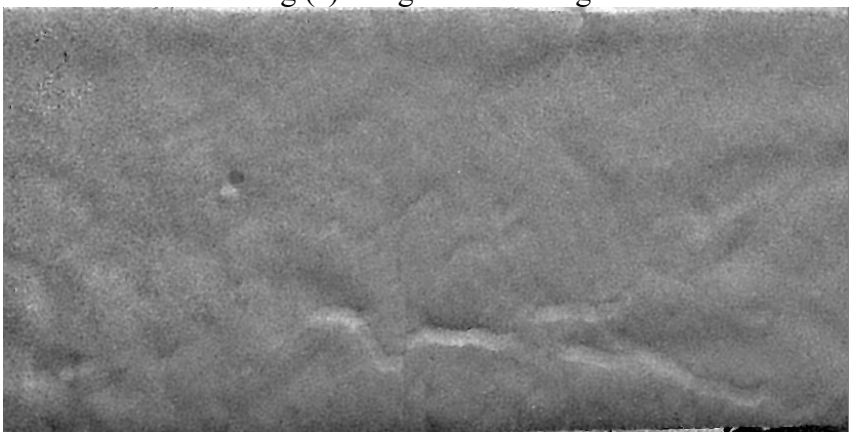

(a)

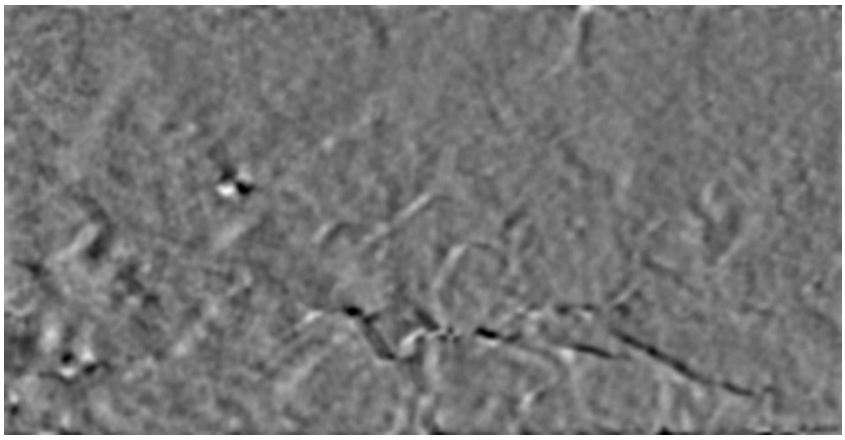

(b)

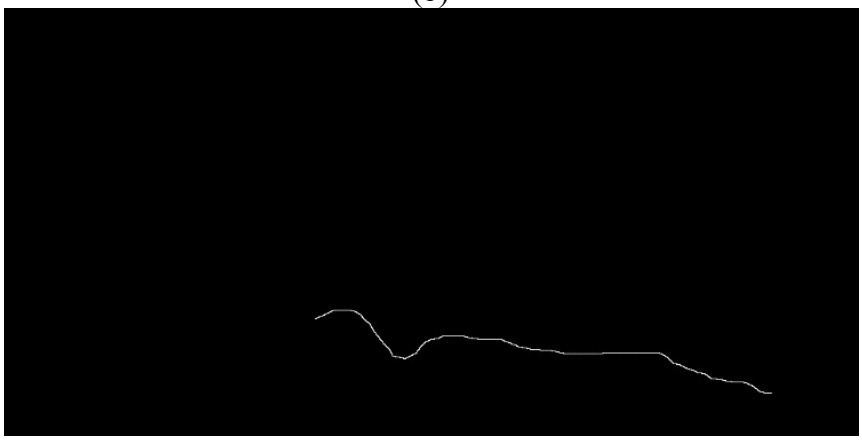

(c)

Figure A.142 TX2 Section 2B-Y at 548 days after cast (a) original image (b) Image after filtering (c) Image after tracing and Mask

(a)

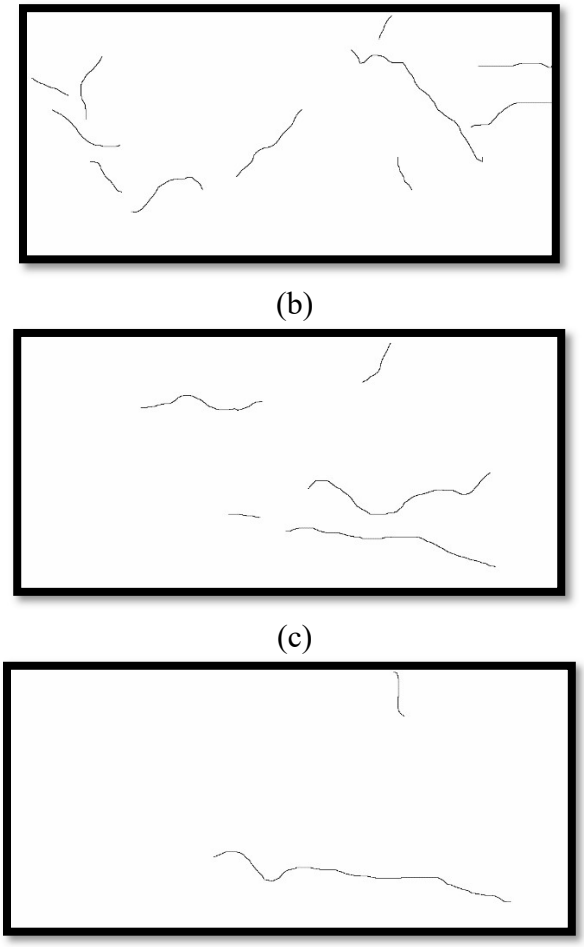

(b)

(c)

(d)

Figure A.143 Section 2B TX2 Mask X and Y shear direction combined traced cracks and inverted (a) 45 Days (b) 97 Days (c) 467 Days (d) 548 Days

**References**

Day, R. L., 1992, “The Effect of Secondary Ettringite Formation on the Durability of Concrete:” A Literature Analysis of Portland Cement Association. Skokie, IL.

Kennerly, R. A., 1965, “Ettringite Formation in Dam Gallery,” ACI Journal, pp. 559-576.

Fu, Y. and Beaudoin, J. J., 1996, “Microcracking as Precursor to Delayed Ettringite Formation in Cement Systems,” Cem. Concr. Res., Vol. 26, No. 10, pp. 1493-1498.

H.F.W. Taylor, C. Famy, K.L. Scrivener “Delayed ettringite formation,” Cem, Concr. Res., Vol 31.

Bruno Godart, Loïc Divet. Lessons learned from structures damaged by delayed ettringite formation and the French prevention strategy. Fifth international conference on Forensic Engineering, Institution of Civil Engineers, Apr 2013, France. 12p. hal-00945667

Diamond, S., 1996, “Delayed Ettringite Formation – Processes and Problems,” Cem. Concr. Composites, Vol. 18, pp.205-215.

Mielenz, R. C., Maursin, S. L., Hime, W. G., and Jugovic, Z. T., December 1995, “Investigation of Prestressed Concrete Railway Tie Distress,” Concrete International, Vol. 17, No.12, pp. 62-68.

Vitousova, L., April 1991, “Concrete Sleepers in CSD Tracks,” International Symposium on Precast Concrete Sleeper, Madrid pp. 253-264.

Ceesay, J. (2007). “Characterization of damage in mortar and concrete specimens due to delayed ettringite formation (def)” (Doctoral dissertation, University of Maryland, College Park, 2007). University of Maryland.

Ceary, M. (2007). “ Characterization of Delayed Ettringite Formation in Maryland Bridges” (Doctoral dissertation, University of Maryland, College Park, 2007). University of Maryland.

Khong, H. (2007). “Application of Laser Shearography for detecting microcracks in concrete” (Master dissertation, University of Maryland, College Park, 2007). University of Maryland.

Cooley, J. Tukey, J. “An algorithm for the Machine Calculation of Complex Fourier Series” American Mathematical Society August 17 1964.

Yin, Zhaozheng & Ker, Elmer & Kanade, Takeo. (2011). Restoring DIC Microscopy Images from Multiple Shear Directions. Information processing in medical imaging : proceedings of the ... conference. 22. 384-97. 10.1007/978-3-642-22092-0_32.

Newman, J. and Amde, A. M., “Development of Prototype Compact Shearography System, Analysis Method and Software for Micro-Crack Detection" (Contract Number DTRT57-08-C-10001), SBIR Report, USDOT – FHWA, March 24, 2011, 104 pages.